RECEIVED
AUG 07 1998
OSTI
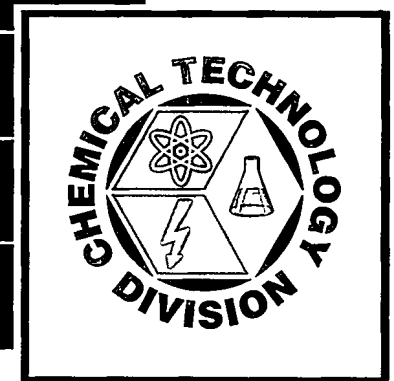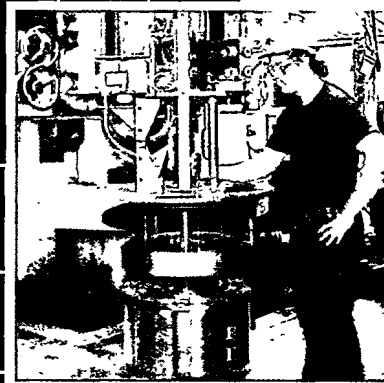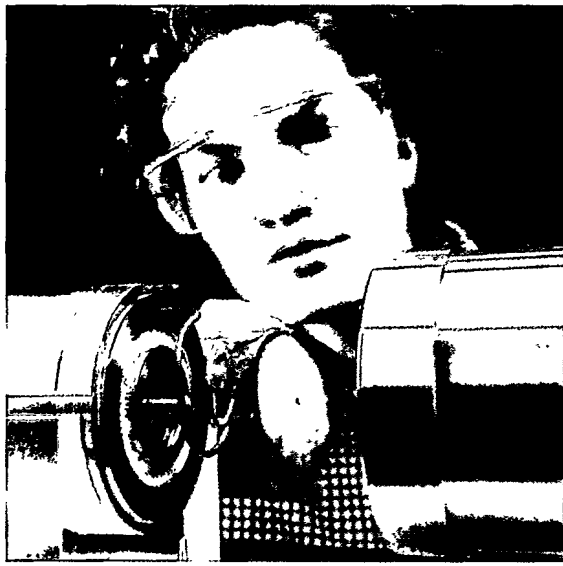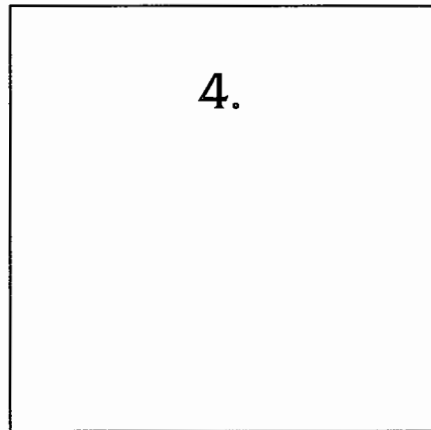
Chemical Technology Division

Annual Technical Report

1997

Applying Chemical Innovation to Environmental Problems

CHEMICAL TECHNOLOGY DIVISION

MASTER

Argonne National Laboratory

DISCLAIMER

Portions of this document may be illegible
electronic image products. Images are
produced from the best available original
document.

RECEIVED
AUG 0 7 1998
U S T

Argonne National Laboratory
9700 South Cass Avenue
Argonne, IL 60439

1997

Chemical Technology Division

Annual Technical Report

J. J. Laidler   Division Director
K. M. Myles   Electrochemical and Basic Science Department
R. E. Einziger   Waste Management Department
C. C. McPheeters   Nuclear Technology Department
D. W. Green   Analytical Chemistry Laboratory

June 1998

TABLE OF CONTENTS

TABLE OF CONTENTS (contd)

TABLE OF CONTENTS (contd)

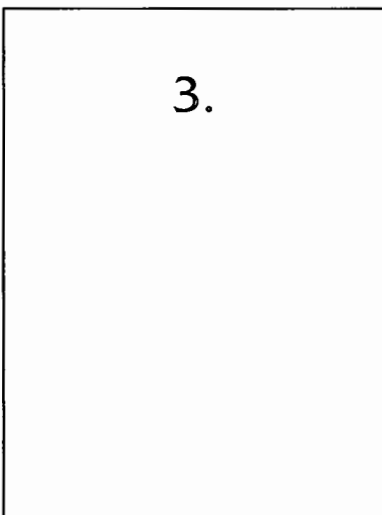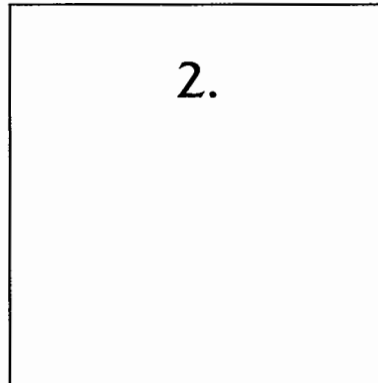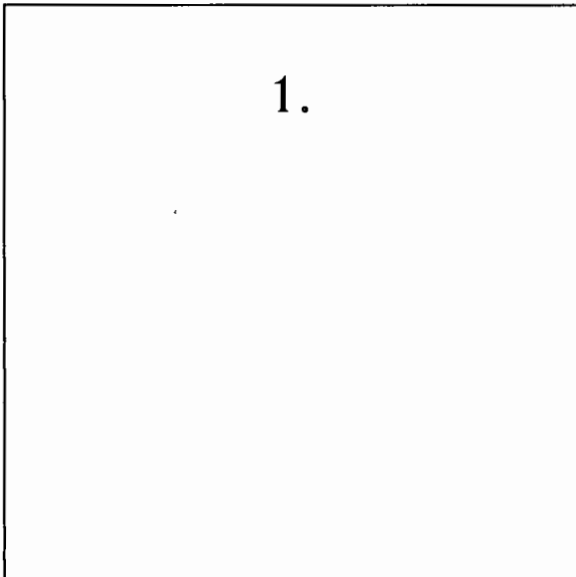# 1997

Chemical Technology Division

Annual Technical Report

Abstract

The Chemical Technology (CMT) Division is a diverse technical organization with principal emphases in environmental management and development of advanced energy sources. The Division conducts research and development in three general areas: (1) development of advanced power sources for stationary and transportation applications and for consumer electronics, (2) management of high-level and low-level nuclear wastes and hazardous wastes, and (3) electrometallurgical treatment of spent nuclear fuel. The Division also performs basic research in catalytic chemistry involving molecular energy resources, mechanisms of ion transport in lithium battery electrolytes, and the chemistry of technology-relevant materials and electrified interfaces. In addition, the Division operates the Analytical Chemistry Laboratory, which conducts research in analytical chemistry and provides analytical services for programs at Argonne National Laboratory (ANL) and other organizations. Technical highlights of the Division's activities during 1997 are presented.

Summary

Electrochemical Technology

The CMT Division conducts research, development, testing, and technical evaluation studies of advanced power sources for vehicle propulsion, utility load-leveling, and other energy storage applications. The technical management of industrial contracts for the Department of Energy (DOE) is also being carried out on the development of fuel cells for transportation applications.

In the battery R&D program, the Division is working with 3M Corp. and Hydro-Québec to develop lithium-polymer batteries for transportation applications. These batteries show promise for meeting the demanding performance requirements of electric vehicles and operate at low temperature (typically 60°C). Recent effort has focused on investigating a V_2O_5 cathode, which offers high theoretical capacity (440 mAh/g) and is relatively inexpensive. Measurements by AC impedance indicated that an interfacial oxide layer between the bulk oxide and polymer layers is the source of an increase in impedance that occurs with charge-discharge cycling.

A potentially attractive electrode material for 3-V secondary lithium batteries is α-MnO_2. Researchers in CMT have replaced the water component in α-$MnO_2 \cdot H_2O$ materials with Li_2O to fabricate "lithia-stabilized" electrodes that show significantly superior electrochemical performance to the parent α-MnO_2 material. The structures of hydrated, dehydrated, and lithia-stabilized α-MnO_2 samples were determined by the Rietveld profile refinement technique combined with time-of-flight neutron diffraction data. The findings have implications for designing improved manganese oxides that will be more tolerant to lithium insertion and extraction reactions, particularly for secondary 3-V lithium cells. Structural studies are also in progress on vanadium oxide insertion electrodes.

A new program has been started to develop a high-power energy storage device for a hybrid vehicle that couples this device with a fuel cell. We are investigating the integration of the galvanic properties of battery "insertion" electrodes and the high surface area of supercapacitors to form a lithium-ion based galvanic stack. Testing of a $Li_4Ti_5O_{12}/LiCoO_2$ cell couple has yielded promising results. We have developed a conceptual design for a 400-V galvanic stack based on a $Li_4Ti_5O_{12}/LiNi_{0.82}Co_{0.18}O_2$ system.

The Electrochemical Analysis and Diagnostic Laboratory in CMT includes a test laboratory to conduct battery evaluations under simulated application conditions. During 1997, performance and life evaluations were conducted for nickel/metal hydride modules fabricated by various industrial firms and for cells and modules in the lithium-polymer battery program. In addition, nickel/metal hydride cells built by Ovonic Battery Co. were subjected to post-test analysis after life evaluations, and the results helped to identify specific areas where changes in design or the materials of construction would improve cell performance. Examinations were also completed for Commonwealth Edison Co. and Duke Power on lead-acid cells (used for standby

power in nuclear generating stations) that had undergone an abrupt capacity fade. The root cause of this problem was identified.

Fuel cells convert chemical energy directly into electricity by electrochemical reaction, eliminating the need for heat engines and rotating machinery. Since fuel cells have very low environmental emissions and high efficiencies, interest in their development continues to grow.

To aid the development of fuel cells for transportation applications, CMT staff are developing a fast-response fuel reformer that converts hydrocarbon fuels into a hydrogen-rich gas for low-temperature fuel cells (polymer electrolyte and phosphoric acid fuel cells). During the past year, we discovered a new class of catalytic materials that yield high hydrogen concentrations (approximately 70%) in the partial oxidation of hydrocarbon fuels, including gasoline. Different crystal structures of these catalysts are also being investigated.

One of the major contaminants in the reformate of low-temperature fuel cells is carbon monoxide, which must be reduced to less than 100 ppm to avoid significant degradation in fuel cell output. Treatment with a CuCl-impregnated sorbent has been shown to provide acceptable removal of carbon monoxide in the reformate of light-duty vehicles. To aid in the development of a fuel cell vehicle, we are also developing a computer model that will work with various configurations of fuel cell systems in light-duty vehicles.

A polymer electrolyte fuel cell that operates directly on methanol (no reformer needed) is under development for small applications requiring a lightweight and easily portable power source. This work is focused on overcoming a major obstacle to commercialization of this fuel cell: low electrocatalytic activity of the anode catalyst for the methanol oxidation reaction. We have found that platinum-based alloy catalysts improve the methanol oxidation activity. An isothermal, steady-state model of the anode in the direct-methanol fuel cell has been developed to design a liquid feed anode that will yield optimal performance at a given set of operating conditions.

Effort continues on developing a molten carbonate fuel cell for utility applications. In molten carbonate fuel cells, the present NiO cathodes have dissolution/precipitation problems that limit cell lifetime under pressurized operating conditions, and a search is underway for alternative conductive materials that are stable in the high-temperature (650°C) cell environment. Low electrical resistivity has been demonstrated with a $LiFeO_2$-$LiCoO_2$-NiO cathode. An inexpensive method of fabricating this cathode has yielded promising preliminary results. Another problem with the present molten carbonate fuel cell is segregation of the Li_2CO_3-K_2CO_3 electrolyte, which increases the potassium concentration near the cathode and leads to increased cathode solubility and performance decline. Tests with carbonate-wetted $LiAlO_2$ strips and bench-scale cells indicated that the problem of electrolyte segregation could be minimized by use of a Li_2CO_3-Na_2CO_3 electrolyte containing 67 to 75 mol% of the lithium carbonate. Work is also underway to develop materials that will prevent corrosion of the metal hardware in the molten carbonate fuel cell.

The Division continues to provide support to the DOE Office of Transportation Technologies and the DOE Office of Buildings Technology in the form of technical management

of R&D contracts with industrial developers of fuel cells and related components. Major ongoing projects managed by CMT include contracts with General Motors Corp., Ford Motor Co., Chrysler Corp., and fuel-cell component suppliers.

Hazardous and Mixed Waste Research

A major challenge facing DOE is management of the massive quantity of hazardous and mixed (hazardous/radioactive) waste that has accumulated at various DOE sites as a result of nuclear-defense production and other activities conducted for more than four decades at these sites. A new technology, aqueous biphasic extraction, has been developed at CMT for removal of heavy metals and toxic materials from solid wastes and wastewater streams and is a prime candidate for large-scale application. The extraction systems are generated by combining an aqueous salt solution with an aqueous polymer solution such as polyethylene glycol. Experimental studies of aqueous biphase formation indicate that recovery of the extracted metal complex can be achieved by contacting the polymer-rich phase with a water-immiscible alcohol at elevated temperatures (60-80°C). The polymer can be recovered from the alcohol phase by back extraction into a dilute salt solution at low temperatures. Aqueous biphasic extraction has also been tested for lead removal from contaminated soil. In extraction tests using soil with a low humate content, the lead content was reduced from 2000 to 600 mg/kg.

Staff in CMT are developing a zinc phosphate glass for disposal of the fission products and transuranic elements that accumulate in the chloride salt used in the electrometallurgical treatment of spent nuclear fuels. Advantages of this new waste form include a low glass transition temperature and high salt loading. Preliminary corrosion tests of small-scale samples have yielded promising results.

The interactions of multivalent actinide species with bacteria are being investigated as part of a larger effort to identify key processes that lead to both the immobilization and mobilization of actinide species in subsurface groundwaters on DOE sites. Effort was devoted to determining the interaction of the actinide-nitrilotriacetic (NTA) complex with the NTA-degrading microbe *Chelatobacter heintzii* in aqueous solution. A key feature of this research is the extensive integration of computer modeling with laboratory experimentation. Our results to date have shown that actinide toxicity is dependent upon the oxidation state and isotope of the actinide in the aqueous system. For example, in contrast to the radiolytic toxicity in the Pu(IV) system, Np(V) inhibits the activity of *C. heintzii* via chemical toxicity, similar to other heavy metals. In other work, studies have been initiated to extend and develop X-ray synchrotron (XRS) radiation techniques to determine the chemical structure of aqueous, adsorbed, and solid actinide species of importance to environmental and nuclear waste management. Emphasis is on both collecting XRS data on actinide systems and modeling these data by improved calculational methods and theory.

The Waste Isolation Pilot Plant (WIPP) in Carlsbad, New Mexico, has been selected as a possible disposal site for transuranic radioactive wastes resulting from defense-related activities at DOE sites. Work for this project in this past year involved determining actinide stability and solubility in various simulated WIPP brines with pH values from 5 to 10. One finding from these studies was that steady-state concentrations of Pu(VI) were maintained in WIPP brine throughout

the 18-month duration of the experiments. Addition of reducing agents relevant to the WIPP brines reduced the Pu(VI) to Pu(IV) and lowered the steady-state concentrations of plutonium in the brine solution. These data are being used to test and challenge the Actinide Source Term model being developed for the WIPP project.

Radiolytic gas generation studies are in progress on a chemically bonded phosphate ceramic (Ceramicrete) being developed for encapsulating transuranic-bearing wastes from DOE sites. Because of the presence of radionuclides, hydrogen is produced by radiolysis of the water present in the waste form. Measurements are given for the number of hydrogen molecules per 100 eV of radiation deposited in various Ceramicrete samples. These values are being used to calculate acceptable transuranic loadings in the waste form.

Nuclear Waste Management

Work is being performed to support programs on the disposal of high-level nuclear waste and spent fuel in the candidate repository site at Yucca Mountain in southwestern Nevada. Several series of laboratory tests are being performed to determine the corrosion behavior of high-level waste glasses upon exposure to liquid water or water vapor. These tests are being conducted to determine the corrosion behavior of high-level radioactive waste forms under the hydrologically unsaturated conditions anticipated at the proposed Yucca Mountain site and are designed to assist DOE in demonstrating that the Defense Waste Processing Facility (DWPF) and the West Valley Demonstration Project (WVDP) will produce a waste glass product that will perform well in an unsaturated environment typical of what may be expected at Yucca Mountain.

On the basis of long-term dissolution tests, a three-stage model of glass corrosion has been developed. In the first stage, the glass dissolves at a rate controlled by the glass composition, solution pH, and temperature. In the second stage, the buildup of dissolved glass components controls the rate. In the third stage, the formation of alteration phases on the glass surface affects the solution chemistry. This model has facilitated the comparison of results from different test methods as well as the results of tests conducted with different glasses.

Samples of natural obsidian and basalt glasses and nuclear waste glasses have been reacted in vapor hydration tests at 75°C and relative humidity of 95 and 100% for up to 7 years. The results indicate that vapor hydration tests can be used to replicate (at least qualitatively) the corrosion behavior that occurs over many thousands of years in nature within a few years in the laboratory. The same test method can be used to forecast the long-term behavior of nuclear waste glasses under similar conditions. Vapor hydration tests have also been performed to characterize the corrosion behavior of Environmental Assessment glass, a benchmark glass for DWPF glasses.

Long-term drip tests are underway with glasses representative of those that may be produced at DWPF. The data after 10 years of testing indicate that insoluble elements, including U, Pu, and Am, are incorporated into alteration phases as the glass reacts and are subsequently released with particulate or colloidal matter as the alteration products spall from the glass. Recent trends have shown that the releases of Pu and Am, while initially quite low compared to those of soluble elements (such as B and Np), eventually are accelerated as the alteration phases spall

from the glass surface and enter the test solution. Trends in technetium release follow those of B and Np. A similar multiyear test series with a WVDP-type glass has indicated that a thorium-rich alteration phase appears to play a substantial role in the corrosion behavior of this glass.

Long-term and accelerated tests are being conducted with several glasses similar to anticipated forms of immobilized low-activity radioactive waste (ILAW) for disposal of Hanford wastes. Tests to date have shown that sodium is released from candidate ILAW glasses faster than other glass components, probably through ion exchange. The release behavior of technetium is under study by a variety of static dissolution tests because it was calculated to contribute the greatest dose to man in a preliminary assessment of the Hanford disposal system. In another project, we developed a test method for determining ILAW product acceptance and formulated a glass to be used as a standard in that test.

Besides the glass studies, long-term tests with unirradiated UO_2 pellets and spent fuel are in progress to determine radionuclide release rates when these materials are exposed to repository-relevant conditions. Results from drip tests with UO_2 pellets for over 12 years indicated that uranium release was rapid during the first one to two years of testing and has remained relatively low in the remaining testing period. Another test method is being developed to measure the solution composition in contact with spent fuel during the reaction processes important in the drip tests. This information is needed as input for model development and confirmation. Tests have also been ongoing for almost four years with spent fuel samples under drip conditions. Results are reported for the amount of released plutonium and the percentage in colloidal form at selected test intervals. The results indicated that thin-film flow is a possible transport pathway for release of radionuclides from the spent fuel.

The DOE is examining options for placing surplus plutonium from the weapons program into a form that is inaccessible for use by others. One such option is immobilization, where the plutonium would be fixed into a glass or ceramic waste form that meets safety and security objectives. Our main task over the past two years has been to provide characterization and corrosion data to DOE so that an informed choice could be made between glass and ceramic. The DOE has decided that ceramic will be the preferred material for the immobilization of excess plutonium.

Other projects in nuclear waste management include static testing of a new ceramic waste form in different leachants, a study of transmutation effects in a ^{137}Cs-bearing ceramic sample, development of a method for pretreating radioactive or mixed waste vitrification feeds, and fundamental research on the nature of the electronic interaction and chemical bonding properties of radionuclides in waste forms.

Separation Science and Technology

The Division's work in separation science and technology is concerned with (1) developing methods for treating radioactive, mixed, and hazardous waste and (2) determining the feasibility of substituting low-enriched uranium for the high-enriched uranium currently used in the production of ^{99}Mo for medical diagnostic applications.

The main project in the first area involves R&D on solvent extraction processes for the cleanup of nuclear waste solutions. Work in the past year focused on advising engineers at Idaho National Engineering and Environmental Laboratory concerning their hot demonstration of the SREX (strontium extraction) process on actual acidic high-level waste stored at the site. A demonstration was successfully completed with a 24-stage centrifugal contactor built at ANL. With this contactor, 99.995% of the ^{90}Sr in the aqueous raffinate was removed. Analysis of the stage-to-stage strontium data showed that the contactor worked well, with a mass-transfer efficiency of 97% in the extraction section and 98% elsewhere. In other solvent-extraction work, we have been collaborating with Oak Ridge National Laboratory and Pacific Northwest National Laboratory on developing a Sr and Tc extraction process for alkaline waste solutions (SRTALK). This process will be able to separate alkali-metal pertechnetate salts from alkaline supernate that comes directly from nuclear waste tanks. In a test with a 12-stage centrifugal contactor and simulated tank waste, the SRTALK process was very successful at removing and concentrating ^{99}Tc. Work for the next year will focus on testing Cs and Sr extractability with the SRTALK process.

We have continued working with the ANL Waste Management Organization to help them solve problems associated with waste storage and treatment. For example, much of the transuranic waste on site is stored as highly acidic solutions that require stabilization for long-term storage until a disposal site is available. As a simple method to stabilize the waste, we have helped them set up a glovebox in which the waste will be neutralized and solidified by treatment with a commercially available setting agent.

A project is ongoing to develop a low-enriched uranium (LEU) target and a processing method for production of ^{99}Mo to be used for medical applications. It is our objective in switching to LEU to maintain the process for molybdenum recovery and separation from uranium (and its fission and absorption products) as close as possible to the current Cintichem process for high-enriched uranium. To that end, we determined the behavior of three fission products (I, Rh, and Ag) during molybdenum recovery and purification by the Cintichem process. We concluded that contamination of the molybdenum product by these three fission products should not be a problem. In other work on Cintichem processing, we are in the process of developing and testing a procedure for separating and recovering actinide elements from the purified ^{99}Mo product that will allow low dose, facile, and effective measurement of alpha contamination in the ^{99}Mo. Development of LEU metal-foil targets has led to the use of thin metal barriers (to fission recoil) between the uranium foil and target walls. Several studies are in progress on the effectiveness of zinc as a barrier material. In mid 1998, we plan to demonstrate the processing of a fully irradiated LEU metal foil at the PUSPIPTEK Radioisotope Production Center in Indonesia.

Electrometallurgical Treatment Technology

The CMT Division is developing an electrometallurgical process for treatment of spent nuclear fuels. It is capable of handling most types of spent fuel and is especially intended for fuels at risk of chemical reaction with the groundwater in the repository. These "at risk" spent fuels include metal fuels with various cladding and matrix materials, reactive compounds, and highly enriched fuels. The central feature of the electrometallurgical treatment is electrorefining of the spent fuel in a molten salt electrolyte at 500°C. After electrorefining of the spent fuel, the

fuel cladding and fission products are placed in two stable waste forms (one a ceramic, the other metal), which are suitable for disposal in a geologic repository. There are no other high-level wastes, and only negligible amounts of low-level waste are generated.

An effort has been underway to develop an advanced electrorefiner having high throughput (>40 kg uranium per hour) and large batch size (>100 kg) for treating large quantities of spent fuel, such as the N-reactor fuel from the Hanford site. Effort this past year focused on testing a high-throughput electrorefiner with a diameter of 25 in. (0.6 m) and a batch size of 150 kg uranium. The test samples were unirradiated N-reactor fuel elements from the Hanford site. The number of ampere-hours (31,219 Ah) passed through this electrorefiner during the most recent test was nearly twice the number of ampere-hours (17,018 Ah) passed through the electrorefiner during all of our earlier runs. To date, about 75 kg of uranium product has been collected from the tests, and about 50 kg of that uranium has been transferred to a cathode processor for consolidation. A new design of scraper for removing uranium from the electrorefiner cathode has shown promise of a large improvement in sustained operation of the high-throughput electrorefiner.

The feasibility of electrometallurgical treatment of oxide and metallic spent fuel has been demonstrated over the past several years. This treatment has now been tested for other types of fuels, including (1) a uranium fluoride fuel that was dissolved in a mixture of molten fluoride salts as part of the Molten Salt Reactor Experiment (MSRE) conducted at Oak Ridge National Laboratory and (2) aluminum alloy fuels, 128 metric tons of which will be shipped to the Savannah River Site over the next 40 years. The test results with simulated MSRE (fluoride) salt clearly showed that zirconium (along with other noble metals) is separable from the salt by deposition on an iron cathode mandrel; this electrotransport product can be alloyed with iron to make a stable metal waste form. Also, the concept of using Li_3Bi as anode material was proven. This is very important in reducing waste volumes in the treatment of MSRE salt. Laboratory-scale tests (2-g batch size) with pure aluminum and U-Al-Si alloy demonstrated the aluminum electrorefining step in the flowsheet for electrometallurgical treatment of aluminum-based fuels. Engineering-scale tests (6-kg batch size) are planned.

Ceramic and metal waste forms to contain the high-level waste from the *electrometallurgical treatment are being developed, along with methods and equipment for* isolation of waste components and fabrication of waste forms. The main isolation equipment includes pyrocontactors for the selective redox removal of constituents from process fluids (mainly uranium from electrorefiner electrolyte) and zeolite ion-exchange columns for removal of waste components from the electrolyte. Single-stage pyrocontactors had previously been shown to be effective in conducting redox extractions between molten salt and liquid cadmium; this work was completed, then extended to operation and successful testing of a four-stage countercurrent device this year. A zeolite ion-exchange column at the laboratory scale is being tested to determine the optimum operating conditions for a full-scale unit. To date, these tests have indicated that temperature has little effect in performance between 500 and 600°C, and flow rates below 1.4 cm/min at 550°C appear to significantly increase removal of rare earths from the salt.

The ceramic waste form contains the transuranic elements and the most easily oxidized fission products that accumulate in the electrorefiner salt. The development of this waste form has focused on two composites: zeolite-glass and sodalite-glass. The zeolite-glass has a higher capacity for salt, while the sodalite-glass composite is more thermally stable. In October 1997, the sodalite-glass composite was selected as the reference ceramic waste form for the project.

With regard to the metal waste form, those components of the high-level waste that are chemically unaffected by the electrometallurgical process—cladding hulls, zirconium alloying additions, and noble metal fission products—are combined with small amounts of particulate materials from electrolyte filters and melted to form a highly durable waste form. Depending on the cladding (stainless steel or Zircaloy), the basic alloy composition is stainless steel-15 wt% zirconium or Zircaloy-8 wt% stainless steel. Recent work has concentrated on the alloy with 15 wt% Zr. Metallurgical studies indicated that this alloy will accommodate all noble metal fission products from any type of fuel treated by the electrometallurgical process, and that zirconium compositions below 15 wt% may become saturated at high fission product loadings. Also, a qualification test matrix has been established for the metal waste form. This matrix is intended to provide a qualification-relevant data base for future repository acceptance: it contains attribute tests, characterization tests, accelerated tests, and service condition tests.

Pyrochemical Process Applications

The electrometallurgical treatment of spent oxide fuels requires that the oxides first be reduced to metals that can be processed in the electrorefiner. A lithium reduction process has been selected to convert the spent oxide fuels into metals. In the process, the spent oxide fuel is treated by reaction with lithium at 650°C in the presence of molten LiCl to reduce the actinide oxides to the corresponding metals and Li_2O. The Li_2O, which is soluble in LiCl, is subsequently removed from the salt in an electrowinning cell.

During the past year, work continued to develop both the reduction and electrowinning portions of the lithium reduction process, with an emphasis on process scaleup. Laboratory-scale experiments indicated that stirring of the bulk salt had a noticeable effect on the reduction rate of crushed UO_2 but little effect on clad UO_2 pellets. One of the difficulties encountered in our electrowinning work has been recombination of the lithium and oxygen in the electrowinning cell to produce Li_2O. This parasitic reaction has been, in some cases, so efficient as to leave no net lithium production. During this period, work has been focused on the development of a porous metal cathode for the electrowinning cell that eliminates this problem. The porous metal cathode works because the lithium wets the porous metal (stainless steel) and is incorporated into the pores below the salt level. The lithium is not released from the cathode under normal operating conditions unless the pore capacity of the cathode is exceeded. Small- and large-scale laboratory experiments have demonstrated the effectiveness of the porous metal cathode. In related work, alternative materials to the expensive Pt-Rh anode in the electrowinning cell are being sought. The candidate materials identified as promising are Fe_3O_4, SnO_2, and NiO. A new fabrication method has been developed for the Fe_3O_4 anode. Evaluating the manufacture and performance characteristics of this material is planned.

An engineering-scale series of experiments is underway to obtain design information and operating experience needed for scaling up the reduction and electrowinning processes to plant size required for processing DOE oxide spent fuels. To meet this objective, the facility used for these experiments was designed to support the reduction of kilogram quantities of fuel. In a test in this facility, 3.6 kg of crushed UO_2 was completely reduced in about 50 h, while 2.9 kg of clad UO_2 pellets was only 40% reduced in 120 h. This experiment provided valuable input into the design of fuel baskets and fuel loading for the next engineering-scale test.

An effort is underway to evaluate whether the electrometallurgical treatment can be applied to the nonmetallic fuel types presently at Idaho National Engineering and Environmental Laboratory. Issues being evaluated include the nature of any required head-end treatment to prepare the spent fuel for the electrometallurgical process, and the chemistry and operating conditions of the electrorefining step.

In support of design work being performed on the pilot-scale reduction facility planned for ANL-West, a series of tests was performed to evaluate the corrosion resistance of candidate materials for the reduction and electrowinning vessels. Test coupons included tantalum, stainless steels, and 2¼ Cr-1Mo. In the tests under reduction conditions, the tantalum suffered minor attack, while none of the other test coupons had any measurable corrosion. For the electrowinning conditions, all coupons were severely corroded. Alternative materials for the electrowinning vessel are thus being sought.

Basic Chemistry Research

Basic chemistry research is being pursued in several areas: fundamental chemistry associated with catalyses in systems that involve molecular energy resources, mechanisms of ion transport in lithium battery electrolytes, materials chemistry of electrified interfaces and molecular sieve materials, and the theory of materials properties.

Recent research in the catalysis program has included *in situ* spectroscopic investigations of the chemistry associated with the conversion of some key industrial homogeneous processes to more energy efficient and more environmentally benign supercritical ones. The various processes designed to achieve the commercial hydroformylation of olefins comprise the largest scale use of homogeneous catalysts and are the subject of the program's current efforts in supercritical fluid catalysis. In recent research, we have completed the first thermodynamic measurements of the key equilibria associated with phosphine-modified hydroformylation catalysis of the type used commercially by the Shell Chemical Company. Equilibria that were measured include not only the important catalyst hydrogenation step, but also carbon-monoxide-induced salt formation that has so far prevented the phosphine-modified cobalt hydroformylation reaction from being conducted in a supercritical fluid. This latter reaction stems from the phosphine's intrinsic basicity and converts the catalyst to an unreactive salt that precipitates from the supercritical medium, thereby making the catalyst ineffective. The results indicate that use of phosphines having lower basicity than conventionally used might allow a potentially desirable supercritical phosphine-modified cobalt hydroformylation catalyst system to be feasible for the first time.

Another catalysis program involves research in hydrocarbon activation aimed at achieving the controlled catalytic functionalization of methane and other hydrocarbons via activation of their C-H bonds. Current research focuses on developing catalytic strategies based on the extremely robust phthalocyanine nucleus. During the past year, CMT researchers synthesized some new catalysts for the epoxidation of olefins and the hydroxylation of alkanes. A high valent $Fe^{IV}=O$ complex of unusual stability was also prepared and characterized.

The mechanism of ion transport in lithium-polymer electrolyte battery materials is being investigated by using *in situ* magnetic resonance imaging developed in our catalysis program. Research in this area in the past year has focused on using the CMT-developed toroid cavity imager to characterize the ion depletion zone near the cathode in these batteries. Nondestructive *in situ* spectroscopic techniques have been developed by CMT researchers for measuring ionic mobilities and the size of the electrolyte depletion zones. Distance resolution of 3 μm has been achieved with the magnetic resonance imager. These techniques make it possible to systematically study the effect of plasticizers, temperature, and alterations in the polymer backbone on the lithium ion transport properties.

The Division's program on materials and interface chemistry is exploring a variety of research areas: corrosion, decontamination of metal surfaces from nuclear facilities, interfacial and electrochemical processes prevalent in fuel cells and batteries, and heterogeneous catalysis related to environmental problems. The work on corrosion/passivation of metals has focused on the structure and chemical composition of oxide-containing films on metals that are (1) used extensively in heat transport and cooling systems (e.g., copper) and (2) the principal constituents of radionuclide-contaminated structures at DOE nuclear facilities (e.g., Ni and Fe). In the past year, results obtained by electrochemical, spectroscopic, and synchrotron X-ray methods have yielded significant new insights concerning the mode of incorporation of elements like Ce and Sr in passive films on nickel.

Recently completed research on the $Cu^{2+}/Cu^{+}/Cu^{0}$ electrode reaction sequence, a troublesome reduction reaction that facilitates corrosion in the steam generators of light water nuclear reactors, has provided new information about the temperature dependence and mechanism of the rate-limiting reaction $Cu^{2+} \rightarrow Cu^{+}$. This study has relied on an integration of transient electrochemical measurement methods with first-principle theoretical calculations to produce findings that elucidate various features of the relevant electron transfer processes.

Two new research projects that explore processes occurring in metal oxide-based ultracapacitors and in lithium polymer batteries are underway. Using the $RuO_2(100)$ surface as a model system, CMT researchers are employing synchrotron X-ray reflectivity techniques to characterize the reconstruction that occurs on ultracapacitor surfaces during charging and discharging. A combination of *ab initio* molecular orbital theory and molecular dynamics simulations has produced interesting conceptual models of the electromigration of lithium ions through polymer electrolytes of the type used in lithium polymer batteries.

Development of the now widely used Gaussian-2 quantum chemical method has continued. Originally, the method was tested against 125 reaction energies, chosen because they have well-established experimental values. This very popular and useful test set has been

significantly expanded with the inclusion of molecular energy values for nearly 100 new species. Coupling of density functional theory methods with the Gaussian-2 method is allowing us to treat systems containing larger numbers of atoms and elements with higher atomic numbers. This expanded computational capacity is being used to explore (1) the mechanisms and energetics of carbocation catalysis in molecular sieve materials and (2) the growth of nanocrystalline diamond films. In other theoretical studies, we have obtained new data on the interaction of ethane with the acid site in a model zeolite cluster and have identified a C_2 addition mechanism that nucleates the growth of diamond surfaces.

Analytical Chemistry Laboratory

The Analytical Chemistry Laboratory (ACL) is administratively within CMT, its principal client, but collaborates as a full-cost-recovery service center with many technical divisions and programs at ANL. In addition, the ACL conducts research in analytical chemistry and provides analytical services for governmental, educational, and industrial organizations.

During the past year, ACL was involved in a diverse array of analytical activities. These included analyses in support of the ANL projects to develop an electrometallurgical treatment for spent nuclear fuels and high-temperature superconductors; continuous monitoring of a plasma arc furnace developed to treat radioactive waste at ANL-West; characterization of products from the recycling of automobile shredder "fluff"; preparation and characterization of simulated waste samples in support of the Waste Isolation Pilot Plant; screening of radioactive samples of solidified waste for semivolatile organic compounds; characterization of used laboratory exhaust filters for disposal; determination of leach resistance in samples being tested for use as phosphate-ceramic-stabilized hazardous waste; analysis of scale and filter residues in cooling-water systems at ANL's Advanced Photon Source; determination of minerals and metals in milk contaminated by radioactive ^{137}Cs; analysis of lithium aluminate prepared for use in tritium production targets; characterization of residues from pitchblende ore processed to extract uranium at a weapons production site; Fourier transform infrared analysis of oil samples from Fermi National Accelerator Laboratory; determination of compounds formed as a result of simulated arcing of electrical cables; and analysis of environmental samples submitted for the determination of hazardous or radiological components.

The ACL was also involved in the development of new technology based on solid-phase extraction for radioisotope determination in aqueous samples; a comprehensive program to provide DOE with information on data quality from laboratories analyzing environmental and waste samples; a procedure that allows the accurate determination of interference-prone elements by inductively coupled plasma/mass spectrometry; and automated methods for real-time analysis of chemical sensor data from environmental samples.

I

Electrochemical Technology

The ANL Electrochemical Technology Program in CMT undertakes (1) in-house research, development, testing, post-test analysis, and technical evaluation studies of advanced battery and fuel cell systems and (2) support research, technology transfer, and technical management for industrial R&D contracts to develop these systems. During the past year, in-house battery R&D has focused on lithium-polymer and lithium-ion systems. The testing, evaluation, and post-test analysis of a variety of advanced batteries fabricated by industrial firms are performed in CMT's Electrochemical Analysis·and Diagnostics Laboratory. Potential uses of these battery systems include vehicle propulsion, utility load-leveling, and other energy storage applications. In-house R&D is also being conducted on fuel cells, where the CMT Division continues to be the premier DOE laboratory in fuel-cell technology development. We are engaged in R&D on the solid oxide fuel cell and the molten carbonate fuel cell, which are targeted for utility applications, and we are heavily involved with fuel processing development for the polymer electrolyte fuel cell for transportation applications.

A. Advanced Battery Research and Development

The primary objective of this program is the scientific evaluation of new materials for electric-vehicle batteries and for batteries for consumer products such as laptop computers and cellular phones. This program uses a complementary experimental and theoretical approach to study the structures and electrochemical properties of electrode materials. It centers on transition metal oxide electrodes for nonaqueous lithium batteries.

1. Lithium-Polymer Electrolyte System

The lithium-polymer battery is a lightweight, high-energy system that can operate at moderate temperatures (typically 60-80°C). With a polymer electrolyte, this all-solid-state battery can be manufactured by using high-speed film-laminate technology. The battery's low weight translates into high specific energy. The Li/Li$^+$ redox reaction (negative electrode, 3.0 V) gives

the battery its high power. The positive electrode is a reversible chemical host for intercalating lithium cations. Thus, during discharge, the lithium cations insert into the host material with simultaneous electrochemical reduction of the host's closest-neighbor redox sites. The host structure is highly reversible to both redox and insertion reactions; this allows the lithium cations to exit upon recharge.

The lithium-polymer battery for electric-vehicle applications is being developed under a Cooperative Research and Development Agreement (CRADA) with 3M Corp. and Hydro-Québec. Under the CRADA, Argonne provides technical support related to all aspects of battery development, including component, cell, and battery testing and characterization; post-test diagnostic analysis; electrochemical cell modeling and battery design; and electrode materials evaluation and optimization.

a.   System Description

Rechargeable lithium batteries with either metallic lithium or lithium carbon as the anode use transition metal oxides as the cathode, for example, oxides of V, Mn, Co, or Ni. These transition metal oxide electrodes have host structures into which lithium can be inserted during electrochemical discharge; the insertion of lithium is accompanied by a concomitant reduction of the transition metal ion. The reverse process occurs during charge.

The structural stability of a host electrode to the repeated insertion and extraction of lithium is undoubtedly one of the key properties for ensuring that a lithium cell operates with good electrochemical efficiency. In transition metal oxides, both stability of the oxygen-ion array and minimum displacements of the transition metal cations in the host are required to ensure good reversibility. For example, structures with a cubic-close-packed oxygen array are more stable to lithium insertion/extraction than hexagonal-close-packed structures, which tend to shear on lithium insertion in response to electrostatic interactions between the incoming lithium ions and transition metal cations in face-shared octahedral sites. The shear process is often accompanied by displacements of the transition metal cations within the oxygen lattice. These structural modifications tend to degrade the integrity of the insertion electrode, particularly when it is subjected to repeated charge and discharge.

Structures of transition metal oxide insertion electrodes are, in general, not tolerant to overcharge or overdischarge. It is, therefore, critically important to carefully control fabrication conditions so that the composition of the electrode corresponds to that of the most stable host structure of the metal oxide system. Furthermore, cell operating conditions, such as voltage limits and current drain, must be carefully controlled to ensure that the structural integrity of the electrodes is not destroyed on cycling. Materials development within the lithium-polymer battery project is focused on the synthesis and characterization of metal oxide electrodes that offer superior electrochemical behavior to state-of-the-art materials. Of particular interest is the V_2O_5 cathode material because of its high theoretical capacity (440 mAh/g).

b.   Lithium Diffusion in Vanadium Pentoxide

To isolate the oxide aging effects occurring in the composite cathode, thin (2000, 4000, and 7000 Å) V_2O_5 layers were sputtered onto nickel substrates by 3M Corp. A dense V_2O_5 layer cathode (as opposed to a composite cathode) establishes a well-defined geometry where the electrochemical active area is equal to the cell area (4 cm^2) and the current distribution is uniform. The relatively small cathode active area compared to standard laboratory cells makes the cathode kinetics and transport easier to measure.

In general, cycling results from the sputtered-cathode cells agreed well with those from typical lithium-polymer laboratory cells containing V_2O_5 cathodes. The loss of capacity in the sputtered-cathode cells was somewhat greater and the charge/discharge curves were slightly more linear than found in typical laboratory cells. The increase in the area specific impedance with cycling was similar to that observed for laboratory cells. The data on area specific resistance also indicated that lithium transport in the sputtered V_2O_5 layer is the primary problem.

Measurements by AC impedance were used to elucidate the transport properties in the sputtered-cathode cells. A typical complex impedance plot for a fully charged sputtered-cathode cell (7000 Å) is given in Fig. I-1. The impedance plot confirms that the cell impedance is dominated by low-frequency transport effects. As a first step, an interfacial oxide layer (denoted layer number 2) between the bulk oxide (denoted layer number 1) and polymer layers was hypothesized as the source of the increase in transport impedance. The theoretical model describing the transport of lithium in each of the layers has two fitted parameters for each layer, a characteristic resistance and time. From earlier work, the electrolyte transport impedance was known to be small enough that it has little effect on the overall results.
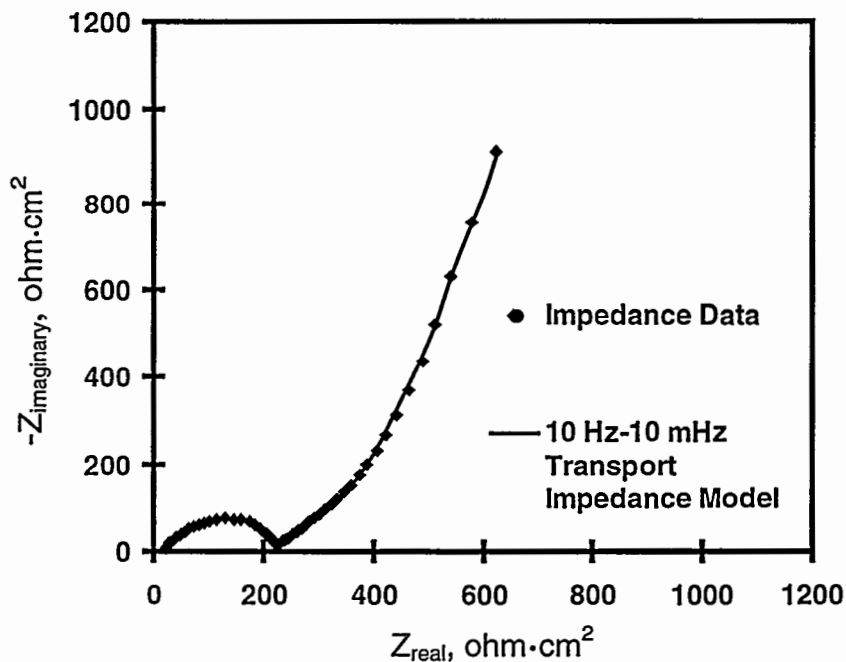
Fig. I-1. Complex Impedance Plot for Sputtered-V_2O_5 Cathode Cell. Cathode-layer thickness is 7000 Å.

A fitting routine was used to determine the characteristic resistance and time constant for the two layers from AC impedance data on a fully charged sputtered-cathode cell (7000 Å) taken every 10 cycles. A typical fit of the data is given in Fig. I-1. The change in characteristic resistance and time constant with cycling for the bulk and interfacial oxide layers is given in Fig. I-2. Clearly, the greatest values are associated with the interfacial layer, indicating that it is the primary source of the increased impedance with cycling.
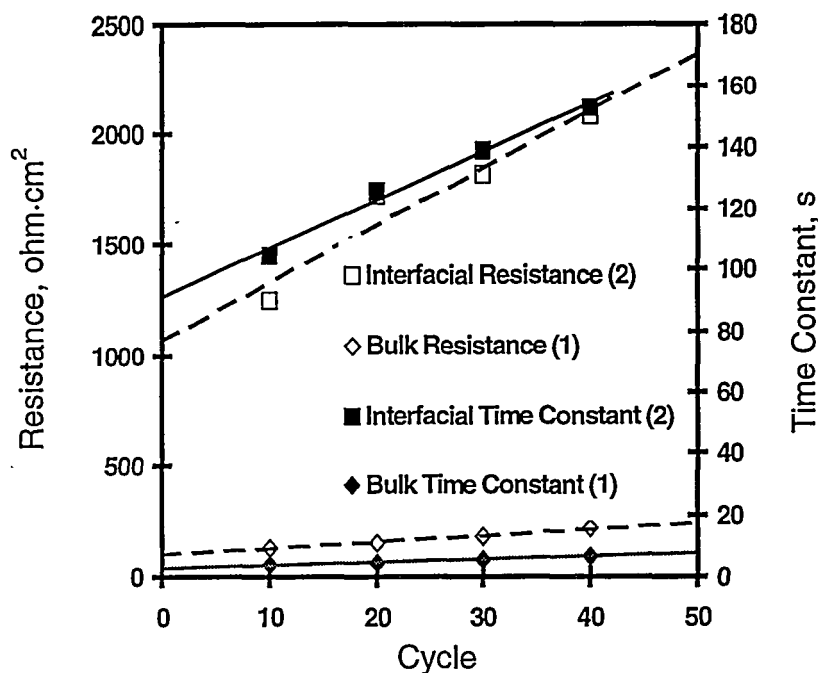
Fig. I-2. Time Constant and Characteristic Resistance
for Bulk and Interfacial Oxide Layers as
Function of Cycle Number

This analysis was further extended by utilizing the open-circuit voltage curve that was previously determined in another study. Table I-1 gives the thickness and the lithium diffusion coefficient that were calculated from the open-circuit voltage curve and the characteristic resistances and time constants. The agreement between the last column in the table

Table I-1. Diffusion Coefficient (D) and Thickness (L) of Interfacial and Bulk Oxide Layers from AC Impedance Data on 7000 Å Sputtered-Cathode Cell. The numbers (1) and (2) indicate bulk and interfacial oxide layers, respectively.

Cycle Number	L(1), Å	D(1), cm²/s	L(2), Å	D(2), cm²/s	L(1)+L(2), Å
10	1784	8.1×10^{-11}	4891	2.3×10^{-11}	6675
20	1267	3.9×10^{-11}	3313	8.7×10^{-12}	4580
30	1825	6.2×10^{-11}	4500	1.5×10^{-11}	6325
40	1773	4.7×10^{-11}	4173	1.1×10^{-11}	5946

and the known thickness of the oxide layer (7000 Å) is a strong indicator that the interfacial layer is indeed part of the oxide layer. The lower lithium diffusion coefficient of the interfacial layer is indicative of the damage done to the oxide by cycling.

These studies are now being expanded to other oxides to examine the effect of cycling on the transport of lithium in the structure.

2. Lithium Battery Electrode Materials

The objective of this effort is development of new electrode materials for lithium batteries. Work this past year focused on α-MnO$_2$ and Li$_x$V$_3$O$_8$ materials.

a. Structural and Electrochemical Studies of α-MnO$_2$

Manganese oxides are of interest as insertion electrodes for primary and secondary lithium batteries.[1] For example, heat-treated γ-MnO$_2$ electrodes are used in commercial 3-V primary cells, electrodes consisting of an intergrowth structure of lithiated γ-MnO$_2$ and spinel-related MnO$_2$ are used in commercial 3-V rechargeable cells, and the spinel system Li$_x$[Mn$_2$]O$_4$ (0<x<1) is being developed for 4-V rechargeable lithium cells. Manganese oxides are also of interest for lithium-polymer electrolyte cells. The rechargeability of 3-V manganese oxides tends to be limited by the anisotropic expansion and contraction of the crystallographic unit cell when lithium is inserted into, and removed from, γ-MnO$_2$ or spinel-related electrode structures. Crystallographic distortions in lithiated manganese oxides can be attributed largely to a Jahn-Teller effect, when the concentration of Mn^{3+} ions within the oxygen array reaches a critical value, typically when the mean oxidation state of manganese falls below 3.5.[2]

There are alternative 3-V lithium-manganese-oxide electrodes, such as the intergrowth structure of lithiated γ-MnO$_2$ and spinel-related MnO$_2$, which offer significantly superior electrochemical cycling compared with the 3-V Li$_x$[Mn$_2$]O$_4$ spinel electrode; however, improved performance of the 3-V MnO$_2$ electrodes is still needed in terms of both electrode capacity and cycling stability. A potentially attractive alternative material for 3-V rechargeable lithium battery systems is α-MnO$_2$.[3] Other workers[4-5] have already demonstrated that a highly pure and crystalline α-MnO$_2$ product can be synthesized by a simple acid digestion of Mn$_2$O$_3$. Also, X-ray and neutron diffraction studies have shown that this α-MnO$_2$ product is devoid of any "stabilizing" cation or molecule, other than H$_3$O$^+$ or H$_2$O within the (2 x 2) tunnel.[6] The

[1] M. M. Thackeray, M. H. Rossouw, A. de Kock, A. P. de la Harpe, R. J. Gummow, K. Pearce, and D. C. Liles, *J. Power Sources* **43-44**, 289 (1993).

[2] R. J. Gummow, A. de Kock, and M. M. Thackeray, *Solid State Ionics* **69**, 59 (1994).

[3] M. A. Humbert, P. Biensan, M. Broussely, A. Lecerf, A. Dollé, and H. Ladhilly, *J. Power Sources* **43-44**, 681 (1993).

[4] J. Brenet, *J. Power Sources* **39**, 349 (1992).

[5] M. H. Rossouw, D. C. Liles, and M. M. Thackeray, *Prog. Batteries & Bat. Mater.* **15**, 8 (1996).

[6] M. H. Rossouw, D. C. Liles, M. M. Thackeray, W. I. F. David, and S. Hull, *Mater. Res. Bull.* **27**, 221 (1992).

electrochemical properties of dehydrated α-MnO$_2$ electrode materials, however, are disappointing; the electrodes provide capacities of only 120 mAh/g after 20 cycles.

At ANL we have replaced the water component in α-MnO$_2$·nH$_2$O materials with lithia (Li$_2$O) to fabricate "lithia-stabilized" electrodes that show significantly superior electrochemical properties to the parent α-MnO$_2$ material.

The structures of hydrated, dehydrated, and lithia-stabilized α-MnO$_2$ samples were determined by using the Rietveld profile refinement technique combined with time-of-flight neutron-diffraction data collected at the ANL Intense Pulsed Neutron Source. As shown in Fig. I-3, water molecules in α-MnO$_2$·nH$_2$O products reside in the (2 x 2) channels of the structure, with the oxygen ions from the water being located at the (0.0, 0.0, 0.48) position, which is close to the position normally occupied by "stabilizing" cations such as K$^+$ in cryptomelane (KMn$_8$O$_{16}$). The water can be entirely removed from α-MnO$_2$ without structural collapse; this α-MnO$_2$ framework is stable to at least 300°C.
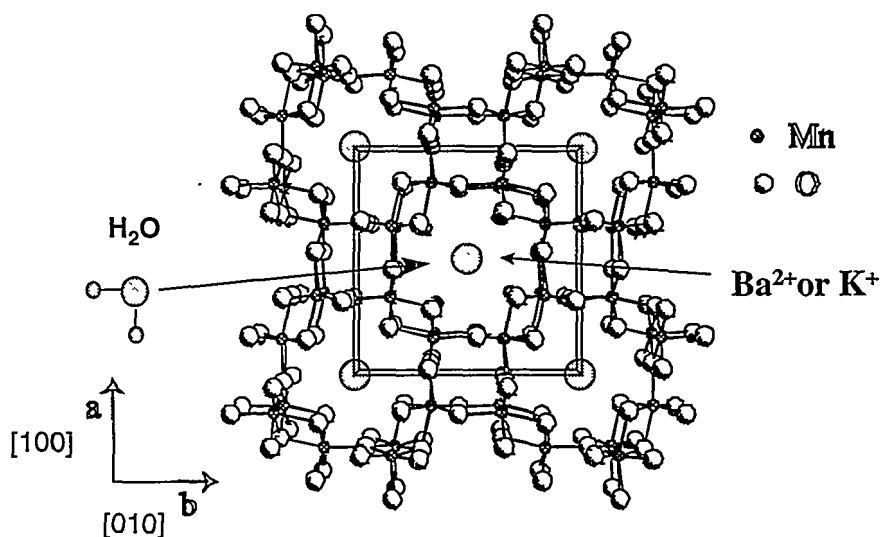
Fig. I-3. Structure of α-MnO$_2$

The structure of a lithia-stabilized α-MnO$_2$ sample of composition 0.15Li$_2$O·MnO$_2$ is depicted in Fig. I-4. A difference Fourier map provided evidence that the oxygen ions from the Li$_2$O molecule were located at (0.0, 0.0, 0.40), close to the position that was occupied by the oxygen ion of the H$_2$O molecule in the hydrated compound. Interatomic Li-O distances showed that the lithium ions were coordinated more strongly to the oxygens of the framework structure than to the oxygens in the (2 x 2) tunnels. If an oxygen ion completely occupied the site at (0.0, 0.0, 0.5), then a distorted hexagonal-close packed oxygen array would result, similar to that found in γ-MnO$_2$ structures. These data, therefore, demonstrate that lithia stabilizes α-MnO$_2$ structures with (1) oxygen-occupying sites in the defect oxygen array of the α-MnO$_2$ framework and (2) the charge-compensating lithium ions occupying newly created interstitial sites.
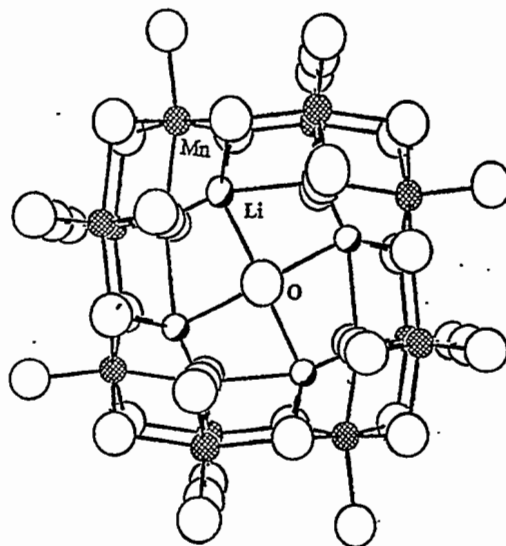
Fig. I-4. Structure of $0.15Li_2O \cdot MnO_2$

Our analysis also showed that the volume of the unit cell of α-MnO_2 increases significantly (3.27%) when stabilized by Li_2O. In addition, the unit cell volume expands by an additional 4.58% when 0.26 Li is inserted into $0.15Li_2O \cdot MnO_2$, either electrochemically or chemically, by reaction with n-butyl lithium at room temperature. The volume expansion occurs predominantly because of an increase in the *a* (and *b)* lattice parameter of the tetragonal unit cell, while the *c* parameter, which reflects an O-O distance, remains effectively constant. From crystallographic symmetry, we expect that the Jahn-Teller distortion which occurs when the average manganese oxidation state reaches 3.5 will be accommodated in tetragonal α-MnO_2 materials in two dimensions, rather than in one dimension, as is the case in the spinel system $Li_x[Mn_2]O_4$, which undergoes a cubic-tetragonal distortion when x exceeds 1.[7] This observation has implications for designing improved manganese oxide materials that will be more tolerant to lithium insertion and extraction reactions, particularly for rechargeable 3-V lithium cells.

We also prepared Li/α-MnO_2 coin-sized cells and galvanostatically cycled them at 0.1 mA between 3.8 and 2.0 V. The initial discharge capacity delivered by the Li/α-MnO_2 cell was 218 mAh/g. The capacity on the second cycle was 157 mAh/g, reflecting a significant capacity loss (28%). On continued cycling, capacity was lost slowly and steadily, yielding 136 mAh/g after 10 cycles. This performance represents a capacity loss of approximately 4% per cycle. By contrast, lithia-stabilized electrodes showed a significant increase in capacity and improvement in capacity retention on cycling; the cells delivered an initial discharge capacity of 222 mAh/g and 204 mAh/g after 20 cycles, reflecting a capacity loss of only 0.4% per cycle. Furthermore, Li/$0.15Li_2O \cdot MnO_2$ cells showed excellent coulombic efficiency (98.9%) when discharged and charged over the same voltage range and at the same current (0.1 mA). Continued improvement of cells with α-MnO_2 electrodes will be sought.

---

[7]   M. M. Thackeray, W. I. F. David, and J. B. Goodenough, *Mater. Res. Bull.* **17,** 785 (1982).

b.   Structural Studies of Vanadium Oxide Insertion Electrodes

Among the desired properties of transition-metal oxide insertion electrodes for lithium batteries are high capacity, which is related to the extent to which lithium can be accommodated by a host structure, and long cycle life, which is related to structural stability upon lithium-ion insertion and extraction. A detailed characterization of atomic structure and phase stability as a function of lithium-ion insertion is a valuable complement to electrochemical measurements for assessing the capabilities of a candidate electrode material, as well as for suggesting strategies for improving the materials. It is frequently difficult, however, to obtain a comprehensive characterization of atomic structure by experiment alone. Computational theory is a valuable additional tool for elucidating structural issues. Different levels of computational theory may be considered, ranging from molecular dynamics to semi-empirical tight-binding to *ab initio* methods. Implementation of local density functional theory is of considerable interest, since it is the most rigorous treatment currently feasible.

Monoclinic $Li_xV_3O_8$ has a layered structure and is of interest as an electrode for 2.5- to 3.0-V lithium batteries. We thus calculated the structure and electrochemical potential of $Li_xV_3O_8$ with local density functional theory and plane-wave-pseudopotential methods. Special attention was given to the compositions near $x = 1.2$ and $x = 4$, for which X-ray diffraction structure refinements are available.[8] The location of the tetrahedrally coordinated lithium ions in the calculated low-energy configuration for $x = 1.5$ (designated the α-phase) is consistent with the structure measured by X-ray diffraction for $x = 1.2$. The calculated low-energy configuration for $x = 4$ (designated the β-phase) is consistent with the three lithium sites identified in X-ray diffraction measurements and can be used to predict the position of the fourth unobserved lithium ion.

vacancy site	ΔE (eV)
Li(3)	0.33
Li(2)	0.37
So(2)	0.00
So(1)	0.27
Li(1)	0.44
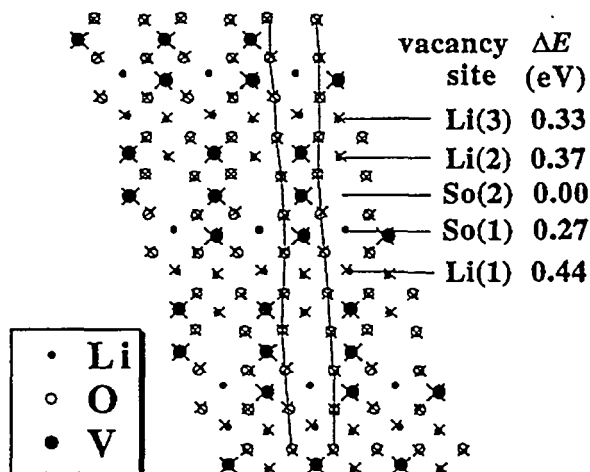
Fig. I-5.

Calculated (open and filled circles) and Experimentally Determined (crosses) Atomic Positions in (010) Layer of $Li_4V_3O_8$ with Vacancy at So(2). The calculated energies for other possible lithium vacancy locations are indicated. Vertical rows of oxygen bend toward vanadium trimers and away from lithium dimers.

---

[8]   L. A. de Picciotto, K. T. Adendorff, D. C. Liles, and M. M. Thackeray, *Solid State Ionics* **62**, 297 (1993).

Figure I-5 superimposes theoretically predicted (circles) and experimentally determined (crosses) coordinates in a single (010) layer of $Li_4V_3O_8$. The root-mean-square (rms) deviation between theoretical and experimental positions is very low, about 0.15 Å. An important qualitative feature of the structure is the curvature of the rows of oxygen, which reflects the stronger bonding to the vanadium than to lithium. Calculations were also performed for the α- and β-monoclinic phases at intermediate compositions, for which no structural information is available from experiment. Calculations at these compositions were based on hypothetical lithium configurations suggested by the ordering of octahedral-site vacancy energies for $Li_4V_3O_8$ (β) and tetrahedral site energies in $Li_{1.5}V_3O_8$ (α). The internal energy curves for the two phases were determined to cross near $x = 3$, in good agreement with electrochemical data.[9] Predicted electrochemical potential curves have been shown to agree reasonably well with experiment. Structural studies of vanadium oxide insertion electrodes will continue into the next year.

3. *High-Power Energy Storage System*

In 1993 the Partnership for a New Generation of Vehicles (PNGV) established a research program between the U.S. government and the U.S. Council for Automotive Research (which represents Chrysler Corp., Ford Motor Co., and General Motors Corp.) with the objective of developing the next generation of automobiles. This passenger car will achieve up to 80 mpg (34 km/L); have negligible environmental emissions and long range; and be safe, fuel efficient, and capable of running on alternative fuels. The PNGV program goal is the development of a production prototype of a six-passenger sedan in the year 2004. It is unlikely that one power system alone will be capable of meeting such a demanding goal, but a hybrid system could. We believe that the best hybrid vehicle will incorporate a fuel cell coupled with an energy-storage device having high-power capability.

The high-power energy storage device is the subject of this work. We are investigating the concept of integrating the galvanic properties of battery "insertion" electrodes and the geometric high surface areas of supercapacitors to engineer a device, referred to hereafter as a "galvanic stack," that would meet the power and energy requirements of a hybrid electric vehicle. A hybrid system made from the combination of a fuel cell and a galvanic stack can provide the power and energy characteristics that are required without sacrificing the energy density, cycle life, and overall cost of the system. The galvanic stack should have high power capability (1-5 kW/kg) and very good specific energy (15-22 Wh/kg) and should be able to rapidly store and release large quantities of energy over hundreds of thousands of cycles.

We are developing a lithium-ion-based galvanic stack as the high-power energy source. The approach is based on transition metal oxide electrodes, which have the capability of accommodating a significant amount of lithium within the host electrode structure. Lithium insertion and extraction reactions are accompanied by the galvanic reduction and oxidation of the metal cations within the host. By restricting to shallow limits of charge and discharge, the

---

[9] K. West, B. Zachau-Christiansen, S. Skaarup, Y. Saidi, J. Barker, I. I. Olsen, R. Pynenburg, and R. Koksbang, *J. Electrochem. Soc.* **143**, 820 (1996).

structural integrity of the electrodes is maintained. This results in high cycle life and permits energy recovery during regenerative braking. Initial cell data look very promising; indications are that a specific energy of 15-22 Wh/kg can be obtained with a life of hundreds of thousands of cycles.

Safety is a key concern for the galvanic stack due to its very large power-to-energy ratio, on the order of 100:1. Such a high power demand necessitates a system that is inherently safe. Consideration has been given to the present "state-of-the-art" lithium-ion technology, which consists of a negative electrode of lithiated carbon/graphite, a positive electrode of transition metal-doped lithium cobalt oxide, and an electrolyte of lithium salt in an organic solvent. However, this system has several areas of concern with regard to safety during high power pulses. Namely, carbon/graphite intercalates lithium at approximately 100 mV (vs. lithium metal), and under high power charge pulses, the negative electrode can be polarized to the extent that lithium metal forms. If the thermal management system fails or is inadequate, this lithium could create a hazardous catastrophic failure by reacting with the electrolyte or positive electrode.

The present graphite/carbon-based system also suffers from a lack of end-of-charge indicator in the voltage profile, as can be seen in Fig. I-6, which is a comparison of a graphite electrode and a $Li_4Ti_5O_{12}$ electrode, both against a $LiCoO_2$ positive electrode. Thus, overcharging with the graphite electrode is more likely because of uncertainty regarding the true state of charge. This could result in damaging structural effects at the positive electrode, such as oxygen release. (Severe overcharging is an even more dangerous situation due to the presence of lithium metal and free oxygen.)
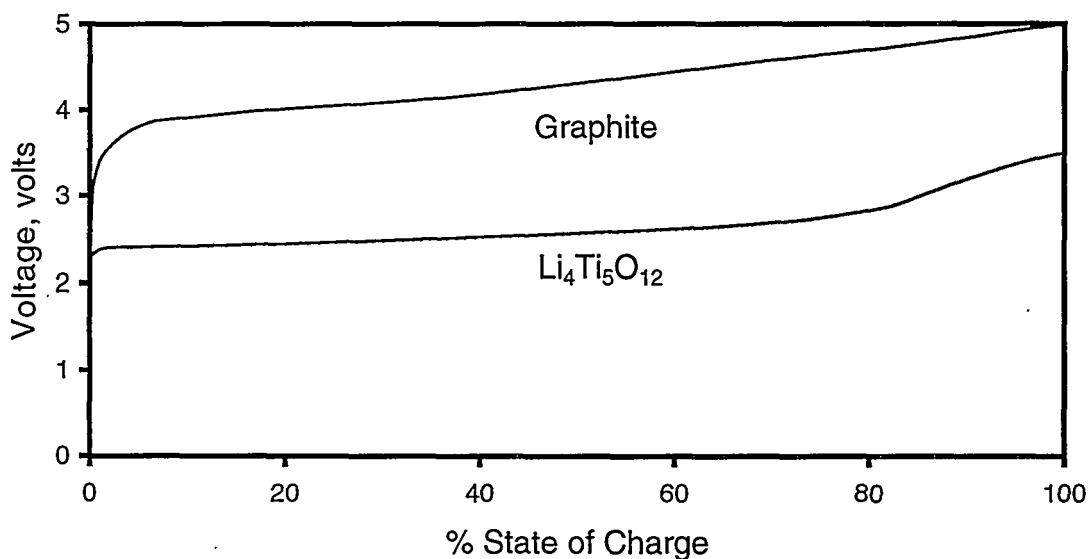
Fig. I-6. Voltage Profiles for Graphite and $Li_4Ti_5O_{12}$ Negative Electrodes. Determined in cells with $LiCoO_2$ positive electrodes.

Our approach to solving these safety/life problems is to replace the graphite/carbon negative electrode with an electrode that exhibits stronger two-phase behavior further away from lithium potential. Characteristic of a two-phase electrochemical reaction is a flat voltage

response. A distinct change in voltage is evident as one phase becomes depleted, thus providing an end-of-charge indicator (see Fig. I-6). The $Li_4Ti_5O_{12} \leftrightarrow Li_7Ti_5O_{12}$ reaction was thus found to be an attractive candidate as the negative electrode because of its two-phase electrochemical reaction and 1.55 V plateau (vs. lithium metal).

Initial efforts have been devoted to testing the $Li_4Ti_5O_{12}/LiCoO_2$ cell couple in small button-sized cell assemblies. Testing followed the 100-Wh Life Cycle Test Profile defined by PNGV. Each life cycle is 60-s long and consists of a 9-s discharge pulse, followed by an 18-s rest, followed by a 10-s charge pulse, and then followed by a 23-s slow charge to make the capacity slightly charge neutral. The life-cycle requirement with this profile is 50,000 cycles for a fast response engine and 120,000 cycles for a slow response engine.

In keeping with the 4:3 ratio in voltage limits (mandated by the PNGV), the $Li_4Ti_5O_{12}/LiCoO_2$ cell couple was operated between 2.7 and 2.0 V, with an open-circuit voltage slightly below 2.4 V at 50% state of charge. The cells have achieved excellent voltage stability over 112,000 life cycles to date (test ongoing). The cell cost would decrease if much of the cobalt in $LiCoO_2$ were replaced with nickel. Such substitution would have little effect on the voltage window and theoretical capacity.

We have developed a conceptual design of a 400-V galvanic stack based on the $Li_4Ti_5O_{12}/LiNi_{0.82}Co_{0.18}O_2$ system. The stack units consist of 144 spiral wound cells divided into eight modules of 18 cells enclosed in a thermally controlled jacket (Fig. I-7). (Other configurations can be utilized depending on the available space in the hybrid vehicle.) The cells
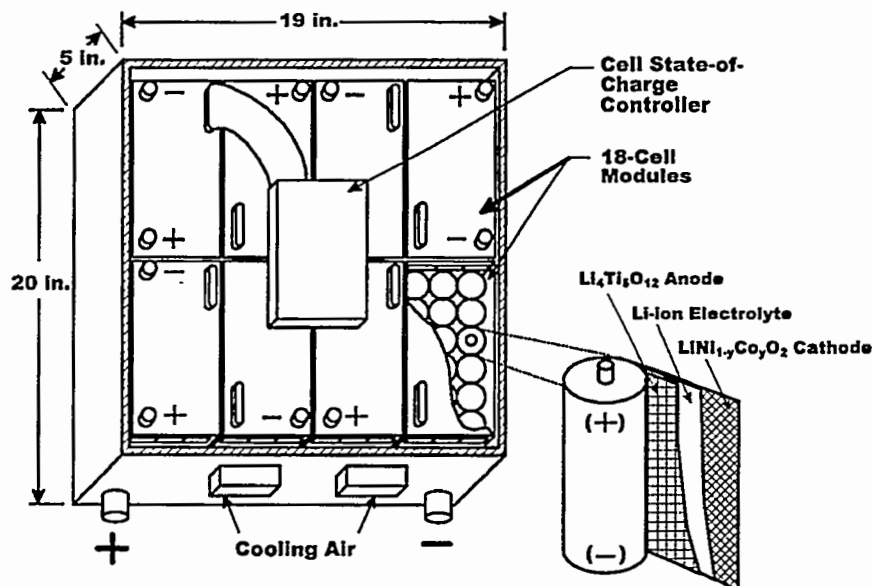
Fig. I-7. Design of Galvanic Stack for Fuel-Cell Powered
Vehicle. Cylindrical wound-cell design will be used
for initial developmental efforts.

are cooled by air blown through finned intercell connectors, which provides cooling directly to the cell terminals. A modeling program developed at ANL, which is part of a Microsoft Excel spreadsheet, was used to calculate the energy, power, weight, volume, and cooling system parameters for components and the entire system. From this modeling work, we determined that this cell couple would meet the performance goals stated by the PNGV.

To simplify the preliminary design of the galvanic stack, we assumed that the electrodes and separator materials are wound to form a $Li_4Ti_5O_{12}/LiNi_{0.82}Co_{0.18}O_2$ cylindrical cell. Considerable savings in volume (and weight) may be realized by considering flat-wound cell designs and also hexagonal packing within the module. The area specific impedance for this cell was assumed to be 9 Ω-cm^2 in the spreadsheet calculations. However, the present $Li_4Ti_5O_{12}/LiCoO_2$ cells have an area specific impedance that was measured to be approximately three times this value (30 Ω-cm^2). The bulk of the future effort in this work will be devoted to reducing the area specific impedance to the required value as predicted by the spreadsheet model (9 Ω-cm^2).

Ongoing and future efforts to develop a high-power galvanic stack that is safe will be focused in three general areas. First, following the encouraging performance obtained from the $Li_4Ti_5O_{12}/LiCoO_2$ system and results from the modeling studies, we plan to continue the study of "galvanic supercapacitors" in an attempt to optimize the preparation and performance of the electrode materials, as well as cell design and construction. Second, fundamental modeling will be used to determine the concentration, current, and potential distributions developed inside lithium-ion cells under PNGV testing regimes. Third, safety-related issues will be identified by measurement of thermal effects in small cells by means of electrochemical calorimetry studies.

B. Electrochemical Analysis and Diagnostics Laboratory

The Electrochemical Analysis and Diagnostics Laboratory (EADL) was established at ANL to study advanced battery systems for applications such as electric vehicles and utility load management. The facilities include a test laboratory to conduct battery experimental evaluations under simulated application conditions. Evaluations are performed for DOE, the Electric Power Research Institute, the U.S. Advanced Battery Consortium (USABC), and others to provide insight into those factors that limit the performance and life of advanced battery systems. The results of these evaluations help identify the most promising R&D approaches for overcoming these limitations and provide battery users, developers, and program managers with a measure of the progress being made in battery R&D programs, a comparison of battery technologies, and basic data for modeling.

1. Performance and Life Evaluations

Performance and life evaluations in the EADL were continued under a CRADA with the Advanced Battery Consortium. The tasks under the original CRADA (initiated in the last quarter of 1992) were completed in December 1997. A second CRADA having an increased scope of work was started in March 1997. The first CRADA focused on (1) testing of nickel/metal-

hydride (Ni/MH) modules from an Advanced Battery Consortium contract with Ovonic Battery Co. and (2) a study to assess the suitability of modules that have reached the end of their electric-vehicle battery lives for other applications, such as standby power, uninterruptible power sources, utility load management, and commercial/industrial vehicles such as golf carts and fork lift trucks. Activities under the second CRADA included evaluation of Ni/MH cells and modules from USABC battery cost reduction contracts with GM-Ovonics (GMO) and SAFT (France). The EADL has also assisted 3M Corp. and Hydro-Québec by providing additional cell and module testing and characterization efforts to their lithium-polymer battery development program with the USABC. The results of these tests and analyses will be released by the USABC at a later date.

Also completed during this past year was the evaluation of an electric-vehicle battery pack from Chrysler Corp. (constructed with Ovonic Ni/MH modules). This study was started under Chrysler sponsorship but was later funded by DOE because the battery exceeded initial life estimates. Also initiated during 1997 was a study for DOE to assess the technical status of foreign electric-vehicle batteries. This study started with the testing of two Ni/MH modules from Yuasa Corp. (Japan) under the guidance of their U.S. partner, Exide Battery Corp. In addition, leasing and data disclosure agreements are also being prepared with AEG (Germany) and Matsushita Battery Industrial Co. and Panasonic EV Energy Co. to evaluate their sodium/nickel-chloride "Zebra" battery and Ni/MH electric-vehicle modules, respectively. The results of these tests and analyses will be released by DOE at a later date.

Besides performance and lifetime evaluations, Argonne has supported the Advanced Battery Consortium by having representatives on the Ovonic Nickel/Metal-Hydride Working Group and the Battery Testing Procedures Tiger Team. Argonne has also participated in USABC battery readiness review meetings to verify proper test planning, instrumentation, and data acquisition before the start of unique tests.

In 1998, evaluations will be continued for the Advanced Battery Consortium's GMO and SAFT Battery Cost Reduction Programs, and the lithium-polymer battery development program of 3M Corp. and Hydro-Québec. The study to assess foreign electric-vehicle battery technologies for the DOE will also be continued.

2. Post-Test Analysis

A number of Ovonic Ni/MH cells underwent post-test analyses after life evaluations in the EADL. This activity was sponsored by the Advanced Battery Consortium to assist Ovonic staff in identifying and focusing their resources on critical design issues facing their technology. On occasion, the post-test analyses performed at ANL have involved the active participation of Ovonic researchers. These activities have declined, and our post-test analysis laboratory has been closed since the evaluation of Ovonic modules has been completed.

Examinations were also completed for Commonwealth Edison Co. and Duke Power on circular lead-acid cells used for standby power requirements at their nuclear generating stations. These cells had exhibited an abrupt capacity loss, which caused the power station to fail its

periodic standby power test. Argonne was asked to identify the root cause(s) for this capacity loss. The results of these examinations revealed a grid corrosion problem that led to a high internal cell resistance and reduced capacity.

C.   Fuel Cell Research and Development

Fuel cells convert chemical energy directly into electricity by electrochemical reaction mechanisms, eliminating the need for heat engines and rotating machinery. Since such systems have very low environmental emissions and offer high efficiencies, interest in their application continues to grow. In the past year, several automotive companies have made major commitments to develop fuel cells as the prime power source for electric vehicles.

The CMT Division continues to address the fuel processing issues related to development of fuel cell systems for transport applications. We are also modeling these systems in close cooperation with the automotive users. Our research on a low-temperature solid oxide fuel cell for the transportation application was terminated by the sponsor, because it was viewed as too long range. In support of the developers of fuel cell systems for stationary power plants, we are fine-tuning the composition of an alternative cathode material for molten carbonate fuel cells and are exploring new electrolytes to improve long-term performance. In addition to these laboratory activities, we are participating in several national and international committees: the polymer electrolyte and solid oxide fuel cell annexes of the International Energy Agency; the Russian-American Fuel Cell Consortium, which has the primary purpose of helping the Russian nuclear weapons laboratories become engaged in civilian R&D; and the Information Exchange Program with the Japanese energy development agency.

1.   Transportation Applications

Vehicles powered by fuel-cell propulsion systems offer superior fuel economy, very low to zero pollutant emissions, and the option to operate on alternative and/or renewable fuels (e.g., methanol). To aid the development of fuel cells for transportation applications, we are developing methods that will convert conventional and alternative automotive fuels into hydrogen and will remove carbon monoxide contaminant from the reformate gases. We are also modeling fuel cell systems under various modes of operation.

a.   Fuel Reforming

Because conventional fuel cells run on hydrogen, liquid fuels must be converted to hydrogen on-board the vehicle in real time to meet the fluctuating power demands of the drive train. We have been investigating catalytic partial-oxidation reforming for the generation of hydrogen from conventional (gasoline and diesel) and alternative (methanol, ethanol, propane, naphtha, and natural gas) automotive fuels for use in fuel cell-powered automobiles and other light-duty vehicles. Such fuel processors need to be compact, lightweight, efficient, and capable of rapid startup and good dynamic response to changing fuel processing rates.

For the partial-oxidation reforming of a generic hydrocarbon fuel, $C_nH_mO_p$, the idealized general reaction is

$$C_nH_mO_p + x(O_2+3.76N_2) + (2n-2x-p)H_2O \rightarrow nCO_2 + (2n-2x-p+m/2)H_2 + 3.76xN_2 \qquad (1)$$
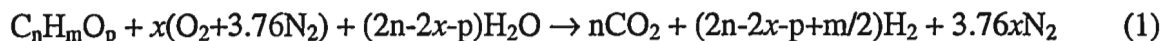
where x is the oxygen/fuel molar ratio. This reaction can be conducted most efficiently in a catalytic reactor because catalysts provide high conversions and product selectivity at relatively low temperatures. We set up a micro-reactor apparatus to test various materials for their ability to catalyze the desired reaction. The tests were conducted with oxygen rather than air as the oxidant to eliminate the dilution effects of nitrogen in the air. A number of catalytic materials, including Fischer-Tropsch-type catalysts, were tested for this purpose. The best performance, however, was obtained with a new class of materials that was developed in our laboratory. This new Argonne catalyst was tested with various individual hydrocarbons (iso-octane, toluene, 2-pentene, cyclohexane) to represent the different types of hydrocarbons (paraffins, aromatics, olefins, and naphthenics, respectively) present in typical gasolines. Methanol, ethanol, and natural gas—often considered as alternative fuels for transportation—were also tested.

Figure I-8 shows the effect of temperature on the composition of the product gas obtained using iso-octane as the fuel and the new catalyst material. For these experiments, the oxygen-to-fuel and the water-to-fuel molar ratios were set at 4 and 9, respectively. With increasing temperature, the unreacted iso-octane percentage decreases while the hydrogen percentage increases. At 630°C, the iso-octane is almost completely reacted, and the hydrogen concentration is over 60% (on a dry basis). For the reactant feed proportions used, the maximum hydrogen concentration achievable theoretically is 68.8%. Thus, the product gas contained 87%
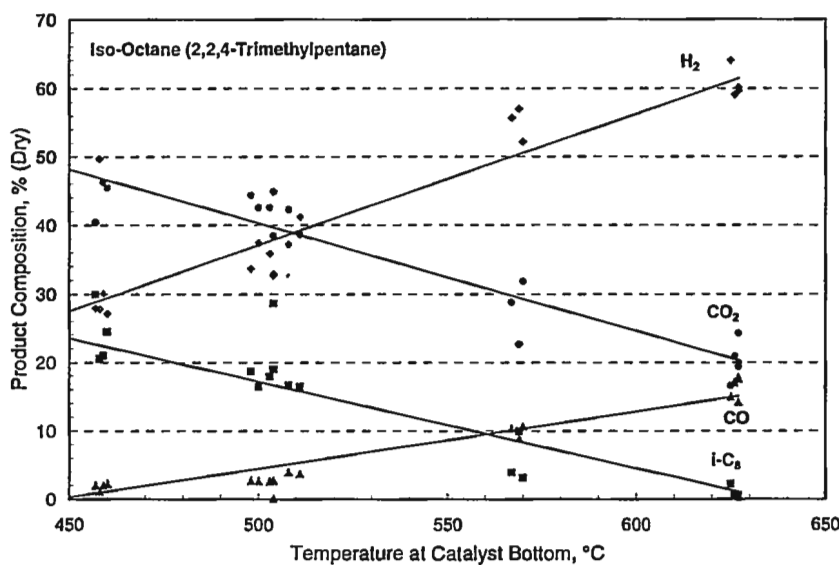
Fig. I-8. Product Gas Distribution Obtained from Partial-Oxidation Reforming of Iso-Octane with Novel Argonne Catalyst

of the hydrogen theoretically available. The remaining hydrogen would be produced by the conversion of carbon monoxide by the water-gas shift reaction:

$$CO + H_2O \rightarrow CO_2 + H_2 \tag{2}$$

The product gas distribution as a function of temperature was also determined for the partial-oxidation reforming of pipeline natural gas. The natural gas contained 93% methane, the balance being propane and butane. At 690°C, the unreacted methane was less than 0.5%, and the hydrogen concentration was 70%. The theoretical maximum at the experimental feed proportions ($O_2/CH_4 = 0.5$, $H_2O/CH_4 = 1.6$) is 75%. The catalyst did not show any deactivation after several days of operation—this is particularly significant because the natural gas contained a small amount of sulfur compounds (odorizer). Thus, the catalyst is resistant to sulfur poisoning. Similar high hydrogen concentrations were obtained from the other fuels tested with partial oxidation reforming.

As part of the development of a partial-oxidation catalyst, we tested the effect of crystal structure on the product distribution of the catalytic reforming process. A simple hydrocarbon, pentane, was used as the fuel, and the ratio of $C_5H_{12}:H_2O:O_2$ was fixed at 1:3:2.8. This ratio was selected to provide sufficient oxygen and water for the reaction:

$$C_5H_{12} + 3H_2O + 2.5O_2 \rightarrow 2CO + 3CO_2 + 9H_2 \tag{3}$$

We tested two catalyst materials with different crystal structures (proprietary). The concentrations of H_2, CO, and CO_2 in the product gas were comparable for the two catalysts in the temperature range of 700–750°C. The only difference between the two materials was the minimum temperature at which the pentane (C_5H_{12}) was completely converted. With the first catalyst, a complete conversion was achieved at 630°C; while the second catalyst required 675°C for complete conversion of the pentane. Studies of catalyst structure will continue.

b. Removal of Carbon Monoxide from Reformate

Because of their low operating temperatures, polymer electrolyte fuel cells are being targeted for the transportation application. For this fuel cell system, the fuel gas from the reformer must be cooled, humidified, and purified to obtain the best performance from the fuel cell stack. One of the major contaminants in the reformate is carbon monoxide, which must be reduced to less than 100 ppm to avoid significant degradation in fuel cell output. We are investigating a regenerable CO sorption process based on the complexing of CO with CuCl. This sorption process is based on the reversible complex formation and dissociation reactions between

CO and CuCl. Such a complex process may take several forms, as documented in the literature[10-13]:

$$2CO + 2H_2O + 2\ CuCl \leftrightarrow [Cu(CO)ClH_2O]_2 \tag{4}$$

$$CO + CuCl\ (sol) \leftrightarrow CuCl(CO)\ (sol) \tag{5}$$

$$CO + CuCl\ (aq\ HCl\ or\ KCl) \leftrightarrow Cu(CO)Cl\downarrow \tag{6}$$

$$CO + CuCl + 3X \leftrightarrow [Cu(X)_3CO]^+\ Cl^-,\ \text{where}\ X = NH_4Cl\ or\ NH_3\ (aq) \tag{7}$$

$$nCO + Cu^I\text{-}ZSM\text{-}5\ (zeolite) \leftrightarrow (ZSM\text{-}5)Cu(nCO),\ \text{where}\ n = 1\text{--}3 \tag{8}$$
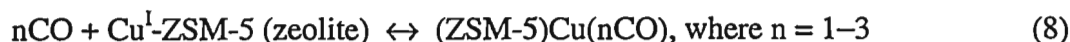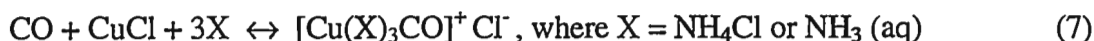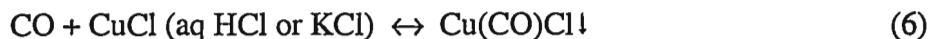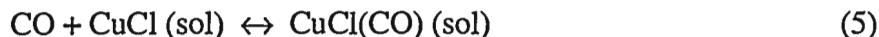
We have conducted two series of experiments to prove the concept. In the first series, a gas mixture containing 0.93% CO, 3.02% H_2O vapor, and balance N_2 was bubbled through an aqueous KCl or HCl solution that contained CuCl (Eq. 5). The experiment was carried out at room temperature and atmospheric pressure. Results of the experiment showed that CO was readily removed by CuCl in both KCl and HCl solutions, and that the solution was easily regenerated by passing N_2 through the solution. In the second series, CuCl was supported and dispersed on a porous, high-surface-area, solid substrate by wet impregnation followed by heat treatment. This sorbent was then tested for the CO uptake in a thermal-gravimetric apparatus with the test gas containing a range of CO concentrations (3.0 to 30.1 vol%) in N_2. As was observed in the solution tests, the solid sorbent also readily captured CO from the gas stream and was easily regenerated by N_2. The rates of CO sorption and desorption were relatively rapid and reproducible. Results of these two series of experiments demonstrate that this concept is valid.

During the past year, we also studied the CO sorption limitations of CuCl-impregnated sorbent (activated bauxite) as a function of the test-gas composition, CO concentration, and temperature. In these studies, the amount of CO taken up by the sorbent was found to depend on the chemical composition of the test gas to which the sorbent was exposed. In tests at room temperature and atmospheric pressure, the sorbent captured 97% more CO from a test gas containing 3% CO in N_2 than a simulated reformate test gas of 3% CO, 50.6% H_2, and 18.6% CO_2 (balance N_2). The sorbent readily captured H_2O vapor from the reformate test gas, and the amount of CO removed decreased with increasing H_2O vapor uptake by the sorbent. However, the after-test sorbent was reactivated by a subsequent heat treatment at temperatures greater than 150°C. The CO sorption capacity of the sorbent also increased with increasing

[10] N. V. Sidgwick, Ed., *The Chemical Elements and Their Compounds,* University Press, Amen House, London, Vol. I, pp. 131-132 (1950).

[11] Y. Xie, N. Bu, J. Liu, G. Yang, J. Qiu, N. Yang, and Y. Tang, "Adsorption for Use in the Separation of Carbon Monoxide and/or Unsaturated Hydrocarbons from Mixed Gases," U.S. Patent No. 4,917,711 (April 17, 1990).

[12] G. Spoto, A. Zecchina, S. Bordiga, G. Ricchiardi, G. Martra, G. Leafanti, and G. Petrini, *Appl. Catal. B: Environmental* **3**, 151-172 (1994).

[13] X. D. Peng, T. C. Golden, R. M. Pearlstein, and R. Pierantozzi, *Langmuir* **11**, 534-537 (1995).

concentrations of CO in the test gas, but the increase was not linearly proportional to the CO concentration. In contrast, the amount of CO sorbed decreased linearly with temperature from room temperature to 160°C, as shown in Fig. I-9. As indicated by the figure, CuCl loses its complexing capability with CO totally at 160°C. However, even at 100°C, the sorbent maintained 82% of its CO sorption capacity measured at the normal operating temperature (80°C) of the polymer electrolyte fuel cell. This finding indicates that, if thermal runaway of the upstream fuel processing system generates reformate at temperatures 80-100°C, then the CuCl-impregnated sorbent will still provide sufficient safeguard for the downstream fuel cell stack by effectively removing CO.
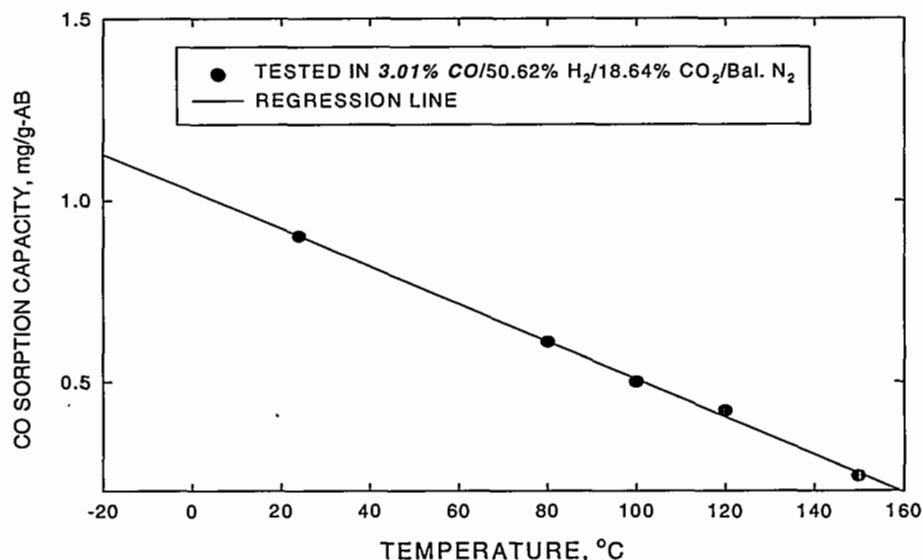
Fig. I-9. Carbon Monoxide Sorption Capacity as Function
of Temperature for CuCl-Impregnated Activated
Bauxite (AB)

Results of these studies show that the CuCl-impregnated sorbent possesses unique CO-sorption characteristics that make it potentially suitable for CO removal in light-duty vehicles. In future work, we will develop CuCl dispersion techniques on high-surface-area substrate to increase CO sorption/desorption rates and sorbent utilization. We will also develop methods to improve the sorbent resistance to water vapor in the reformate, investigate other potential chemical sorbents, and test this process with actual reformate from gasoline or alcohol reforming.

c.   Modeling and Systems Analyses

In this effort, we are developing computer simulations of various configurations of fuel cell systems for use in light-duty vehicles. The major activity is directed toward the design and analysis of polymer electrolyte fuel cell systems and components; alternative fuel cell systems and components are also modeled, as needed. The objectives are to determine (1) key design parameters and operating efficiencies and (2) the influence of component design on

startup and dynamic performance. We have developed a system design and analysis code (GCTool) that consists of component models (as C data structures), mathematical utilities, property utilities, and thermodynamic data. The code permits modeling of variable system configurations and is capable of performing parametric analyses, optimizations, and time integrations.

Work this year focused on analyses of hydrogen-fueled and gasoline-fueled vehicles operated on various driving schedules. Vehicle performance and equivalent fuel economy were determined for present-day and future vehicles. In these analyses, we worked closely with technical teams in the DOE Partnership for a New Generation of Vehicles: the Systems Analysis Team for fuel-cell system operation at design and partial load and for performance of warm and cold systems; the Vehicle Engineering Team for a packaging study taking into account component weights, volumes, flow rates, etc.; and the Fuel Cell Team for startup and dynamic performance on different driving schedules.

One example of such analyses is the drive-cycle performance that we conducted for hydrogen-fueled fuel cell vehicles. For this example, two vehicles were considered: an aluminum-intensive vehicle, the Mercury Sable (AIV Sable), and the P2000 vehicle, both from Ford Motor Co. The P2000 vehicle is lighter (1043 vs. 1491 kg) and has a lower drag coefficient (0.25 vs. 0.33) than the AIV Sable. The fuel economies for the two vehicles with 40- and 80-kW fuel cell systems were calculated for three driving schedules: the Federal Urban Driving Schedule (FUDS), a highway schedule, and a combination of the two. Results are given in Fig. I-10. For all three driving schedules, the P2000 vehicle showed the best fuel economy, and the two fuel cell systems did not appear to make much difference in fuel economy for each vehicle. In future work we will analyze the effect of system design variables on system efficiency.

2. Direct Methanol Polymer Electrolyte Fuel Cells

a. Anode Catalyst Development

Work is in progress to develop a polymer electrolyte fuel cell fueled directly by methanol. The direct methanol fuel cell (DMFC) is an attractive power source for portable, lightweight application (military or consumer electronics) due to the high energy density of methanol, the portability and ease of distribution of liquid rather than gaseous fuel, and elimination of the fuel reformer. One of the major obstacles impeding development of this power source is the low activity of the anode catalyst for methanol oxidation. We are developing improved anode catalysts using X-ray absorption spectroscopy, X-ray diffraction, and electrochemical studies. The following summarizes our electrochemical investigation of platinum-based catalysts for their methanol oxidation activity.

The platinum-based catalysts were in the form of small particles (1–10 nm), either unsupported or supported on carbon powder. The catalyst powders (see Table I-2) were mixed with a solubilized form of Nafion® to form an ink, which was applied to the polished face of a glassy-carbon rod. The catalyst was then tested for its ability to oxidize methanol in an aqueous
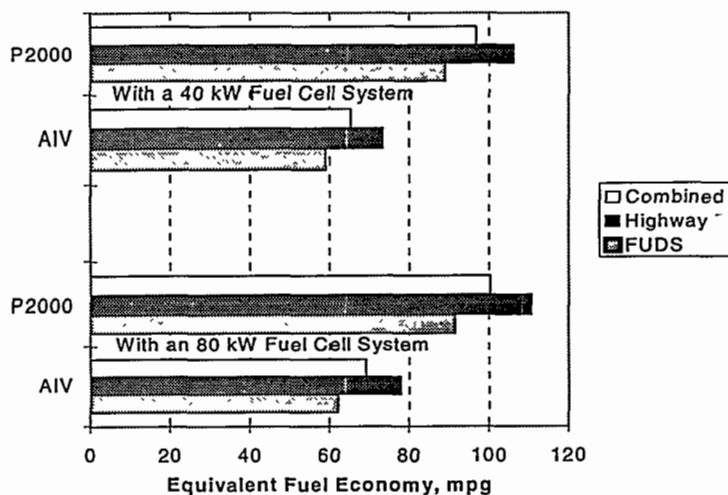
Fig. I-10. Fuel Economies (miles per gallon) Calculated for AIV Sable and P2000 Vehicles Powered by 40- and 80-kW Fuel Cell Systems

electrochemical cell with a platinum-wire counter electrode and a mercury/mercuric sulfate reference electrode.

Table I-2 gives the potentials at which methanol oxidation current was first observed during the anodic voltammetric scan. Some of the catalysts are listed twice to facilitate comparison. The first group of catalysts illustrates the effect of the addition of alloying metals to platinum, which are known to form oxide species at lower potentials than platinum. Both Ru and Os were found to lower the methanol oxidation potential as compared with pure platinum. As shown in the first and second groups in Table I-2, the catalyst with the lowest methanol oxidation potential is $Pt_{0.5}Ru_{0.5}$, with no effect of the support on the initiation potential. The third group of catalysts in Table I-2 illustrates the effect of increasing the Pt:Ru ratio in the unsupported catalysts. The methanol oxidation potential increased with decreasing fraction of ruthenium in the alloy. We found that Pt/Ru/Os alloys have lower initiation potentials for the methanol oxidation reaction than the mixed metal-metal oxide, $PtRuO_x$. No further work in this area is planned.

b. Modeling of Direct Methanol Fuel Cell

We are developing a comprehensive model of a polymer electrolyte-based DMFC. As part of that activity, an isothermal, steady-state model of the anode has been developed. This anode is considered to be a porous electrode consisting of an electronically conducting catalyst structure that is thinly coated with an ion-selective polymer electrolyte. The pores are filled with the aqueous feed solution of 2 $\underline{M}$ methanol. Four different species are transported in the anode: water, methanol, hydrogen ions, and carbon dioxide. In the model, four species move in the x-direction through the depth of the electrode. Species movement in the y-direction is taken into account for water, methanol, and carbon dioxide by use of an effective mass-transfer coefficient.

Table I-2. Platinum-Based Catalyst Powders Tested for Methanol Oxidation Electroactivity and Initial Potential for Methanol Oxidation

Catalyst Composition (mole ratio)	Carbon Support	Weight % Metal	Methanol Oxidation Potential,[a] V vs. RHE
Pt	yes	20	0.373
Pt/Ru (1:1)	yes	20	0.188
Pt/Os (8:2)	yes	20	0.237
Pt/Ru/Os (5:3:2)	yes	20	0.230
Pt/Ru (1:1)	yes	20	0.188
Pt/Ru (1:1)	yes	50	0.222
Pt/Ru (1:1)	yes	60	0.203
Pt/Ru (1:1)	yes	80	0.218
Pt/Ru (1:1)	no	100	0.189
Pt/Ru (1:1)	no	100	0.189
Pt/Ru (7:3)	no	100	0.201
Pt/Ru (9:1)	no	100	0.220
Pt Black	no	100	0.287
Pt/RuOx (1:1)	no	100	0.315

[a]All potentials were converted to the reversible hydrogen electrode (RHE) reference scale. Voltammetric scans were taken at 5 mV/s from 0 to 1.23 V in a quiescent 2 $\underline{M}$ methanol/0.5 $\underline{M}$ sulfuric acid solution.

The model predictions have been verified with experimental data, as shown in Fig. I-11. The experimental data were obtained from a polymer electrolyte membrane fuel cell operated with an aqueous methanol feed to the anode and hydrogen feed to the cathode; for this condition, the cathode is equivalent to a reversible hydrogen electrode after subtraction of the potential drop due to the membrane resistance. Therefore, the experimental data could be reasonably interpreted as the potential drop through the anode. The standard deviation of the model prediction from the observed data is only 4 mV up to a current density of 1 A/cm^2.

A sensitivity analysis was performed to identify the critical parameters affecting the anode performance. Kinetic limitations, the conductivity of the polymer electrolyte, and the anode thickness were found to be the key parameters affecting the performance of the anode in the typical operating range of 0.5–0.6 V.

This model can be used to design a liquid feed anode for the DMFC that yields optimal performance at a given set of operating conditions. The water concentration profile through the anode's polymer electrolyte can be used to predict dehydration. The model can also be used to calculate the amount of methanol crossover through the membrane, based on the predicted methanol concentration at the anode/membrane interface. In addition, the anode's volume fractions of polymer electrolyte and catalyst can be effectively varied with the knowledge that the potential drop through the anode is caused by kinetic and ohmic limitations but not mass-transfer effects. The model is being expanded to predict the performance of a complete polymer electrolyte fuel cell by including the membrane and cathode.
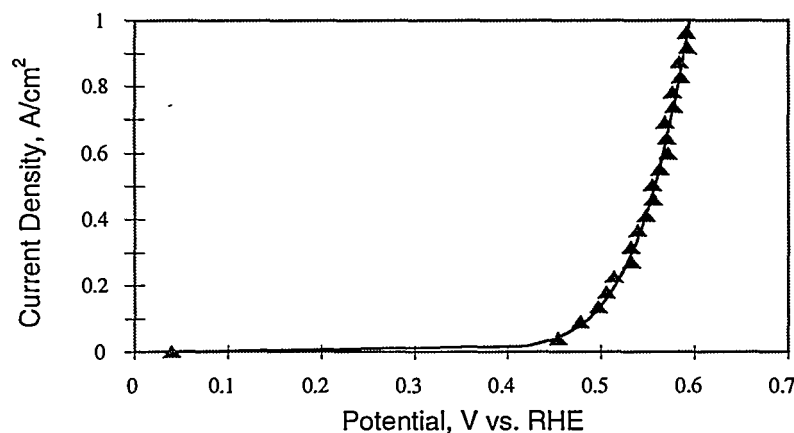
Fig. I-11.   Model Predictions (solid curve) and Experimental Data (triangles) for Performance of Direct Methanol Fuel Cell Having Polymer Electrolyte

3.   Molten Carbonate Fuel Cells

The CMT Division has a program on development of the molten carbonate fuel cell for utility applications, which offers the possibility of higher efficiency compared with other technologies. At present, the molten carbonate fuel cell consists of a porous nickel anode, a porous nickel oxide cathode, a semi-fluid $(Li,K)_2CO_3$ + $LiAlO_2$ electrolyte, and a metal bipolar plate. The operating temperature is 650°C. The molten carbonate fuel cell program is engaged in efforts to develop alternative cathodes, develop nonsegregating electrolytes, and improve the corrosion resistance of the cell components. The goal of these efforts is to extend cell life, increase power density, and decrease cost.

a.   Alternative Cathodes

In the present technology, lithiated NiO is used as the cathode. Over the lifetime of the cell, however, Ni^{2+} ions tend to transport to the anode, where they are reduced to metallic

nickel.[14] With increased CO_2 partial pressure, the nickel transport increases because of the increased solubility of NiO in the carbonate electrolyte. Although this process is slow in molten carbonate fuel cells operated at atmospheric pressure (100 kPa) and low CO_2 partial pressure (about 10 kPa), transport of nickel to the anode may be excessive at a higher pressure (about 300 kPa) and CO_2 partial pressure (about 30 kPa). This transport is expected to lead eventually to poor cell performance and/or short circuiting.

Several alternative-cathode compositions have been explored to reduce cathode solubility in the molten carbonate electrolyte. For example, $LiCoO_2$ has been studied extensively as a potential cathode material. The $LiCoO_2$ cathode has a low resistivity, about 1 $\Omega \cdot cm$ at the cell operating temperature of 650°C, and can be used as a direct substitute for NiO. However, the high material cost may prevent large-scale implementation.

We are developing advanced cathodes based on lithium ferrate ($LiFeO_2$), which is attractive because of its very low solubility in the molten $(Li,K)_2CO_3$ electrolyte.[15] In contrast to Co^{2+}, Fe^{2+} is not reduced at the anode. However, the $LiFeO_2$ cathode, because of its high resistivity (about 300 $\Omega \cdot cm$), cannot be employed as a direct substitute for the lithiated NiO cathode. A solid solution consisting of $LiFeO_2$, $LiCoO_2$, and NiO is expected to possess some properties of these materials. The $LiFeO_2$ will lower the solubility of the material in $(Li,K)_2CO_3$ electrolyte, and $LiCoO_2$ and NiO will lower the resistivity to an acceptable level (about 1 $\Omega \cdot cm$). Transport of nickel- and cobalt-containing species to the anode is also expected to decrease because of their lower activities in the cathode.

Using mixed oxide and the glycine-nitrate methods, we have prepared many compositions in the $LiFeO_2$-$LiCoO_2$-NiO system. They were characterized in terms of phase distribution and resistivity. The phase distribution data vs. composition are represented in the phase diagram shown in Fig. I-12, along with proposed solid-solution boundaries. Two regions of homogeneity are visible in Fig. I-12. One extends from the $LiCoO_2$ corner to about 12 mol% $LiFeO_2$ and about 6 mol% NiO. In this region, the materials crystallize with a layered, hexagonal crystal structure similar to that of $LiCoO_2$. A larger region of homogeneity extends from the $LiFeO_2$-NiO join to about 15–20 mol% $LiCoO_2$. Here, the materials crystallize with the rock-salt (NaCl) structure.

As expected, the resistivity of $LiFeO_2$ at the cell operating temperature (650°C) is lowered by solid-solution formation. The combination of a small amount of $LiCoO_2$ with $LiFeO_2$ lowers the resistivity of the solid solution much more than with a comparable amount of NiO. For example, incorporating about 6 mol% $LiCoO_2$ lowers the resistivity from 300 $\Omega \cdot cm$ to less than 10 $\Omega \cdot cm$, which is an order of magnitude lower than that of the binary with 6 mol% NiO. Indeed, in the high-$LiFeO_2$-containing ternary solutions, compositions were found with

---

[14] N.Q. Minh, *J. Power Sources* **24**, 1-19 (1988).

[15] D. Shores and Y. Qu, "Dissolution of Oxides in Molten Carbonates," Proc. Third Int. Symp. on Carbonate Fuel Cell Technology, 183rd Electrochem. Soc. Meeting, Honolulu, HI, May 16-21, 1993, Vol. 93-3, pp. 356-367 (1993).
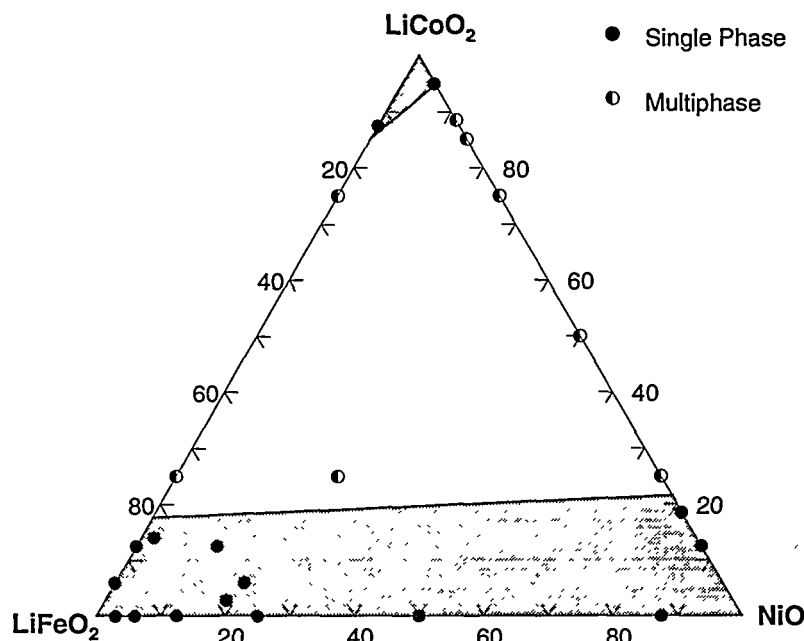
Fig. I-12. Phase Diagram for LiFeO₂-LiCoO₂-NiO Ternary System Showing Proposed Regions of Solid Solution

resistivities close to that of $LiCoO_2$; for example, 75 mol% $LiFeO_2$-12.5 mol% NiO-12.5 mol% $LiCoO_2$ has a resistivity of only 2.6 Ω·cm. In the future, cell tests are planned using the $LiFeO_2$-$LiCoO_2$-NiO materials. Here, the crucial issues are chemical stability in the molten carbonate electrolyte and electrochemical performance.

A potentially less-expensive method to fabricate cathode structures is to use Fe-Ni-Co alloy preforms. Here, the basic structure is formed by oxidizing and lithiating the alloy to form the final cathode composition. We determined that good phase formation with this alloy depended upon the particle size of iron metal. A heat-treatment study with 48.5% Fe-48.5% Ni-3% Co mixtures was also carried out to determine the optimal conditions to form the metal solid solution. These mixtures were heated at 650, 750, and 850°C for 4 h in 0.5% H_2/Ar atmosphere. X-ray diffraction analysis of all the heat-treated samples indicated the desired phase conversion to γ solid solution.

Heat treatment serves two functions: a mixture of Fe, Ni, and Co is converted to a metal solid solution, and a sintered metal preform is made. Diffusion also causes sintering, which decreases porosity in the cathode. An optimized heat-treatment process is being sought to maximize phase formation kinetics while maintaining a porous microstructure.

In addition to proper phase formation, microstructural development of the metal preform is important for cathode performance. A significant volume fraction of porosity is required for gas permeation and liquid-salt entrainment during operation of the molten carbonate fuel cell. To create more pores in the cathode, rice starch was added to the Fe-Ni-Co cathode materials (minus Li_2CO_3). The starch created pores when burned out during the sintering process.

Varying amounts of starch (up to 20 wt%) were added to the batches to study the effect on porosity. As can be seen from Fig. I-13, a monotonic density decrease was observed with increasing starch content. Further research will focus on obtaining a porous metal preform that can be lithiated.
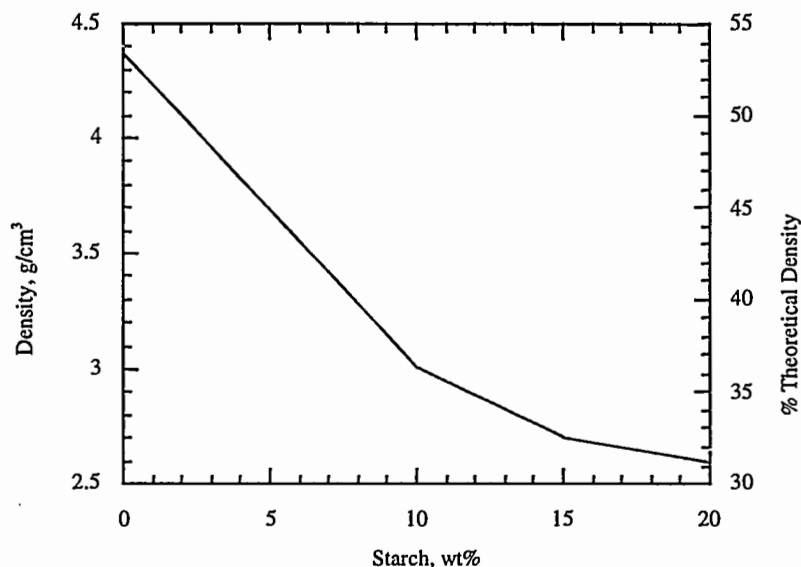
Fig. I-13. Density of 48.5% Fe-48.5% Ni-3% Co Metal Preforms as Function of Starch Content. All heat treatments were for 0.3 h at 750°C in a 0.5% H_2/Ar atmosphere.

b.   Nonsegregating Electrolytes

Electrolyte segregation has been reported[16] to occur within both the individual molten carbonate fuel cell and stack of cells. In the cell, the segregation increases the potassium concentration near the cathode, which, in turn, leads to increased cathode solubility and performance decline. In a stack of fuel cells, the high potential difference along the manifold gaskets causes electrolyte migration and cation segregation, which, in turn, lead to severe performance decline of the "end" cells.

We have screened electrolyte compositions for segregating behavior by using 12-cm-long strips that were wetted with carbonate and exposed to 5- to 20-V potential gradients. These conditions simulate the gasketing strip of an externally manifolded molten carbonate fuel cell. In our case, strips of carbonate-wetted $LiAlO_2$ were made from cold-pressed powders. The strip was purged with a 1:2 O_2:CO_2 gas mixture at 655°C. After 72 h at 20 V, the potential distribution in the strip reached equilibrium. The strips were quenched under load and later examined by metallography. These strips were sectioned for chemical analysis by inductively coupled plasma/atomic emission spectroscopy (ICP/AES). From the ICP/AES results, cation

---

[16] H. R. Kunz, *J. Electrochem. Soc.* **134**, 105 (1987).

ratios and electrolyte fill in each of the sections were calculated. The variation in cation composition vs. strip length was linear; therefore, these deviations were represented as a single cation separation value, or "segregation factor," given in units of mole percent per centimeter. The ICP/AES results are presented in a plot of electrolyte segregation factor vs. Li_2CO_3-Na_2CO_3 electrolyte composition (see Fig. I-14). The plot indicates that the nonsegregating range is 67-75 mol% Li_2CO_3. Surprisingly, the eutectic carbonate (52 mol% Li_2CO_3) displays the greatest cation segregation. Even on the sodium-rich side of the eutectic composition (40 mol% Li_2CO_3), the electrolyte exhibits lower cation segregation than does the eutectic.

Nominal mol% Li₂CO₃
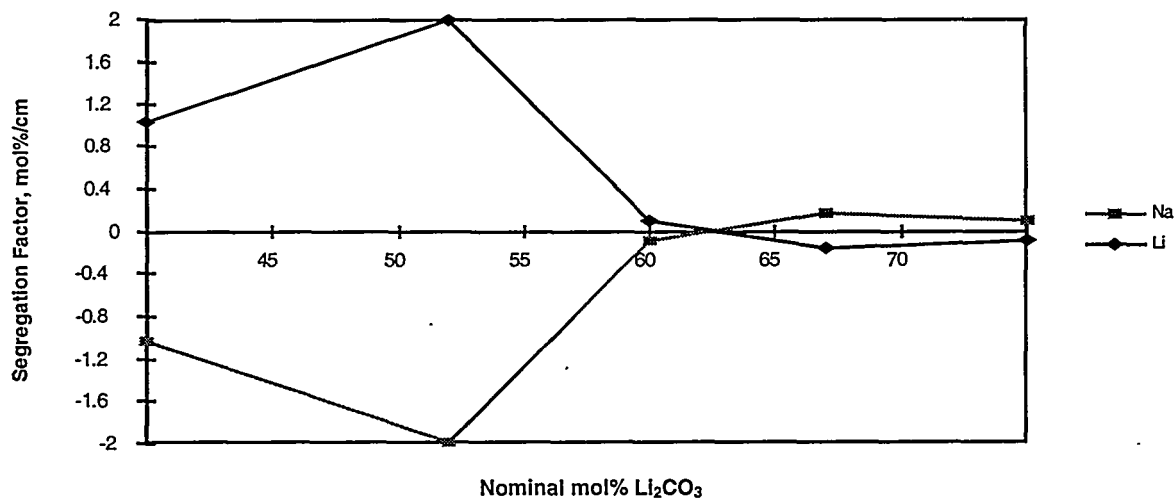
Fig. I-14. Segregation Factors versus Composition for Range of Li/Na Carbonate
Electrolytes Containing from 40 to 75 mol% Li_2CO_3

Performance data from bench-scale cells were used to compare the performance of Li_2CO_3-Na_2CO_3 electrolyte compositions. Data on cell impedance, cell voltage, and electrode performance at various utilizations and current density operations were collected as a function of time at 650°C and 1 atm with laboratory standard oxidant (air + 28% CO_2) and humidified fuel (80% H_2 + CO_2). Figure I-15 shows the polarization curves for bench-scale cells with six electrolyte compositions. The cell tests displayed improved performance in the nonsegregating electrolyte range. Compared to the eutectic (52 mol% Li_2CO_3) composition, cell voltage increased about 100 mV at 160 mA/cm^2 for the off-eutectic carbonate compositions, 65-75 mol% Li_2CO_3.

Cell area-specific impedances, a combination of IR losses and electrode polarization, for the cell tests have been correlated with the segregation factor derived from the strip screening tests. This correlation suggests that the composition of the carbonate at the electrodes plays a significant role in the performance of the molten carbonate fuel cell. Only a minor portion of the reduced cell polarization can be attributed to increased electrolyte conductivity that is associated with the increased Li_2CO_3 content of the nonsegregating electrolyte composition. Post-test examination of molten carbonate cells will investigate this observation further.
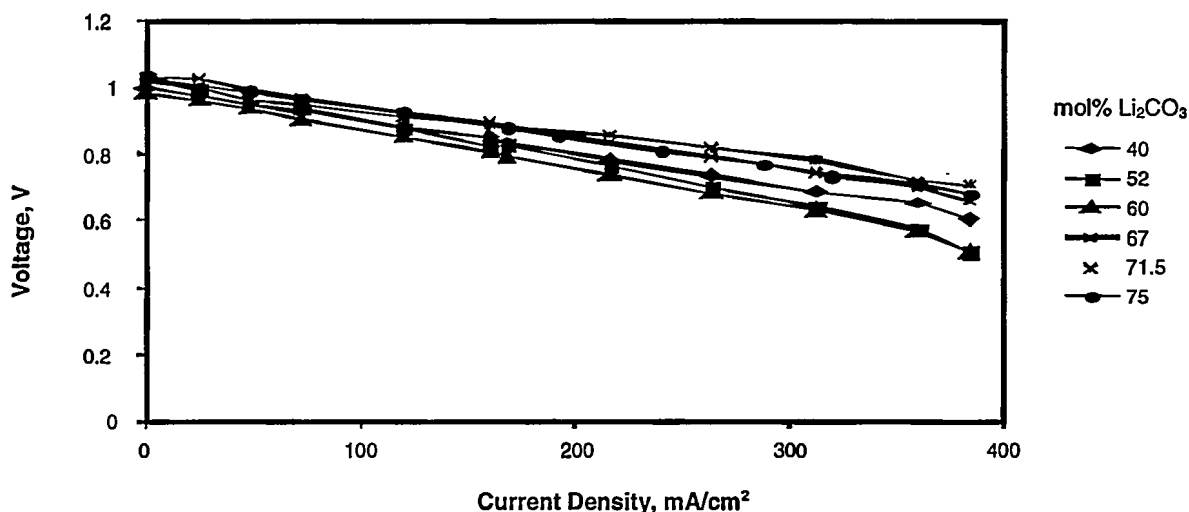
Fig. I-15. Polarization Curves in Cell Tests with Various Electrolyte Compositions. The Li_2CO_3/$NaCO_3$ compositions (in mol%) are 40/60, 52/48, 60/40, 67/33, 71.5/28.5, and 75/25.

c.   Cell Hardware

The temperature, gas compositions, electrolyte composition, and chemical potential differences in the molten carbonate fuel cell lead to corrosion of the metal hardware. Two regions in the molten carbonate cell experience high corrosion rates, the bipolar plate and the wet seal area. We are determining the mechanism of this corrosion and investigating methods to mitigate it.

The bipolar plate in the molten carbonate fuel cell consists of nickel-clad stainless steel. Here, the nickel-clad side is exposed to the anode compartment and the bare steel side, to the cathode. A $LiFeO_2$-based oxide scale forms on the bare steel during cell operation, which lowers cell performance because of its high resistivity. Our approach to the corrosion problem is to develop alternative metals and alloys that form oxide scales with lower resistivity. On the basis of the $LiFeO_2$ cathode work (Sec. I.C.3.a), solid-solution formation with NiO and $LiCoO_2$ dramatically lowered resistivity. Thus, if an Fe-Co-Ni alloy is formed with the metal ratios equal to those of the conductive $LiFeO_2$ solid solution, then the solid solution may form on the metal surface during the corrosion process.

This study has provided data that show promise for powder metallurgy of Fe-Co-Ni alloy). The two major obstacles to be overcome are porosity and secondary phases. We have been able to reduce secondary phases to insignificant amounts simply by using very fine metal powder (on the order of 10 μm). Sintering at temperatures closer to the melting point improves the kinetics of reaction and, consequently, reduces secondary phases as well as pores. Future work will focus on corrosion and *in situ* resistivity measurement in a cathode environment.

4. Technical Management

The CMT Division, through the ANL Electrochemical Technology Program, provides support to the DOE Office of Transportation Technologies and to the DOE Office of Buildings Technology in the form of technical management of R&D contracts with industrial developers of fuel cells and related components. In this capacity, we prepare work statements, evaluate proposals, and conduct progress reviews. Major ongoing projects managed by CMT include DOE contracts with General Motors Corp., Ford Motor Co., Chrysler Corp., and fuel-cell component suppliers.

The DOE/General Motors project managed by the Electrochemical Technology Program completed the third year of a $35 million contract to develop a methanol-fueled polymer electrolyte fuel cell system for automotive applications. During 1997, a 50-kW polymer electrolyte fuel cell stack was built by Ballard Power Systems (under a subcontract to General Motors). This stack achieved a specific power of 480 W/kg and a power density of 700 W/L, meeting program performance targets. Delphi Automotive Systems also built an improved 50-kW stack of their own design, to be tested in 1998. General Motors completed the scaleup of a partial oxidation reformer for methanol to a size suitable for a 50-kW fuel cell; this effort represents a successful technology transfer from Argonne, where the concept was developed, to General Motors.

Under the DOE/Ford project, International Fuel Cells (IFC) Corp. successfully fabricated a high-efficiency 50-kW fuel cell system and delivered the unit to Ford for testing. Operating on hydrogen fuel, the system achieves an efficiency of 60% at partial power and 50% at full power. Unlike many fuel cell systems, the IFC unit operates without an air compressor. Eliminating the need for a compressor greatly simplifies the system and decreases the auxiliary power consumption, which results in greater energy efficiency.

The DOE/Chrysler project was completed during 1997. In this project, AlliedSignal (under subcontract to Chrysler) successfully built and tested a 100-cell stack operating on hydrogen fuel. AlliedSignal's cost analysis projected a fuel cell cost of $108/kW, based on current performance, and $68/kW, based on targeted performance, at an assumed production level of one million per year. System integration tests, conducted by PEI Electronics, Inc., on the AlliedSignal stack using simulated automotive driving cycles, validated Chrysler's conceptual design of a light-duty vehicle powered by a fuel cell with a battery load-leveling unit for peak power and recovery of braking energy.

The CMT Division is constructing a Fuel Cell Test Facility, which will fulfill DOE's need for an independent source for validating the performance of fuel cells fabricated by industrial developers under DOE sponsorship. The facility will have the capability for testing either fuel cell stacks or complete systems (fuel processor and stacks) with a size up to 60 kW of electrical power output. The test room has been constructed, and bulk hydrogen storage via compressed gas tubes has been installed. A gas management system has been procured to control the pressure, temperature, humidity level, and flow rate of both the fuel and oxidant gas supplies to the fuel cell. Argonne will complete the Fuel Cell Test Facility, commission it, and initiate the

independent evaluation of fuel cells for DOE in 1998. A **30**-kW fuel cell stack built by Ballard Power Systems is the first system scheduled to be evaluated in the test facility.

II

Hazardous and Mixed Waste Research

A major challenge facing DOE is management of the massive quantity of hazardous and mixed (hazardous/radioactive) waste that has accumulated at various DOE sites as a result of nuclear-defense production conducted for more than four decades at these sites. Cleanup and disposal of this waste in an environmentally sound and cost-effective manner is now a major DOE mission. In addition, minimization of hazardous waste production and safe and efficient management of any hazardous waste that is produced are becoming increasingly important considerations in the commercial sector. We are investigating a variety of approaches aimed at treating and disposing of hazardous and mixed wastes in support of DOE's waste management mission. In addition, we are investigating whether the technologies developed for DOE applications could also be used for hazardous waste minimization in industry.

A.   Development of Aqueous Biphasic Extraction Processes

Aqueous biphasic extraction (ABE) is a highly adaptable separation technique that can be used in a wide range of applications. We have been evaluating various types of ABE systems for possible applications in the treatment of solid radioactive wastes, liquid nuclear wastes, and contaminated soils, and in the removal of organics from aqueous salt solutions. Below, we summarize the recent developments in our efforts to design efficient systems for metal separation and soil decontamination.

1.   Metal Separations

The ABE extraction systems are generated by combining an aqueous salt solution and an aqueous polymer solution. This produces two distinct liquid layers that are as immiscible as oil and water, yet each liquid layer contains at least 70 to 80 wt% water. The biphasic systems that we have been working with consist of immiscible polyethylene glycol (PEG) and salt solutions. Some inorganic salts that promote biphase formation with PEG solutions include the sodium/potassium salts of sulfate, carbonate, phosphate, and hydroxide. A major difficulty

encountered when designing ABE systems for metal ion extraction has been an inability to efficiently back extract solutes from the polymer-rich phase. This is primarily due to the relatively high salt concentrations that are required to maintain the aqueous biphase system. Proposed flowsheets that involve treating the loaded polymer phase with ion-exchange resins or back extraction into secondary salt-rich phases are inefficient and generate significant amounts of waste.

We have found that the recovery of the extracted metal complex can be achieved by contacting the loaded PEG-rich phase with a water-immiscible alcohol phase (e.g., n-butanol) at elevated temperature (60-80°C). The elevated temperature provides the thermodynamic driving force for the selective partitioning of the PEG from the aqueous phase into the alcohol phase. The partition coefficient for PEG with a molecular weight of 4000 in the n-butanol/water/salt/PEG system at elevated temperature is ≥ 15, while the partition coefficient for the salts is $\leq 10^{-3}$. Partition data for the butanol/water system at 60°C are summarized in Table II-1. The mass transfer of PEG into the alcohol phase results in significant phase volume change so that even though the partition coefficient for PEG is marginal, we still achieve >99.4% PEG recovery. In general, increasing temperature and PEG molecular weight lead to more favorable partitioning of the polymer into the alcohol phase:

Table II-1. Partitioning in n-Butanol/Water/Sulfate/PEG
System at 60°C

Species	Partition Coefficient[a]
PEG-4000	15
PEG-10,000	~35
Sulfate	0.001
n-Butanol	12.7

[a]The PEG phase was prepared by equilibrating equal volumes of 15 wt% PEG-3400 and 12 wt% Na_2SO_4 solution at 60°C. An initial phase volume ratio of butanol/PEG solution of one produced an equilibrium phase volume ratio of five.

The polymer can be recovered from the alcohol phase by back extraction into a dilute salt solution at low temperature ($\leq$20°C). The tie-line composition of the polymer-rich phase from the PEG/salt/water phase diagram can be used as a guide in choosing the appropriate salt composition for this back extraction step. Partition coefficients for PEG-4000 during back extraction at 5 and 20°C are given in Table II-2.

As in the forward extraction, there is also a large phase volume change during back extraction because of the mass transfer of large amounts of polymer. For the three cases listed in Table II-2, initial phase volume ratios (polymer-to-salt) of one produced, at equilibrium, phase volume ratios of 0.3. The data in Tables II-1 and -2 for the PEG-4000 species show that temperature is the primary factor in determining partitioning behavior of this polymer.

Table II-2. Back Extraction of PEG-4000 from n-Butanol
at 5 and 20°C

[Na₂SO₄], wt%	PEG-4000 Partition Coefficient	
	20°C	5°C
0	0.048	0.025
0.01	0.044	0.028
0.05	0.047	0.028

An example ABE flowsheet for the removal of actinides from high-ionic-strength salt solutions, similar to those used in the decontamination of concrete surfaces, is shown in Fig. II-1. Prior to the first extraction section, a metal complexant, such as chlorophosphonazo III, is added to the salt stream at a concentration of 0.005-0.01 wt% to selectively complex the actinides (e.g., Pu^{4+}, UO_2^{2+}, Th^{4+}). In the first extraction section, any excess chlorophosphonazo III and the complexed actinides are extracted into the PEG-rich phase. This produces an actinide-free salt solution that can be recycled back to the decontamination operation. The net result of the first two extraction sections in Fig. II-1 is the production of an aqueous stream in which the actinide concentrations increase while the salt concentration decreases. The actinide concentrate can then be sent directly to a vitrification process prior to final disposal.
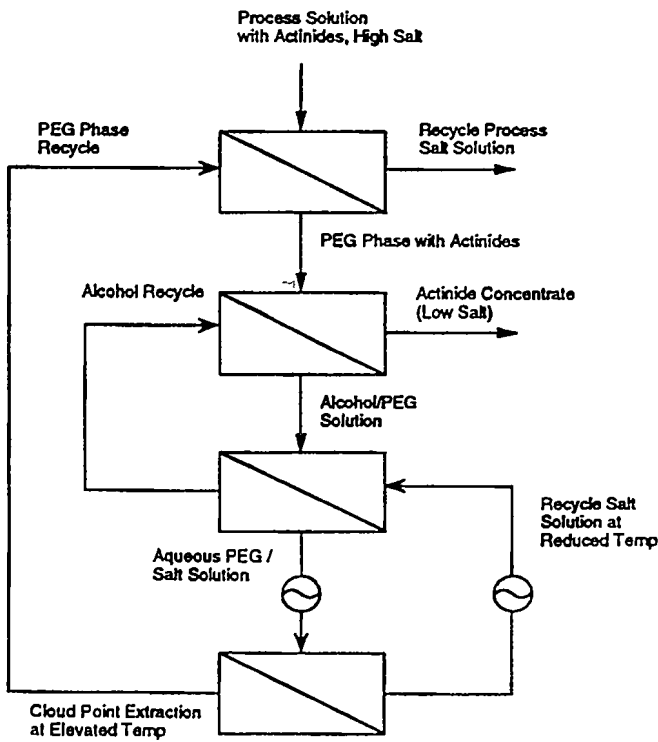
Fig. II-1.

Flowsheet for Aqueous Biphasic Extraction of Actinides from High-Ionic-Strength Salt Solutions

In the last section of the flowsheet, a cloud-point extraction is used to generate a polymer solution for recycle. This is achieved by raising the temperature of the polymer/salt solution above its cloud point, causing it to split into two phases—a polymer-rich phase and a salt-rich phase. Both solutions can then be recycled.

2. Removal of Lead from Contaminated Soils

The removal of heavy metal contaminants from clay-rich soils has the potential to achieve significant volume reduction in cleanup efforts. However, it is beyond the capabilities of traditional soil washing techniques. During 1996, we began a study to determine the feasibility of using ABE technology for removal of lead from clay-rich soils. This work continued in 1997. The sources of the two contaminated soil samples used in the ABE studies are two inactive firing ranges at ANL.

The treatment flowsheet includes a combination of conventional particle-classification technologies together with the treatment of the fine-particle-size fraction by the ABE process. Conventional particle classification of the soil samples was carried out by Metcalf & Eddy, Inc. The soil samples were classified according to size and density. The major fraction of the soil (150 mesh) had lead concentrations ranging from 500 to 1400 mg Pb/kg, which is above industrial cleanup standards (e.g., 400 mg Pb/kg). During the past year, four continuous, countercurrent ABE runs were completed.

Unfortunately, during ABE extraction of the humate-rich soil, there were no significant reductions in the lead content of the clay fraction. We postulated that possible surface activation by humates may have been responsible for the lack of lead separation. To test this hypothesis, we conducted a test in which we calcined the soil prior to ABE extraction.

Calcination of the soil to remove naturally occurring organics (e.g., humates) from the soil was found to expose the iron oxide coatings on the soil particles, which changed the color of this soil from black to red. During the biphase extraction, practically all of the lead partitioned to the salt phase; however, the exposure of the iron coatings on the clay resulted in coextraction of the clay into the salt phase. The net result was no selective partitioning of lead away from the clay.

In extraction tests using soil with a very low humate content (this sample was supplied by Metcalf & Eddy, Inc.) the lead content was reduced from about 2000 to 600 mg/kg. While the lead reduction was not low enough to meet cleanup standards, the improved performance suggests that the ABE system is sensitive to surface activation of soil contaminants by naturally occurring organics. We are now examining alternative methods to improve mass transfer of lead during ABE treatment. One of these includes preleaching the soil with dilute sodium carbonate solution in an attempt to selectively remove organic coatings from lead particles. Another approach involves calcination of the soil and the use of a phase transfer agent to selectively partition the lead into the polymer-rich phase.

B. Development of Low-Temperature Phosphate Glasses for Waste Disposal

During the electrometallurgical treatment of spent nuclear fuels (see Sec. IV), fission products and transuranic elements accumulate in the LiCl-KCl electrolyte. The transuranic elements and fission products can be recovered by using zeolite ion exchange. In current process flowsheets, the spent zeolite is prepared for final disposal by incorporation into a composite ceramic waste form that contains borosilicate glass. In the baseline flowsheet, the waste form is fabricated by hot isostatic pressing. Because of the inherent scaleup limitations of hot isostatic pressing, we have begun to examine a possible alternative process, which involves incorporation of the zeolite into a ceramic waste form that contains a low-temperature phosphate glass.

The zinc phosphate glasses that we are studying have a glass transition temperature (T_g) in the range of 325 to 375°C. The low T_g means that relatively low processing temperatures (e.g., 450-700°C) can be used to encapsulate a wide variety of radioactive waste particulates. In addition to the low processing temperatures, which significantly reduce losses of volatile metals (e.g., ^{137}Cs, ^{99}Tc, Cd), the zinc phosphate glasses are capable of direct incorporation of chloride salts at significant loading levels (e.g., 10-15 wt%). This capability is advantageous for the planned electrometallurgical treatment of Experimental Breeder Reactor-II fuel, where it is not feasible to recycle the LiCl-KCl eutectic electrolyte because of the high sodium content of the fuel.

We have been able to prepare small-scale composite monoliths containing several particulate materials currently being considered for radioactive waste disposal, including cesium-loaded crystalline silicotitinate, zeolite, and sodalite. The monoliths were fabricated by cold pressing and sintering at 460°C. Cesium release from these materials during standard leach tests (MCC-1) for 3 days was extremely low and ranged from 0.02 to 0.04 wt%. We have also begun to evaluate the performance of salt-loaded phosphate glasses. Glasses with 10 wt% salt loading were prepared by heating the glass precursors with the chloride salt at 900°C for 2 h in a covered crucible. Cesium release during MCC-1 tests at 90°C for 3 and 7 days was approximately 10^{-4} wt%. This is the same fractional release that was observed for Zn, Na, K, and Li from the salt-free glass and suggests that cesium is not preferentially leached from the glass.

We will continue our efforts to optimize the glass composition with respect to corrosion resistance and waste loading capacity and will begin to scale up the process. We will also be examining the feasibility of directly incorporating salts into a glass melt at temperatures as low as 700 to 800°C. The lower processing temperatures will reduce even further the losses of volatile radionuclides such as ^{137}Cs and ^{99}Tc.

C. Fundamental Studies of Actinide Behavior

The behavior (i.e., complexation, oxidation state, and aggregation) of radionuclides is being investigated under conditions relevant to subsurface groundwaters on DOE sites. Emphasis is on factors that affect mobilization/immobilization of actinides. Results of this work will

establish key factors concerning the chemistry of actinide-organic mixtures in the presence of microbes, inorganic substrates, and metal cations.

1.   Microbiological-Actinide Interactions in Subsurface Environments

Understanding the interactions between actinides and microorganisms in subsurface environments is essential to assess actinide fate during organic contaminant bioremediation efforts and to help predict the fate of radionuclides in the proposed nuclear waste repositories. An important class of organic compounds at contaminated DOE sites includes organic chelating agents, such as nitrilotriacetic acid (NTA), which can increase dissolved actinide concentrations and lead to enhanced radionuclide migration in the groundwater. Improving our ability to predict the effects of chelate biodegradation on the fate of actinides in the subsurface has broad applicability, since the properties of many natural organic compounds and microbially derived byproducts found in the subsurface mimic the behavior of anthropogenic complexants.

Our past research has focused on elucidating the key interactions in aerobic actinide-NTA-*Chelatobacter heintzii* systems. In these model systems, we have investigated the effects of Pu(IV) and Np(V) on NTA biodegradation and studied the fate of the actinides during chelate degradation. This work has been expanded during the past year to include actinide-microbe interactions in the presence of other chelating agents and under oxygen-limited and anaerobic microbiological conditions. A key feature of our research is the extensive integration of modeling with laboratory experimentation. In this collaborative effort, experimental data obtained at CMT are used to help develop and test a Northwestern University computer code (CCBATCH) designed to couple biological and chemical reactions. Concurrently, model simulations help identify areas where additional laboratory work is needed.

In the past year, we made significant progress in determining additional mechanisms of actinide toxicity toward microorganisms. Our results show that actinide toxicity is oxidation state and isotope specific. For example, in contrast to the radiolytic toxicity noted in the Pu(IV) system, Np(V) inhibits the activity of *C. heintzii* via chemical toxicity, similar to other heavy metals. Several sets of experiments were performed to separate radiolytic from chemical toxicity in the Np-NTA system. To determine radiolytic effects, the viability of the organism as a function of increasing neptunium concentration (0.2 to 125 μM) was monitored in a 5.2 mM NTA-12 mM phosphate solution, which ensured that all the neptunium was present in complexed form during NTA degradation. In this case, there was no significant bioassociation of neptunium with the organism, and no inhibition was observed at neptunium concentrations up to 125 μM. These findings indicate that at environmentally relevant concentrations, complexed Np(V) shows no radiotoxicity toward *C. heintzii*.

Heavy metal toxicity toward microorganisms is usually related to the concentration of specific metal aqueous species, often the aquo metal ion concentration. To study the potential chemical toxicity of Np(V), experiments were conducted in fixed-pH, minimal-growth medium so that no background ligand was available to complex neptunium during NTA biodegradation. Modeling simulations showed that neptunium speciation was dominated by the concentration of

NTA in solution. As NTA was biodegraded, re-equilibration of the aqueous speciation increased the concentration of the aquo NpO_2^+ ion. As the total neptunium concentration increased, the degradation of NTA was inhibited. Modeling simulations of these results linked the observed inhibition to the concentration of the aquo NpO_2^+ ion.

In other chelate systems, we conducted preliminary studies designed to investigate the potential toxicity of depleted U(VI) toward the bacterium *Pseudomonas fluorescens* during the degradation of citric acid. The use of depleted uranium in these experiments enabled us to rule out radiolytic inhibition. Colony forming unit counts during citrate degradation clearly indicated that increasing the total U(VI) concentration inhibited the organism. However, unlike the Np(V)-NTA system, experiments conducted in the absence of complexing ligands showed no toxicity toward *P. fluorescens* at near-neutral pH. This finding indicates that the U(VI)-hydroxide and -carbonate species present did not chemically inhibit the organism. Because of the special status of citric acid in biological reactions,[1] our working hypothesis for future experiments is that the presence of citrate is the key factor contributing to U(VI) toxicity.

In parallel with our actinide toxicity studies, we conducted experiments designed to investigate the impact of biological activity on actinide speciation. Biological degradation reactions often strongly affect the pH of aqueous systems by directly consuming or producing acids, bases, and hydrogen ions. The biodegradation of NTA by *C. heintzii* consumes hydrogen ions, causing an increase in pH in weakly buffered systems that influences actinide aqueous speciation. Because of the high solubility of actinides in the V oxidation state, we were especially interested to determine if the pH shift during chelate degradation would reduce actinide mobility. Figure II-2 shows the fraction of neptunium precipitated as a function of time for Np(V) concentrations at 0.2 to 125 μM. The greater extent of partitioning with time was due to a rise in the solution pH as the NTA present was biodegraded. The experiments were performed in the presence of a phosphate buffer to minimize the increase in pH. A pH increase from 7.0 to 7.9 was
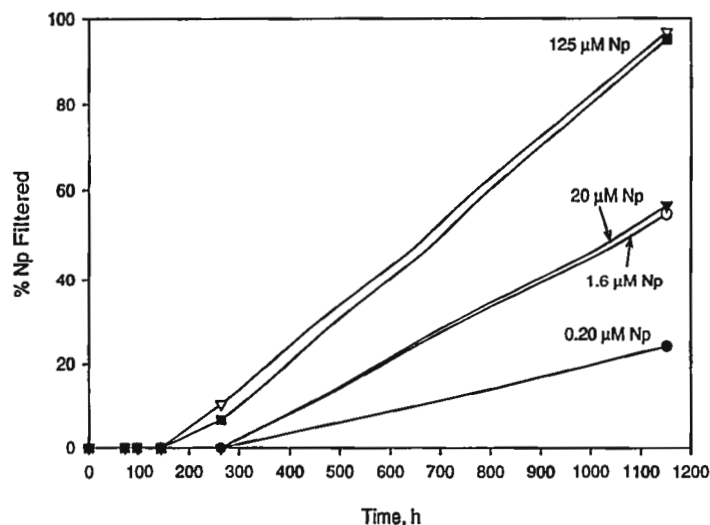
Fig. II-2.

Fraction of Np(V) Precipitated during NTA Degradation by *C. heintzii*.

---

[1] M. T. Madigan, J. M. Martinko, and J. Parker, *Brock Biology of Microorganisms*, 7th ed., Prentice Hall, Upper Saddle River, NJ (1997).

observed during the degradation of NTA, again mediated by *C. heintzii*. The biologically induced pH increase caused the precipitation of an unidentified neptunium-phosphate phase. This finding will be investigated further, since phosphorus is a required biological nutrient, and many *in situ* bioremediation efforts require supplemental phosphorus additions.

In subsurface environments, anaerobic microbial activity may affect actinide speciation by altering the overall redox potential or by directly utilizing actinides as electron-donor or -acceptor substrates. Additionally, microbial activity in closed systems often results in elevated carbonate concentrations that can dramatically increase actinide solubility. We have recently initiated experiments to study the fate of neptunium under sulfate-reducing conditions. Our initial results show that Np(V) is stable under anaerobic conditions for more than 6 months, and that the presence of low concentrations of Np(V) does not inhibit the activity of the organisms. In future work, we will investigate the stability of the V oxidation state during anaerobic microbial activity.

2. Actinide Stability/Solubility Studies in Support of the Waste Isolation Pilot Plant

The Waste Isolation Pilot Plant (WIPP) in Carlsbad, New Mexico, has been selected as a possible disposal site for transuranic radioactive wastes. The goal of the actinide stability/ solubility project is to provide experimental data for WIPP on actinide solubility and oxidation state distribution in WIPP brine. These data are being used to test and challenge the Actinide Source Term (AST) model developed by Sandia National Laboratories.

In this project, we are investigating the stability and steady-state concentrations of three actinides (U, Np, and Pu) in the VI oxidation state in WIPP-relevant brine. We are also determining the effects of organic chelating agents (oxalate, citrate, and ethylenediaminetetraacetic acid) on the oxidation state stability. The experiments are performed in the following simulated WIPP brines: G-Seep at pH 5 and 7, ERDA-6 at pH 8 with carbonates, and ERDA-6 at pH 10 with and without carbonate. They are conducted in an oxygen-free environment with a hydrogen atmosphere of ~1000 torr, at 25°C, and in 1-L polypropylene bottles. The starting actinide concentrations are ~10^{-4} $\underline{M}$. Gas and liquid sampling is done periodically.

In the results obtained to date (18 months), the actinide(VI) oxidation state persisted as a stable truly dissolved species under the following conditions: Pu(VI) in ERDA-6 brine with/without carbonate present, Np(VI) at pH 8 and 10 in ERDA-6 brine with carbonate, and U(VI) at pH 5 in G-Seep and pH 10 with carbonate in ERDA-6. The concentration profiles for the Pu(VI) experiments are shown in Fig. II-3 for the ERDA-6 brine. Plutonium(VI) was stable in WIPP brine throughout the 18-month experiments under all conditions tested. Lower steady-state concentrations were observed for U(VI) in G-Seep at pH 7. Neptunium(VI) was rapidly reduced to Np(V) in G-Seep brine and was stable only when carbonate was present in ERDA-6 brine.

The addition of reducing agents relevant to the WIPP resulted in the reduction of Pu(VI) to Pu(IV) and, subsequently, the establishment of low steady-state concentrations of plutonium in the brine system. The effect of iron coupons on the plutonium concentration is shown in Fig. II-4.
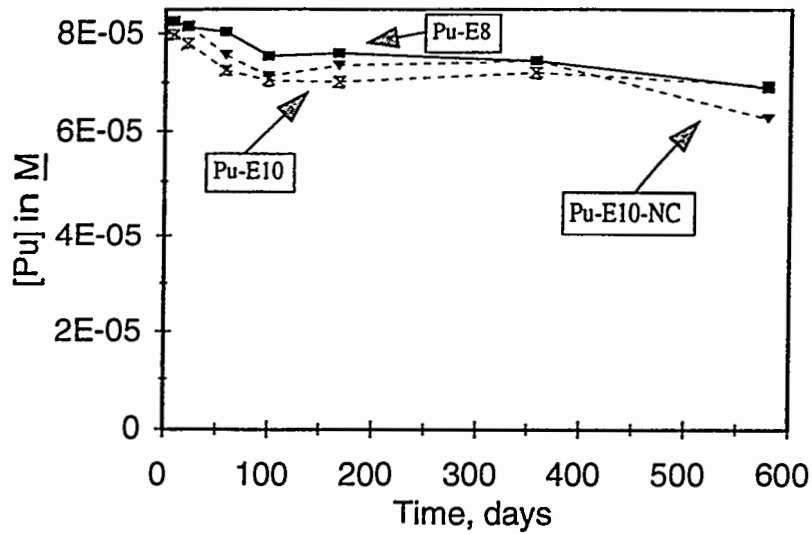
Fig. II-3. Concentration of Trace Plutonium as Function of Time in ERDA-6 Brine. Designations are Pu-E8, pH 8 brine, with carbonate; Pu-E10, pH 10, with carbonate; Pu-E10-NC, pH 10, without carbonate.
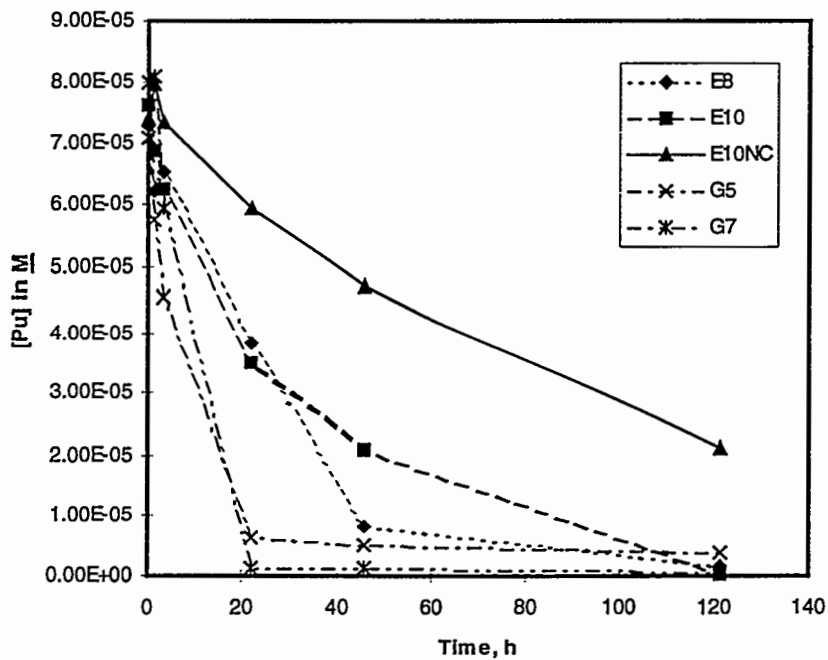
Fig. II-4. Effect of Presence of Iron Coupons on Concentration of Plutonium in Experiments with Various WIPP Brines. Designations are E8, ERDA-6 brine with carbonate at pH 8; E10, ERDA-6 brine with carbonate at pH 10; E10NC, ERDA-6 brine, no carbonate at pH 10; G5 and G7, G-Seep at pH 5 and 7, respectively.

More rapid reduction was noted when the iron was added as aqueous Fe^{2+}. Organic chelating agents expected to be present in the WIPP also caused the reduction of Pu(VI) and Np(VI). In the presence of organics, Pu(VI) and Np(VI), with one exception, were reduced to form organic complexes of lower oxidation states. The one exception was Pu(VI) at pH 10 in the presence of carbonate, which was stable as a Pu(VI) carbonate complex.

Two areas will be emphasized in future studies. In collaboration with Sandia National Laboratories, the long-term data generated are being modeled to challenge their current high-ionic-strength models for actinide solubility. Additionally, more detailed studies are being conducted to study the mechanism and rate of the reduction of Pu(VI) and Np(VI) by organic chelating agents.

3.   Synchrotron-Based Studies of Actinide Species

Studies are in progress to extend and develop X-ray synchrotron radiation (XSR) techniques to determine the chemical structure of aqueous, adsorbed, and solid actinide species of importance to environmental and nuclear waste management. This will help resolve a number of fundamental structural issues related to the speciation (e.g., complexation, oxidation state, and aggregation) of actinides in subsurface environments. Emphasis is on both collecting XSR data on actinide systems and modeling these data by improved calculational methods and theory. Experiments are planned for the ANL Advanced Photon Source.

Actinide speciation is an important issue in many aspects of nuclear waste management. The chemical structure and geometry of actinide complexes and phases are often the missing pieces of information in characterizing the actinide species. Structural information is needed to define key aqueous complexes, redox chemistry, surface-adsorbed species, and microbiological interactions in the subsurface. Improved speciation information will lead to greater accuracy in predicting migration and to improved remediation/reprocessing strategies.

The theoretical aspect of the work initially focused on electronic structure calculations to determine geometries and oxidation states of the actinides in solution. X-ray absorption spectra were calculated from first principles to help interpret experimentally obtained spectra. Preliminary calculations of the uranium $L_{2,3}$ edge with X-ray absorption near edge spectroscopy (XANES) have been performed for small cluster models of UO_2, including both first and second nearest neighbor atoms. The results are now being analyzed.

Several experiments were performed in the area of actinide microbiological interactions to generate well-characterized samples for our XSR studies. The biodegradation of the uranium-citrate complex by *Pseudomonas fluorescens* showed biosorption to be an important process. These experiments generated samples of bio-associated uranium and aqueous uranyl complexes for further characterization by XSR techniques. Absorption spectra were also obtained to help establish/define the aqueous speciation.

The XANES spectra of four actinide solids were taken at the National Synchrotron Light Source of Brookhaven National Laboratory. The purpose of these experiments was to establish baseline/reference spectra for synchrotron applications to actinide samples and establish the

relationship between the edge energy and the oxidation state of the actinide. The solids analyzed were PuO_2, PuF_3, $PuBr_3$, and Ba_3PuO_6.

The XANES spectra for the actinide solid samples are shown in Fig. II-5. The experiments were performed by monitoring the fluorescence at 14.4 keV, which corresponds to absorption at the L_3 edge of plutonium. These results compare well with XANES spectra taken on aquo species of the various plutonium oxidation states. A slightly less than 2 eV shift to higher energy was noted for each oxidation state increase. These data indicate that XANES spectra may be useful in identifying oxidation states of plutonium in environmentally relevant systems.
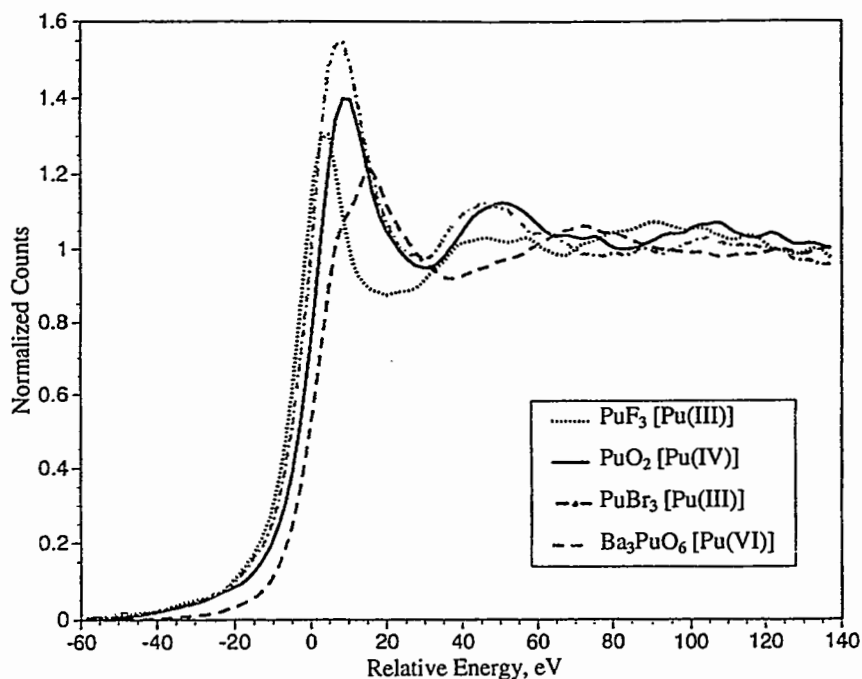
Fig. II-5. X-ray Absorption Near-Edge Structure for Various Actinide Solids

Future plans are to continue the work on characterizing the XANES spectra of both solid and aqueous actinide species and eventually expand this to determine the structure of key aqueous complexes in the environment. The ongoing theoretical work will be emphasizing calculation of the near-edge structure for plutonium species.

D.   Radiolytic Gas Generation Studies

Chemically bonded phosphate ceramic (Ceramicrete), developed by the ANL Energy Technology Division, is being investigated as a waste form for encapsulating transuranic (TRU) wastes from DOE sites. Because of the presence of radionuclides, gases, primarily H_2 and to a lesser extent O_2, are produced by radiolysis of the water present in the waste form. Other gases, such as CO, CO_2, CH_4, and low-molecular-weight hydrocarbons may also be produced by radiolysis of organic materials present in the waste. The accumulation of radiolytically produced

H_2 and volatile organic compounds in the waste canister is an important safety issue for storage and transportation operations. The objective of this work is to measure the "G-value" (i.e., number of molecules produced per 100 eV of radiation deposited in the sample) for various TRU wastes encapsulated in Ceramicrete waste forms. These G-values are used in calculating acceptable TRU loadings in the waste form to meet waste acceptance criteria for a geologic repository.

The test matrix consisted of three plutonium-laden Ceramicrete samples: one sample (I) containing a UO_2-PuO_2 mixture, and two samples (II and III) containing a TRU combustible residue. For a comparison basis, gas generation by a sample of the TRU combustible residue (IV), not incorporated into Ceramicrete, was also measured. A more detailed description of the various samples is provided in Table II-3. Studies are still in progress on Samples II-IV.

Table II-3. Samples Investigated in Gas Generation Studies. All G-values were calculated under the assumption that 100% of the decay energy is deposited into the entire mass of the sample.

Sample No.	Description	Composition, wt%					G-value (molecules H_2/100 eV)
		Pu	Waste	Binder	Class C Flyash	Water	
I	Ceramicrete containing U-Pu oxide mixture	5.245	20.98	58.94	0	20.08	0.13
II	Ceramicrete containing TRU combustible residue	7.87	24.75	31.65	22.61	20.99	0.10
III	Ceramicrete containing TRU combustible residue and bakellite	5.00	25.7[a]	31.65	21.63	20.99	Decreasing, with a maximum of 0.96[b]
IV	TRU combustible residue	31.8	100	0	0	0	0.007

[a]Broken down into 10 wt% bakellite and 15.7 wt% waste.
[b]Based on the amount of H_2 observed after first sampling, which occurred after 48 h.

The number of molecules of H_2 generated as a function of the decay energy in the three plutonium-loaded Ceramicrete samples and the TRU combustible residue is shown in Fig. II-6. The G(H_2) values are summarized in Table II-3. The G(H_2) value measured for Samples I and II are constant and approximately equal, 0.10 and 0.13 molecules H_2/100 eV, respectively. The measured G(H_2) value for Sample III is decreasing, with a maximum G(H_2) value of 0.96 molecules H_2/100 eV after the initial 0.16×10^{20} 100 eV of decay energy (48 h). It should be noted that Samples I and II were cured for 21 days, whereas Sample III was not cured prior to initiation of the study. The TRU combustible residue (not incorporated in Ceramicrete) has a measured G(H_2) of 0.007 molecules H_2/100 eV.

It has been suggested that free or unbounded pore water is the primary source of H_2 for cementitious materials.[2] To establish whether or not pore water is the primary source of H_2, a sample of a plutonium-loaded Ceramicrete (5.0 wt% PuO_2 and 18.9 wt% H_2O) was dewatered by

---

[2] E. W. McDaniel and D. B. Delzer, "FUETAP Concrete," Chapter 9 in *Radioactive Waste Forms for the Future*, Eds., W. Lutze and R. C. Ewing, Elsevier Science Publications, New York, pp. 565-588 (1988).
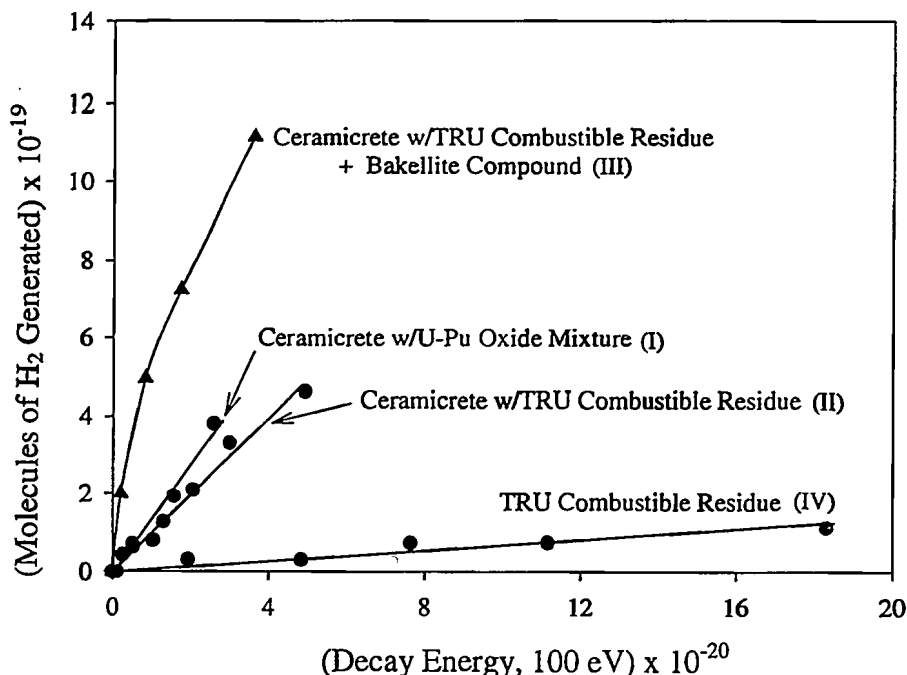
Fig. II-6. Molecules of H_2 Generated by Radiolysis for Three Plutonium-Laden Ceramicrete Samples and Sample of TRU Combustible Residue. The decay energy is defined as the product of the number of decays in a given time period multiplied by the average energy of the emitted alpha particle per decay for each radionuclide present in a given sample. It is assumed that 100% of the energy is deposited in the sample.

heating at $110 \pm 5°C$ for 1 h in a nitrogen atmosphere. On the basis of the difference in weight of the sample before and after heating, the water content of the sample had decreased from 18.9 to ~1 wt%. The hydrogen yield was measured for the un-dewatered (18.9 wt%) and dewatered (~1 wt%) samples. The $G(H_2)$ of 0.04 molecules $H_2/100$ eV measured for the dewatered sample is an order of magnitude lower than the $G(H_2)$ of 0.37 molecules $H_2/100$ eV measured for the un-dewatered sample, as shown in Fig. II-7.

On the basis of the similarity in water content and the measured $G(H_2)$ values for Samples I and II, the $G(H_2)$ value of 0.10-0.13 molecules $H_2/100$ eV may represent the rate of H_2 production by radiolysis of pore water in TRU-loaded Ceramicrete waste forms. This $G(H_2)$ value is significantly less than the $G(H_2)$ value of 1.6 molecules $H_2/100$ eV for alpha-particle deposition in pure water.[3] Currently, it is not understood why the $G(H_2)$ value for Sample III is decreasing. If radiolysis of pore water is the primary reaction occurring, a constant $G(H_2)$ would be anticipated for Sample III. Since Sample III was not cured for 21 days prior to initiation of the

[3]   G. Draganic and Z. D. Draganic, *The Radiation Chemistry of Water*, Academic Press, New York (1971).
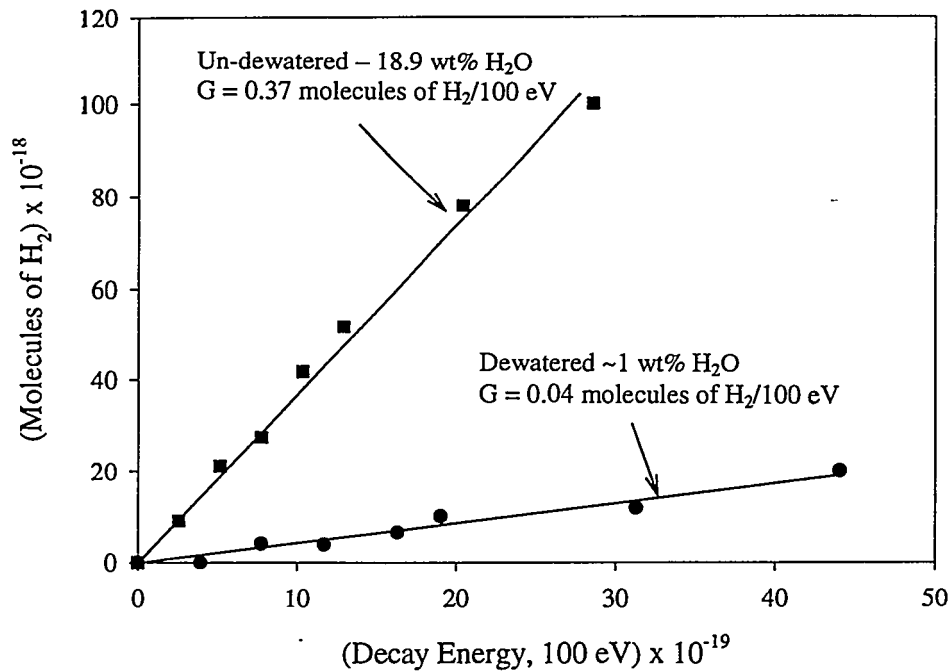
Fig. II-7. Effect of Water Content on Rate of Radiolytic H_2 Generation for Plutonium-Laden Ceramicrete Sample (5.0 wt% PuO_2 and 18.9 wt% H_2O). The decay energy is defined as the product of the number of decays in a given time period multiplied by the average energy of the emitted alpha particle per decay for each radionuclide present in a given sample. It is assumed that 100% of the decay energy is deposited in the sample.

study, one cannot draw firm conclusions by comparing the $G(H_2)$ value for Sample III to the $G(H_2)$ values for Samples I and II. The data for Sample III represent only a 34.8-day period (40 days after synthesis). Gas studies were not initiated on Samples I and II until >35 days after synthesis. (The 21-day curing period is included in the >35 day period.) Since the gas generation study on Sample III is still in progress, a better comparison will be the $G(H_2)$ measured for >35 days to the $G(H_2)$ values for Samples I and II. The $G(H_2)$ after 35 days should be constant and approximately equal to 0.1-0.13 molecules $H_2/100$ eV if radiolysis of pore water is the primary source of H_2. If not, alternative explanations must be pursued. Future work will involve gas generation studies on pilot-scale waste forms as this technology advances toward implementation.

E. Technical Support

In this effort, we are providing technical consulting support to the DOE Advanced Energy Projects and Technology Research Division and are assisting the DOE Richland Operations initiative to privatize treatment of the high-level radioactive waste currently stored in underground tanks at Hanford.

The technical support included providing technical review and advice on program direction and project selection for the Advanced Energy Projects (AEP) and for the Small Business Technology Transfer program. The mission of the AEP is to explore the scientific feasibility of novel energy-related concepts that are high risk, in terms of scientific feasibility, yet have a realistic potential for a high technological payoff. The technology transfer program provides support to small businesses for research that is conducted jointly with nonprofit research institutions.

The continuing support to the DOE Richland effort to privatize treatment of the radioactive wastes stored in underground tanks at Hanford involved participation in review and evaluation of the "Standards Approval Packages" which have been developed by the two private organizations (British Nuclear Fuels, Ltd., and Lockheed Martin Advanced Environmental Systems) that have been selected to compete for services related to tank waste treatment. The Standards Approval Packages are the first major deliverables and provide part of the basis for design of the facilities that are to be built to accomplish the waste pretreatment and vitrification.

III

Nuclear Waste Management

Before nuclear waste can be buried in a geologic repository, its corrosion behavior over long time frames must be known. In the CMT nuclear waste programs, a variety of laboratory tests with simulated and fully radioactive waste glasses are performed to obtain corrosion information that is used to support development of a geologic repository in an unsaturated environment similar to that expected for the candidate site at Yucca Mountain in southwestern Nevada. These tests are primarily directed at determining the interactions between groundwater and various nuclear waste forms, including high-level waste glasses and spent nuclear fuel, under unsaturated conditions. Tests are also underway to support development of vitrified forms of low-level waste generated at the DOE Hanford site, as well as ceramics and glasses for the disposal of surplus plutonium and plutonium-bearing wastes. In most cases, extensive analyses are conducted with both the reacted solids and the test solutions to develop a full understanding of the corrosion mechanism and to relate the test results both to long-term corrosion behavior under disposal conditions and to mechanistic corrosion models that are being developed to calculate waste form performance in specific disposal systems.

A.   Preparation of Review Documents

In this effort, we are compiling and interpreting previously published data that address the effects of several important parameters on the reactions between glass and repository groundwater. Over the last several years, critical reviews were completed on the effects of temperature, glass composition, radiation, and ratio of glass surface area to water volume (S/V) on glass reaction, as well as the status of glass reaction modeling. Two more critical reviews will be completed in the future: one on the effects of unsaturated conditions on glass durability, and the other on the corrosion behavior of natural analogues to the waste glass.

B.   Static Tests with Savannah River and West Valley Glasses

Tests are being conducted under the auspices of the DOE Office of Environmental Waste Management to characterize the corrosion behavior of several glasses developed for the Defense Waste Production Facility (DWPF) at the Savannah River Site and the West Valley Demonstration Project (WVDP). The goal of these tests is to gain insight into the corrosion mechanism and long-term behavior of waste glasses under the unsaturated conditions of the proposed Yucca Mountain repository. The dissolution of waste glasses is important because glass is a source of radionuclides, and glass components will affect the durability of other materials in the repository system. Since tests cannot be conducted on the time scale over which radionuclides must be contained, which exceeds 10,000 years, predictions of long-term behavior must be based on an understanding of the corrosion mechanism and the effects of environmental factors.

Tests are being conducted with glasses made with radioactive sludge from DWPF and WVDP and with glasses made with nonradioactive surrogates to compare their responses and evaluate whether or not simulated waste glasses are reliable surrogates. Tests are also being conducted to evaluate whether or not consistency requirements that must be met during vitrification can also be used to demonstrate that the waste forms are suitable for disposal. This is being done by evaluating the long-term corrosion behavior of the benchmark glass for vitrification, namely, the Environmental Assessment (EA) glass,[*] and by comparing the short-term and long-term behaviors of several glasses. Progress in several ongoing tasks is summarized below.

1.   Dissolution Tests

Several tests are being performed to characterize the corrosion behavior of vitrified waste forms and develop a mechanistic description of the long-term corrosion behavior. Static dissolution tests have been conducted at 90°C to assess the effects of S/V (10, 340, 2000, and 20,000 m^{-1}) and radiation on the glass corrosion behavior and the release of radionuclides and to evaluate the use of S/V as an accelerating parameter. The presence of radiation was found not to have a significant effect on glass corrosion. The S/V was found to accelerate corrosion in that the solution concentrations of dissolved glass components increased faster in tests at high S/V than in tests at low S/V over the same time period. However, the fact that the solution pH also increased faster at high S/V complicates the use of the S/V to accelerate corrosion.

The results of various tests have been interpreted in terms of a reaction progress variable that measures the transformation of a glass to thermodynamically more stable alteration phases. Different test conditions provide insight into different stages of corrosion progress. The dissolution kinetics can be divided into three stages. In the first stage, the glass dissolves at a rate

---

[*] A glass composition that was used as part of the environmental assessment for the DWPF at the Savannah River Site.

that is controlled by the glass composition, solution pH, and temperature. In the second stage, the buildup of dissolved glass components controls the rate. The formation of alteration phases may affect the solution chemistry and, thereby, the dissolution rate in the third stage. Tests with several glasses have shown the corrosion to increase to a high rate after zeolites and other phases form. The degree to which the rate increases in Stage III is probably the most important aspect of the long-term corrosion behavior with regard to repository performance.

This model has facilitated the comparison of the results from different test methods as well as the results of tests conducted with different glasses. The reaction progress that is attained in a particular test depends on the test method and the glass composition. Equally important, the model is compatible with the computer simulation models used to calculate long-term corrosion behavior. The reaction progress model provides a means of relating, in a single plot, laboratory tests conducted under conditions that simulate the disposal environment, conditions used to measure variables for the dissolution rate model, and conditions that accelerate certain corrosion processes. The influence of the glass composition on its long-term corrosion behavior is of key interest, since the composition is what is controlled during waste form production. Preliminary results of a model that is being developed to relate the glass composition to its long-term behavior are promising.

2.   Vapor Hydration Tests

Vapor hydration tests (exposure to vapor-saturated air at temperatures from 70°C to 200°C) have been performed on the EA glass. Although not a high-level nuclear waste glass, the EA glass is considered to be representative of the least durable high-level waste glass that might be produced at the DWPF, as indicated by the high release of B, Na, and Li in product consistency tests (7 days at 90°C and S/V = 2000 m^{-1}). This low durability is reflected in the rapid corrosion during vapor hydration tests. In the vapor hydration tests, the initial hydration of EA glass proceeded with an apparent $t^{1/2}$ dependence. The corrosion rate increased at high temperatures (150-200°C) coincident with formation of analcime ($NaAlSi_2O_6 \cdot H_2O$) and tobermorite [$Ca_5(OH)_2Si_6O_{16} \cdot 4H_2O$], and at lower temperatures (<120°C) with the formation of analcime. The distribution of phases, particularly calcium silicates, formed during glass corrosion was influenced by temperature, although the overall reaction kinetics was not affected significantly by the presence of calcium-bearing phases. The final alteration phases observed in the 175 and 200°C tests were albite ($NaAlSi_3O_5$), as well as calcium and sodium silicates.

In vapor hydration tests at 175°C and 200°C, zirconium appeared to have become incorporated into the analcime alteration phase. Similar behavior has been noted by Bakel et al.[1] for a Hanford low-level waste glass reacted at 200°C under vapor hydration conditions. The $Zr(OH)_x^{4-x}$ complex has a minimum activity at solution pH 4-6 but is the dominant aqueous form of zirconium above pH 8. The log stability constants for the reaction:

$$Zr^{4+} + 5H_2O = Zr(OH)_5^- + 5H^+ \qquad (1)$$

---
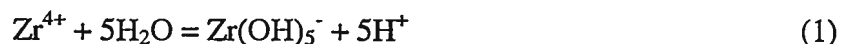
[1]   A. J. Bakel, W. L. Ebert, and J. S. Luo, *Ceram. Trans.* **61**, 515-522 (1995).

are -16 at 25°C, -11.62 at 100°C, and -8.82 at 200°C,[2] demonstrating a potential for this complex to be dominant at high temperatures. Complexes of the type $Zr(OH)_x^{4-x}$ may be incorporated into the analcime, and this reaction (Eq. 1) may occur in the high pH conditions that appear during corrosion of EA glass at ≥175°C. The form of zirconium in analcime will continue to be investigated.

Although the EA glass contains no radionuclides, a number of trace elements may be effective surrogates for some radionuclides. In particular, the fate of lanthanum can be used to predict the behavior of other rare earths and, perhaps, some actinides. In previous studies,[3] we demonstrated that plutonium follows rare earths into some alteration products on a SRL 200 glass made with DWPF sludge. Manganese has been used by Abdelouas et al.[4] to simulate technetium behavior; however, its use in this manner is questionable. In our tests, all the transition metals (Mn, Fe, Ti, and Ni) tended to reside in the smectite clay layer.

Lanthanum was observed to occur in the clay layer in our 70°C tests; however, in higher temperature tests, it was found with calcium in tobermorite. This suggests that actinides could become incorporated into related silicate phases under some reaction conditions; indeed, this has been observed in tests with a glass that contains high concentrations of plutonium.[5] Further study of this behavior is needed.

3. Critical Review and Testing of Natural Analogues

A comprehensive critical review has been completed on the present state of knowledge regarding the use of natural glasses as analogues for the long-term behavior of nuclear waste glasses. The information regarding important corrosion processes was obtained by studying a variety of naturally reacted glasses (tektites, obsidians, and basaltic) that had been recovered from a wide range of geologic environments and by experimentally studying the water/glass interactions under controlled laboratory conditions. The understanding of glass behavior and the effects of reaction environments has also advanced through analysis of the data reported in the literature. From these studies, it became clear that the conditions specific to an unsaturated repository may be quite different from the natural conditions under which naturally occurring basalt glasses have been altered. Consequently, the data from studying naturally occurring glasses may not be directly applied to project the long-term behavior of waste glass. Nonetheless, natural analogue studies do provide a link to the repository conditions for those reaction processes that occur even in non-repository conditions.

Samples of natural obsidian and basalt glasses and nuclear waste glasses have been reacted in vapor hydration tests at 75°C and relative humidities (RH) of 95 and 100% for up to

[2]   J. H. Adair, H. G. Krarup, S. Venigalla, and T. Tsukada, *Mater. Res. Soc. Symp. Proc.* **432**, 101-112 (1997).

[3]   E. C. Buck and J. A. Fortner, *Ultramicroscopy* **67**, 69-75 (1997).

[4]   A. Abdelouas, J. L. Crovisier, W. Lutze, B. Grambow, J. C. Dran, and R. Müller, *J. Nucl. Mater.* **240**, 100-111 (1997).

[5]   J. A. Fortner, C. J. Mertz, and J. K. Bates, "Plutonium Alteration Phases from Vapor Hydration of Lanthanide Borosilicate Glass for Weapons Disposition: A TEM Study," Proc. of Microscopy and Microanalysis Meeting, Cleveland, OH, August 10-14, 1997, pp. 663-664 (1997).

7 years. Reacted samples have been microscopically examined to compare their alteration with that of the same natural glasses that occurred over long times by natural processes. Tests with obsidian glass resulted in the formation of birefringent layers identical to those formed in nature; the layers formed in nature are called "perelite." The extent of hydration was similar at both RHs. Reaction of synthetic basalt glass in vapor resulted in the formation of alteration layers at both RHs. The thickness and crystallinity depended strongly on the RH. In tests at 95% RH, the layer consisted of an amorphous gel layer, whereas in tests at 100% RH, the alteration layer consisted mainly of saponite clay, and no gel layer was detected. Naturally altered basalts have layers (called "palagonite") that contain both amorphous and crystalline phases.

The results of tests with obsidian and basaltic glass indicate that vapor hydration tests can be used to replicate (at least qualitatively) the corrosion behavior that occurs over many thousands of years in nature within a few years in the laboratory. The same test method can be used to forecast the long-term behavior of nuclear waste glasses under similar conditions. The alteration of the waste glasses was found to depend on not only RH but also glass composition. A glass made with SRL 131 frit and a PNL 76-68 glass, which both contain about 43 wt% SiO_2, were more reactive than SRL 165 glass, which contains about 52 wt% SiO_2. Analyses indicated that the alteration layers formed on all three glasses were primarily smectite clay, a phase that is also frequently observed on naturally reacted basalt. The similar alteration behavior of basalt and waste glasses suggests that the same fundamental processes control their corrosion. However, our studies also indicate that the reaction kinetics of a particular glass may be significantly affected by the reaction conditions and the composition of the glass selected.

C.   Drip Tests of Savannah River and West Valley Glasses

Unsaturated Glass Tests, designated the N2 tests, were initiated in February 1986 on actinide- and technetium-doped DWPF glass, SRL 165. These tests are still in progress and have been sampled intermittently during the ensuing period of over 10 years, with regular sampling at 26-week intervals since December 1993. Designed to simulate potential conditions at the proposed Yucca Mountain Repository, these tests combine slowly dripping, tuff-equilibrated groundwater (EJ-13 water) with a monolithic waste glass sample, sensitized 304L stainless steel, and water vapor. Test results are used to determine synergistic interactions possible in a compromised pour canister under unsaturated conditions. Semi-annual analyses of the leachate are performed to monitor release of glass components, including actinides. Details of the test procedure and test results can be found elsewhere.[6,7]

Particulate and colloidal materials released to solution are also analyzed by analytical transmission electron microscopy and by sequential filtering with alpha spectroscopy (for transuranic content). These combined data indicate that insoluble elements, including U, Pu, and Am, are incorporated into alteration phases as the glass reacts and are subsequently released with particulate or colloidal matter as the alteration products spall from the glass. Recent trends have

---

[6]   J. A. Fortner and J. K. Bates, *Mater. Res. Soc. Symp. Proc.* **412**, 205-211 (1996).

[7]   J. A. Fortner, S. F. Wolf, E. C. Buck, C. Mertz, and J. K. Bates, *Mater. Res. Soc. Symp. Proc.* **465**, 165-172 (1997).

shown that the releases of Pu and Am, while initially quite low compared to those of soluble elements (such as B and Np), eventually are accelerated as the alteration phases in which they are entrained spall from the glass surface and enter the test solution.[7] Ultimately, the release of these actinides will be determined by the transport of the particulates suspended in solution.

Figure III-1 shows the cumulative normalized mass release for B and Li in the vessel rinse from three N2 tests as a function of time. The normalized mass release rate is defined as

$$N_i = M_i/(\Delta t\; c_i\; A) \tag{2}$$

where M_i is the measured mass of element i in the leachate solution, c_i is its element fraction in the source glass, Δt is the time interval between tests, and A is the surface area of the glass monolith (1.36×10^{-3} m^2). The release of these elements is an important gauge of the glass corrosion, as they are not expected to form secondary phases, are not major components of the EJ-13 water, and are not present in the steel vessel. Negligible amounts of B and Li were measured in acid strip solutions. Normalized release values for these elements appear in Fig. III-1. Note the nearly identical behavior of these two elements, an indication that they are remaining in solution (dissolved) and are released from the glass congruently. Note also that, in the 8- to 10-year period, while the data from the three replicate samples may differ, the N2-10 sample releases both B and Li the fastest, and the N2-9 sample releases both elements the slowest. The differences in measured reaction rate are real and are reflections of the inherent variability in elemental release for this type of test over a 10-year period. Trends in technetium release follow those of B and Np. We are analyzing the technetium content of the source glass (from an archive sample) to allow direct comparison of normalized release rates for this element.
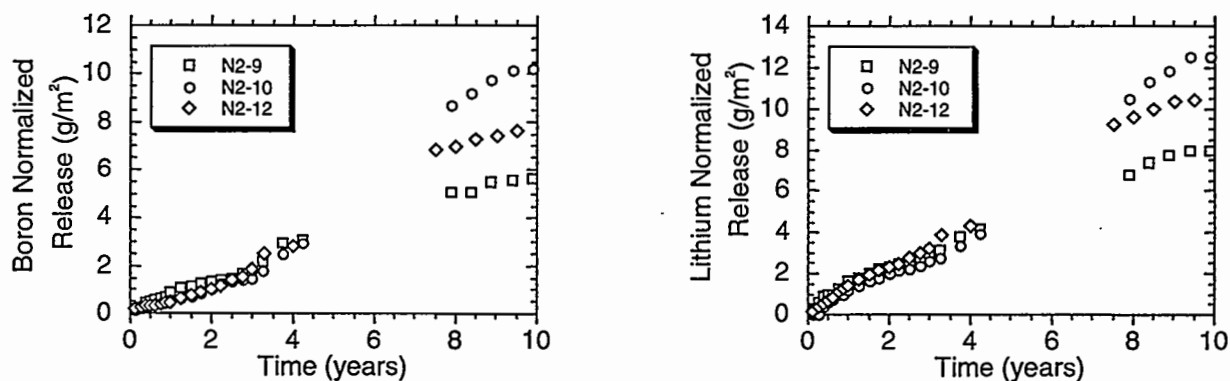
Fig. III-1. Normalized Cumulative Release of B and Li from
N2 Tests as Function of Elapsed Time

Unsaturated Glass Tests, designated the N3 tests, are also being conducted with an actinide- and technetium-doped WVDP glass, ATM-10. These tests were begun in July 1987 and remain ongoing with regular sampling at 26-week intervals. The ATM-10 glass is a former reference glass for the WVDP, and its composition differs only slightly from the present WVDP reference glass.

The WVDP-type glass used in the N3 test is unusual in that it contains a large amount of thorium relative to most other waste glasses. This element is found to concentrate in alteration phases.[6,8,9] The N3 tests continue to release thorium at the relatively low rate of 1.5 ($\pm$0.5) x 10^{-5}g/(m^2·day), about 100 times less than the normalized elemental release rates for B and Li (Table III-1). This low release rate suggests that the thorium alteration phases are mostly remaining with the waste package, although they have been observed in colloidal particles from the test solution.[8,9]

Table III-1. Normalized Release Rates for Selected Elements from N3 Test Series after 10 Years

Test Series	Normalized Release Rates,[a] g m^{-2}·day^{-1}						
	Li	B	Th	U	Np	Pu	Am
N3-9	4.0×10^{-3}	3.4×10^{-3}	1.3×10^{-5}	2.6×10^{-4}	9.6×10^{-4}	4.7×10^{-5}	3.0×10^{-5}
N3-10	1.8×10^{-3}	1.7×10^{-3}	2.1×10^{-5}	4.3×10^{-4}	6.6×10^{-4}	4.7×10^{-5}	2.2×10^{-5}
N3-12	2.6×10^{-3}	2.3×10^{-3}	1.1×10^{-5}	3.7×10^{-4}	4.9×10^{-4}	1.0×10^{-4}	3.6×10^{-5}

[a]Error is approximately $\pm$30% for each of the rates.

D.   Testing of Glass Waste Forms for Low-Level Waste

Long-term and accelerated tests are being conducted with several glasses similar to anticipated forms of immobilized low-activity radioactive waste (ILAW) for disposal of Hanford wastes. Results from these tests will provide data for the performance assessment of the Hanford disposal system, including development of glass corrosion models, measurement of model parameters, and characterization of the disposition of radionuclides as the glass dissolves. Tests to date have shown that sodium is released from candidate ILAW glasses faster than other glass components, probably through ion exchange. Long-term glass dissolution is currently modeled to be controlled by matrix dissolution reactions, which proceed at very low rates as dissolved glass components accumulate in solution. The observed preferential release of sodium raises the concern that highly soluble radionuclides could be released from the glass at a rate that is much higher than the matrix dissolution rate over extended periods at the low temperatures anticipated for a low-activity waste disposal system (about 20°C). Although the dissolution rate is quite low, this must be taken into account in the development of the glass corrosion model. The release behavior of ^{99}Tc is of particular interest because it was calculated to contribute the greatest dose to man in the preliminary assessment of the Hanford disposal system.[10]

To study the release behavior of technetium from a glass that is representative of likely ILAW forms for Hanford, we added NaTcO$_4$ to LD6-5412 glass and remelted the mixture to make a glass that we refer to as the "LD6Tc7" glass. Although the LD6-5412 glass will not be

[8] J. A. Fortner, T. J. Gerding, and J. K. Bates, *Ceram. Trans.* **61**, 455-462 (1995).

[9] J. A. Fortner, J. K. Bates, and T. J. Gerding, *Analysis of Components from Drip Tests with ATM-10 Glass*, Argonne National Laboratory Report ANL-96/16 (1997).

[10] F. Mann, *Impacts of Disposal System Design Options on Low-Level Glass Waste Disposal System Performance*, Westinghouse Hanford Company Report WHC-EP-0810, Revision 1 (1995).

used to immobilize waste, the release of technetium from this glass is assumed to be representative of its release from the silicate glasses with high soda contents being developed for waste immobilization. To facilitate analyses, the LD6Tc7 glass contained 0.18 wt% technetium, which is much more than can be present in waste forms meeting low-level (Class C) requirements. A series of MCC-1, product consistency, and vapor hydration tests is being performed with this glass to study the release of technetium under various conditions. The concentrations of technetium in solutions from 3-day MCC-1 tests conducted at 40 and 90°C were too low to be measured. In product consistency tests (PCTs) at 40 and 90°C, the normalized release of technetium was intermediate between that of Si and Na. While the dissolution rate of LD6-5412 glass increased significantly when alteration phases precipitated in PCTs at 90°C between about 3 and 6 months, similar phases have not yet formed in tests with LD6Tc7 glass under the same test conditions through 6 months. Long-term tests are ongoing. Vapor hydration tests at 200°C show that the same phases form during the corrosion of LD6-5412 and LD6Tc7 glasses. The altered glasses are being examined to characterize the release mechanism of technetium from LD6Tc7.

E. Testing of Spent Fuel

Spent nuclear fuel contained in an engineered barrier system surrounded by consolidated volcanic tuff is the current reference design for the potential repository at Yucca Mountain. This multiple barrier system will be designed to limit the radionuclide release from the spent fuel. Long-term tests with unirradiated UO_2 and spent fuel are in progress to determine the behavior of, and radionuclide release from, spent fuel under unsaturated conditions.

1. Unsaturated Tests with UO_2 Samples

The objective of this effort is to evaluate the reaction of unirradiated Zircaloy-clad UO_2 pellets after exposure to dripping EJ-13 water at 90°C. Results from these tests will be used to characterize the dissolution behavior of UO_2, formation of alteration phases, and rates and mechanisms of uranium release. The tests will also serve as a pilot study for drip tests with spent UO_2 fuel.

Drip tests on UO_2 pellets are continuing into their thirteenth year. These tests are being conducted in stainless steel vessels, with UO_2 pellets supported on a Teflon stand. Uranium release from UO_2 samples was rapid during the first 2 years of testing. This has been followed by lower release rates during the subsequent 10 years. The rapid release period correlated with an episode of preferential corrosion along UO_2 grain boundaries and spallation of micrometer- to sub-micrometer-sized UO_2 particles from the pellet surfaces. Scanning electron microscopy and optical examinations on two cross-sectioned samples revealed a reaction front that penetrated an average two to four grains into the pellets (~10 to 20 μm) ahead of the exposed pellet surface. This reaction front was variable, containing regions with little or no visible corrosion and regions with more extensive penetration (up to ten grains deep). After 2 years of reaction, the formation of a dense mat of U(VI) alteration phases enveloped the loosened UO_2 grains. This mat reduced the spallation of UO_2 particles, lowering the uranium release rates. Solution aliquots from the 11-12 year reaction interval were analyzed, and uranium concentrations were found to be similar to

values in previous samplings, when similar drip tests were conducted with stainless-steel support stands (instead of Teflon) and sampled for the 7-8 year reaction interval. The surfaces of the pellets show evidence of reaction products; however, these have not been identified yet. The surfaces and Zircaloy cladding have yellow-green coatings, consistent with previous samples that had alteration layers of dehydrated schoepite, $UO_3 \cdot 0.9H_2O$.

Another test method is being developed to measure the solution composition in contact with spent fuel during the reaction processes important in the drip tests. This information is needed as input for model development and confirmation. Development of the preliminary test method is being done with UO_2; these tests are given the name "petri-dish tests" (PDTs). These experiments are designed to help understand the reactions that occur in the thin water film that forms on the surfaces of UO_2 and spent fuel in drip tests. The PDTs are batch tests that are run at 90°C in stainless steel vessels (45 mL) with a small amount (0.5 mL) of EJ-13 water on the bottom. A small amount (0.2 g) of UO_2 powder is placed on a stainless-steel screen attached to a steel hanger and lowered into the vessel. The water is wicked through the screen and onto the powdered sample, where it forms a thin film. Preliminary results from the PDTs, conducted with unirradiated UO_2, indicate that small changes in solution compositions can be observed and correlated with solid uranium-bearing alteration products that form on the surface of the UO_2.

Several PDTs were conducted with and without a small amount of H_2O_2 added (0.1 $\underline{M}$) to the EJ-13 water. This addition was intended to mimic the increased oxidation potential associated with radiolytic products formed in drip tests on spent fuel. Phases identified in the PDTs include metaschoepite, dehydrated schoepite, soddyite, uranophane, and (possibly) sodium-compreignacite. These are the same phases found in drip tests on UO_2. In addition to our apparent success in reproducing the alteration products and phase paragenesis observed in the drip tests, reactions in the PDTs also appear to be accelerated somewhat. The UO_2 samples in tests with H_2O_2 added reacted faster than samples in either the drip test or the PDT without H_2O_2 and precipitated dehydrated schoepite rather than metaschoepite. Also, the dissolved concentrations of uranium in the tests with H_2O_2 were higher than in tests with unmodified EJ-13 water, and the pH values were lower. Lower pH may reflect increased corrosion of steel in tests with H_2O_2. A lower pH would also lead to enhanced UO_2 oxidation and dissolution. Results from the PDTs continue to be analyzed.

2.   *Unsaturated Tests with Spent Fuel Samples*

Spent fuel is being tested under unsaturated conditions at 90°C to evaluate its long-term behavior in the potential repository at Yucca Mountain. The tests are on two commercial irradiated UO_2 fuels, ATM-103 and ATM-106, from a pressurized water reactor. The EJ-13 leachant was produced by reaction of water from well J-13 with Yucca Mountain tuff for approximately 80 days at 90°C. The tests monitor the dissolution behavior of the spent fuel matrix, the release rate of individual radionuclides, the form in which the radionuclides are released, and the mode of reaction. Examined this past year were the amounts of plutonium in colloidal form and the potential for thin-film flow in drip and vapor tests, respectively.

For drip tests at high rates (0.75 mL/3.5 days), plutonium retention in colloids collected in the leachate in the test intervals between 1.6 and 3.7 years was examined, and the results are

summarized in Table III-2. At most test intervals, the amount of plutonium released is greater for the ATM-103 fuel, and a large fraction of this material (about 30% on average) is in a colloidal form. The amount of plutonium released for the ATM-106 fuel is as much as two orders of magnitude less than that for the ATM-103 fuel, and the average fraction that is in colloidal form is about 10%. The composition of the colloids is unknown, but a goal of future work is to determine their composition since colloidal transport has been identified as an important release pathway at the Yucca Mountain site.

Table III-2. Percentage of Released Plutonium in Colloidal Form from High-Drip-Rate Tests[a]

Interval, yr	ATM-103		ATM-106	
	Colloids, ng	Percentage	Colloids, ng	Percentage
1.6	20	68	0.3	24
2.1	0.2	21	0.06	6
2.6	0.05	8	0.05	3
3.1	30	35	0.06	10
3.7	0.4	15	0.002	0.3

[a]The burnups are 30 MW·d/kg U for ATM-103 and 45 MW·d/kg U for ATM-106.

In the vapor test, the calculated amounts of radionuclides transported by thin-film flow were compared to the measured amounts after 3.7 years of reaction. The calculated amounts were based on the minimum thin-film flow rate (7.5 x 10^{-7} L/d) for a Van der Waals liquid on quartz multiplied by the expected concentration in a drop of liquid. The drip concentrations for Tc, U, and Sr in the vapor tests after 3.7 years were represented by the radionuclide concentrations found early in the high-drip-rate tests, before excess Na and Si appear in solution.

Table III-3 presents the measured amounts of transport for Tc, U, and Sr and the calculated amounts (range for low and high concentrations). In all cases, the measured amount of radionuclide transported was greater than, or about equal to, the lower range for the calculated values. This result is evidence of the importance of thin-film flow as a transport pathway for release of radionuclides. This result will be verified with tests done using different fuel types.

3. Characterization of Reacted Spent Fuel Samples

Analytical transmission electron microscopy (AEM) is a versatile technique for examining the microstructure of corroded spent fuel. During AEM examination of corroded ATM-103 from both the vapor and high-drip-rate tests, we found regions that possessed anomalously high concentrations of plutonium (see Fig. III-2). The enrichment of plutonium in

Table III-3. Experimental Evidence for Thin-Film Transport in Vapor
Tests at 3.7-yr Interval

	Measured Thin-Film Transport, g		
	Tc	U	Sr
ATM-103	2×10^{-7}	7×10^{-9}	3×10^{-9}
ATM-106	6×10^{-10}	3×10^{-8}	3×10^{-9}
	Calculated Thin-Film Transport,[a,b] g		
	Tc	U	Sr
Low Range	2×10^{-10}	4×10^{-9}	2×10^{-11}
High Range	2×10^{-7}	4×10^{-7}	2×10^{-9}

[a]The minimum thin-film flow rate is 7.5×10^{-7} L/d.
[b]The steady-state concentrations in the high-drip-rate tests
were assumed to be representative of those in the vapor tests.
The concentrations were as follows: Tc (10^{-8} to 10^{-5} $\underline{M}$),
U (10^{-7} to 10^{-5} $\underline{M}$), and Sr (10^{-8} to 10^{-6} $\underline{M}$).
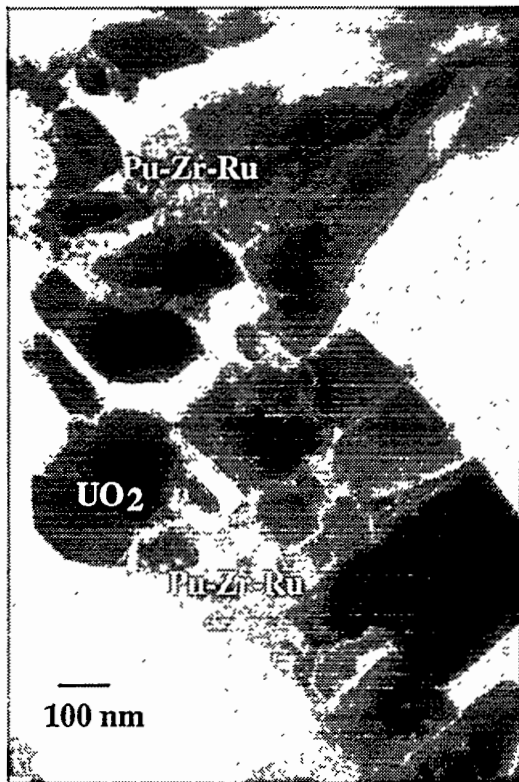
Fig. III-2.

Transmission Electron Microscopy
Image of Plutonium-Rich Regions in
Vapor Test of ATM-103

these regions far exceeded those reported in the uncorroded fuels.[11] X-ray energy dispersive analysis indicated significant amounts of Zr and Ru in these regions. The source of the zirconium is probably the fuel cladding, although the spent fuel does contain zirconium as a fission product. Electron energy loss spectrometry (EELS) indicated anomalously low concentrations of rare earths. From microstructural analysis of European high-burnup fuels, Kleykamp et al.[12] have reported the existence of a perovskite-type phase [Ba(U,Pu,Zr,Mo)O$_3$]; however, these types of phases have not been identified in low-burnup fuels from pressurized water reactors.[11] Although the perovskite phase has not been reported in low-burnup fuels, its existence in these fuels at the tens of nanometer scale cannot be ruled out. Therefore, it is not possible to conclude that the plutonium-enriched regions in the ATM-103 sample were produced during oxidative corrosion of the fuel.

Burns et al.[13] have reported the possibility of the substitution of Pu$^+$ for U^{6+} or the substitution of Pu^{4+} into uranyl oxide hydrates (particularly ianthinite) and uranyl silicates during testing of spent fuel samples. In the high-drip-rate tests, pseudomorphic transformation of the spent fuel (UO$_2$) to uranyl phases would probably require isomorphic substitution of plutonium for uranium sites in uranyl phases. To date, we have not found evidence for this substitution; however, we do have supporting evidence for the accumulation of plutonium into discrete areas in the corroded fuel. Regardless of their origin, the presence of enriched regions of plutonium suggests that, if these regions become friable, plutonium-bearing colloids could be released. The AEM technique will continue to be exploited for analysis of the reacted spent fuel samples.

F.   Immobilization of Plutonium

Several alternatives are being considered by DOE for the long-term disposal of surplus plutonium resulting from the dismantlement of nuclear weapons and the cleanup of weapon production sites. One such alternative is immobilization, where the plutonium would be fixed into a glass or ceramic waste form that meets safety and security objectives. Argonne is participating in the Fissile Materials Disposition (MD) Program by (1) characterizing a ceramic waste form being developed at Lawrence Livermore National Laboratory (LLNL), (2) corrosion testing of the ceramic material prepared at LLNL, and (3) corrosion testing of plutonium-loaded glasses prepared at Westinghouse Savannah River, Pacific Northwest National Laboratory, and Argonne National Laboratory. Our task this past two years was to provide characterization and corrosion data to the MD program so that an informed choice could be made between glass and ceramic. The DOE has decided that ceramic will be the preferred material for the immobilization of excess plutonium. Our focus now is to obtain data that will advance our understanding of the corrosion mechanism of the ceramic form.

---

[11] R. J. Guenther, D. E. Blahnik, T. K. Campbell, U. P. Jenquin, J. E. Mendel, L. E. Thomas, and C. K. Thornhill, *Characterization of Spent Fuel Approved Testing Material—ATM-103,* Pacific Northwest Laboratory Report PNL-5109-103 (1988).

[12] H. Kleykamp, J. O. Paschoal, R. Pejsa, and F. Thommler, *J. Nucl. Mater.* **130**, 426-433 (1985).

[13] P. C. Burns, R. C. Ewing, and M. L. Miller, *J. Nucl. Mater.* **245**, 1 (1997).

1. Ceramic Characterization

A titanate-based ceramic waste form, rich in phases structurally related to zirconolite and pyrochlore, is being developed for immobilizing excess plutonium. As part of this program, LLNL has produced several ceramics that are being characterized at ANL. The plutonium-loaded ceramics contain a number of titanate-based phases, such as zirconolite, brannerite, and rutile. However, other types of phases have been found, including perovskites and undissolved plutonium as PuO_{2-x}. Analytical transmission electron microscopy has been used to determine the plutonium oxidation state in the zirconolite.

The oxidation state of the plutonium in a zirconolite phase was determined with an EELS technique described by Fortner and Buck.[14] The value obtained from the zirconolite phase (Fig. III-3) indicated that its plutonium may be a mixture of Pu^{4+} and Pu^{3+}. The Pu-$N_{4,5}$
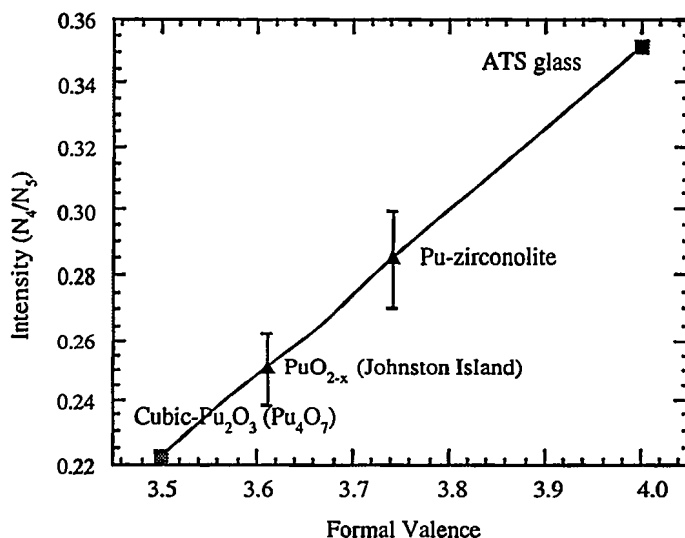
Fig. III-3. Plot of N_4/N_5 Intensities and Formal Valences for Various Plutonium-Bearing Phases. The plutonium valence in plutonium-bearing zirconolite was determined from the ratio of the intensity of N_4-to-N_5 "white lines" and the line drawn between two reference points: alkali-tin-silicate (ATS) glass and reduced plutonium oxide present in the ceramic waste form (+3.5).

absorption edges exhibit sharp "white line" transitions in the EELS spectrum, and these $4d_{3/2} \rightarrow 5f_{5/2}$ (N_4) and $4d_{5/2} \rightarrow 5f_{7/2}$ (N_5) transitions were used to determine the chemical state of the plutonium in the zirconolite. The ratio of N_4/N_5 absorption edges for a range of other actinide-bearing phases, as well as other plutonium phases, was found to decrease with increasing $5f$-orbital occupancy. In the plot shown in Fig. III-3, the alkali-tin-silicate glass was determined by

[14] J. A. Fortner and E. C. Buck, Appl. Phys. Lett. 68, 3817-3819 (1996).

optical methods to contain only Pu^{4+}. The plutonium oxide was assumed to be in the +3.5 state, based on electron diffraction analysis of this phase; this suggested that it was Pu_4O_7, which is sometimes referred to as "cubic-Pu_2O_3." The N_4/N_5 ratio from a partially reduced plutonium oxide obtained from contaminated soil taken in the Johnston Island is also shown in Fig. III-3 for comparison.

Although this procedure apparently allows determination of the plutonium oxidation state, the $N_{4,5}$ edges are complicated by multiple scattering, multiple effects, and interactions between the bound states and the continuum. This method is still undergoing evaluation for determining the plutonium oxidation state.

2. Glass Testing

Static dissolution testing (MCC-1, product consistency, and vapor hydration tests) is being performed with two plutonium-doped glasses (LaBS, a lanthanide borosilicate glass, and P5, an alkali-tin-silicate glass) at S/V ratios from 10 to 20,000 m^{-1}. The objective is to determine the extent of corrosion and the disposition of plutonium.

The dissolution rate, based upon boron, for LaBS and P5 glasses obtained from the MCC-1 tests (3 days at 90°C and S/V = 10 m^{-1}) indicates that the leach resistance of the LaBS glass is very similar to that of the P5 glass, 0.8 ± 0.1 and 1.1 ± 0.1 g/(m^2·day), respectively. Figure III-4 compares the corrosion behavior from PCT-B (90°C and 20,000 m^{-1}) between LaBS and P5 over 182 days. While normalized mass loss values for B and Si indicate that the LaBS glass is more durable than the P5 glass, the NL(Pu) values from LaBS are approximately an order of magnitude greater than those for the P5 glass. The Pu and Gd are dissolved nearly congruently from both glasses (see Fig. III-4b). The extent of corrosion in the glasses from vapor hydration tests (exposure to humidified air at 200°C for up to 56 days) indicates that the hydration of the LaBS occurs more rapidly than the ATS glass. In these tests, the crystalline alteration phases (plutonium-rare earth-silicates) that formed on the glass surface were found to segregate the plutonium and rare earth elements in the LaBS. Alteration layers on the P5 glass reacted under vapor hydration conditions were very thin and similar in composition to the unreacted glass, indicating a hydrated glass alteration layer. Additional long-term PCT-B tests continue, although early results suggest that the LaBS composition is not as leach resistant for Pu and Gd as the P5 composition.

3. Ceramic Testing

Titanate ceramics have been developed for incorporation of a wide variety of radioactive materials. Most recently, titanate ceramic was selected as the immobilization material for disposition of surplus plutonium. The advantages of titanate ceramics include their ability to accept various cations as substitutions within its structure and their high resistance to aqueous corrosion. Ceramics formulated at LLNL as part of the MD program are composed primarily of zirconolite ($CaZrTi_2O_7$). We performed a suite of static corrosion tests to investigate different aspects of the corrosion behavior of the plutonium-loaded ceramic. Our results from ceramics
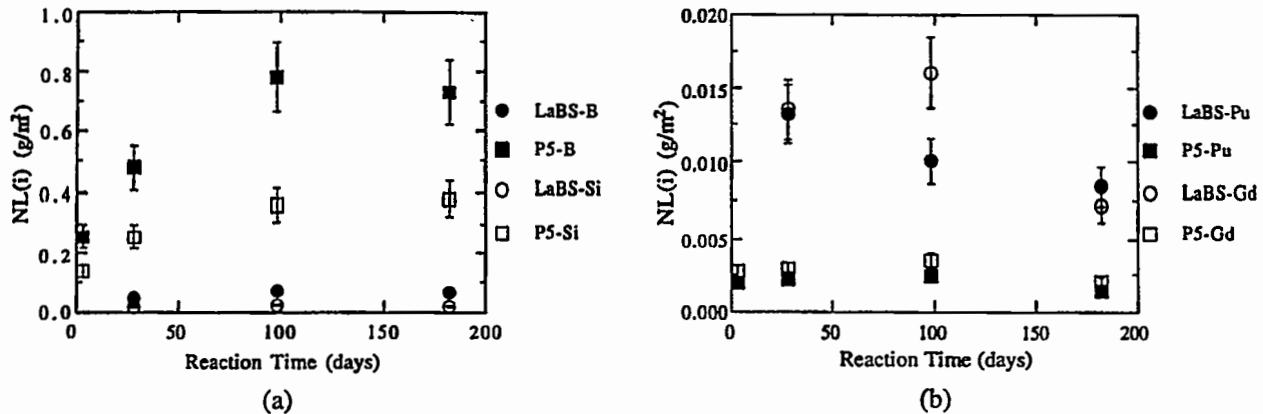
Fig. III-4. Normalized Mass Loss for (a) Boron and Silicon and (b) Plutonium and Gadolinium from LaBS and P5 Glasses in PCT-B

were compared with similar results from tests with the plutonium-doped glass with the intent that one candidate waste form would be selected.

Results from MCC-1 tests (3 days at 90°C and 10 m^{-1}) were used to estimate the initial corrosion rate of the ceramic and showed that the corrosion was nonstoichiometric. The following normalized release rates were measured [units of g/(m^2·day)]: Ca, 0.1; Zr, 0.004; Ti 0.0004; Pu, 0.004; and Gd, 0.01. These results show that each element is released at a different rate during MCC-1 tests. Release rates calculated from PCT-A results (7 days at 90°C and 2000 m^{-1}) are lower than the release rates calculated from MCC-1 tests and range from 0.00002 g/(m^2·day) for titanium to 0.005 g/(m^2·day) for calcium. These results indicate that the more concentrated solutions in PCT-A tests slow the release of all elements from this ceramic. We believe that the differences in release rates for the different elements reflect differences in release processes and elemental solubilities.

We will continue to test ceramics developed for the MD program during the next year. The ceramic composition currently being developed contains hafnium instead of zirconium and contains pyrochlore [Ca(Zr, Hf)Ti$_2$O$_7$] as the major phase.

G.   Development, Characterization, and Testing of Various Waste Forms

1.   Development of Test Method for Product Acceptance

Several sites in the DOE complex are interested in privatizing the immobilization task for tank wastes. The immobilized low-activity waste (ILAW) forms produced will be required to meet contractual product specifications to ensure their suitability for handling and disposal. A standard product acceptance test (PAT) and standard material that will allow quantitative determination of test accuracy are required. To meet these needs, we have developed a test method and formulated a glass (Low Activity Reference Material-1, LRM-1) to be used as a

standard material in that test. The glass was formulated to be similar in composition to ILAW forms for Hanford and other DOE sites.

The bulk composition of the glass was determined by analyses with inductively coupled plasma/mass spectrometry, inductively coupled plasma/atomic emission spectroscopy, and ion chromatography. The microstructure of the glass was examined with scanning electron microscopy and transmission electron microscopy to verify that the phases in the glass had not separated, and that no phases had precipitated in the glass. Several properties of the glass were measured to assess its compliance with requirements specified by Hanford and its possible use as a test standard. Although LRM-1 is intended only as a standard for the PAT, it may later be developed as a standard for the measurement of other waste form requirements. The density of the glass was measured by buoyancy to be 2520 kg/m^3; the average leachability index for sodium was measured to be 15.4 ± 0.1; and the compressive strength was measured to be 226 ± 57 MPa. These values are well within the acceptance levels for Hanford ILAW.

We have subjected LRM-1 glass to replicate dissolution tests to determine the effects of key test parameters on the mean and variance of the glass response. The glass was subjected to replicate tests in a matrix designed to determine the effects of temperature (20, 40, and 70°C), glass/water mass ratio (1:10 and 1:1), and test duration (3 and 7 days) on glass response. On the basis of the test results, we have recommended that the PAT be conducted for 7 days at a glass/water mass ratio of 1:10 and 40°C. These parameters will result in a reproducible test that is run under conditions relevant to the qualification of ILAW. The LRM-1 glass is suitable for use as a standard test material in determining product acceptance. A round-robin test program will be conducted by ANL to measure the interlaboratory reproducibility of the test when conducted with LRM-1 glass. The test method will be submitted to the American Society for Testing and Materials for standardization.

2.   Qualification Testing of Ceramic Waste Form

Glass-bonded zeolite (referred to as the "ceramic waste form") is being developed as a potential waste form for the long-term disposal of fission product and transuranic elements associated with the electrometallurgical treatment of spent nuclear fuel (Sec. IV). The goal is to provide qualification testing and associated activities that may be applied toward acceptance of this ceramic waste form into the Civilian Radioactive Waste Management System.

The qualification testing will require investigations of the long-term corrosion behavior of the ceramic waste form, with emphasis on repository-relevant durability testing. We have provided technical information about testing methodology and aided in the development of a testing program that will be used to ascertain the corrosion behavior of the ceramic waste form in a geologic repository.

Initial vapor hydration, product consistency, and MCC-1 tests with durations up to 364 days have been completed with glass-bonded zeolite containing waste constituent components. Three leachants were tested: deionized water, EJ-13 well water, and a Mg-Na-K-Cl brine. The samples had the greatest amount of glass corrosion in the deionized water, but the Mg-Na-K-Cl brine created the greatest release of fission products. The effects of the

Mg-Na-K-Cl brine may be related to the dependence of zeolite retention on pH. The results from tests with EJ-13 were similar to those from tests with deionized water.

Along with the standard durability tests, methodologies were developed to characterize both the short- and long-term behavior of the ceramic waste form with relatively short duration tests to provide useful information for evaluating the overall behavior. It was concluded that these methodologies are sufficiently sensitive to allow determination of the behavior of different waste constituents and comparison of the products that are produced with different processes.

The effects of water washing were investigated to determine whether there is a problem with the premature release of accessible free salt during the preparation of the ceramic samples. The results from these investigations indicated that washing with deionized water removes significantly more salt compared to ethanol, such that the use of water in the sample preparation processes should be limited or eliminated, and that the wash times with ethanol should be minimized for maximum salt retention in the ceramic waste form.

A large suite of qualification tests will be initiated with the ceramic waste form and constituent components during the next two years. This work will focus on the reference ceramic waste form being developed for the EBR-II fuel conditioning project at ANL-West. The reference ceramic waste form will contain two or more distinct phases, with sodalite being the primary crystalline component.

3.   *Transmutation Effects in Crystalline Waste Forms*

This work is carried out by a team from two national laboratories who will be determining the effects of transmutation in samples of ^{137}Cs-bearing pollucite $(CsAlSi_2O_6)$ obtained from a French company. These samples are unique in that the pollucite was made with various amounts of ^{137}Cs, which was then sealed in welded stainless-steel capsules to be used as tumor irradiation sources. Over the past 18 years, the ^{137}Cs has been decaying to stable barium in the absence of atmospheric effects. We are studying this material as an analogue to crystalline waste forms in which a transmutation such as this could possibly disrupt the integrity of the original ceramic waste form.

Work this year consisted of determining the construction of the capsules and state of the pollucite in the absence of details about the pollucite preparation. We have opened one capsule containing nonradioactive pollucite. The information on the construction of the stainless-steel capsule is useful for the work that we are preparing to do on capsules containing radioactive pollucite. Microscopic characterization (electron energy loss spectroscopy and energy dispersive X-ray spectroscopy) of the nonradioactive pollucite revealed two compounds in addition to pollucite: cesium silicate and a cesium aluminosilicate $(CsAlSiO_4)$. These compounds may complicate the interpretation of the X-ray absorption spectroscopy results that are used to characterize the pollucite in unopened capsules. Preparations have been started to study the radioactive samples at the Stanford Synchrotron Radiation Laboratory. Our calculations show that, by thinning the base of the capsules, we should be able to obtain about a factor of ten increase in the fluorescence signal. Procedures are in place for thinning capsules containing the radioactive pollucite and examining the samples at Stanford.

We have investigated the stability of pollucite to β-radiation damage by use of 200 keV electrons in the transmission electron microscope. The samples investigated became amorphous in about 10 min. This is equivalent to many more years of β-radiation damage than under normal decay of the ^{137}Cs. In fact, the dose was equivalent to several thousand years of normal radiation damage from the decay of ^{137}Cs. Of course, there would not be any ^{137}Cs remaining after that period of time because the half-life of ^{137}Cs is 30 yr. Additional work with less intense beams or in an ion accelerator will be performed next year to better simulate the damage to the pollucite crystal structure from the decay of cesium to barium.

4. Pretreatment of Radioactive or Mixed Waste Vitrification Feeds

Vitrification has been selected as a final waste form technology in the U.S. for long-term storage of high-level radioactive wastes. The presence in high concentrations of certain elements (e.g., transition metals) in the high-level waste may cause unwanted crystalline material in the final glass product. This may be a problem during vitrification at some DOE sites. The formation of spinel compounds, such as Fe_3O_4 and $FeCrO_4$, may result in devitrification and would reduce the lifetime of the melter used in vitrification. A superconducting, open-gradient, magnetic separation (OGMS) system is being developed at ANL for the removal of the deleterious transition elements (e.g., Fe, Co, and Ni) and other elements (actinides) from vitrification feed streams. This system exploits the ferromagnetic or paramagnetic nature of these elements and is designed to deflect and collect paramagnetic minerals on the basis of the mineral interactions with a magnetic field gradient. This system has the potential to reduce significantly the volume of high-level waste for vitrification and ensure a stable product. Design of an efficient superconducting OGMS system requires a fundamental understanding of the physical and chemical properties of the waste feed streams. Both simulated and radioactive samples of fly ash and sludge from the Savannah River, Rocky Flats, and the Hanford sites are being studied with several techniques to characterize and predict the separation capability and limitations of a superconducting OGMS system.

5. Microscopic Radiation Damage in Waste Forms

The objective of this new cooperative research between the Chemistry Division and CMT is to conduct fundamental research on the nature of the electronic interaction and the chemical bonding properties of radionuclides in analogue waste forms. The work at CMT includes investigation of microscopic effects of radiation damage in crystalline and glass waste forms with state-of-the-art analytical electron microscopy (AEM) téchniques.

During the past year, single crystals of $LuPO_4$ doped with ^{244}Cm (III) (half-life of 18.1 years) were examined with AEM. The crystals, which are structural analogues for proposed ceramic waste forms, had been doped with ^{244}Cm at a concentration of ~1 wt% about 17 years ago. Electron microscope images indicated that the majority of the waste matrix remained intact, although electron diffraction analysis indicated that an amorphous phase was present. Moreover, nanometer-sized bubbles were frequently observed within crystals, which may be related to local segregation of gaseous He or O species that were generated during decay of ^{244}Cm. These results provided new insights into the metamictization of crystalline materials containing radionuclides.

Our current effort is focused on determination of the structure and elemental species in the crystalline domains and the amorphous region. The goal is to achieve a clear understanding of the microscopic nature of radiation damage and its effects on the long-term behavior of high-level waste forms.

IV

Separation Science and Technology

The Division's work in separation science and technology during the past year was in two areas:

- Treatment of radioactive, mixed, and hazardous waste
- Substitution of low-enriched for high-enriched uranium in the production of ^{99}Mo

The major activity in the waste treatment area involves R&D on solvent extraction processes for the cleanup of acidic and alkaline nuclear waste solutions. In another project, we are assisting in the development of an evaporator/concentrator system for treating low-level radioactive waste at the Savannah River Site. We also continue to provide technical support for the Waste Management Organization at ANL.

The largest R&D effort being pursued is development of low-enriched uranium targets and processing methods for production of ^{99}Mo for use in medical diagnostic applications. In this activity, we are working to convert all current processes, worldwide, that use high-enriched uranium to low-enriched uranium.

A. Solvent Extraction Technology

Although our separation science and technology activities have broadened into other areas, solvent extraction R&D remains a significant fraction of our development work. Work during the past year was focused on advising engineers at Idaho National Engineering and Environmental Laboratory (INEEL) on their demonstration of the SREX (Strontium Extraction) process on actual high-level waste stored at the site. (The SREX process was invented by researchers in the Chemistry Division at ANL.) The demonstration was conducted with a 24-stage centrifugal contactor built at ANL. After the test runs, the GTM (Generic TRUEX Model) and its SASSE (Spreadsheet Algorithm for Stagewise Solvent Extraction) module were used as a means to better understand the test results. We also provided engineering and modeling

support and tested a flowsheet for researchers at Oak Ridge National Laboratory for the SRTALK (Strontium and Technetium Extraction for Alkaline Solution) process.

1. Demonstration of SREX Process

We provided support for INEEL researchers at the Idaho Chemical Processing Plant as they tested the SREX process using sodium-bearing waste from tank WM-183. The SREX test with actual nuclear waste was demonstrated with the flowsheet shown in Fig. IV-1. The test was done in a 24-stage "minicontactor" (2-cm rotor), which was designed, built, and tested at Argonne. The minicontactor is now located in a shielded-cell facility at Idaho, where actual sodium-bearing waste can be easily obtained for flowsheet tests. The SREX solvent composition for the test was 0.15 $\underline{M}$ bis-4,4'(5')[(*tert*-butyl)cyclohexano]-18-crown-6 (CE) and 1.5 $\underline{M}$ tributyl phosphate (TBP) in Isopar®L. The ^{90}Sr in the sodium-bearing waste feed was removed by the solvent in the extraction section (stages 1-10). In the scrub section (stages 11-12), other components in the solvent were washed back by the scrub feed. In the first strip section (stages 13-16), dilute acid stripped ^{90}Sr out of the solvent, as well as any potassium. In the second strip section (stages 17-20), a complexant (ammonium citrate) stripped lead and actinides from the solvent. Finally, in the wash section (stages 21-24), the solvent was reacidified so that it could be recycled to stage 1. In this test, because the availability of the waste solution was limited, the SREX solvent was not recycled.
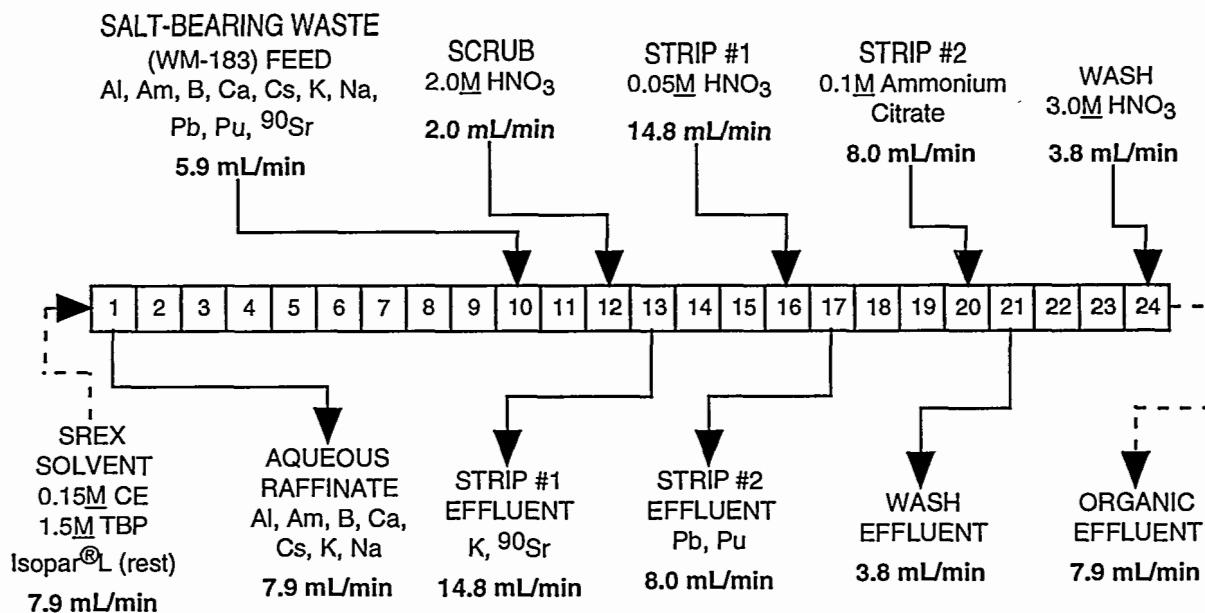
Fig. IV-1. The SREX Flowsheet Tested with Tank Waste at INEEL

Our review of the hot SREX demonstration at INEEL determined that the test went very smoothly, with 99.995% of the ^{90}Sr being removed from the aqueous raffinate. With this removal efficiency for ^{90}Sr, the activity of ^{90}Sr was reduced from 201 to 0.0089 Ci/m^3, which is well below the Nuclear Regulatory Commission's limit for Class-A low-level waste of 0.04 Ci/m^3 (1.48 x 10^9 Bq/m^3) for ^{90}Sr. Analysis of the stage-to-stage strontium data showed that the

minicontactor worked well. The mass-transfer efficiency was 97% in the extraction section and 98% elsewhere. About 5% of other elements (Ba, Cd, K, Pb, Pu, Zr, and probably U) were extracted along with the ^{90}Sr. While these elements have low concentrations and will not hinder the separation of ^{90}Sr from the nitrate salts in the tank waste, the effect of their presence needs to be addressed to ensure that they do not pose any problems downstream of the SREX process. The successful operation of the SREX process in the minicontactor with actual Idaho waste indicates that a full-scale plant for processing this waste would also work well.

2.   Demonstration of SRTALK Process

Over the past year, we have been working with Oak Ridge National Laboratory (ORNL) and Pacific Northwest National Laboratory (PNNL) on the SRTALK (Sr, Tc, and Cs alkaline-side extraction) solvent-extraction process. This process is able to separate alkali-metal pertechnetate salts from alkaline supernate that comes directly from nuclear waste tanks. It could replace ion-exchange columns that are currently planned to remove pertechnetate from alkaline wastes. The two key advantages of the SRTALK process over ion exchange are that the technetium is recovered (1) free of the other salts in the tank supernate and (2) without any added chemicals (e.g., tin, ethylene diamine) required to strip technetium from the ion-exchange columns. These factors would greatly reduce the number of glass cannisters subsequently generated for waste disposal and potentially reduce the overall cost of waste disposal. The SRTALK solvent, which consists of 0.04 $\underline{M}$ CE and 1.8 $\underline{M}$ TBP in Isopar®L, extracts technetium from the feed with a distribution ratio of 6 to 10 and can be subsequently stripped of technetium with water or dilute nitric acid.

The SRTALK concept was first demonstrated in a test tube. Then, we developed a 12-stage process flowsheet and tested it in a minicontactor. The final flowsheet, shown in Fig. IV-2, has a scrub section so that the aqueous strip effluent is free of the other salts in the tank supernate and employs 0.01 $\underline{M}$ HNO_3 to strip the technetium so that the strip effluent is essentially free of added chemicals. In addition, use of a low organic-to-aqueous (O/A) flow ratio in the extraction section and a high O/A flow ratio in the strip section increases the technetium concentration in the strip effluent by a factor of 10 compared with that in the aqueous feed. At the same time, the decontamination factor for technetium in the aqueous raffinate is kept >6.4, as required.

As part of this work, we correlated technetium extraction data from ORNL and, using analytical mathematical techniques developed at CMT, developed the SRTALK flowsheet. Then, the alkaline conditions required for this flowsheet were evaluated with both dispersion-number tests and hydraulic-performance tests in a single-stage minicontactor. Finally, the SRTALK flowsheet was tested in a multistage contactor with a simulated tank waste. The technetium results (both calculated and measured), given in Fig. IV-3, show that the ^{99}Tc concentration of 6 x 10^{-5} $\underline{M}$ in the extraction feed to stage 5 is reduced by a factor of ten, to 6 x 10^{-6} $\underline{M}$, in the extraction effluent at stage 1. At the same time, the ^{99}T concentration in the strip effluent from stage 8 is 6 x 10^{-4} $\underline{M}$, an increase by a factor of ten from its concentration in the extraction feed. Thus, this test of the process flowsheet was very successful at both removing and concentrating the ^{99}Tc. Work for the next year will focus on adding Cs and possibly Sr extractability to the SRTALK process.

SIMULATED ALKALINE TANK
SUPERNATE FEED
Al, K, Na, NO$_3$, OH, ^{99}Tc

20.6 mL/min

SCRUB
0.5$\underline{M}$ NaOH

4.4 mL/min

STRIP
0.01$\underline{M}$ HNO$_3$

1.93 mL/min

| 1 | 2 | 3 | 4 | 5 | 6 | 7 | 8 | 9 | 10 | 11 | 12 |

Extraction (1-5)   Scrub (6-7)   Strip (8-12)

SRTALK
SOLVENT
0.04$\underline{M}$ CE
1.8$\underline{M}$ TBP
Isopar$^®$L (rest)
8.0 mL/min

AQUEOUS
RAFFINATE
Al, K, Na, NO$_3$, OH
25.0 mL/min

STRIP
EFFLUENT
^{99}Tc
1.93 mL/min

USED
SRTALK
SOLVENT
8.0 mL/min
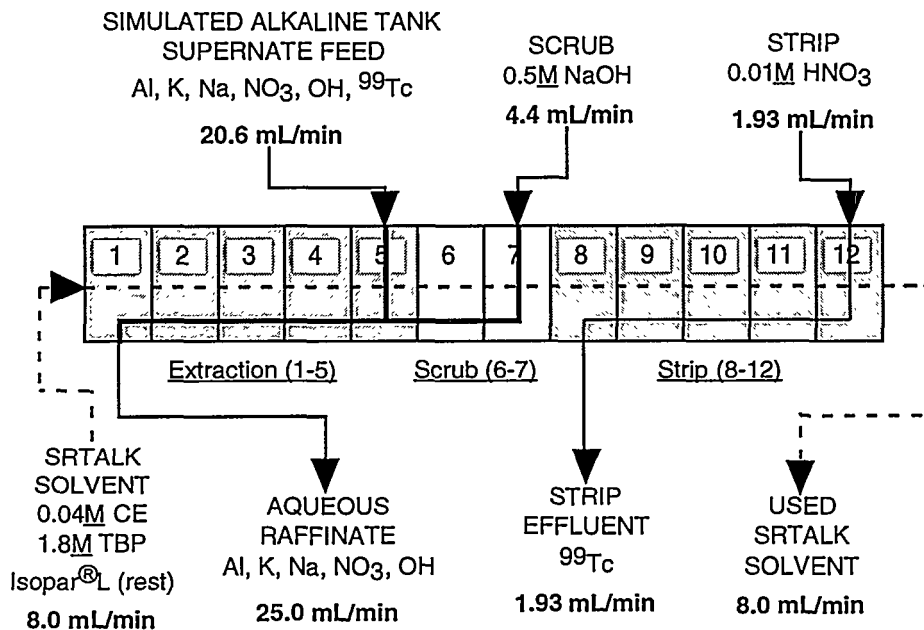
Fig. IV-2. Flowsheet for SRTALK Demonstration
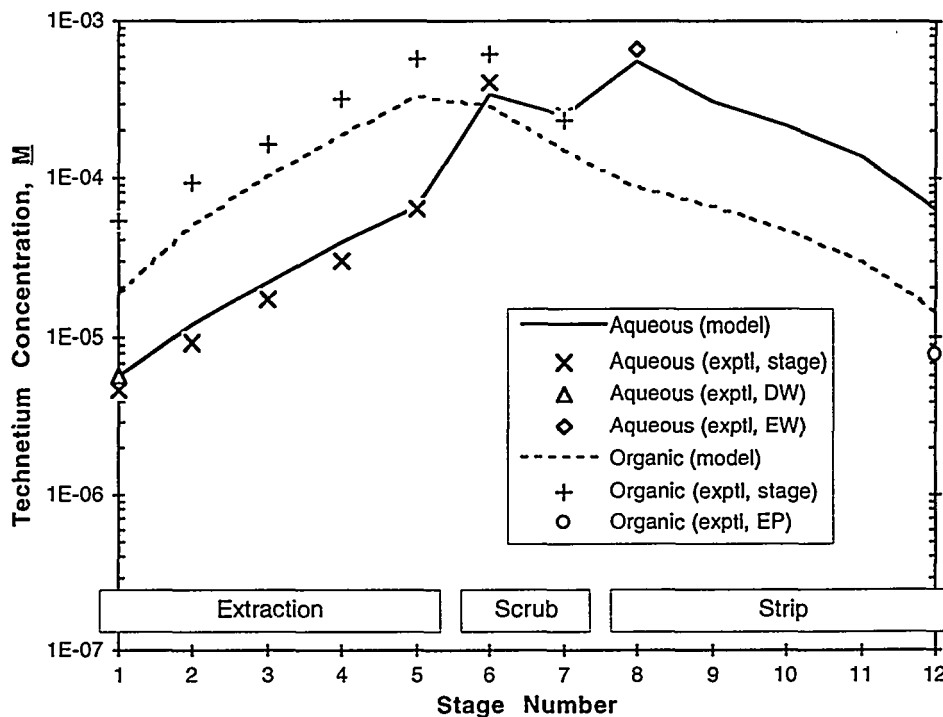
Fig. IV-3. Stage-to-Stage Technetium Concentrations in Test of
SRTALK Flowsheet. Both model calculations and
experimental results are plotted. The symbols in legend are
defined as follows: DW = aqueous raffinate, EW = aqueous
strip effluent, EP = used organic solvent.

B. Advanced Evaporator Technology

A new program was started to evaluate whether feed to the saltstone process used at the Savannah River Site (SRS) can be concentrated to increase waste loading. Saltstone produces an acceptable waste form from salt solutions containing 10 to 32 wt% soluble sodium salts. Salt solution is processed to produce saltstone based on the water content of the salt solution. According to present projections, as much as 490 million liters of salt solution containing 20 to 25 wt% sodium salts will be generated from processing existing high-level waste stored at SRS. This will require about 120 vault cells (ten 12-cell vaults in the present vault configuration) for disposal in the Salt Disposal Facility at SRS. Projected treatment and disposal costs for salt solution converted to saltstone are $1 per liter of solution (about $0.50 per liter of saltstone). By simply evaporating the existing salt solution from the current specific gravity of 1.23 to a specific gravity of 1.30, one could reduce the volume of saltstone generated by as much as 20%. This would effectively eliminate the need for at least one of the disposal vaults in the Salt Disposal Facility and the processing of at least 50 million liters of waste into saltstone; this corresponds to a savings of $40 to $60 million in disposal costs for saltstone. One challenge to processing SRS salt solutions is the potential release of toxic organic compounds (e.g., benzene). This work will provide the data necessary for design and deployment of a full-scale evaporator system at SRS.

C. Technical Support to ANL Waste Management

We have continued working with ANL Waste Management staff to help them solve their technical problems associated with waste storage and treatment. Much of their transuranic-bearing waste is stored as highly acidic solutions that require stabilization for long-term storage until a disposal site is available. As a simple method to stabilize this waste, we have helped them set up a glovebox to neutralize the waste and solidify it by adding a commercially available setting agent. After the waste has been neutralized and solidified, it will be removed from the glovebox and placed into a 55-gal drum for storage on site. We have also produced training documentation for using the glovebox. We will continue to act as technical consultants as future operations are planned and implemented.

D. Production of Molybdenum-99 from Low-Enriched Uranium

Molybdenum-99 ($t_{1/2}$ = 66.02 h) decays by beta emission to ^{99m}Tc ($t_{1/2}$ = 6.02 h). The latter nuclide is used in many nuclear-medicine diagnostic applications. For clinical use, it is prepared first in the form of pertechnetate ion (TcO$_4^-$) and then suitably changed to other chemical forms, depending upon the intended application. The TcO$_4^-$ is washed from an alumina-column generator that contains the parent ^{99}Mo. This washing is accomplished by elution with a saline solution. Much of the world's supply of ^{99}Mo is produced from fissioning of high-enriched uranium (HEU).

The Reduced Enrichment for Research and Test Reactors (RERTR) program has been active for 20 years at ANL and many countries throughout the world. Its objective is to modify

reactor and fuel designs so that reactors could switch from HEU to low-enriched uranium (LEU) with no or little loss in flux or cycle time. Many reactors have converted to LEU, and many more are in the process. While conversions of reactor fuel have proceeded, the amount of HEU being exported from the United States for use in [99]Mo production has become an ever more visible proliferation concern.

As a part of the RERTR program, we are studying two LEU target designs, uranium metal foil and UO_2/Al-dispersion fuel. At present, either electrodeposited UO_2 or various UAl_x alloys are used in HEU targets. The uranium metal foil and UO_2/Al dispersion fuel are both being developed as the LEU substitute for UAl_x/Al-dispersion targets, in processes where the aluminum-clad target is dissolved in base. The uranium metal foil is also being developed as the LEU substitute for electrodeposited UO_2, which is dissolved from the inner target wall with acid.

1.   Cintichem Processing of LEU Targets

The present Cintichem process produces, recovers, and purifies [99]Mo from HEU targets that consist of a thin coating of UO_2 on the inside of a cylindrical target, which is also used as a dissolver vessel for the irradiated HEU. Our R&D effort is focused on modifying the target and the recovery and purification procedures so that they can be used to process LEU targets consisting of uranium metal foil that is 0.13-mm thick.

We are collaborating with the National Atomic Energy Agency (BATAN) of Indonesia to develop and demonstrate the use of LEU targets in the Cintichem process. It is our objective to maintain the process for molybdenum recovery and separation from uranium (and its fission and absorption products) as close as possible to the current Cintichem process. It is also our goal to make improvements that will mitigate any economic detriment resulting from conversion to LEU. To this end, we are exploring the use of a LEU metal-foil target and have modified the dissolver solution to contain only nitric acid instead of a nitric/sulfuric acid mixture (sulfate in the high-activity waste complicates waste treatment and/or disposal[1]). During 1997, we focused on three areas:

- Determining the behavior of three fission products (I, Rh, and Ag) during molybdenum recovery and purification by the Cintichem process

- Measuring the effects of using zinc fission barriers for uranium-foil targets

- Developing a procedure that will measure alpha contamination in the [99]Mo product

In mid 1998, we plan to demonstrate the processing of a fully irradiated LEU metal foil at the PUSPIPTEK Radioisotope Production Center in Serpong, Indonesia.

---

[1] E. P. Gause, L. G. Stang, D. R. Dougherty, E. Veakis, and J. Smalley, *Characterization of the Radioactive Large Quantity Waste Package of the Union Carbide Corporation*, Brookhaven National Laboratory Report BNL-NUREG-30247R (July 1982).

a.   Behavior of Fission Products

The behavior of three radioisotopes (I, Rh, and Ag) has been studied this year. Radioiodine has been an impurity problem for BATAN. Rhodium and silver behaviors were studied because the low gamma yield of their radioisotopes makes it difficult to prove that they are not present in the ^{99}Mo product.

Most of the radioiodine in the Cintichem dissolver solution should be present as I_2 following dissolution in the nitric acid/sulfuric acid cocktail or in nitric acid alone. It will, therefore, be removed from the solution by evacuating the vapor in the dissolver. The iodine is collected in an iodine trap. What passes through the iodine trap is held by the cold trap at liquid nitrogen temperatures. However, other iodine species (I^-, IO_3^-, and IO_4^-) may have formed during fissioning. The rate of isotopic exchange between I^- and I_2 is rapid, while isotopic exchange between either iodate or periodate and all other iodine species is slow.[2] Therefore, once radioiodine is in the form of iodate or periodate, addition of iodide or iodine carriers will have little effect on changing its oxidation state. For this reason, we studied the chemical behavior of iodate and periodate in molybdenum purification steps.

In the Cintichem process, precipitation of silver iodide and sorption by activated charcoal (AC) and silver-coated activated charcoal (ACAC) are employed to remove radioiodine.[3] These methods would remove radioiodine in the form of molecular (I_2) or iodide ion (I^-). We looked at the effectiveness of these steps at removing these species, as well as iodate (IO_3^-) and periodate (IO_4^-).

Iodide ion should be almost completely precipitated out of solution by the addition of silver nitrate since the solubility product of AgI is 8.3×10^{-17}. Silver iodate also has limited solubility, but its solubility product is significantly larger than that of AgI (3.1×10^{-8}).[4] It is likely that silver periodate is more soluble than the iodate. Molecular iodine is not expected to precipitate with silver ion but does react with silver metal to form the insoluble AgI. Because carrier precipitation is a likely mechanism for increasing the removal of ions to a greater extent than their solubility products predict, we studied the coprecipitation of periodate on AgI and AgCl precipitates. Experimental results confirmed that coprecipitation is a likely mechanism for removal of the iodate and periodate forms. In both cases, the amount of periodate ion in solution was dropped by a factor of about 20. None of the periodate ion would have precipitated without being carried by the AgCl or AgI, given the extremely low concentration of the tracer (5×10^{-11} $\underline{M}$).

---

[2] M. Kahn and J. Kleinberg, *The Radiochemistry of Iodine*, National Academy of Sciences, National Research Council, Springfield, VA (1977).

[3] C. D. Massey, D. L. Miller, S. D. Carson, T. A. Wheeler, S. W. Longley, R. L. Coats, E. J. Parma, M. McDonald, M. E. Vernon, S. C. Bourcier, S. G. Mills, A. J. Trennel, and K. R. Boldt, *Feasibility Study of Medical Isotope Production at Sandia National Laboratories*, Sandia National Laboratories Report SAND95-2703 Rev. O (1995).

[4] D. A. Skoog and D. M. West, *Fundamentals of Analytical Chemistry*, Holt, Rinehart, and Winston, New York, p. 770 (1963).

We also studied the sorption of iodine species by AC and ACAC. The general trends of the data, summarized in Table IV-1, are that (1) iodide and iodine are sorbed to a limited degree by AC and very well by ACAC, and (2) neither iodate nor periodate is sorbed on AC or ACAC. For reference in interpreting the data in Table IV-1, a distribution coefficient (K_d) of ~10 mL/g will allow the separation of a species from solution; however, it would not be an efficient process and would require large amounts of sorbent to achieve a high decontamination factor. On the other hand, a K_d of 1000 mL/g would provide an extremely efficient decontamination process. Our results show that ACAC provides such a process for I^- and I_2.

In the Cintichem process, columns of hydrated zirconium oxide (HZO), AC, and ACAC are used in the purification process. During 1997, we investigated the uptake of ^{101}Rh tracer by these solids from 0.2 $\underline{M}$ NaOH, the solution from which ^{99}Mo is purified during processing. Measurements of distribution coefficients for rhodium between 0.2 $\underline{M}$ NaOH and the three solid sorbents were complicated by the instability of the solutions. As the alkaline solution aged, the ^{101}Rh activity in solution dropped. Initially, the 0.2 $\underline{M}$ NaOH solutions were measured to contain between 93 and 103% of the ^{101}Rh activity pipetted from the stock solution (5 x 10^{-11} $\underline{M}$). However, the ^{101}Rh concentration in solution dropped 20% in 15 minutes, 40% in an hour, and 98% in 13 days. Because the tracer was initially in the form of RhCl$_3$, it is likely that this effect is due to the conversion of Rh(III) from the soluble trichloride to an insoluble hydroxide. The chemistry of Rh(III) is quite complex and generally not easily predictable[5]; however, one can infer from these data that the solubility of Rh(III) in 0.2 $\underline{M}$ NaOH is $\leq 10^{-12}$ $\underline{M}$ based on the amount still in solution after 13 days.

Table IV-1. Distribution Coefficients for Sorption of ^{125}I Tracer on Activated Charcoal (AC) and Silver-Coated Activated Charcoal (ACAC) from 0.2 $\underline{M}$ NaOH Solution

Species	Distribution Coefficient,[a] mL/g	
	AC	ACAC
I^- (Iodide)	4	1,400
I_2 (Iodine)	5	3,700
IO_3^- (Iodate)	<1	<1
IO_4^- (Periodate)	<1	<1

[a]Average values for contacts with different (1) ratios of mass of sorbent to volume of solution, (2) contact times, and (3) preparation of iodine species. Differences in values for varying experiments were experimentally indistinguishable. Most measurements were done at room temperature using 0.2 g of solid in 2 mL of solution.

The loss of soluble rhodium with time complicates the measurement of its K_d for partitioning between 0.2 $\underline{M}$ NaOH and the three solid sorbents. To deal with this problem, we determined two K_d values for each sorbent at each mixing time. The first was based on the total

[5] G. R. Choppin, *The Radiochemistry of Rhodium*, National Academy of Sciences, National Research Council, Springfield, VA (1960).

concentration of rhodium added, and the second was based on the expected amount of rhodium remaining in solution without the sorbent present. These data indicate that (1) all three materials are effective sorbents for soluble and insoluble Rh(III)-Cl/OH species from 0.2 M NaOH, and (2) the order of sorbent effectiveness is ACAC better than AC better than HZO.

According to the calculations we presented at the 1996 International RERTR Meeting,[6] a typical 18-g LEU-foil target would contain 700 Ci of ^{99}Mo and 100 Ci of ^{105}Rh 24 hours after the end of irradiation in the BATAN reactor. The volume of the 0.02 M NaOH solution would be ~40 mL. Neglecting all other rhodium that may be in solution as other fission-product isotopes and carrier, we calculated that the rhodium concentration in this solution is 3×10^{-5} M, a concentration ~10^7 higher than the above solubility data allow. Adding to that factor is the high affinity for rhodium by the sorbents in the molybdenum-purification columns, which, conservatively, may provide another decontamination factor of 100. To meet a specification of 0.05 μCi/mCi-^{99}Mo would require a rhodium decontamination factor of ~3000 for the process. On the basis of the (1) low solubility of Rh(III) species in the process solution and (2) the effectiveness of the sorbents at removing rhodium from solution, attaining this decontamination should be no problem for the Cintichem process.

Although the decontamination factors needed for silver fission products are small ($\leq$10), the silver impurity levels in the ^{99}Mo are difficult to measure because they have no gamma-ray emissions. Therefore, we measured the decontamination factors for irradiated-silver tracer in each step of the LEU-modified Cintichem process. The silver decontamination factors for the (1) initial molybdenum recovery step was >70, (2) the first purification column was >40, and the (3) second purification column was >40. Multiplying the three decontamination factors gives an overall decontamination factor of >10^5; silver should, therefore, not be a contamination problem in the Cintichem process.

b.   Effects of Zinc Barriers on LEU-Foil Processing

Development of LEU metal-foil targets has led to the use of thin (10-15 μm) metal barriers between the uranium foil and the target walls. Because the uranium foil target is now being developed as the primary LEU target for ^{99}Mo-production processes that begin by dissolving HEU-aluminide-dispersion targets in base, we needed to select and test the use of a base-soluble metal as a fission-recoil barrier. Neither Cu, Ni, nor Fe dissolves in base. Therefore, a challenging task in process development was identifying a suitable metal for a barrier material that could dissolve in alkaline solution and meet other mechanical and chemical criteria. Zinc is an active electropositive element and forms a strong anion with oxygen. It also dissolves readily in sodium-hydroxide/nitrate solution. Work on barrier materials for targets to be processed by dissolution in base has, therefore, focused on zinc. Because of the appeal of developing just one target for all processes, a zinc fission barrier is also being considered for the target in acid-side processing.

---

[6]   D. Wu, S. Landsberger, and G. F. Vandegrift, "Progress in Chemical Treatment of LEU Targets by the Modified Cintichem Process," Proc. of 19th Int. Meeting on Reduced Enrichment for Research and Test Reactors, Seoul, Korea, October 6-10, 1996, pp. 172-179 (1996).

The ORIGEN2 computer code was used to calculate the neutron activation of a zinc fission barrier employed in the irradiation of an LEU foil target in the Indonesian BATAN reactor. The neutron activation products formed from the impurities were also examined. It was found that zinc has a lower neutron absorption than Cu, Fe, or Ni. Irradiation of the target would produce 700 Ci of ^{99}Mo and 1.3 Ci of radioactive isotopes from the zinc. Copper and cadmium impurity levels in the zinc may produce more radioactivity than the zinc itself. For the zinc foil we purchased, for example, 20 ppm cadmium and 15 ppm copper would produce 0.41 and 1.65 Ci of radioactive isotopes.

Zinc dissolves very quickly in 8 M nitric acid. However, our recent studies have shown that a U/Zn compound may form at the interface during heating (and perhaps during irradiation), and that it dissolves in nitric acid at a much lower rate than does zinc or uranium. The U/Zn compound is described in Sec. IV.D.4. This processing concern will be addressed in 1998. Low-enriched uranium with zinc fission barriers formed by electroplating will be irradiated and processed in Indonesia in mid 1998.

c.   Measurement of Alpha Contamination

Irradiation of an LEU target will produce about 30 times more ^{239}Pu than an HEU target producing the same quantity of ^{99}Mo. However, a typical HEU target is substantially more enriched in ^{234}U than a typical LEU target. A typical LEU target with the same amount of ^{235}U as an HEU target will have only two-thirds of the short-lived ^{234}U. Therefore, even with substantially greater production of ^{239}Pu, the total alpha activity of an irradiated LEU target is only about 20% higher than an equivalent HEU target.

Although the total alpha activity in an irradiated LEU sample is not far different from that in a comparable HEU target, the concern over plutonium toxicity has made the measurement of alpha contamination an important focus of our efforts. Therefore, we are in the process of developing and testing a procedure for separating and recovering actinide elements from the ^{99}Mo product that will allow low dose, facile, and effective measurement of alpha contamination in a sample of $<10^{-7}$ μCi-α/mCi-^{99}Mo. This technique is a modification of a procedure developed by Eichrom Industries (Darien, IL) for measuring dilute concentrations of actinides in urine and fecal samples.

The stringent alpha-contamination limit for the ^{99}Mo product necessitates quantitative removal of the alpha emitters from the ^{99}Mo. A typical sample for analysis would contain ~180 mCi of ^{99}Mo and, therefore, must contain less than 2 x 10^{-5} μCi (41 dpm) of alpha-emitters to meet the alpha purity specifications. Without separation from the molybdenum, interference from the ^{99}Mo beta/gamma makes counting this low level of alpha nearly impossible. Also, handling the counting plate would give a high dose to analytical personnel. We are investigating the use of TRU-Resin™ columns (Eichrom Industries) to separate the alpha-(hard-) emitting isotopes (U, Np, and Pu) from the ^{99}Mo. Chromatographic studies are underway to determine the behavior of molybdenum and the three actinides in the form of Pu(IV), Np(V), and U(VI). The known chemical properties of this column and the feed solution indicate that actinides in the (III), (IV), and (VI) oxidation states should all be strongly sorbed by the column, and that Mo(VI) should pass through. Conditions in the feed solution are set to reduce Np(V) to

the strongly sorbed (IV) oxidation state. These same redox conditions will affect plutonium in the (III) oxidation state.

Briefly, the chromatographic procedure calls for addition of a small aliquot (e.g., 10 µL) of the ^{99}Mo product solution to 1-10 mL of a 'feed containing 3 $\underline{M}$ HNO$_3$ and 1 $\underline{M}$ Al(NO$_3$)$_3$ and a yet-to-be-determined concentration of oxalic acid. The feed solution may also contain ascorbic acid and ferrous sulfamate. The feed is passed through the column and followed by a 5- to 15-mL wash of 2 $\underline{M}$ HNO$_3$. (At this point, "all" the molybdenum should be removed from the column. However, at the time of writing, we have yet to find the proper conditions for complete molybdenum separation.) The actinides are stripped from the column with 10 mL of 0.1 $\underline{M}$ NH$_4$(HC$_2$O$_4$). The actinides can then be electrodeposited on a plate for alpha counting.

Figure IV-4 shows Np(V) elution results for three oxalic acid concentrations. Shown in this figure are results of three column runs where samples of the effluent were taken approximately every milliliter. Data points are not shown at regular intervals (~3/column-volume) in the first six column volumes because the activity in the samples was not detectable. The feeds for all three actinides contained the reductants. The results are very encouraging. All of the neptunium in the feed was sorbed by the column and remained on the column during washing for all three oxalic acid concentrations. The only difference was more tailing in the strip for solutions with lower amounts of oxalic acid in the feed. However, in all cases, stripping was essentially quantitative. The behaviors of U(VI) and Pu(IV) were comparable.
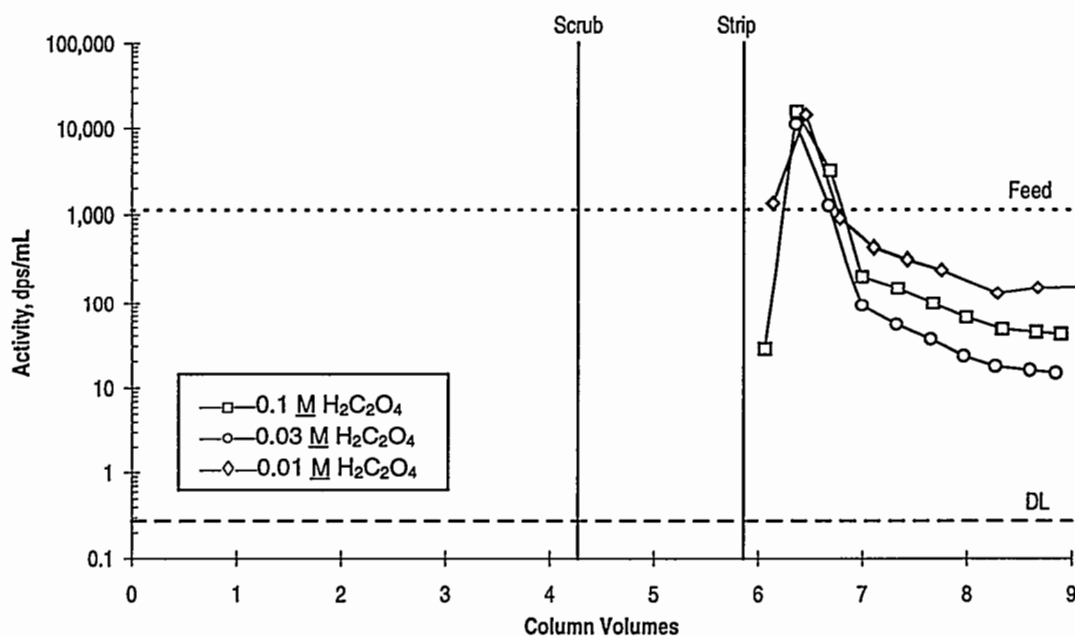
Fig. IV-4. Elution Profile of Neptunium on TRU-Select Column with Feed Concentration of H$_2$C$_2$O$_4$ Varied from 0.01 to 0.1 $\underline{M}$. The symbol DL indicates the detection limit for ^{239}Np.

Three column experiments were run to study the behavior of molybdenum as the oxalic acid in the feed was varied from 0 to 0.1 $\underline{M}$. The results shown in Fig. IV-5 indicate that molybdenum does not move unhindered through the column. As expected, the higher concentrations of oxalic acid do show more ability to hold back the molybdenum from sorbing onto the column. We are conducting experiments where the concentrations of the reducing agents and oxalic acid are varied over a wider range, and the volume and composition of the column scrub solution are also varied. We are confident that the chromatographic procedure will work but still need to find the proper conditions for maximum separation of the actinides from the ^{99}Mo.
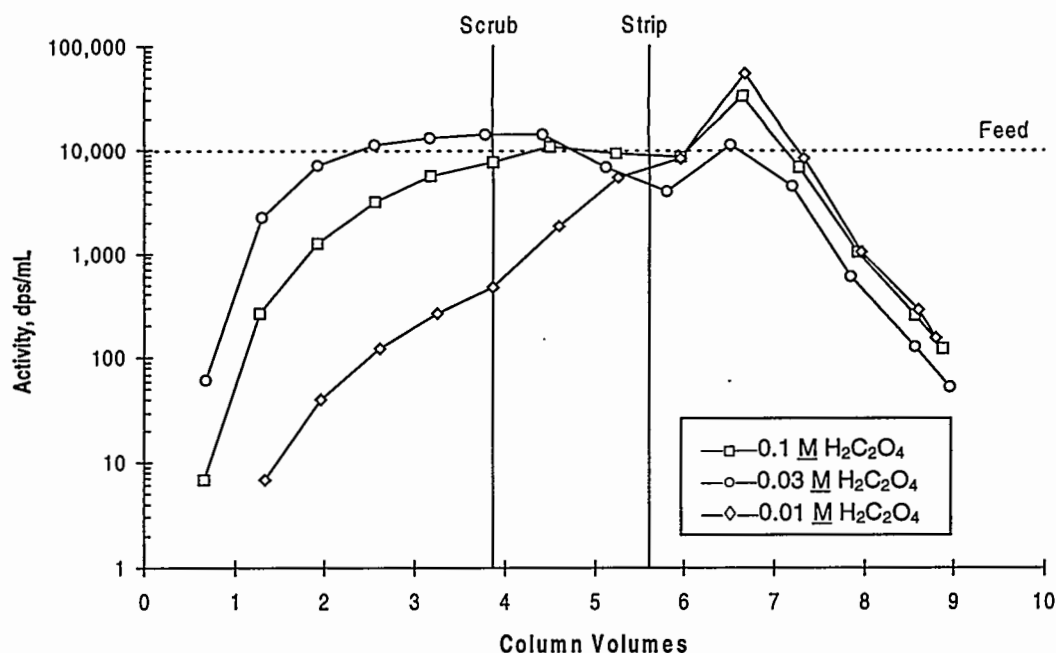
Fig. IV-5. Elution Profile of Molybdenum on TRU-Select Column with Feed Concentration of $H_2C_2O_4$ Varied from 0 to 0.1 $\underline{M}$

2.   *Electrodeposition of Zinc and Nickel onto Uranium Foil*

The principal difficulty in electroplating onto uranium foil is that it oxidizes readily in air and aqueous media. The resulting oxide layer prevents formation of a true metallurgical bond. A mechanical bond can be obtained by thorough surface preparation. We found that the procedure used to prepare uranium foils prior to actual plating had a major impact on the quality of the plating. A descaling step was necessary to remove the pre-existing oxide scale. The simplest and most consistent method of descaling the foil surface was immersion in 8 $\underline{M}$ HNO_3. Next, an etching step was needed to roughen the surface. The etching agents investigated included chloride salts of Fe, Ni, and Zn in concentrations that ranged from 0.45 to 9.0 $\underline{M}$. The 5.33 $\underline{M}$ $FeCl_3$ became the standard based on its ability to dissolve a predictable quantity of uranium in a reasonable time. Finally, the foil was "pickled" in the nitric acid solution to remove the dark scale left by the etching treatment.

Issues concerning foil surface preparation were largely resolved through a series of zinc-plating experiments. The zinc electrolyte was a commercially obtained solution containing sodium zincate, sodium hydroxide, and a proprietary additive to promote uniform deposition. With adjustment of surface preparation procedures, the quantity of uranium lost in pretreatment was consistently controlled at acceptable levels (~10%) without losing plating adherence. An example of an acceptable electroplating onto an adjusted LEU test foil is shown in Fig. IV-6.

Fig. IV-6.

Uniform, Continuous, and Adherent Zinc Plating on a Uranium Substrate (220X)

Our experiments in nickel electroplating uncovered a new concern, the maintenance of uniform coating thickness over the full area of the foil. The greater throwing power of the nickel sulfamate solution also resulted in a much broader edge-to-center variation in coating thickness. Overplating at the edges exceeded the tolerances needed to maintain the desired fit within the target assembly. Full-size foils, rather than the smaller test foils, were used to explore electroplating modifications because the degree of thickness variation was also dependent on foil geometry. Copper was substituted for uranium to conserve cost and minimize waste. The techniques studied to date include: reductions in current density, new nickel-anode geometries, perimeter-shielded foils, and auxiliary or "robber" cathodes around the perimeter of the foil. Each full data set was consolidated into three subsets representing the average thickness along the vertical edge, 0.5 cm from the vertical edge, and 0.5 cm from the vertical midline. To normalize for slight differences in deposited nickel, the thickness values were divided by the gravimetrically determined average thickness for that foil.

In Fig. IV-7, one set of curves depicts the measured thickness variation under what had been our standard plating conditions. The coating along the edge is still four to five times thicker than the central region, even when the bottom edge is excluded. (The bottom edge exaggerates the overplating effect because the anodes are much longer than required.) The second set of curves was generated for a foil electroplated at a reduced current and tested in conjunction with a
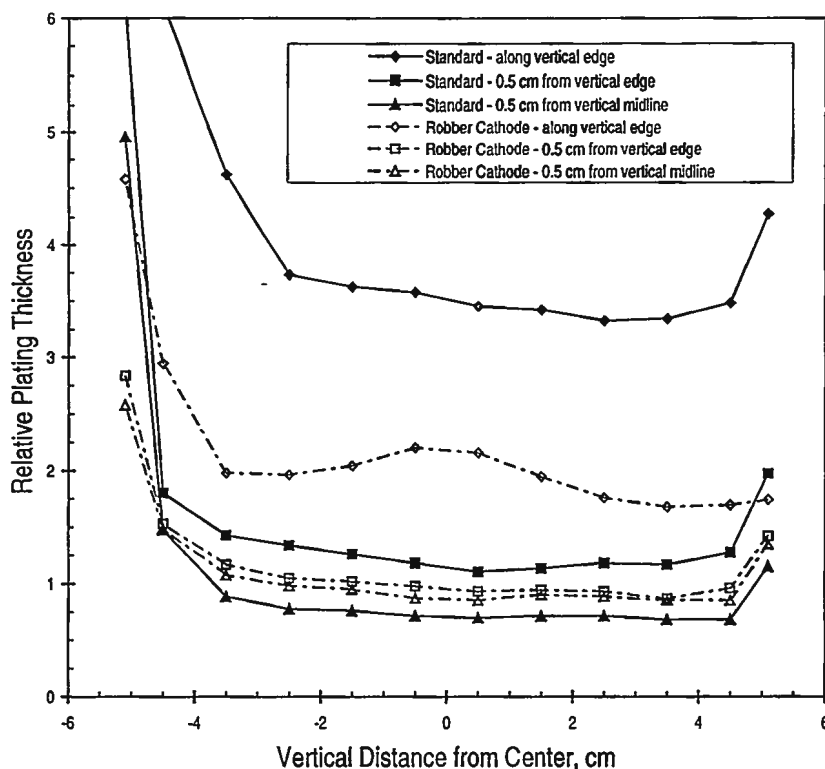
Fig. IV-7. Relative Plating Thickness for ~16-μm Nickel
Platings on Full-Size Foils

robber cathode. The edge-to-center variation has been reduced to a factor of two. This level of variation is very close to the existing tolerance limit for the foil target.

In summary, the feasibility of electroplating zinc and nickel barriers layers on uranium foils has been demonstrated. A surface preparation procedure that combines good foil adherence with complete coverage has been developed. Promising methods of preventing overplating at the foil perimeter have been investigated. Future work will couple the use of a robber cathode with other techniques to ensure that the coating thickness is held within design limits. By early 1998, electroplated LEU foils will be ready for evaluation as [99]Mo production targets.

3.   *Alkaline Dissolution of UO₂ Targets*

Work on recovering [99]Mo from a UO_2/Al dispersion target has continued. Several experiments were run to determine the dissolution rate of UO_2 in alkaline peroxide solutions. From these experiments, an empirical rate model was generated of the form:

$$R = k \cdot [H_2O_2]_i^{0.5} [OH^-]_i^{0.5}$$ (1)

where k is an empirical rate constant, and the molecules in brackets are the initial hydrogen peroxide and base concentrations. A plot of dissolution rate vs. $[H_2O_2]_i^{0.5}[OH^-]_i^{0.5}$ is shown in Fig. IV-8. As seen in this figure, a fairly linear relationship is present over several orders of magnitude. The slope of the best fit line is equal to the rate constant k = 1.26.
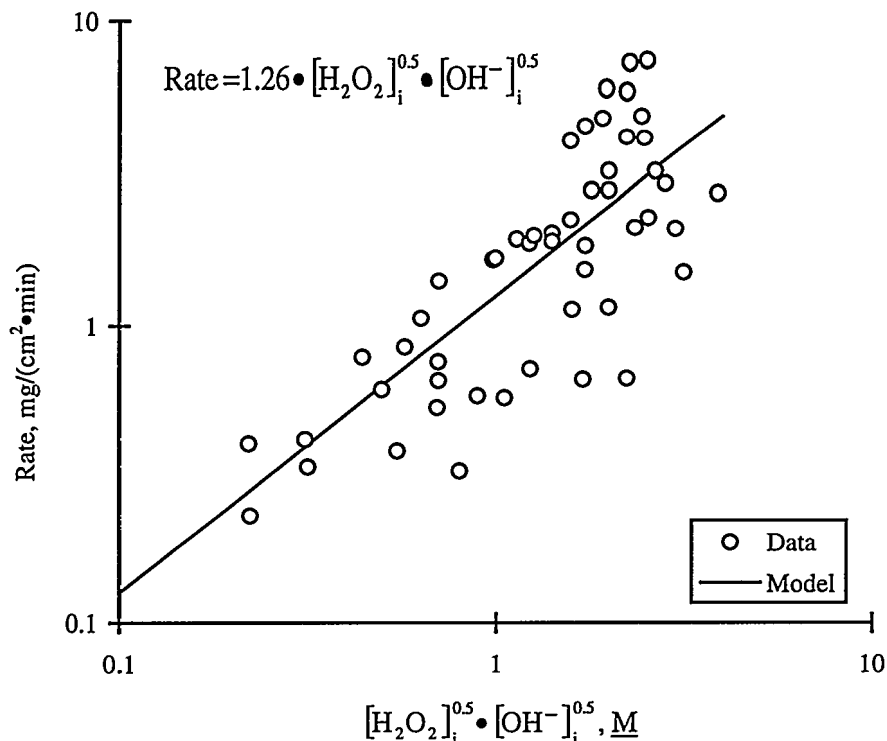
Fig. IV-8. Measured and Calculated Dissolution of UO_2 in
Alkaline Peroxide

Once it was shown that UO_2 would dissolve at acceptably high rates in alkaline peroxide solutions, compacts of aluminum powder and UO_2 were prepared and dissolved. These compacts simulate the "meat" of an aluminum-clad UO_2/Al dispersion target. Some compacts were then irradiated to low burnup, and the distribution of uranium and activation and fission products was measured through the various dissolution steps. Results of these tests showed that (1) the UO_2 compacts dissolve, and (2) fission products distribute soluble and insoluble fractions as predicted by their known chemical behaviors.

4.   Alkaline Dissolution of LEU Metal Targets

Since 1995, dissolution of LEU metal foil with alkaline peroxide has been studied as a replacement for processing of the HEU aluminide targets.[7,8] An LEU-foil dissolution kinetics

---

[7]   D. Dong and G. F. Vandegrift, *Nucl. Sci. Eng.* 124, 473-481 (1996).

[8]   D. Dong and G. F. Vandegrift, *Nucl. Sci. Eng.* 126, 213 (1997).

model was proposed in the same year. During 1996, work was focused on reducing the consumption of hydrogen peroxide during uranium foil dissolution in alkaline peroxide solution and optimizing the uranium dissolution process. During 1997, the effects of using zinc as a fission barrier were studied.

Three solutions for dissolving zinc were studied: NaOH, NaOH/H$_2$O$_2$, and NaOH/NaNO$_3$. A variety of NaOH/NaNO$_3$ compositions gave dissolution rates well above the desired 2 mg/(cm^2·min). A solution of 2.5 $\underline{M}$ NaOH/1 $\underline{M}$ NaNO$_3$ at 70°C is our standard for rapid dissolution of pure zinc metal. Experiments have confirmed that a zinc coating electroplated onto the uranium-foil surface is also dissolved rapidly by this solution. Analysis by energy dispersive spectroscopy of the foils left after dissolution showed that all of the zinc plate was dissolved from the uranium. Liquid scintillation counting of the dissolution solution showed that virtually none of the uranium foil was dissolved with the zinc.

Because of radioactive-decay heat generated within the irradiated LEU, we were concerned that a zinc barrier might melt during transport of the target from the reactor pool to the processing hot cell. The biggest hindrance to the transfer of heat from the target during transport is the relatively small surface area from which heat can be transferred. Calculations were made for natural convection in the air immediately after the target leaves the cooling pool and for the possibility that the target will be placed in a cask and shipped over a 24-h period. Although exact temperatures to be experienced by the zinc barriers cannot be predicted, calculations show that temperatures in the range of 300-400°C are likely. Although this is very close to zinc's melting point (420°C), it is expected that the zinc will not melt. However, when a zinc-plated uranium foil was heat treated at 375°C overnight in an evacuated glass tube, an intermetallic U/Zn compound formed.

The intermetallic U/Zn compound is visually distinct from the unheated zinc-plated uranium foil when viewed through a microscope with a magnification of about 440X. Figure IV-9 presents two micrographs of a zinc-plated depleted-uranium foil after heat treatment. Figure IV-10 is a micrograph of another section of the foil before this heat treatment. In the sample shown in Fig. IV-10, the uranium was badly etched during surface preparation for electrodeposition; however, the adhesion of the zinc to the uranium was excellent. (See Sec. IV.D.2 for details on surface preparation for electrodeposition.) Good adhesion of the zinc to the uranium has been found to be important to forming the intermetallic compound during heating. With this intermetallic compound, the interface between the zinc and the uranium is almost indistinguishable (Fig. IV-9), whereas it had been pronounced before (Fig. IV-10). Notice the dendrite-like formations along the edge of the foil in Fig. IV-9a. Even if the target is held at low overall temperatures during transport, the fission-product recoil that the zinc barrier is designed to absorb will result in localized heating and will most likely result in the formation of this intermetallic compound at the U/Zn interface.

Solutions suitable for dissolving the intermetallic U/Zn compound were investigated. Attempts to dissolve the zinc from this foil showed that this intermetallic would not dissolve as the zinc plate had from the unheated foils (at 70°C with a solution of 2.5 $\underline{M}$ NaOH and 1 $\underline{M}$ NaNO$_3$). On the other hand, a solution of 1.5 $\underline{M}$ NaOH/5 $\underline{M}$ H$_2$O$_2$ appears to dissolve the

intermetallic compound faster than it does pure zinc or pure uranium. Additional experimental work is necessary to clarify the rate of dissolution.

5.   Conclusion

We will continue to move toward demonstration of both the acid- and base-side processes in 1998. A top priority of the program is to form a cooperative agreement with a commercial producer that employs an alkaline-dissolution process. The commercial partner will act to focus our research and to demonstrate the LEU target and process in the same facilities being used for HEU target irradiation and processing.
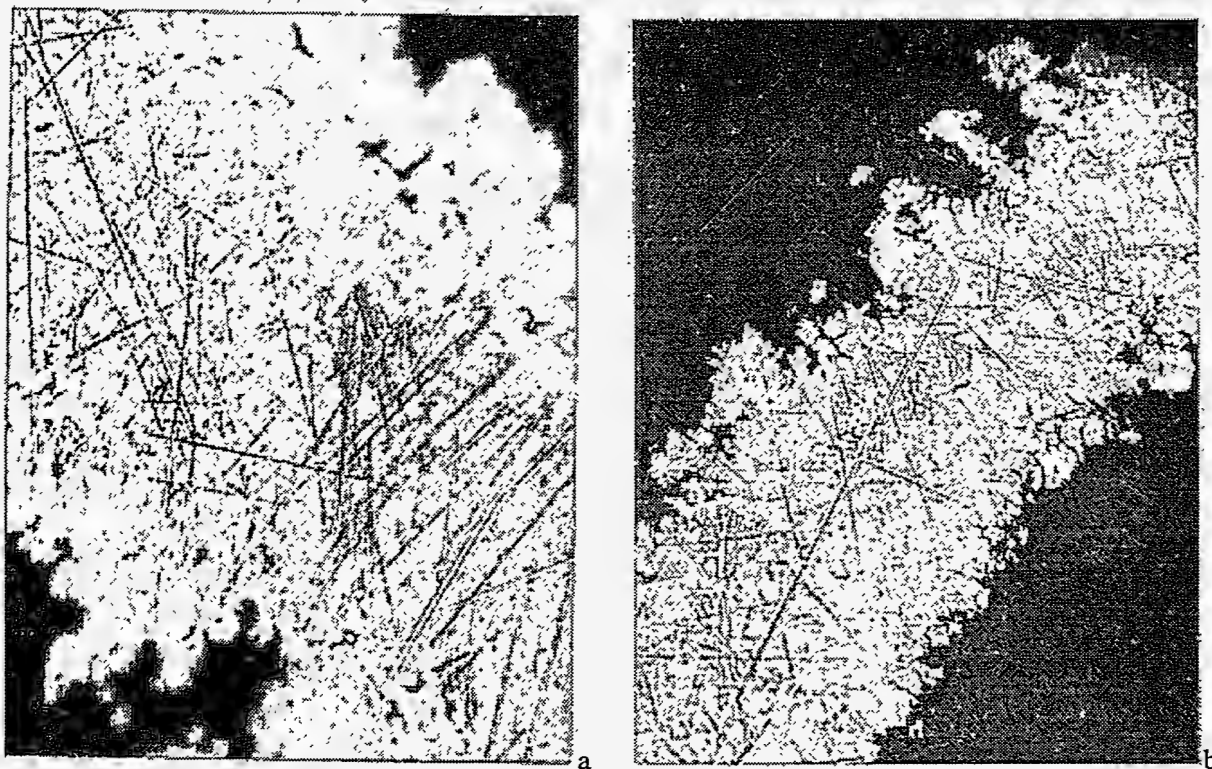
Fig. IV-9. Two Sections of Zinc-Plated Depleted-Uranium Foil after Heating at 375°C Overnight
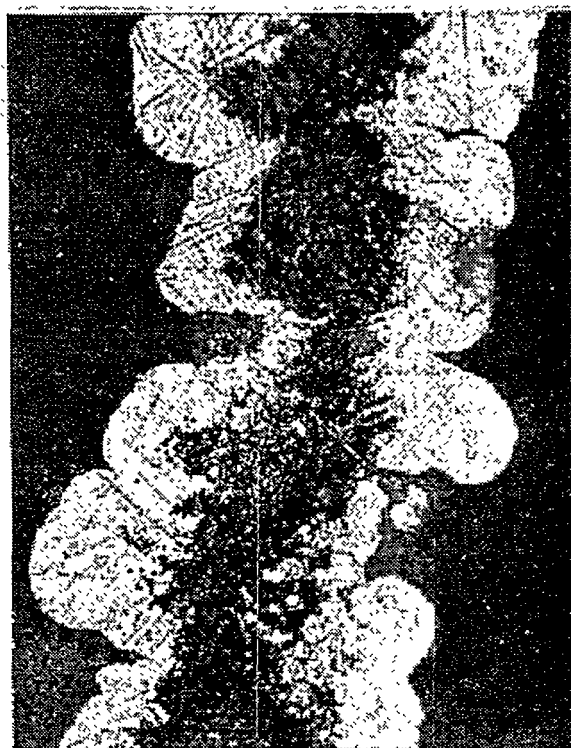
Fig. IV-10. Early Zn-Plated Uranium Foil
            Showing Considerable Loss of
            Uranium during Etching

V

Electrometallurgical Treatment Technology

The CMT Division is developing an electrometallurgical process for treatment of spent nuclear fuels for disposal in a geological repository. It is capable of handling most types of spent fuel and is especially intended for fuels at risk of chemical reaction with the groundwater in the repository. These "at risk" spent fuels include metal fuels with various cladding and matrix materials, reactive compounds, and highly enriched fuels. The central feature of the electrometallurgical treatment is electrorefining of the spent fuel in a molten salt electrolyte at 500°C (773 K). The LiCl-KCl eutectic electrolyte is formulated to contain about 2 mol% UCl_3. When a potential is applied between the anode and cathode, uranium, active fission products, and transuranic (TRU) elements dissolve at the anode, while pure uranium product is deposited on a solid cathode. The fission products and TRU elements are left behind to accumulate, either in the anodic dissolution basket (more noble fission products) or in the molten salt electrolyte (active fission products and TRU elements). The TRU elements and more active fission products may be extracted by passing the molten salt through anhydrous zeolite. The loaded zeolite may then be combined with a suitable glass frit and hot pressed to make a stable waste form for repository disposal. Fuel cladding, assembly hardware, and the noble metal fission products left in the anodic dissolution basket are melted together to form a Zr-Fe-based metal waste form for repository disposal. The TRU elements could also be placed in this metal waste form for disposal.

All the electrorefining process steps were developed in laboratory-scale experiments and have now been demonstrated at the engineering scale (10-kg batch size). Past work also demonstrated the feasibility of using this process for treatment of N-Reactor fuel (Zircaloy-clad uranium), single-pass reactor fuel (aluminum-clad uranium), and Experimental Breeder Reactor-II (EBR-II) fuel (steel-clad uranium alloy). Select topics from the electrometallurgical programs in CMT are discussed below.

A.   Electrorefining Development

Work continues on development of uranium electrorefining, the key step in electrometallurgical treatment of metallic spent nuclear fuel. This electrorefining separates pure uranium from the spent fuel, thus greatly reducing the volume of high-level waste. Also being investigated is use of the electrometallurgical treatment for other materials, including aluminum-alloy fuels and the waste salt remaining from the Molten Salt Reactor Experiment.

1.   Advanced Electrorefiner

Electrometallurgical treatment of the large quantities (about 2700 metric tons) of spent fuel remaining from the N-Reactor, EBR-II blanket, and foreign and domestic research reactors would require development of a high-throughput electrorefiner (HTER). The uranium concentration in these fuels covers the range from high to low enriched. The HTERs must be designed to provide systems that are not only high throughput but also safe based on criticality analyses.

Effort has continued on developing an HTER having a throughput >40 kg uranium per hour and batch size >100 kg of uranium. During this reporting period, testing of a 25-in. (0.6-m) dia HTER was initiated. This HTER contains 20 stainless steel anode baskets and has a batch size of 150 kg of uranium. The cathode consists of five concentric steel tubes that form four channels in which the anode baskets are positioned. Uranium scrapers are attached to the anode baskets. As the baskets are rotated in the cathode channels, the uranium that is electrodeposited on the cathode tubes is knocked off them by the uranium scrapers. The uranium is then collected in a basket that is attached at the bottom of the outer cathode tube.

Several features of this HTER design are favorable for high throughput and provide the flexibility to meet the criticality concerns for different types of spent fuel. For high throughput, the anodes and cathodes are separated by a short distance (maximum separation of 0.635 cm), which provides low resistance. Electrodes with large surface areas can be used to provide high currents for high throughput. The HTER batch size can be controlled by the volume and number of the anode baskets. The anode baskets can be sized to accommodate large batch sizes. Thus, the present HTER has the design needed for high throughput and the flexibility to meet the criticality limitations required to treat the DOE spent metallic fuels.

The objective of the initial tests of the 25-in. (0.6-m) HTER was to determine the effects of current density, rotation speed of the anode assembly, and electrode-scraper configuration on the performance of the cathode scrapers, sustained operation of the HTER, and the characteristics of the granular uranium cathode product. The test samples were unirradiated N-reactor fuel elements from the Hanford site. The initial uranium surface area exposed to the molten salt was 5625 cm^2.

A summary of the test results to date is given in Table V-1. All of these tests were terminated after the anode drive stalled owing to uranium buildup between some anode baskets and the cathode tubes. The uranium buildup was caused by the inability of the scrapers to

accommodate the uranium throughput rate or failure of some scrapers. In an attempt to provide sustained operation of the HTER, we increased the anode rotation speed from 20-30 rpm to 40 rpm; this step reduced the amount of uranium that was scraped off of the cathode tubes per revolution. Similarly, the electrodeposition current was reduced from 600 to 200 A to reduce the uranium throughput rate. These changes were needed to accommodate the limited (one scraper blade per revolution) number of uranium scrapers provided in the present HTER. From these results, we concluded that three uranium scraper blades per revolution may make it possible to provide sustained operation of the HTER at 0.07 A/cm^2 (600 A) and an anode assembly rotation speed of 40 rpm. A current density of about 0.07 A/cm^2 is the goal for HTERs that could be used to treat the spent N-Reactor fuel stored at the Hanford site.

Table V-1. Results of Tests with 25-in. (0.6-m)
High Throughput Electrorefiner

Electrodeposition Ampere-Hours	Current, A	Anode Rotation Speed, rpm
5272	500-600	20-30
1960	300-500	50
4982	300	40
3066	200	30
1738	200	30
31,219	200	40

The results of tests to date with the HTER have identified two factors that are barriers to sustained operation. One of these barriers, uranium buildup between some anode baskets and cathode tubes, was discussed earlier. The second barrier is the buildup of a dense uranium deposit on some areas of the cathode tubes. The thickness of this deposit increased with electrodeposition ampere-hours. Subsequently, this dense uranium deposit damaged some of the uranium scrapers.

The number of ampere-hours (31,219 Ah) passed through the HTER during the most recent test was nearly twice the number of ampere-hours (17,018 Ah) passed through the electrorefiner during all of our earlier tests. This result indicates that the increased anode rotation speed and decreased electrodeposition current were effective in eliminating uranium buildup between the electrodes. Stripping was also used during the most recent test. It was effective in controlling the thickness of the dense uranium deposit on the cathode tubes. As used in this test, stripping involved the electrotransport of a small amount of the uranium on the cathode, less than 30% of the uranium on the cathode tubes, back to the anode baskets.

To date, about 75 kg of uranium product has been collected from the HTER tests, and about 50 kg of uranium has been transferred to the cathode processor for consolidation. After the salt is separated from the uranium in the cathode processor, this uranium weight will be used to calculate the uranium mass balance for the HTER tests.

In conclusion, results from the initial tests of the 25-in. (0.6-m) HTER show that the scaleup of the HTER was successful. The resistance of this HTER (150 kg of uranium) is only 0.6 mΩ, compared with 1.0 mΩ for the 8-in. (0.2-m) HTER (5 kg of uranium) developed and tested earlier.[1] Progress has also been made in determining operating conditions that increase the operating time of the HTER and reduce the number of mechanical failures. Further improvement in the performance of the HTER will be achieved by making improvements in the uranium scraper design and configuration.

2. *Metallic Spent Fuel from Experimental Breeder Reactor-II*

a. Electrorefiner Development

The EBR-II blanket operations planned for the Fuel Conditioning Facility (FCF) electrorefiner at ANL-West will demonstrate throughput rates of 150 kg uranium per month. The "Mark V" high-throughput electrorefiner [10-in. (0.2-m) dia] will be used in this demonstration. In HTER tests at ANL-East, similated, unirradiated EBR-II blanket fuel is being electrorefined to verify the conditions needed for a throughput rate of 30 kg of uranium per day. These tests are being used to determine the effects of anode basket geometry, electrode separation, cathode scraper design, and operating conditions on the performance of the HTER.

To similate electrotransport in the Mark V HTER, the two baskets in the inner channel of the 25-in. (0.6-m) HTER [channel formed by 8.5-in. (22-cm) ID and 6-in. (15-cm) OD tubes] were loaded with chopped, clad uranium-zirconium-fissium (U-Zr-Fs) fuel segments. The U-Zr-Fs composition is given in Table V-2. The objective of this test was to determine the effect of a new cathode scraper design on the performance of the HTER and to determine anode designs and operating conditions that will retain noble metal fission products in the anode baskets.

Table V-2. Composition[a] of Uranium-Zirconium-
Fissium Alloy Used in HTER Test

Component	Weight Percent, wt%
U	88.2
Zr	10.4
Mo	0.76
Ru	0.36
Pd	0.14
Rh	0.093

[a]Composition was measured by inductively coupled
plasma/mass spectroscopic (ICP/MS) analysis.

---

[1] J. J. Laidler et al., *Chemical Technology Division Annual Technical Report, 1996*, Argonne National Laboratory Report ANL-97/13, pp. 101-104 (1997).

The HTER was operated at a current density between 0.1 and 0.2 A/cm^2, the anode drive rotation speed was 40 rpm, and the cutoff voltage was 0.45 V. No scraper failures or uranium holdup occurred during the test. About 80% of the uranium was anodically dissolved, and 100% of the zirconium was retained in the anode baskets.

The new cathode scraper design showed promise of a large improvement in sustained operation of the HTER. In this scraper design, uranium is knocked off of the cathode tubes so that it falls in the space between the rotating anode baskets. In previous designs, the uranium was knocked off the cathode in the narrow space between the electrodes. Steps are being taken to install this cathode scraper configuration in the outer channel of the 25-in. (0.6-m) HTER so that the effect on sustained operation can be determined. The partially dissolved fuel will be placed back into the HTER for further uranium electrotransport, until 98.5% of the uranium is dissolved. Other operating conditions and anode basket designs in noble metal retention tests are being investigated. Preliminary results are presented in Sec. V.A.2.c.

b.   Synthesis of UCl$_3$ for the Mark V Demonstration

In uranium electrorefining of the irradiated, sodium-bonded spent fuel from EBR-II, uranium chloride from the electrolyte is consumed. A *chemical* reaction occurs at the cell anode between UCl$_3$ from the electrolyte and some elements in the fuel feedstock, and this reaction forms chlorides that are thermodynamically more stable than UCl$_3$. The elements (metals) become chlorides and dissolve in the electrolyte, and the uranium metal that is formed in the chemical reduction of the UCl$_3$ deposits at the site of the chemical reaction (the cell anode). Elements in the fuel that act in this manner include Na, Pu, Nd, Ba, and Cs.

In electrorefining, it is necessary to maintain the UCl$_3$ concentration in the electrolyte within limits, so means must be taken to compensate for the uranium chloride loss that occurs through chemical reaction. There are a number of ways to compensate and maintain the desired level of UCl$_3$ concentration. These include addition of (1) chlorinating agents to the electrorefiner electrolyte, (2) UCl$_3$, and (3) salt mixtures rich in UCl$_3$. In the past, high-purity CdCl$_2$, a chlorinating agent, has been added to the salt. Cadmium metal, a byproduct of the chlorination, was not a problem because the current generation of electrorefiners was designed with a large pool of molten cadmium in the bottom of the electrorefiner, and the added cadmium did not alter the cell environment. The next generation of electrorefiner designs (HTER), however, eliminates the cadmium pool and seeks to eliminate all cadmium metal from the cell environment. Therefore, new means are being sought to compensate for the UCl$_3$ consumption in the next-generation electrorefiners.

The near-term need is a source of large quantities of UCl$_3$ for loading and startup of the Mark V electrorefiner being used to treat spent EBR-II fuel at ANL-West. Outside procurement (relied on in the past) from vendors of chemicals has not been successful. Therefore, it has become necessary that we make this material in-house.

There are two parts to this program. The first part involves producing enough material to meet the short-term needs as quickly as possible. To meet that goal, we have chosen to use high-purity CdCl$_2$, which we either already have available or on order from a vendor, as

the chlorinating agent. We are using this reagent and, with minor alterations, existing glovebox equipment to produce approximately 110 kg of UCl_3. The second part of the program calls for the production of 1 metric ton of UCl_3 for use in later electrorefiners at ANL-West. How to produce this large amount of material in the most economic fashion is under study.

To meet present needs, we are preparing a salt of 46 mol% LiCl-24 mol% KCl-30 mol% UCl_3. This ternary eutectic has a melting point of 418°C and is rich in UCl_3 (73.4 wt%, 45 vol%). To prepare pure UCl_3 from $CdCl_2$, we would need to work with liquid salts in the temperature range 568-842°C. This results in bulk distillation of cadmium, which we could not handle in our laboratory. With minor alterations of our equipment, however, we were able to prepare 20 kg batches of the ternary eutectic (14.5 kg UCl_3). One batch has been prepared, and a second batch is in process. The first batch has been sampled, and preliminary results of the analytical chemistry indicate that an acceptable product was produced.

Another synthesis that we have explored is use of manganese chloride as an oxidant to form UCl_3 *in situ*. Two laboratory-scale experiments were conducted to evaluate this synthesis route. These experiments were performed by adding uranium metal to a molten LiCl/KCl/$MnCl_2$ salt. These experiments are used to simulate a technique to form UCl_3 in the Mark V electrorefiner at ANL-West. The laboratory-scale setup consisted of a stainless steel crucible with a 8-cm diameter and a 14-cm height. A stainless steel basket, which was covered with a 100-mesh screen to retain any fines, was used to add uranium metal to the molten salt. After the UCl_3 had formed, it was determined whether manganese remained in the mesh basket.

In the first experiment, the uranium was added in stoichiometric quantities based on the equation:

$$2U + 3MnCl_2 \rightarrow 2UCl_3 + 3Mn \tag{1}$$
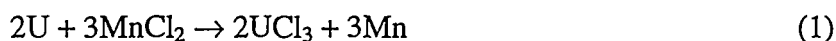
In the second experiment, a 10 mol% excess of uranium metal was added to the molten salt per Eq. 1.

Inductively coupled plasma/atomic emission spectroscopy (ICP/AES) was used to determine the composition of the salt 2 h after addition of uranium metal. The manganese remaining in the salt was found to be 4.14 wt% in the first experiment and 0.52 wt% in the second. This concentration of manganese in the salt is unacceptable for electrorefiner operation. X-ray diffraction analysis of the salt before the addition of uranium metal showed that $MnCl_2$ forms a $KMnCl_3$ phase with KCl. The formation of the $KMnCl_3$ phase may be the reason for the 0.52 wt% Mn that remained in the salt.

c.   Noble Metal Retention with Uranium Dissolution

One of the proposed high-level waste streams in the electrometallurgical treatment of spent nuclear fuel is produced by trapping the noble metal fission products in the anodic dissolution baskets. To test noble metal retention in the electrometallurgical treatment, we used the U-Zr-Fs alloy (simulant fuel) given in Table V-2. The goal of these tests was to

electrotransport 98.5% of the uranium, while retaining 80% of the zirconium in the anode baskets. To aid in retaining the zirconium, noble metals, and fines in the anode baskets, the baskets were lined with 325-mesh steel screen.

Two experiments have been performed with a laboratory-scale HTER. In the first experiment, a small amount (five pieces of chopped fuel) of simulant fuel was added to each anode basket. After the electrorefiner had been operated until theoretically all of the uranium had been electrotransported (10 Ah), the entire content of the anode baskets was analyzed by ICP/AES. In the second experiment, we filled the anode baskets with 343 g of the simulant fuel and ran the electrorefiner until theoretically all the uranium had been electrotransported (104 Ah).

Results of the first experiment showed that the goal of electrotransporting 98.5% of the uranium was achieved. Anode samples show that 98.64 wt% U was removed from the U-Zr-Fs alloy. However, our goal of retaining 80% of the zirconium in the anode baskets was not met. Only 75 wt% of the zirconium remained in the anode. Chemical analyses of fuel segment samples from the anode baskets of the second experiment have not been completed. Further experiments are needed to address the problem of zirconium retention.

3.   Waste Salt from Molten Salt Reactor Experiment

In the 1960s, Oak Ridge National Laboratory (ORNL) carried out the Molten Salt Reactor Experiment (MSRE). The reactor was shut down on December 12, 1969, and the irradiated molten fluoride salt fuel [LiF-BeF$_2$-ZrF$_4$-(^{233}U)F$_4$] containing actinides and fission products was drained into storage tanks, where the salt solidified. Subsequently, there has been some deterioration of the salt (radiolytic decomposition with formation of fluorine and gaseous UF$_6$), with spread of activity through the connecting piping and off-gas systems. To minimize the spread of activity and to prevent possible criticality, ORNL initiated a remediation project, the purpose of which was the conversion of the fuel salt into acceptable high- and low-level waste forms. Oak Ridge also asked for help in formulating a possible treatment that will allow this to happen.

One form of remediation proposed by ANL[2] is electrometallurgical treatment to separate the salt into actinides (for recovery), fisson products (for disposal as high-level waste), and bulk salt (for disposal as low-level waste). The laboratory equipment for experimental work was previously described.[3] In the ANL proposal, the MSRE salt is to be processed in 30-L batches in a lightly shielded facility. The total fuel salt volume is about 2000 L, so that 67 batches would be processed. Each batch would be processed in about one week. During the past year, we conducted 17 tests using a solid cathode and simulated MSRE (fluoride) salt to investigate removal of zirconium and its electrochemical separation from uranium. Afterwards, we

---

[2]   J. J. Laidler et al., *Chemical Technology Division Annual Technical Report, 1995*, Argonne National Laboratory Report ANL 96/10, p. 81 (1996).

[3]   J. J. Laidler et al., *Chemical Technology Division Annual Technical Report, 1996*, Argonne National Laboratory Report ANL-97/13, p. 100 (1997).

conducted three tests using Li-Bi alloy as chemical reductant. Further work was stopped at that point per DOE's order.

a.   Experimental

For the 17 electrotransport runs (MSRE-1 through -17), the matrix salt (6178 g) was placed in the electrorefiner crucible at room temperature, power to the furnace was turned on, and the salt allowed to melt. When the salt was clearly molten, the cathode assembly (containing the mixer and anode) was lowered into place. The matrix salt was mixed, and then 12.71 g BaF_2, 11.71 g CsF, 14.35 g CeF_3, and 13.28 g ThF_4 were added through the fill tube. The salt temperature during these additions was 551°C. Afterwards, 92.54 g UF_4 was added and the salt mixed; shortly thereafter, 0.689 g of plutonium was added. After thorough mixing, molten salt samples were taken.

Prior to each run, Li-Bi alloy was loaded into the anode baskets. To start a run, the cathode assembly was lowered into the molten salt in the crucible, and current passage was started. During cell operation, temperature, mixing rate, and cell voltage were monitored and recorded. The cathode assembly was then raised and allowed to cool at room temperature. The cell crucible containing the salt remained at operating temperature. Visual observations were made during the lift sequence and the cool-down period. Photographs were taken of each deposit. Samples of the product material and of the molten salt were taken after each test.

b.   Results

The analytical data from salt and cathode product samples that were taken from the electrorefiner experiments indicated that the product from the tests MSRE-1 through -16 was zirconium metal, which contained occluded salt. Uranium was deposited in test MSRE-17. The analysis of the zirconium deposits, which were dendritic or plate-like, indicated essentially pure zirconium. The other elements that were associated with these deposits can be accounted for by salt (which contains these elements as fluorides) accompanying the products. These results are important in that they support our position that zirconium will be removed before uranium deposits, and that no other metals (other than noble metals) present in the simulated salt will deposit. These results are consistent with thermodynamic calculations performed to predict the deposition sequence. These calculations indicate that the deposition sequence on a solid cathode should be in the order Zr, U, Be, Pu, Th, Cs, Ce, and Ba. Our product results are consistent with this predicted sequence.

The analytical results of salt samples taken after each test indicate that we obtained the expected increase in lithium concentration accompanying the decrease in zirconium concentration. These trends are shown in Fig. V-1. This figure shows good agreement between the measured and predicted values. For these calculations, we used the electrochemical data, assumed that LiF and Zr were formed, and corrected for the weight change occurring in the salt resulting from LiF formation. The differences noted in this figure are attributed to analytical
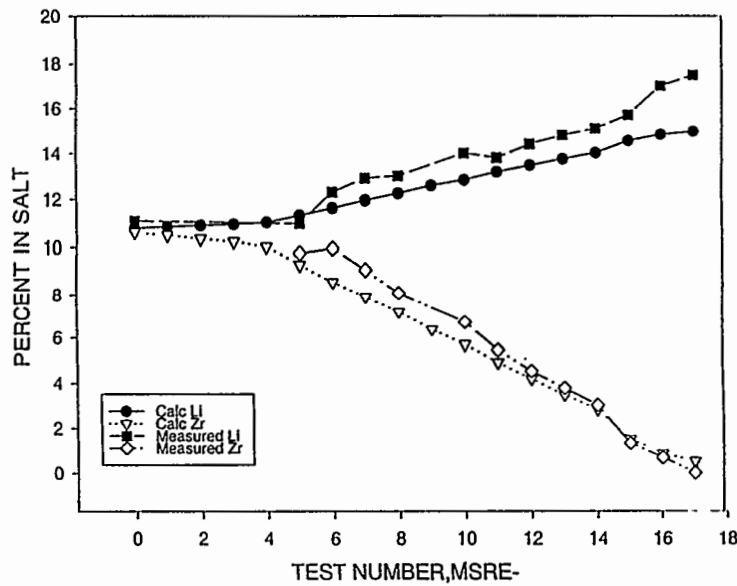
Fig. V-1. Measured vs. Calculated Lithium and
Zirconium Content of Fuel Salt from the
Molten Salt Reactor Experiment

uncertainties in the Li and Zr values (estimated to be 10-15%) and errors introduced by ignoring the Zr and Li removed due to sampling or that occluded in the products.

Uranium data are a matter of concern to us because they indicate an initial drop-off in uranium concentration, which eventually stops. In experiments carried out after the 17 runs, we added ZrF_4 to the salt after removal of ZrF_4 and UF_4 and allowed the contents to equilibrate for some time. The uranium concentration in the salt increased from <0.01 to 0.25 wt%. Similarly, when the electrorefiner vessel was made the anode, zirconium metal was deposited on the cathode, while the uranium concentration in the salt increased from 0.25 to 0.57 wt%. Thus, these brief tests indicated that oxide formation and U-Bi intermetallic formation are likely. We know from ORNL work that the ZrF_4 was added to the LiF-BeF_2 salt to prevent UO_2 formation. When UO_2 is present, ZrF_4 reacts to form UF_4 and ZrO_2. The free energy change for the reaction is such that UO_2 formation cannot occur until at least 90% of the initial ZrF_4 was removed. Thus, UO_2 formation in the early stages of zirconium removal in our studies is not likely from thermodynamic considerations. However, it is possible that UO_2 formation did occur, and once formed, the reaction of UO_2 with zirconium tetrafluoride was slow under the test conditions.

c.   Discussion

The test results clearly showed that zirconium (along with any other noble metal in MSRE salt) is separable from the salt by deposition on an iron cathode mandrel. The product was dendritic and plate-like metal covered with cell electrolyte. As demonstrated in development work connected with processing EBR-II fuel into waste forms, this material can be alloyed with iron to make a stable metal waste form. In the melting and alloying process, the occluded electrolyte on the dendrites may be recovered and recycled.

In tests using the Li_3Bi anode alloy and a solid cathode, a voltage difference of -0.12 V was found between the transport of zirconium and the transport of uranium. On our MSRE flowsheet this means that $\geq 98\%$ of the zirconium and all fission product (and daughters of thorium decay) more noble than zirconium can be removed from the salt, leaving essentially all of the ^{233}U in the salt. The remaining zirconium and all of the uranium were removed from the salt by using a second solid cathode. This result gives us a second option for separating and decontaminating the ^{233}U from MSRE salt. (In our original flowsheet, the remaining zirconium, the uranium, the transuranics, and some fission products are removed with a liquid bismuth cathode.)

The concept of using Li_3Bi (solid→liquid) as anode material was proven. This is very important in reducing waste volumes for the process. The spent anode material, bismuth, was recovered from the anode catch basket crucible. If this were not possible, 1.4 metric tons of bismuth would need to be devoted to making the Li_3Bi. Since bismuth proved to be recoverable after each batch, only about 1.5% of the 1.4 metric tons (20 kg) will be needed for this purpose.

Because of time constraints, we were unable to study the separation of other fission products and transuranics from the salt by electrotransport to a liquid bismuth cathode. However, we did an experiment involving three successive contacts (using a pounder-type contactor) of the salt with $Li_{0.2}Bi_{0.8}$. This reduced all of the fission products (except cesium) in the simulated MSRE salt to or below the detection limit (≤ 0.01 wt%). The use of 20 mol% lithium alloy (as opposed to 75 mol% alloy) prevented reaction with BeF_2 of the matrix salt after removal of the ZrF_4. More research needs to be devoted to explore means for removing cesium from the salt.

With the exception of minor losses of Li-Bi spent anode alloy during the 17 runs, the cell components and hardware worked well, and as expected. In scaleup to process size, we would provide overlap between the anode catch basket and the anode basket (size constraints prevented this in the laboratory-scale electrorefiner). This should resolve the problem with material loss. Given the benefit of the present and applicable past experience, an automated electrorefiner could be designed for use in a lightly shielded inert atmosphere enclosure to process MSRE fuel.

4.   *Aluminum-Based Spent Fuel*

Development work has continued this year on an electrometallurgical process for treating spent aluminum-based fuels. This fuel is predominantly used in foreign and domestic research reactors. Over the next 40 years, 128 metric tons of spent aluminum-based fuel will be shipped to the DOE Savannah River Site from U.S. and foreign research reactors. When originally fabricated, the fuel contained over 55 metric tons of uranium at an average enrichment of approximately 20%. Along with the approach of simply melting the fuel and adding depleted uranium, electrometallurgical treatment of the fuel is considered a backup option for treatment of the spent fuel. The primary options at present are processing the fuel in existing Purex facilities at Savannah River and direct disposal of the fuel in a geological repository.

Because electrometallurgical treatment separates the aluminum from the spent fuel for disposal as low-level waste, the high-level waste volume is reduced by better than 80%. The process is also well suited for operation after 2005, when the rate of spent fuel shipments begins to decline. Additionally, the existing Purex facilities at Savannah River are scheduled to be decommissioned around 2005 as well.

The overall process flowsheet (Fig. V-2) has changed very little from the one described in last year's report.[4] In a high-throughput electrorefiner, aluminum is removed from the spent fuel alloy by electrotransport. After all the aluminum has been removed, the anode baskets contain only the actinides, noble metal fission products, and some of the rare earth fission products. These baskets are then transferred to a second electrorefiner, where uranium is removed by electrotransport. Summarized below is the work conducted this past year in the areas of flowsheet modifications, laboratory-scale tests, and engineering-scale tests.
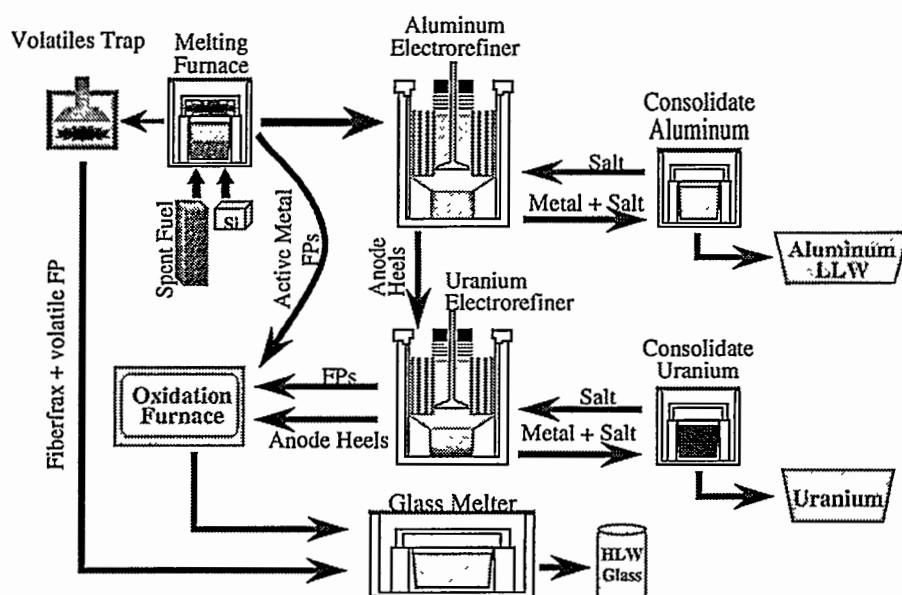
Fig. V-2. Flowsheet for Electrometallurgical Treatment of Aluminum-Based Fuel. (FP = fission product, LLW = low-level waste, and HLW = high-level waste.)

a.   Flowsheet Modifications

In the process flowsheet discussed in last year's report,[4] only the melting step has been modified. In the modified process, the spent fuel is melted under a salt flux, and silicon is then added to the molten fuel. Silicon forms stable intermetallic compounds with uranium and rare earths; it is added to the fuel to enhance the retention of these metals in the anode of the aluminum electrorefiner. The advantage of using a salt flux is that the active metal fission

---

[4]   J. J. Laidler et al., *Chemical Technology Division Annual Technical Report, 1996*, Argonne National Laboratory Report ANL-97/13, pp. 96-98 (1997).

products can be extracted from the spent fuel at this stage. Without a flux salt, the active metal fission products would accumulate in the aluminum electrorefiner. It would be necessary then either to discard the salt or to separate the active metal fission products from the electrorefiner salt. Moreover, the salt used to extract the active metal fission products can be selected to optimize the degree of removal and to simplify the scrubbing of the active metal fission products from the flux salt.

b.   Laboratory-Scale Tests

Many of the steps in the flowsheet shown in Fig. V-2 have been demonstrated as part of other programs. Electrorefining of uranium, for instance, has been demonstrated in the treatment of spent EBR-II fuel at ANL-West. However, the aluminum electrorefining step in the potassium cryolite salt that we have selected had not been demonstrated until this past year.

This year we have successfully demonstrated electrorefining of pure aluminum and a U-Al-Si alloy in laboratory-scale tests (aluminum batch size of 2 g). The electrorefining tests with pure aluminum confirmed that the cathode product is dendritic, that the cathode product can be easily scraped off the cathode, and that the product is denser than the molten potassium cryolite. In another series of tests, we confirmed thermodynamic calculations that predicted alkaline earth fission products, such as Ba and Ca, do not codeposit with aluminum. The same test also confirmed the prediction that rare earth metals, if they are present in the salt as metal fluorides, will codeposit with aluminum.

The purpose of the electrorefining tests with U-Al-Si alloy was to identify conditions under which a pure aluminum product could be obtained. In the best test thus far, the aluminum that deposited at the cathode contained only 500 ppm uranium. In that test, the cell potential was limited to 0.20 V. Analysis of the alloy remaining in the anode at the end of the test revealed that 95% of the aluminum had been removed from the U-Al-Si alloy.

c.   Engineering-Scale Tests

In addition to laboratory-scale tests of aluminum electrorefining from a U-Al-Si alloy, engineering-scale tests are needed. Therefore, an engineering-scale aluminum electrorefiner (aluminum batch size of 6 kg) has been designed and fabricated. The electrorefiner is similar in design to the uranium high-throughput electrorefiner (Sec. V.A.2.a). The U-Al-Si alloy will be loaded into anode baskets that rotate in the annulus between two concentric cathode cylinders. The electrodeposited aluminum metal will be continuously scraped off the cathode surfaces and collected at the bottom of the electrorefiner. Because the electrorefiner will use a potassium cryolite salt, all components have been constructed out of Inconel, a high-nickel alloy. The present test plan calls for installation of this equipment in an engineering-scale glovebox and testing in early 1998.

B.   Waste Isolation from Electrorefiner Salt

As the electrorefiner repeatedly treats batches of fuel, fission product and transuranic (TRU) actinide ions build up in its electrolyte salt (LiCl-KCl of approximately eutectic composition). The salt must be periodically renewed or replaced because of the decay heat load, formation of insoluble phases in the salt, or criticality concerns. Under development for salt purification are zeolite ion-exchange columns and pyrocontactors.

1.   Zeolite Ion-Exchange Column

Zeolite columns continue to be investigated as a means for separating radionuclides from spent electrorefiner salt so that the salt can then be reused. The zeolite sorbs and retains radionuclides from the salt by replacing Li and K ions from within its structure. Zeolite from the column, which is loaded with TRU and fission product ions, is ground, mixed with additional dehydrated zeolite and glass, and hot pressed to form a durable ceramic waste (see Sec. V.C). During the hot pressing process, the zeolite can be converted to sodalite, a stable chloride-bearing mineral.

Columns are not strictly required to process the salt; the spent salt may be discarded by simply mixing it with sufficient dehydrated zeolite to soak up essentially all of the salt, then converting it to a waste form. However, because the column concentrates the radionuclides within the zeolite, the amount of spent salt that is discarded (and thus the amount of waste produced) is reduced significantly.

A laboratory-scale column unit (~2.5-cm dia by 30-cm length) is being tested to determine the operating conditions for a full-scale system (13-cm dia by 76-cm length). Figure V-3 illustrates the change in composition of the effluent salt during a column test. Concentrations of cations normalized to their initial concentrations in the salt (C/C_0) are plotted versus the ratio of the mass of salt passed through the column to the mass of zeolite initially in the column. As can be seen in the figure, the zeolite preferentially sorbs the more highly charged ions.

In the initial laboratory-scale column tests, the effects of temperature and flow rate were examined. The zeolite bed in the initial tests was 2.86 cm in diameter and 30 cm in length. Several tests were run at a superficial salt velocity of 1.4 cm/min and temperatures of 500, 550, and 600°C. These temperatures are well above the melting point of the salt (~360°C) and below the temperature at which the zeolite transforms to other phases (~650°C). Only a moderate change in fission product uptake with temperature was seen. The effect of salt flow rate is being tested by reducing this rate below 1.4 cm/min at a temperature of 550°C. In these ongoing tests, the removal of rare earths from the salt appears to increase significantly with reduced flow rate, but little change in alkali or alkaline earth behavior is seen. Tests with longer columns are also planned.
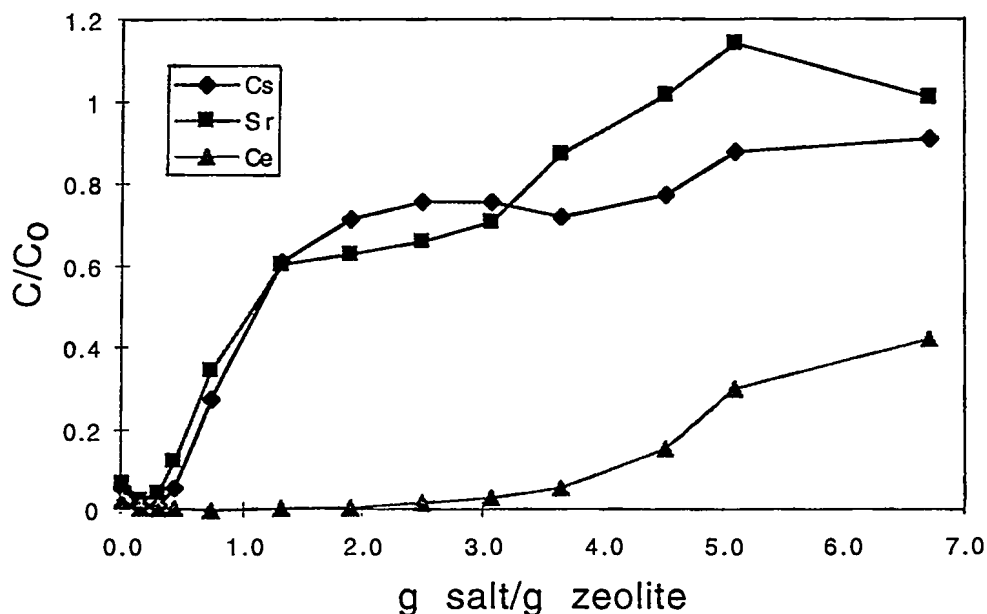
Fig. V-3. Breakthrough Curves for Typical Test with Zeolite Ion-
Exchange Column

2. Pyrocontactor

Pyrocontactors are high-temperature centrifugal contactors that provide intense mixing to effect chemical reactions between solutes in molten salt and liquid metals. They also provide clean separation of these streams. In previous work with a single-stage pyrocontactor,[5] lanthanum was separated from a LiCl-KCl salt containing lanthanum and yttrium chlorides by reduction with cerium in Ce-Cd metal. Stage efficiencies of up to 90% of the theoretical value were measured at contactor speeds of up to 2700 rpm.

This year, a four-stage countercurrent pyrocontactor was successfully tested. A four-stage unit can achieve about 30% better separation efficiencies than a single-stage unit. Three sets of tests were completed: in set one, lanthanum metal was separated from a LiCl-KCl eutectic salt containing $LaCl_3$ and YCl_3 by contact with a Ce-Cd metal. In set two, $CeCl_3$, $LaCl_3$, and YCl_3 in LiCl-KCl eutectic salt were reduced by reaction with a Li-Cd metal. In set three, Li, Ce, and La in cadmium metal were oxidized by reaction with $CdCl_2$ in LiCl-KCl salt. The four-stage pyrocontactor achieved stage efficiencies approaching 99% of the theoretical value at rotor speeds near 3200 rpm. These results indicate that the pyrocontactor will effectively separate TRU elements from the rare earths contained in the spent salt from an electrorefiner. Because the pyrocontactor is better suited to production electrorefining, and because simpler separation methods are more appropriate to the demonstration of pyroprocessing, further development of pyrocontactors is being deferred.

[5] J. J. Laidler et al., *Chemical Technology Division Annual Technical Report, 1994*, Argonne National Laboratory Report ANL-95/24, p. 95 (1995).

C.   Development of Ceramic Waste Form

The TRU elements and the most easily oxidized fission products accumulate in the process salt during electrorefining of spent fuel. These salt-borne wastes are periodically removed and incorporated into a crystal structure; the resulting material is made into a composite ceramic waste form with borosilicate glass. The development of this waste form has focused on two composites: zeolite-glass and sodalite-glass. The zeolite composite has a higher capacity for salt, while the sodalite composite is more thermally stable. Fabrication of the two waste forms is very similar and involves the same processing operations: dehydration of zeolite A, blending of the salt and dehydrated zeolite A, mixing the salt-loaded zeolite A with glass, and hot pressing. Other than the ratio of salt to zeolite that is used, the primary difference is in the hot pressing, since zeolite heated to a relatively high temperature forms sodalite. In October 1997, a sodalite-glass composite was selected as the reference ceramic waste form for the project.

Because the demonstration project of the electrometallurgical treatment underway at ANL-West with spent EBR-II fuel will not use zeolite columns initially, we have, for the most part, developed the ceramic waste form without using the zeolite ion-exchange column as a feed stream. Development of the ion-exchange column is being carried out parallel to the demonstration activities (Sec. V.B.1).

1.   Fabrication

Improvements in waste form fabrication are being sought by testing the effects of additives (tougheners and getters), different salt loadings, larger particle sizes, and alternative consolidation methods to hot isostatic pressing.

a.   Use of Additives

The overall goal of the ceramic waste form development is to produce a highly leach-resistant composite of substantial physical integrity. Both leach resistance and physical integrity might be enhanced by the inclusion of additional phases. We have looked at both tougheners and getters. The toughening additives were intended to enhance the physical integrity of the waste forms by preventing or limiting crack propagation. The getters were intended to enhance leach resistance by improving fission product retention. Approximately 50 zeolite- or sodalite-glass composites were tested. The effectiveness of the additives was gauged by measuring the mass fraction of cesium released by the waste form after immersion for 3 or 28 days in deionized water at 90°C (following the MCC-1 test procedure). However, because it is possible that the effectiveness of the additives will not be determined from these measurements, additional tests are being conducted under more severe conditions.

The toughening additives included fine-grained silica and both fine- and coarse-grained alumina powders. These materials were chosen because of differences in thermal expansion. The getters investigated were dehydrated forms of zeolite 4A, zeolite 5A, and chabazite. As with the toughening additives, our goal was to look for substantial improvement in cesium retention. All samples were hot isostatic pressed to yield either zeolite- or sodalite-glass

composites. Specimens were subjected to leach tests, X-ray diffraction, and density determination.

The cesium mass release data for zeolite- and sodalite-glass composites with tougheners and with getters showed no discernible improvement compared with those obtained for specimens without additives. Leach resistance of the sodalite-glass composites, with or without additives, is such that cesium release data are very near the detection limit of the technique used to determine cesium content in the leach solution, inductively coupled plasma/mass spectrometry. Because the cesium release is roughly an order of magnitude higher for the zeolite-glass composites (for 3-day tests), we can better gauge the effect of tougheners and getters on that waste form composition. It was clear for zeolite-glass composites that no improvement in cesium retention was realized from the inclusion of any of the tougheners or getters in our study. However, the first full-scale waste forms produced at ANL-West contained significant cracks and had poorer fission product retention than comparable laboratory-scale samples. It is possible that additives may improve the waste form in full-scale operations. It is also possible that longer-term leach behavior will benefit from tougheners and getters; this hypothesis is being tested.

b.   Composite Composition

The total volume of ceramic waste form can be reduced by increasing the salt loading in the zeolite or sodalite and/or decreasing the glass content. However, such composition changes may have detrimental effects on waste form behavior. In a series of tests, the salt and glass (binder) contents were varied in 60 specimens prepared by hot isostatic pressing. The effect of these composition changes on cesium release was measured to gauge the relative leach resistance of the final zeolite-and sodalite-glass composites. The salt content in the blended zeolite ranged between 6.5 and 10.5 chloride ions per unit cell (Cl⁻/u.c.) in the zeolite-glass composites and between 3.0 and 4.0 Cl⁻/u.c. in sodalite-glass composites. The amount of glass was varied between 25 and 50 wt% of the total canister charge. Each specimen type was made in triplicate to evaluate canister-to-canister variance.

Both 3- and 28-day leach tests showed that higher salt loadings did not increase the fractional mass release of cesium for either zeolite or sodalite. The cesium release increased significantly, however, when the glass content of the zeolite-glass composites was reduced below ~30 wt%. Sodalite-glass composites, in contrast, showed constant cesium releases down to 25 wt% glass, indicating that the glass content may be reduced further without deleterious effects. Lower glass contents are being investigated.

c.   Particle-Size Distribution

Most of our development work has been done with fine powders (average particle sizes less than 20 μm) because pure zeolite A is only available in this form. Granular zeolite A contains binders, typically clays, which make up 5 to 20 wt% of the material and thus introduce another component to the waste form. Fine powders allow for more intimate contact between the zeolite and salt during blending; small particles also cause the waste form to densify more rapidly--which is important in making zeolite-glass composites. However, fine powders resist

flow, which can pose problems for remote handling. Granular zeolite and glass both flow much more readily than the powders, making them more suitable for remote operations. It may also be possible to improve powder packing (an important factor in rapid and successful densification) by using appropriate particle-size distributions for zeolite and glass.

In replacing fine powders with granulated zeolite, we were initially concerned with whether granules blend efficiently with salt. We also looked for changes in the leach resistance or physical integrity of the composite induced by the binder. Initial tests with zeolite granules up to ~840 μm indicated that the granular material occluded salt as effectively as the fine powder under the same blender conditions. The sodalite-glass waste forms fabricated from granular zeolite showed short-term leach resistance (static immersion tests for 3 days) and physical integrity comparable to samples manufactured from fine powders. Longer leach tests of waste forms made with coarser grained materials are underway.

d.   Sintering

We have examined possible alternative consolidation methods that can potentially increase ease of fabrication and throughput, relative to hot isostatic pressing, without sacrificing waste-form durability. The most promising alternative to date is sintering of sodalite-glass composites. Preliminary results suggest that green or unfired composites with densities ranging from 30 to 60% solids can be sintered to full density. The resulting composites appear to be as leach resistant as comparable hot-isostatic-pressed specimens in 3-day leach tests. The sintering process being developed includes moderate heating and cooling rates (5°C/min) and maximum temperatures ranging from 800 to 850°C. Issues related to scaleup are under investigation with the goal of developing a continuous consolidation process.

2.   *Testing and Characterization*

a.   Testing and Characterization Methods

A wide variety of measurements are made to test and characterize the ceramic waste form. Part of the characterization work involves the development of tests that will be used to quality the waste form for disposal in a geologic repository (Sec. III.G.2). These tests are used to develop the processes required to produce waste forms and to characterize the waste from itself. The properties measured include density, apparent porosity, crystalline structure, microstructure, and leach resistance. The density and apparent porosity are measured by Archimedes method. The crystalline phases are determined from X-ray diffraction patterns of ground waste forms. Scanning electron microscopy/energy dispersive microscopy is used to examine the microstructure of the waste form and to determine qualitatively the chemical composition of specific phases.

As a development test, radionuclide retention was determined by immersion of monolithic specimens in deionized water at 90°C following the MCC-1 test procedure. Nearly all of the development samples had a normalized release rate (NRR, defined in Sec. III) of less than 1 g/(m^2·day) in 28-day tests for all elements released. A release rate of less than 1 g/(m^2·day) was a target initially set for vitrified high-level wastes. A limited number of 56-day leach tests

have also been completed for sodalite waste forms. The NRR for all elements released to solution decreased approximately by half as test duration was doubled to 56 days. The NRR decreased with time for zeolite-glass composites with 35% glass or more. These results suggest that most of the radionuclides are released in the initial segment of the test since the release rate declines significantly as the test proceeds.

Most of the characterization work completed to date has involved ceramic waste forms containing simulated waste salt with Ce, Sr, Ba, and rare earth chlorides but no actinides. Scanning electron microscopic examination of the composites showed that at least some of the rare earths were segregated in clusters. Subsequent X-ray diffraction patterns of zeolite containing salt rich in rare earths suggested that the rare earths were, at least partially, converted to oxychlorides. The NRR values measured for the rare earths were the lowest of all the salt components; this finding indicates that the formation of oxychlorides does not adversely affect the behavior of the ceramic waste form.

As the composition and processing of the ceramic waste form are modified and refined, the properties of the waste form will continue to be measured to determine how its behavior is affected.

b. Characterization of Uranium- and Plutonium-Bearing Waste Forms

Initial scoping studies of waste form fabrication were conducted by immersion of zeolite A in a uranium-bearing salt at 500°C. This immersion resulted in the loss of zeolite crystallinity and production of UO_2. In similar tests, rare earth chlorides dissolved in a LiCl-KCl eutectic salt were observed to form oxychlorides when mixed with zeolite at 500°C. Because even very dry zeolite contains a residual amount of water, we are investigating the role that water plays in these reactions and the extent to which the zeolite framework is attacked by highly charged ions. Thermodynamic calculations indicate that U, Pu, and rare earths dissolved in the eutectic salt react to varying extents to form oxides or oxychlorides in the presence of zeolite and/or water. Uranium is very reactive and should react with both zeolite and water to form UO_2. Rare earths will react with water to form oxychlorides but should not react with zeolite. The reactivity of plutonium is intermediate.

Work has now started to determine if Pu and U will react with zeolite to form oxychlorides or oxides, and if the inclusion of these ions (either as 3+ ions or as oxides) affects overall leach performance of the waste form. The work was divided into several phases: preparation of both salt and salt-loaded zeolite, densification of blended zeolite and glass, and leach testing of the ceramic waste form. Materials are being characterized in every phase. Details of the work over the past year are summarized below.

Salt was prepared with 36 wt% (15 mol%) plutonium by oxidizing plutonium metal with $CdCl_2$ in LiCl-KCl eutectic salt. X-ray diffraction examination of the salt indicated that the plutonium was present as K_2PuCl_5. A similar salt containing 52.4 wt% uranium had an X-ray diffraction pattern consistent with $KU_{1.67}Cl_6$. Additional salts will be prepared with lower concentrations of actinides.

Zeolite 4A powder and the high-plutonium salt were mixed at 500°C. X-ray diffraction examination of this salt-loaded zeolite showed that zeolite 4A and PuO_2 were present. Zeolite 4A mixed with a uranium salt in the same fashion showed formation of UO_2 in the X-ray diffraction patterns; zeolite A and other phases were also present in some uranium-bearing samples.

Both the Pu- and U-loaded zeolites were mixed with glass frit in an analytical mill prior to hot pressing, a process identical to that used to produce reference waste forms. The mixture of glass and uranium-loaded zeolites was consolidated by hot isostatic pressing, following the schedules developed for the ceramic waste form.[6] The plutonium-bearing samples were densified with a hot uniaxial press (because this press could fit in our glovebox containing the plutonium-bearing materials). A small amount of the powder mixture was heated to nearly 700°C and pressed at 5000 psi (35 MPa) until the pressure stabilized, as measured by a load cell.

The results of 28-day leach tests for a plutonium-bearing sample are given in Table V-3 in terms of normalized release rates. These data are compared with NRR data from zeolite 4A specimens (hot isostatic pressed) containing simulated fission products but no plutonium. Although the plutonium-bearing sample contained 6 wt% more salt than the one containing simulated fission products, the NRR for plutonium was comparable to that measured for the rare earths, 0.02 $g/(m^2 \cdot day)$. The NRR values for Al and Si were also comparable in the two samples, but the NRR values for the alkali metals were higher in the plutonium-bearing sample, which can be attributed to its greater salt content.

The formation of plutonium and uranium oxides, as well as rare earth oxychlorides, appears to result from the interaction of the chlorides and the zeolite. We are determining if the oxygen source is the aluminosilicate framework of the zeolite or residual water that is not removed during dehydration. If the framework is degraded, the capacity of the zeolite to occlude salt may be diminished, or the crystalline structure destroyed. If the reaction is with residual water, the problem is less severe, but keeping the zeolite dry becomes paramount. The initial water content of the plutonium-bearing zeolite was not measured, but that of the uranium-bearing zeolite was initially 0.16 wt%. At this low level, the molar quantity of uranium in the mixture was greater than that of water, which may be reacting with the uranium chloride to form uranium oxide.

D. Development of Metal Waste Form

Stainless steel-zirconium (SS-Zr) waste form alloys have been developed to immobilize metallic fission products isolated during the electrometallurgical treatment of spent nuclear fuel. The SS-Zr waste forms comprise spent fuel cladding, noble metal fission products, and in some cases, zirconium metal from alloy nuclear fuels. The designation "noble metal" means a metallic element that is inert, or electrochemically noble, in the electrorefiner system; the cladding and

---

[6] J. J. Laidler et al., *Chemical Technology Division Annual Technical Report, 1996*, Argonne National Laboratory Report ANL-97/13, pp. 112-116 (1997).

Table V-3. Leach Test Results for Plutonium-Containing Ceramic Prepared by Hot Uniaxial Pressing (HUP) and for Sodalite Ceramic Prepared by Hot Isostatic Pressing (HIP)

Species	Normalized Release Rate, $g/(m^2 \cdot day)$	
	HUP	HIP
Pu	0.02	a
Rare Earths[b]	a	0.02
B	0.71	0.05
Al	0.44	0.35
Si	0.23	0.23
Li	0.84	0.34
Na	0.58	0.39
K	0.20	0.06

[a]Not determined.

[b]Rare earths include Ce, La, Nd, and Pr.

zirconium are among the noble metals. Since the cladding typically represents 85 to 99 wt% of the metal wastes from electrometallurgical treatment, the waste form alloys use the cladding as the principal alloying component and thus minimize the waste form volume.

This approach gave rise to the parallel development of two nominal compositions of metal waste form: stainless steel-15 wt% zirconium (SS-15Zr) for stainless steel-clad fuel and Zircaloy-8 wt% stainless steel (Zr-8SS) for Zircaloy-clad fuel. A full-scale process demonstration is underway at ANL-West using EBR-II spent fuel, which includes both driver and blanket fuels. Since the driver and blanket fuels from EBR-II contain stainless steel cladding, the research emphasis for this past year has been on the development and characterization of the SS-15Zr alloy. The development of the Zr-8SS alloy is still proceeding, but at a reduced rate, and will not be discussed in this report.

1. Waste Form Metallurgy

A typical SS-15Zr alloy microstructure is shown in Fig. V-4. It contains two primary phases that form a simple eutectic structure: (1) a ferritic iron solid-solution phase (dark contrast in Fig. V-4), designated as α-Fe(Cr,Ni), that is similar in composition to ferritic stainless steel, and (2) a Zr-Fe intermetallic phase (bright contrast), designated as $Zr(Fe,Cr,Ni)_{2+x}$, that is a Laves-type compound (AB_2 structure). In addition to the primary phases, two minor phases are present in SS-15Zr alloys: an austenitic iron solid-solution phase [γ-Fe(Cr,Ni)] and a second Zr-Fe intermetallic compound, $(Fe,Cr,Ni)_{23}Zr_6$.
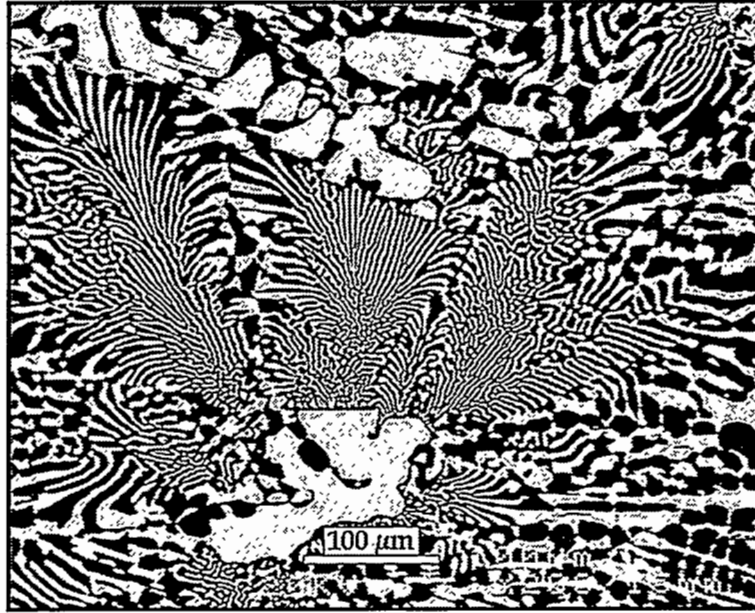
Fig. V-4. Backscattered Electron Image of As-cooled
Stainless Steel-15 wt% Zirconium. The image
reveals eutectic microstructure containing an
iron   solid   solution   (dark)   and   the
$Zr(Fe,Cr,Ni)_{2+x}$ intermetallic (bright).

The elemental composition, crystal lattice parameters, and volume fractions of these phases are reported in Table V-4. The composition data were generated with energy dispersive X-ray spectroscopy, and the crystal structure information was generated from neutron powder diffraction data collected at ANL's Intense Pulsed Neutron Source. The $Zr(Fe,Cr,Ni)_{2+x}$ phase has two crystal structures, which are designated in Table V-4 as Laves C36 (hexagonal) and C15 (cubic). Since these crystal structures cannot be differentiated by scanning electron microscopy, the measured $Zr(Fe,Cr,Ni)_{2+x}$ composition has been arbitrarily assigned to the C36 phase. The composition of the C15 phase may be similar to that listed for the C36 phase in Table V-4. Another interesting point is that the $Zr(Fe,Cr,Ni)_{2+x}$ intermetallics contain only 24 at.% zirconium, a substoichiometry of more than 25% from the expected 33.3 at.% Zr.

The distribution of noble metal fission products in SS-15Zr alloy phases was investigated through the addition of representative, nonradioactive elements such as Ru, Pd, Ag, and Nb. A summary of the elemental distribution in SS-15Zr is presented in Table V-5. In all cases, the noble metals were soluble in the SS-15Zr phases at representative waste form concentrations. Some of the noble metals (Tc, Re, W, Mo, Mn, and Co) were evenly distributed throughout the SS-15Zr, while others (Ru, Nb, Pd, Ta, Ag, Sn, and Si) became concentrated in the intermetallic phases. In general, those elements that became concentrated in the intermetallic tended to have a low solubility in iron.

Since the intermetallic phases are "preferred" locations for several of the noble metals, fission product retention in SS-15Zr is strongly influenced by the volume fraction of the Laves phases, which is, in turn, influenced by the zirconium concentration in the waste form.

Table V-4. Neutron Diffraction and Spectroscopy Measurements from SS-15Zr Alloys

Phases	Elemental Composition, at. %				Lattice Parameters,[a] nm	Vol. Percent
	Fe	Cr	Ni	Zr		
Ferrite (bcc)	67	25	5	<0.1	a = 0.2876	40 ± 5
Austenite (fcc)	71	19	7	<0.1	a = 0.3596	9 ± 1
Laves C36	54	7	12	24	a = 0.4908, c = 1.6016	33 ± 5
Laves C15	—	—	—	—	a = 0.6938	16 ± 2
$(Fe,Cr,Ni)_{23}Zr_6$	58	10	9	20	a = 1.1690	2 ± 1

[a]Accurate to ± 0.0001 nm.

Table V-5. Distribution of Noble Metal Phases in SS-15Zr Alloy

Element	Ratio of Intermetallic to Iron Solid Solution
Ru	~4 : 1
Nb	~8 : 1
Pd	~10 : 1
Tc	~1 : 1
Re	~1 : 1
Ta	~8 : 1
Ag	~5 : 1
Sn	~9 : 1
W	~1 : 1
Mo	<1 : 1
Mn	<1 : 1
Co	~1 : 1
Si	~9 : 1

Therefore, the noble metal distribution was also investigated for alloys containing less than 15 wt% zirconium. In stainless steel alloys with no zirconium, fission products such as Nb, Pd, Ag, and Sn always precipitated to form noble metal-rich phases. In stainless steel-5 wt% zirconium alloys, noble metal precipitates were observed when the $Zr(Fe,Cr,Ni)_{2+x}$ intermetallics became saturated as the total noble metal content increased above ~1 wt% zirconium.

The principal conclusion from these results is that SS-Zr waste forms with 15 wt% zirconium can accommodate all noble metal fission products from any type of fuel treated by the electrometallurgical process. Zirconium compositions below 15 wt% may become saturated at high fission product loadings.

2.   *Testing and Qualification*

Qualification of the metal waste form is a long-term task which involves demonstrating that the waste form material will behave and meet applicable performance requirements. In other words, the material must immobilize and be able to hold onto its radioactive components in a high-level nuclear waste repository. We have performed immersion corrosion tests, electrochemical corrosion tests, and property measurements as part of the development of the SS-15Zr alloy. Results from these tests were summarized in last year's report,[7] and they indicated that SS-15Zr has excellent corrosion resistance and superior mechanical and thermophysical properties for a high-level nuclear waste form. It is now time to move past the developmental research phase by expanding the testing effort to facilitate the repository qualification of the metal waste form.

A standard test method has been established by the American Society for Testing and Materials (ASTM C 1174-91)[8] for the prediction of long-term behavior of nuclear waste materials to be placed in a high-level waste repository. We used this approach to establish a test matrix for the SS-15Zr waste form. The matrix is intended to provide a qualification-relevant data base for future repository acceptance; it contains the following test categories: attribute tests, characterization tests, accelerated tests, and service condition tests.

Attribute tests are designed to quantify the physical attributes of the waste form materials. Characterization tests are designed to generate information on corrosion rates and material alteration mechanisms; test methods include immersion of waste form samples in simulated groundwater at representative repository temperatures for extended times. Accelerated tests are designed to increase the waste form alteration rates beyond those expected under normal conditions; the test results are then analyzed to gain fundamental understanding of the alteration mechanism. Accelerated test methods include electrochemical testing, vapor hydration testing at 200°C, and static immersion testing at 90°C. Service condition tests are designed to simulate the actual conditions encountered in the repository.

The test matrix for the metal waste form defines the number of tests for a particular test method that will be performed on a specified composition of waste form alloy. The matrix has four categories of alloy: "cold," "cold-process variables," "spiked," and "hot." Cold alloys are being generated from nonradioactive ingots containing 5, 15, and 20 wt% zirconium, with and without noble metal additions. Cold alloys are also being generated under various processing conditions, with and without noble metal additions, to examine the effects of impurities and cooling rates on the SS-15Zr behavior. Spiked and hot alloys are being generated at ANL-West and contain technetium, actinide metals, and actual waste from EBR-II fuel.

The implementation of the test plan for the metal waste form is well underway. All of the new SS-15Zr, SS-5Zr, and SS-20Zr ingots needed to prepare the cold test specimens have been

[7] J. J. Laidler et al., *Chemical Technology Division Annual Technical Report, 1996*, Argonne National Laboratory Report ANL-97/13, pp. 109-111 (1997).

[8] American Society for Testing and Materials, *Annual Book of ASTM Standards*, ASTM C 1174-91, Vol. 12.01, Philadelphia, PA, pp. 598-611 (1997).

generated in CMT. The majority of the attribute tests are either completed or underway. The test matrix is scheduled for completion in June 1999, which corresponds to the end of the demonstration of electrometallurgical treatment at EBR-II.

3. Crucible Materials for Waste Form Production

The production of SS-15Zr ingots is accomplished by melting the alloy constituents at 1600°C. This operation is performed in high-temperature, controlled-atmosphere induction furnaces under an argon cover gas at 1 atm pressure (~0.1 MPa). The molten metal is contained in a Y_2O_3 ceramic crucible. Yttrium oxide is a very stable ceramic material that has strong chemical resistance to molten zirconium alloys at 1600°C. Unfortunately, but not unexpectedly, yttrium oxide is not mechanically strong, and it is very brittle. As a consequence, melt crucibles have fractured into multiple pieces during all production runs. On occasion, the melt crucible fractured while the charge was molten. The melt was still contained by the crucible if the fracture was small, but larger cracks can enable the melt to contact the graphite induction susceptor. More frequently, the fracture occurred on cooling when the metal ingot, which had bonded to the crucible wall, thermally shrunk to a greater extent than the crucible wall.

We recognized from the beginning of this effort that yttrium oxide cannot be employed as a full-scale production crucible for the metal waste form. Two alternatives are being pursued: cold and hot crucible melting. Cold crucible melting is a well-established technology for reactive metals, such as Ti and Zr, and for alloys, but the water-cooled hearth presents engineering and nuclear criticality challenges for hot-cell fabrication of metals that will contain enriched uranium (the metal waste form may contain up to ~2 wt% uranium). Recent CMT research has thus focused on overcoming the challenges facing hot crucible melting and developing a crucible material that may be used to contain the waste form alloy.

Our approach to crucible material development has proceeded in two phases. First, a variety of stable ceramic materials were tested in high-temperature interaction studies. Second, the promising materials were refined and tested through further interaction studies and then fabricated into prototype test crucibles. Major parts of this work were carried out under a subcontract with Integrated Thermal Sciences, Inc. (Santa Rosa, CA).

The high-temperature interaction experiment is performed in an inert-atmosphere furnace at temperatures up to ~2100°C. In these experiments, small metal samples of Zr, SS-15Zr, Zr-8SS, and uranium were placed on flat ceramic substrates and heated to a pre-determined test temperature. As an example of the interaction experiment, Fig. V-5 shows a video image taken of zirconium metal "drops" sitting on a ceramic substrate at ~2031°C. The zirconium metal is slightly non-wetting on strontium zirconate ($SrZrO_3$) with a contact angle of ~120° at 2031°C. The molten zirconium is completely non-wetting on the ceramic labeled MYO-B with a contact angle that approaches ~180°, i.e., there is very little contact between the metal and the ceramic. (Some of the materials of interest are proprietary to Integrated Thermal Sciences and cannot be reported at this time.)
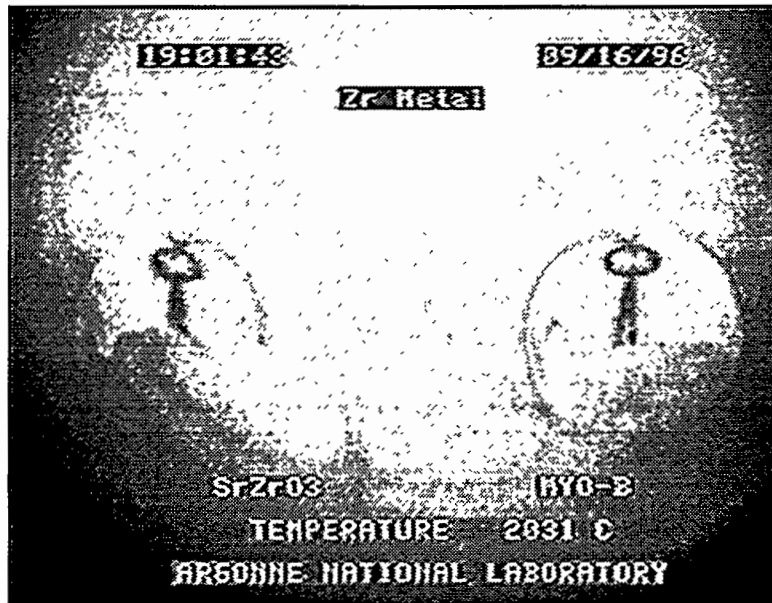
Fig. V-5. Video Image from High-Temperature Inter-
action Experiment Showing Molten Zirconium
on $SrZrO_3$ and MYO-B Substrates

Initial screening tests included interactions between zirconium and SS-15Zr metals and four potential crucible materials (Y_2O_3, BeO, ZrB_2, and carburized tantalum). The results from these tests essentially eliminated BeO, ZrB_2, and carburized tantalum as viable melt crucible materials for zirconium alloys. After these initial tests, a more complete test matrix was performed with 20 candidate substrate materials and Zr, SS-Zr alloys, and uranium. These extended results eliminated numerous materials from consideration and revealed some mixed oxides and stable nitrides that resisted interaction with the molten metals.

Further interaction studies were carried out with Zr and SS-Zr alloys to refine the ceramic processing methods. Two prototype ceramic crucibles (~10 cm diameter by ~15 cm tall) were fabricated and tested. They were designated as the Metal Nitride Prototype (MNP) and the Oxide Ceramic Crucible (OCCR). (Composition of these materials is proprietary.) The MNP crucible was used to generate two SS-15Zr ingots before it failed because of a coating defect, and the OCCR generated only one ingot before it failed because of thermal and mechanical stresses. Since the molten metal must be poured to enable the multiple use of the MNP crucible, further refinements of the MNP material are being investigated.

VI

Pyrochemical Process Applications

The U.S. Department of Energy inventory of spent nuclear fuel consists of ~2700 metric tons of heavy metal and over 100 fuel types. Concerns about the enrichment, chemical stability, and physical condition of many of these fuel types complicate the task of preparing and qualifying them for repository disposal. The electrometallurgical treatment process (see Sec. V) can convert many of these spent fuel types into a uniform set of well-characterized, stable product streams, greatly simplifying the process of preparing and qualifying these fuels for storage or disposal.

The chemical composition of the fuel matrix and cladding determines whether a particular fuel can be directly treated using the electrometallurgical process, or if a pretreatment step is required. For example, oxide fuel types require a pretreatment step that will reduce the actinide oxides to the metallic form prior to electrorefining. The CMT Division has been developing a pretreatment process that uses lithium at 650°C in the presence of molten LiCl to reduce the actinide oxides to the corresponding metals and Li_2O. The Li_2O, which is soluble in LiCl, is subsequently removed from the salt in an electrowinning cell. In this cell, Li_2O is electrolytically decomposed to form lithium metal at the cathode and oxygen at the anode.

During the past year, work continued to develop both the reduction and electrowinning portions of the lithium reduction process, with an emphasis on process scaleup. Corrosion tests were conducted to identify candidate construction materials for a pilot-scale oxide reduction facility planned at ANL-West. In addition, a new program was started to study the applicability of electrometallurgical treatment to the spent fuel types stored at the Idaho National Engineering and Environmental Laboratory (INEEL).

A. Development of Lithium Reduction Process

Before oxide fuels can be electrorefined they require a preliminary treatment that will reduce the actinide oxide components of the fuel to the metallic form. The lithium reduction process uses lithium, dissolved in molten LiCl, at 650°C to reduce the actinide oxides to the

corresponding metals and Li_2O. The Li_2O concentration in the salt is controlled by electrolytically decomposing it to form lithium and oxygen in the electrowinning step. Development work on the reduction step focused on identifying the factors affecting reaction kinetics and improving the transport of lithium to the fuel. Development work on the electrowinning process focused on improving the design of the cell electrodes and obtaining fundamental electrochemical data.

1. Reduction Step

During the past year, progress was made in understanding the factors that control the rate of the UO_2 reduction. A parameter thought to affect the reduction rate is the rate of stirring of the bulk salt. Laboratory-scale experiments were run to investigate the effect of stirring on the reduction rate for two fuel morphologies. The fuel material was selected to simulate what might result from chopping individual spent oxide fuel rods into segments. This material represents a portion of the debris from the Three Mile Island-2 (TMI-2) accident and other disrupted oxide fuels. Crushed UO_2 was used to represent material that might be dislodged from the cladding during the chopping operation. Intact UO_2 pellets (1-cm long), clad with stainless steel, were used to represent material not dislodged from the cladding during the fuel chopping step. The effect of stirring on the reduction rate of crushed UO_2 and of clad UO_2 pellets is shown in Figs. VI-1 and -2, respectively. These results suggest that complete reduction of the crushed UO_2 can be accomplished in as little as 12 h (Fig. VI-1), provided that there is adequate stirring. Stirring had little effect on the reduction rate of clad UO_2 pellets (Fig. VI-2), which required 36 h to be completely reduced whether stirred or not. The difference between the effect of stirring on the two fuel morphologies is thought to result from the different relationship between particle size and the dimensions of the basket used to hold the chopped fuel. Stirring increases the rate of crushed UO_2 reduction because it improves access of bulk salt (and lithium) into the spaces between the particles. Without stirring, the crushed powder tends to act like a single pellet. The relationship between the reduction rate and the stirring speed, fuel morphology, and basket dimensions will be the focus of work in the upcoming year.

2. Electrowinning Step

During the past year, development work on the electrowinning process focused on improving cell and electrode design, obtaining fundamental electrochemical data, and investigating new materials that could be used to fabricate the electrodes.

The most significant technical challenge concerning cell design has been to prevent the recombination of the lithium metal and oxygen produced by electrowinning. This recombination has occurred in two ways. First, because both lithium metal and oxygen gas are less dense than lithium chloride salt, the two products rise to the surface of the melt, where reaction occurs. A less obvious mode of recombination of the reactants has been dissolution/dispersion of the evolved oxygen in the salt. In cell configurations that produce a low anode current density, essentially all the oxygen is evolved at the anode as microscopic bubbles, which become dispersed in the salt by Brownian motion. Previously, ceramic shrouds have been placed around

the anode in an attempt to maintain separation of the lithium and oxygen,[1] but this technique has proven only marginally successful. Separation of the reaction products has been incomplete, or cell performance was decreased due to diffusion/conduction restrictions imposed between the anode and the cathode. In addition, simple shrouds are ineffective against recombination when the oxygen is dispersed throughout the salt.
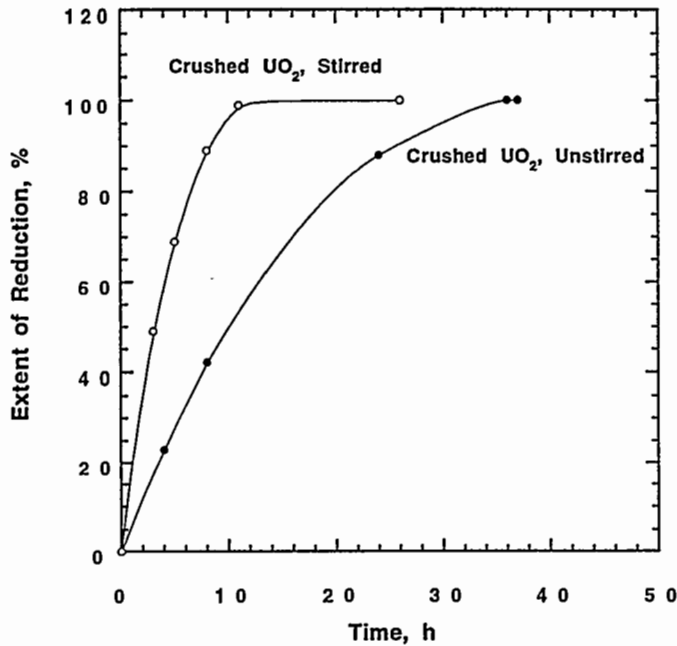
Fig. VI-1.

Effect of Stirring on the Reduction Rate of Crushed UO_2

Fig. VI-2.

Effect of Stirring on the Reduction Rate of Clad UO_2 Pellets (1-cm long)
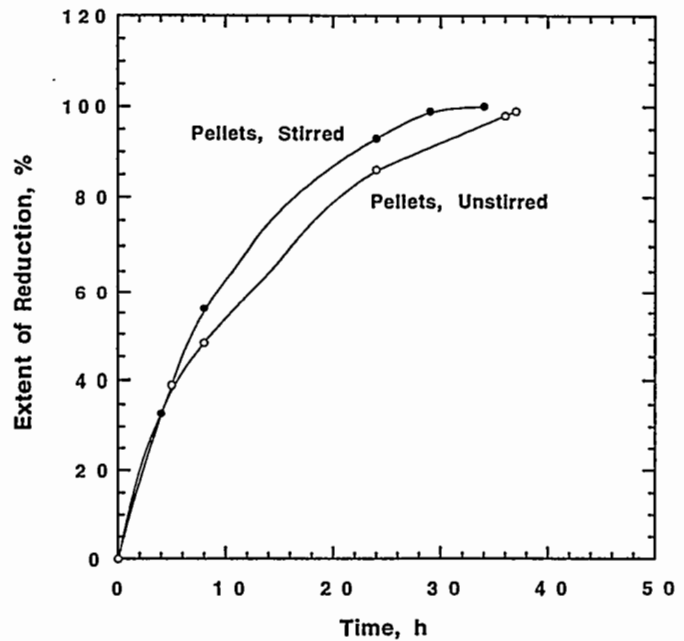
---

[1] J. J. Laidler et al., *Chemical Technology Division Annual Technical Report, 1995*, Argonne National Laboratory Report ANL-96/10, pp. 101-103 (1996).

One approach to solving the problem of oxygen and lithium recombination is to use a porous metal cathode.[2] The advantage of this geometry is twofold. First, all lithium is held below the salt surface so that the surface problem mentioned above cannot occur. This, in turn, allows a cell configuration without any shrouding whatsoever between the anode and cathode. The absence of shrouding allows the anode to run at a higher current density; the high current density not only permits more rapid completion of the experiment, but also causes the production of large oxygen bubbles at the anode, effectively eliminating the problem of dissolution/dispersion. During 1997, laboratory-scale cells were successfully run with no shrouding whatsoever.

In addition to improvements in the cell design, experiments were also performed to determine the maximum acceptable operating voltage of the system. Increasing the cell voltage provides another way to increase the current density. In previous test sequences, we had assumed that the upper limit to this approach is the standard potential for decomposition of LiCl, approximately 3.5 V. Since it is thermodynamically necessary to exceed the decomposition potential of Li_2O (approximately 2.5 V), there would be only a 1 V range of possible operation. Previously, to ensure that LiCl would not decompose, both engineering- and laboratory-scale tests were run at a maximum of 3.0 V at the electrode connections. This imposes a rather significant penalty with respect to maximum current. An experimental examination of the phenomenon of chlorine evolution was undertaken to help clarify this limit on cell operation. No evidence of chlorine evolution was found over a wide range of applied potential. Intentional voltage excursions to ~6-7 V did not exhibit a change in slope of the current-voltage curve. An increased slope is expected at the potential that chlorine evolution begins. Starch-iodide paper, a chlorine indicator, put in the off-gas from the cell never indicated chlorine.

To further investigate the effect of Li_2O on the cell operation and to check system behavior in the limiting case of very low Li_2O concentration, we fabricated a special cell that contained LiCl and no Li_2O. Cell potential was slowly increased while the cell current was monitored. At approximately 3.8 V (measured outside the cell), the current began to rise very rapidly. At the same time, the salt surface was observed to develop a cloudy appearance. This was assumed to be the result of chlorine gas bubbles breaking the surface. A Drager tube was used to sample the cover gas and verified the presence of chlorine. Post-test examination of the platinum anode revealed extensive surface attack, and the salt was found to contain platinum chloride.

Continued work will be needed to determine the precise phenomena that prevent the decomposition of LiCl, but some tentative possibilities can be suggested. One is that the voltage profile and the composition gradients that are established in the electrolysis of Li_2O (beginning at ~2.5 V) do not allow the chloride reduction to begin. Another possibility is that the conditions at the anode during Li_2O reduction prevent the anode overpotential necessary to drive the chloride reduction reaction.

---

[2] J. J. Laidler et al., *Chemical Technology Division Annual Technical Report, 1996*, Argonne National Laboratory Report ANL-97/13, pp. 126-127 (1997).

In addition to the above work, development of materials to replace the expensive Pt-Rh anode has advanced. The candidate materials identified as promising are Fe_3O_4, SnO_2, and NiO. Recent work has focused on fabrication of a Fe_3O_4 anode. The process being pursued involves fabrication of the ceramic electrode inside a metal tube. This method is being developed particularly for Fe_3O_4 because it eliminates problems unique to Fe_3O_4. While Fe_3O_4 is very conductive due to the mixed valence state of iron, the material readily undergoes oxidation/reduction during high-temperature fabrication. The approach being developed is to swage the Fe_3O_4 powder inside a metal tube and subsequently sinter the material while still within the tube. This controls the oxygen partial pressure within the tube so that the Fe_3O_4 stoichiometry remains unchanged. We found that the process works well if the thermal expansion of the Fe_3O_4 and the metal is matched. It was demonstrated that Inconel 600 matches the expansion of the Fe_3O_4 sufficiently well that the Fe_3O_4 can be sintered without cracking. In practice, the Inconel sheath would remain on the anode and would provide protection during shipping and handling, as well as a convenient means of electrical connection to the electrode. Future work will consist of evaluating the manufacture and performance characteristics of each of the three alternative anode materials.

B.   Engineering-Scale Experiments

The purpose of the engineering-scale experiments is to obtain design information and operating experience needed for scaling up the reduction and electrowinning processes to equipment sizes required for processing DOE spent oxide fuels at ANL-West and elsewhere. To meet this objective, the facility used for these experiments was designed to support the reduction of kilogram quantities of fuel. The engineering-scale facility consists of three major components: the reduction vessel, the electrochemical vessel, and the casting station. The reduction vessel holds the salt, fuel, and lithium during the reduction step; the electrochemical vessel holds the molten salt during the electrowinning step that regenerates the spent salt and lithium; and the casting station provides a means to cast the regenerated salt into ingots for storage between process steps. The molten salt and lithium are transferred among these three components through heated transfer lines. All of the equipment is enclosed in a large (7.6 x 2.4 x 2.6 m) argon atmosphere glovebox; the facility is qualified to handle limited quantities of plutonium and other transuranics.

The fourth engineering-scale test (ES-4) was completed in March 1997 and involved the reduction of unirradiated uranium oxide of two fuel morphologies. Crushed UO_2 was used to represent fuel material that might be dislodged from the fuel cladding during a chopping operation. The individual pieces of crushed fuel ranged in size from several millimeters down to 325 mesh. Intact UO_2 pellets (1-cm length), clad with stainless steel, were used to represent material not dislodged from the fuel cladding during chopping. The size and compaction of the fuel material that result from the chopping are believed important because they may determine the time necessary for the reduction step. As the irradiated spent fuel to be processed in the ANL-West pilot facility (currently under design) is expected to be more porous and contain more cracks than our unirradiated simulated fuel, it should reduce more quickly, and thus, the results obtained by ES-4 should be viewed as conservative.

Two fuel basket/pouch assembles were used during ES-4: one was loaded with 3.6 kg of crushed material and the other with 2.9 kg of clad pellets. Each of the fuel basket pouches was 1.5-cm thick, 7.6-cm wide, and 40-cm tall. Figure VI-3 is a schematic diagram of the reduction vessel and fuel baskets. Initially, 760 g of lithium was added to the vessel; 100 g of additional lithium was added near the end of the test to ensure adequate reduction. This second addition was done after it was observed that the Li_2O concentration in the salt had leveled off even though the reduction of the clad pellets was still incomplete (as was seen by examining samples removed from the pellet-containing pouch on a daily basis).
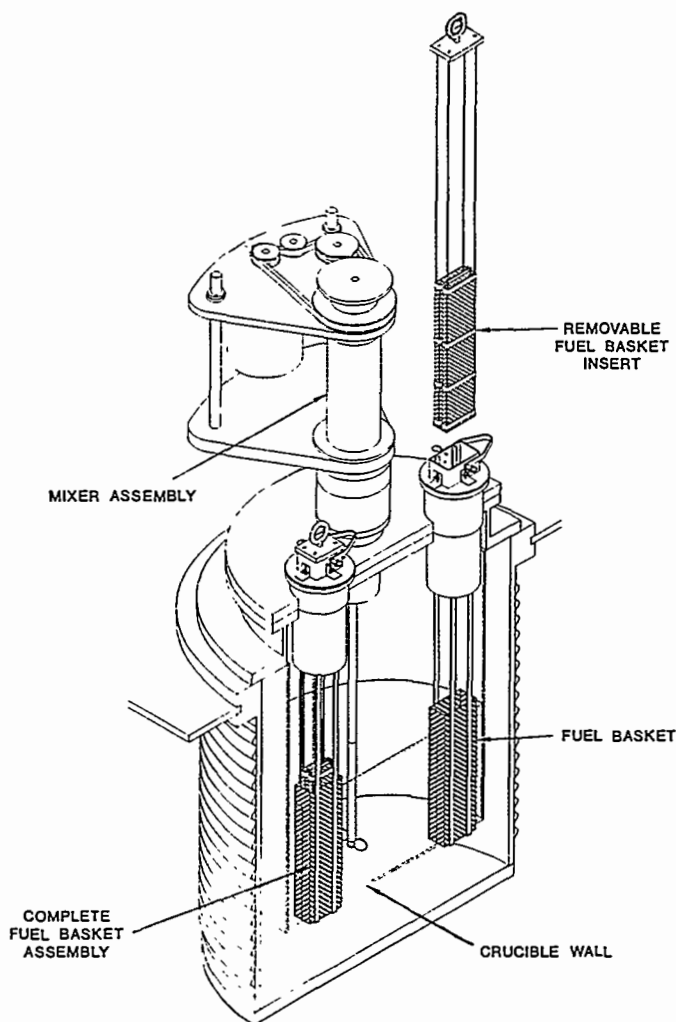
Fig. VI-3.

Cut-away View of Reduction Vessel and Fuel Basket Assemblies Used in Engineering-Scale Experiments

The reduction was terminated after 120 h. Examination of the material in the pouches and determination of the Li_2O concentration in the salt as a function of time indicated that the crushed material was completely reduced in about 50 h, but the pellets were only 40% reduced after 120 h.

A series of laboratory experiments done prior to ES-4 (Sec. VI.A.1) indicated that pellets should have been fully reduced in less than 40 h and crushed material in much less time than 40 h, even in an unstirred system. Several reasons for the differences in reduction time between

the engineering- and laboratory-scale tests are being investigated, including the method of introducing the lithium reductant into the salt. In ES-4, the lithium floated in puddles on the top of the stirred salt melt, where it could have become contaminated with lithium nitride from a reaction with the small amount of nitrogen in the glovebox atmosphere.

The success of ES-4 was in demonstrating complete reduction of one type of fuel morphology in a basket/pouch assembly similar to the design that may be used in the ANL-West electrorefiner operations. This experiment also provided valuable input into the design requirements for the fuel baskets with regard to the reduction of crushed UO_2. This information will be used in designing full basket/pouches and fuel loading for the next engineering-scale test.

C. Treatment of INEEL Spent Fuel

The inventory of spent nuclear fuel at Idaho National Engineering and Environmental Laboratory (INEEL) contains a wide variety of fuel types that are unsuitable for direct repository disposal in their current form. Concerns about the enrichment, chemical stability, and physical condition of these fuel types complicate the task of preparing and qualifying them for repository disposal. The electrometallurgical treatment has the potential to simplify preparing and qualifying these fuels for disposal by converting them into a uniform set of three product streams (uranium metal, a metal waste form, and a ceramic waste form). At ANL-West, a demonstration of the electrometallurgical process is underway with sodium-bonded metallic fuel from Experimental Breeder Reactor-II (EBR-II), the fuel type for which the process was designed. At the same time, we are evaluating whether the electrometallurgical process can also be used to treat nonmetallic fuel types at INEEL. Examples of these include ceramic matrix oxide, hydride, and carbide fuels. Also included are components of metallic fuels that have reacted with water during storage to form uranium oxide and hydride. Issues being evaluated include the nature of any required head-end treatment to prepare the spent fuel for the electrometallurgical process, and the chemistry and the operating conditions of the electrorefining step.

The material used to clad or alloy the uranium determines, in part, the maximum voltage at which the electrorefining process can take place to ensure separation of the cladding or alloying elements from the uranium. Oxide fuels require a preliminary treatment step to reduce the oxide components of the fuels to a metallic form prior to electrorefining. Thus, the first step in the evaluation process was to categorize the "special case" fuels by chemical composition.

In terms of chemical composition, special-case spent INEEL fuel can generally be classified as metallic, oxide, hydride, or carbide. The electrometallurgical process can be applied without substantial changes to all the metallic fuel types, with the exception of U-Al alloy. The ability of the ANL-designed electrorefiner to separate the components of Zircaloy-clad uranium fuel has been demonstrated at the engineering scale using unirradiated fuel from the Hanford N-Reactor.[3] It is anticipated that U-Mo alloy fuel (FERMI-I reactor) can be treated in a manner

---

[3] J. J. Laidler et al., *Chemical Technology Division Annual Technical Report, 1994*, Argonne National Laboratory Report ANL-95/24, pp. 90-93 (1995).

similar to the N-Reactor fuel, but a more detailed characterization of the U-Mo fuel is required, along with laboratory-scale testing of the U-Mo alloy in the electrorefining system. Electrometallurgical treatment of U-Al alloy fuels is possible with some modifications to the current electrorefining technique. Theoretical studies and experimental work using simulated U-Al alloy fuel have been employed to develop a number of process options.

The ability of the lithium reduction process to reduce the principal components of oxide fuel has been demonstrated at the engineering scale.[4] Experimental work done to apply the lithium reduction process to the reduction of simulated TMI-2 fuel debris indicates that it can be used to reduce UO_2-ZrO_2 matrix fuels, although additional work needs to be done on UO_2-ZrO_2-CaO matrix fuel. The existing lithium reduction process can also be used to treat mixed-oxide fuels; for this type of fuel, additional work is required to verify the optimum conditions required to reduce PuO_2. Metallic fuels that have reacted with water during storage may have become oxidized and must also be treated, at least in part, as nonmetallic. This degraded metallic fuel, along with hydride- and carbide-based fuel, requires a head-end step to reduce the fuel to a metallic form prior to electrorefining. The required head-end treatment steps for these fuels are to be studied in the next year.

D.   Materials Evaluation for Pilot-Scale Facility

In support of design work being performed on the pilot-scale oxide reduction facility planned for construction at ANL-West, a series of tests was performed to evaluate candidate materials for vessel construction. Separate tests were conducted for both the reduction vessel and electrowinning vessel because of the difference in conditions between the two. The reduction vessel will contain lithium chloride with varying amounts of lithium metal and lithium oxide. The hardware is exposed to essentially no free oxygen or lithium metal. The salt is at or near saturation with lithium metal during the process; therefore, the conditions are quite reducing. The electrochemical vessel components will be exposed to various concentrations of oxygen in salt and cover gas. The initial tests were run for 30 days, after which the test coupons were removed for evaluation.

. The test conditions for the reduction vessel were the following: argon cover gas, a salt of $LiCl/3.5$ wt% $Li_2O/1$ wt% Li_3N, and an operating temperature of 725°C. The nitrogen in the salt composition was selected in an attempt to simulate the atmosphere conditions that would occur in the oxide reduction facility, where the environment is primarily argon but with a significant amount of nitrogen. Test coupons included tantalum, stainless steel (Types 316L, 422, and 430), and 2¼ Cr-1Mo steel. All coupons were 2.5 cm in width and 7.5 cm in length and had a weld along the full length. Two tantalum samples were used, one as-welded and one with a post-weld heat treatment to relieve stresses. All others were tested in several forms: as-welded, post-weld heat treatment, aluminized, and aluminized and heat treated. The result of the test was that

---

[4]   J. J. Laidler et al., *Chemical Technology Division Annual Technical Report, 1996,* Argonne National Laboratory Report ANL-97/13, pp. 128-130 (1997).

tantalum suffered minor attack, while none of the other test coupons had any measurable corrosion.

The test conditions for the electrochemical vessel were the same as for the reduction vessel, except that the cover gas was argon-10% oxygen. The gas was fed in below the surface of the salt to better simulate the conditions in the electrowinning step. The samples for this test were the same as for the reduction test, except that the two tantalum samples were deleted. In this test, all samples were severely corroded, most beyond recognition. While some attack was expected because corrosion of Type 304 stainless steel had been observed in laboratory-scale electrochemical testing, nothing so severe had been observed. Indeed, corrosion mechanisms and corrosion rates could not be determined because of the extent of the corrosion. It became clear that oxygen attack in this system is extremely severe.

A subsequent test was run to better understand the corrosion and to help rank materials with respect to corrosion resistance. Samples were tested for 6 days at 625°C with a cover gas of argon-10% oxygen and a salt of LiCl-3.5 wt% Li_2O. Sample materials included Type 316L stainless steels (one aluminized, the other not), 304 stainless steel, Inconel 600, and Inconel 625. All stainless steels incurred more corrosion damage than either of the Inconel (nickel-chrome) materials. The aluminizing had no beneficial effect, but later microscopy revealed that the commercially applied aluminizing was quite porous and poorly bonded. Iron aluminide on the stainless steel and the nickel aluminide on Inconels should provide enhanced corrosion resistance. The characterization of the possible aluminization processes has begun, and aluminized samples will be tested. A second 6-day test was completed with nickel-based alloys exclusively (Inconel 600, Inconel 625, Haynes 242, and Krupp alloys 31, 33, 59, 602Ca, and 45TM). The Inconel 600 and Krupp alloy 31 experienced the least attack. Alloy 31 exhibited a generally very thin corrosion layer but had occasional deep penetration. Inconel 600 had a heavier but more uniform corrosion layer.

Future work will continue to focus on finding corrosion-resistant materials for the electrochemical vessel construction.

VII

Basic Chemistry Research

Basic chemistry research is being pursued in several areas: fundamental chemistry associated with catalyses in systems that involve molecular energy resources, mechanisms of ion transport in lithium battery electrolytes, materials chemistry of electrified interfaces (in connection with corrosion and electrochemical devices) and molecular sieve materials (in connection with catalysis), and the theory of materials properties.

A. Chemical Sciences Research

Our program employs *in situ* spectroscopic and mechanistic techniques to examine the reaction chemistry of processes that are used in the chemical industry or are under development for industry. Recent work in fluid catalysis encompasses (1) the first *in situ* nuclear magnetic resonance (NMR) investigation of phosphine-modified catalysts for the hydroformylation of olefins in supercritical fluids and (2) the study of extremely robust polyfluorophthalocyanine catalysts for hydrocarbon activation processes. Also, in a program associated with development of a lithium-polymer battery (see Sec. I.A.1), we are developing toroid cavity imaging techniques for the *in situ* examination of ion transport in lithium-polymer battery materials.

1. Catalytic Chemistry in Supercritical Fluids

Supercritical fluids (CO_2 or water) offer environmentally benign alternatives to toxic organic solvents frequently used in homogeneous catalysis. An additional advantage is the elimination of energy-intensive distillations necessary for product separations and catalyst recovery from organic solvents. Our efforts have focused upon the development of homogeneous catalyst systems in supercritical carbon dioxide ($scCO_2$) and both single- and two-phase $scCO_2$ surfactant and/or solvent mixtures.

The oxo process, in which homogeneous catalysts are used for the hydroformylation of olefins, is one of the largest industrial processes used worldwide today. In this process, carbon

monoxide and hydrogen react with an olefin to selectively produce the desired linear isomers of aldehydes:

$$R = alkyl \qquad\qquad \text{"normal"} \qquad \text{"iso"} \qquad (1)$$
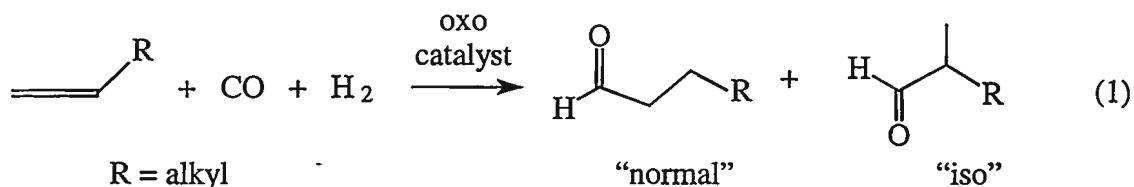
The linear "normal" isomers are desired over the branched "iso" products. Oxo products are used in detergents, plastics, and agricultural products. The capacities of homogeneous oxo processes exceeded 6.6 million tons per year in 1995.[1]

Currently, we are examining high-pressure reactions of phosphine-substituted cobalt carbonyl catalysts with CO, H_2, and excess free phosphine by NMR spectroscopy.[2-5] The reactivity with CO and H_2 is of interest as these gases are requisite for the oxo reaction in Eq. 1. The addition of excess phosphine is thought to inhibit CO substitution for phosphine in the substituted cobalt carbonyl complexes. It is believed that the steric effects from the phosphine in these complexes impart selectivity for the desired normal oxo products.

The phosphine-substituted cobalt system examined most extensively by us has been $[Co(n\text{-}Bu_3P)(CO)_3]_2$, a Shell-type catalyst. Using specially designed *in situ* NMR detectors, we have monitored precatalytic equilibria under the high pressure and temperature regimes at which the oxo process is commercially operated. Solvent polarity effects are pronounced and have been examined in cyclohexane, benzene, dioxane, *i*-butanol, $scCO_2$, and $scCO_2$/toluene mixtures. While supercritical solvent systems offer many advantages, difficulties have arisen with their use. The dimer, $[Co(n\text{-}Bu_3P)(CO)_3]_2$, is moderately soluble in $scCO_2$/toluene; however, upon addition of CO, the dimer concentration in the fluid decreases. We believe that the dimer is converted to a disproportionation salt, and that this salt precipitates out of the $scCO_2$/toluene mixture. The disproportionation reaction is

$$[Co(n\text{-}Bu_3P)(CO)_3]_2 + CO \rightleftharpoons [Co(n\text{-}Bu_3P)_2(CO)_3][Co(CO)_4] \qquad (2)$$
$$\text{[dimer]} \qquad\qquad\qquad\qquad \text{[cation]} \qquad \text{[anion]}$$
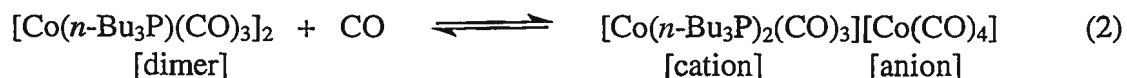
[1] M. Beller, B. Cornils, C. D. Frohning, and C. W. Kohlpaintner, *J. Mol. Catal. A* **104**, 17-85 (1995).

[2] J. W. Rathke, R. J. Klingler, R. E. Gerald, K. W. Kramarz, and K. Woelk, *Prog. Nucl. Magn. Reson. Spectrosc.* **30**, 209-253 (1997).

[3] K. W. Kramarz, R. J. Klingler, and J. W. Rathke, "*In Situ* NMR Spectroscopy Studies of Hydroformylation Catalysts Using High Pressure Toroid Probes," Abstracts of the Sixth Int. Conf. on the Chemistry of the Platinum Group Metals, University of York, July 21-26, 1996, p. 48 (1996).

[4] K. W. Kramarz, R. J. Klingler, and J. W. Rathke, "High Pressure *In Situ* NMR Spectroscopy of Cobalt Oxo Catalysts," Technical Abstracts of the 15th North American Catalysis Society, Chicago, IL, May 18-23, 1997, p. 149 (1997).

[5] J. W. Rathke, *J. Magn. Reson.* **85**, 150-155 (1989).

The formation of the salt from the dimer has been examined in various organic solvents. The thermodynamics of salt formation (see Table VII-1) becomes more favorable as solvent polarity increases (benzene < dioxane < i-butanol). In addition, salt formation increases with decreasing temperatures and higher CO pressures for all of the solvents investigated.

Table VII-1.   Thermodynamics of Salt Formation in Eq. 2. Data given for
equilibrium constant (K_2), enthalpy of formation (ΔH°),
entropy (ΔS°), and free energy (ΔG°).

Solvent	K_2, atm^{-1} at 100°C	ΔH°, kcal/mol	ΔS°, eu	ΔG°, kcal/mol
Benzene	8.0 (±0.8) × 10^{-3}	-14 (±0.2)	-44 (±0.4)	0.3 (±0.3)
Benzene[a]	1.3 (±0.8) × 10^{-3}	-15 (±0.5)	-52 (±1.4)	0.5 (±1.0)
Dioxane	0.013 (±0.003)	-21.5 (±0.6)	-65 (±1.4)	-2.0 (±1.2)
i-Butanol	0.495 (±0.04)	-17 (±0.3)	-47 (±0.8)	-3.0 (±0.6)

[a]In the presence of excess free n-Bu$_3$P (dimer-to-Bu$_3$P ratio of 1:1).

The equilibrium in Eq. 2 becomes complicated at low temperatures. An additional resonance is evident at 20°C, as shown in Fig. VII-1. This new resonance does not occur in the presence of added free phosphine. Therefore, one possibility for this new species is that it is produced by phosphine displacement from the dimer reactant of Eq. 2, as follows:

$$[Co(n\text{-}Bu_3P)(CO)_3]_2 + CO \rightleftharpoons Co_2(n\text{-}Bu_3P)(CO)_7 + n\text{-}Bu_3P \qquad (3)$$
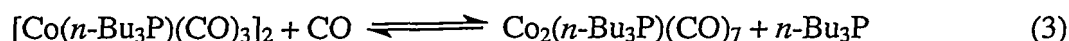
Fortunately, the monosubstituted dinuclear complex can be prepared independently, and its ^{31}P NMR resonance occurs at approximately 56 ppm at room temperature. This complex exhibits a strong and characteristic chemical shift dependence on temperature, as shown in Fig. VII-2. This dependence is most likely due to a bridging/terminal isomerization of the complex's carbonyl ligands, similar to that observed for dicobalt octacarbonyl. Significantly, this characteristic dependence on chemical shift allows the monosubstituted dimer to be eliminated from further consideration because the temperature dependence of the chemical shift for the independently synthesized monosubstituted dimer in Fig. VII-2 is not consistent with the observations under the experimental reaction conditions in Fig. VII-1. Alternatively, the new resonance is tentatively
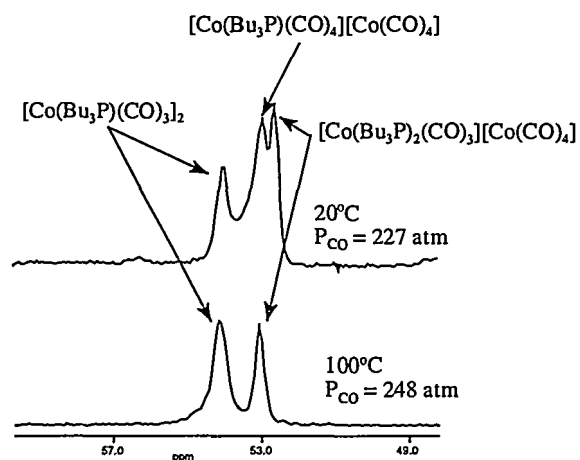
Fig. VII-1.

In Situ ^{31}P NMR Spectra Showing the Resonance for the Monosubstituted Salt at 20 and 100°C
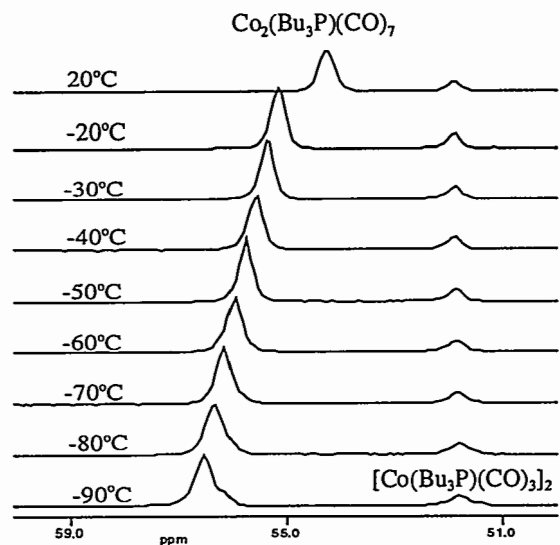
Fig. VII-2.

In Situ ^{31}P NMR Spectra Showing the Chemical Shift Temperature Dependence for $Co_2(Bu_3P)(CO)_7$

assigned to a salt that is analogous to the product in Eq. 2, where one of the phosphine ligands in the cation has been substituted by carbon monoxide to yield $[Co(n\text{-}Bu_3P)(CO)_4][Co(CO)_4]$. Consistent with the proposed CO substitution reaction, the resonance for the new species disappears in the absence of CO at ambient temperature. Preliminary experiments have shown that both salts are formed from $Co_2(n\text{-}Bu_3P)(CO)_7$ at about 300 atm of CO. This would account for the absence of $Co_2(n\text{-}Bu_3P)(CO)_7$ under the aforementioned conditions.

The thermodynamics of the salt/dimer in benzene was reexamined for reactions in the presence of excess free phosphine. As expected from the lack of phosphine dependence for the reaction shown in Eq. 2, the deviation from the data obtained previously was insignificant. However, data were obtainable as low as 50°C without complications arising from the resonance assigned to $[Co(n\text{-}Bu_3P)(CO)_4][Co(CO)_4]$. These observations indicate that there is very little $[Co(n\text{-}Bu_3P)(CO)_4][Co(CO)_4]$ present, if any, at temperatures above 75°C. The thermodynamic data obtained for the equilibrium in Eq. 2 are summarized in Table VII-1.

For a dimer-to-Bu_3P ratio of 1:4, the ^{31}P NMR spectra indicated that all species convert to an uncharacterized species with a resonance occurring at approximately -19 ppm. Free phosphine occurs at -30 ppm; however, it undergoes a fast exchange with the species at -19 ppm, resulting in a chemical shift average of the two species at temperatures above 35°C. This is significant because conditions that decrease the amount of precatalytic dimer decrease the amount of hydride formed just prior to the catalytic cycle.

Future studies will examine the effect of adding many equivalents of free phosphine because the commercial phosphine-modified cobalt carbonyl process (Shell) is typically run in the presence of excess free phosphine. Formation of the hydride in the presence of excess phosphine is thus underway. Preliminary results indicate that the unknown species is present in significant amounts in the commercial process at high CO pressures. Attempts to characterize this species by using ^{13}C NMR are also underway.

2.   Hydrocarbon Activation Chemistry

Selective functionalization of hydrocarbons remains a great challenge to organometallic chemists. Because homogeneous catalysts are better defined and characterized than heterogeneous catalysts, major advances in our understanding of catalytic processes are derived mostly from studies of homogeneous catalysis. In addition, the uniformity of the catalyst sites in these systems makes these catalysts more likely to yield good product selectivity. We have continued our studies of metallophthalocyanine-catalyzed hydrocarbon activation. Metallophthalocyanines are chosen as catalysts because of their high-temperature stability and their similarity in structure to porphyrins, which are the prosthetic groups of heme enzymes that catalyze the aerobic oxidation of hydrocarbons in biological systems.[6,7]

We reported previously that [(RPc)Rh]$_2$ (where RPc = dianion of 1,4,8,11,15,18,22,25-octa-n-pentylphthalocyanine) catalyzes the C-H bond activation by a free radical mechanism initiated by homolysis of the Rh-Rh bond, which is estimated to have a bond energy of 23 kcal/mol.[8,9] To weaken the Rh-Rh bond, we have invoked coordination of ligands on the axial sites. Trimethylphosphine successfully breaks the Rh-Rh bond at ambient temperature. However, six-coordinate (RPc)(PMe$_3$)$_2$Rh, instead of five-coordinate (RPc)(PMe$_3$)Rh, was obtained, even in solutions in which the ratio of PMe$_3$/Rh was unity. Our recent ^{1}H NMR studies show that the initially formed five-coordinate (RPc)(PMe$_3$)Rh simply disproportionates to (RPc)(PMe$_3$)$_2$Rh and [(RPc)Rh]$_2$(PMe$_3$):

$$3(RPc)(PMe_3)Rh \longrightarrow (RPc)(PMe_3)_2Rh + [(RPc)Rh]_2(PMe_3) \qquad (4)$$
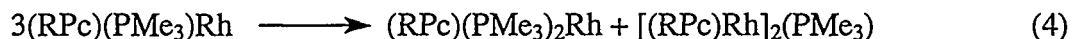
In support of our conclusion that the six-coordinate 19-electron (RPc)(PMe$_3$)$_2$Rh is a ligand-centered radical,[10,11] the electron spin resonance (ESR) spectrum of (RPc)(PMe$_3$)$_2$Rh in Fig. VII-3a shows that it has a g-value (electronic gyromagnetic ratio) very close to the free electron value of 2.0023. A calculated simulation yields $g_{||}$ = 1.989 and $g_\perp$ = 1.995. Shown for comparison in Fig. VII-3b is the ESR spectrum of the corresponding ligand-centered cobalt complex (RPc)(PMe$_3$)$_2$Co, which gives $g_{||}$ = 1.983 (A$_{||}$ = 19.5 G)* and $g_\perp$ = 1.994. The hyperfine couplings to ^{103}Rh were not resolved, neither was the hyperfine coupling to ^{59}Co in the perpendicular direction (A$_\perp$). In contrast, the metal-centered, four-coordinate (RPc)Co in toluene glass has the following g-values: $g_{||}$ = 1.982 (A$_{||}$ = 175 G) and $g_\perp$ = 2.627 (A$_\perp$ = 148 G). These data show the difference in the g-values of metal- and ligand-centered radical Co^{II} complexes.

[6] J. H. Dawson, *Science* 240, 433 (1988).

[7] B. Meunier, *Chem. Rev.* 92, 1411 (1992).

[8] M. J. Chen and J. W. Rathke, *Organometallics* 13, 4875 (1994).

[9] M. J. Chen, L. Nuñez, J. W. Rathke, and R. D. Rogers, *Organometallics* 15, 2338 (1996).

[10] W. E. Geiger, *Acc. Chem. Res.* 28, 351 (1995).

[11] D. R. Tyler, *Acc. Chem. Res.* 24, 325 (1991).

* The symbols A$_{||}$ and A$_\perp$ are the parallel and perpendicular electron-spin nuclear-spin hyperfine coupling constants.
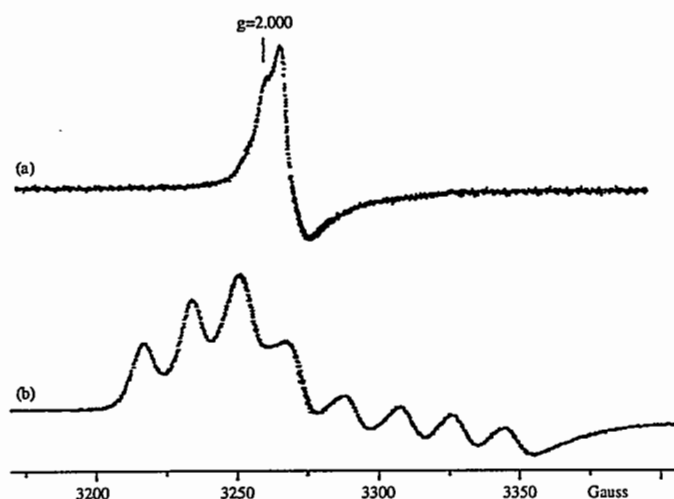
Fig. VII-3.

Electron Spin Resonance Spectra of $(RPc)(PMe_3)_2Rh$ (curve a) and $(RPc)(PMe_3)_2Co$ (curve b) in Toluene Glass at $-263°C$

We have also extended our study of $[(FPc)Fe]_2(\mu\text{-}O)$ [where FPc = dianion of 1,4,8,11,15,18,22,25-octakis(trifluoromethyl)phthalocyanine], which catalyzes the epoxidation of olefins by iodosylbenzene, to include other olefins.[12] For substrates that have alkyl substituents, both epoxidations and alkyl C-H bond oxidations have been observed. Although *trans*-stilbene gives *trans*-stilbene oxide as the only product, *cis*-stilbene gives a mixture of *cis*- and *trans*-stilbene oxides. This finding indicates that epoxidation of *cis*-stilbene, and possibly other olefins as well, proceeds through a non-concerted mechanism.

Although the oxidation of olefins has been shown to be catalytic, the turnover numbers are still low. We suspect that the source of catalyst instability is the eight aromatic hydrogens. Future work will include synthesis of phthalocyanines that have these aromatic hydrogens replaced by halogens or perfluorinated alkyl substituents. We are also working to isolate $(FPc)Fe^{IV}=O$ for further studies. Since $(FPc)Fe^{IV}=O$ is among the least reactive Fe^{IV}-oxo complexes, it offers a good opportunity for studying the chemical and physical properties of these complexes.

3. Electrochemical/Battery Research

This program investigates the mechanism of ion transport in lithium-polymer electrolyte battery materials by using *in situ* magnetic resonance imaging.[13-15] An imaging approach is necessitated by the inhomogenous nature of existing battery systems. For example, in the current generation of lithium-polymer electrolytes, only a small fraction of the ionic current is carried by the electroactive lithium ions. Consequently, the passage of current through these battery

---

[12] M. J. Chen, D. E. Fremgen, and J. W. Rathke, to be published in *J. Porphyrins Phthalocyanines*.

[13] K. Woelk, J. W. Rathke, and R. J. Klingler, *J. Magn. Reson. A* **105**, 113 (1993).

[14] K. Woelk, J. W. Rathke, and R. J. Klingler, *J. Magn. Reson. A* **109**, 137 (1994).

[15] K. Woelk, R. E. Gerald II, R. J. Klingler, and J. W. Rathke, *J. Magn. Reson. A* **121**, 74 (1996).

materials results in large changes in the lithium ion concentration in the region of the electrolyte directly adjacent to the electrodes, and an electrolyte depletion zone is rapidly established. Furthermore, a typical electrolyte depletion zone accounts for a only small volume percent of the total electrolyte material. Accordingly, the electrolyte depletion region is difficult to investigate by conventional spectroscopic methods, and all of the existing NMR literature on lithium ion diffusion coefficients and polymer interactions has been obtained for homogeneously loaded samples. Consequently, very little is known about how the ion mobility or the structure of the polymer is influenced by the electrolyte concentration gradients.

It is generally believed[16,17] that the cations tend to cross-link the polymer chains, thereby influencing the segmental motion of the polymer. Furthermore, the segmental polymer motion is believed to be the most important factor controlling the ionic conductivity in polymer electrolytes.[16,17] Importantly, this causes changes in the region adjacent to the electrodes due to the dynamic nature of the electrolyte concentration gradients. With the NMR imager, it should be possible for the first time to probe for differences in the ion and polymer mobility across the electrolyte concentration gradients by measuring the NMR spin relaxation times, T_1 and T_2, as a function of distance from the working electrode.

Previously, we reported that electrolyte depletion zones can be accurately mapped by using *in situ* NMR imaging.[2] For example, the upper ^{19}F NMR plot in Fig. VII-4 illustrates the lithium triflate concentration as a function of distance from the working electrode before (solid) and after (dashed) electrodepositing lithium. The electrolyte is depleted over a distance of approximately 0.3 mm from the working electrode, where the electrode radius is represented by the gray region in Fig. VII-4. At ambient temperature, the electrolyte concentration gradients produced in this manner are quite stable for periods of many hours. This allows ample time to
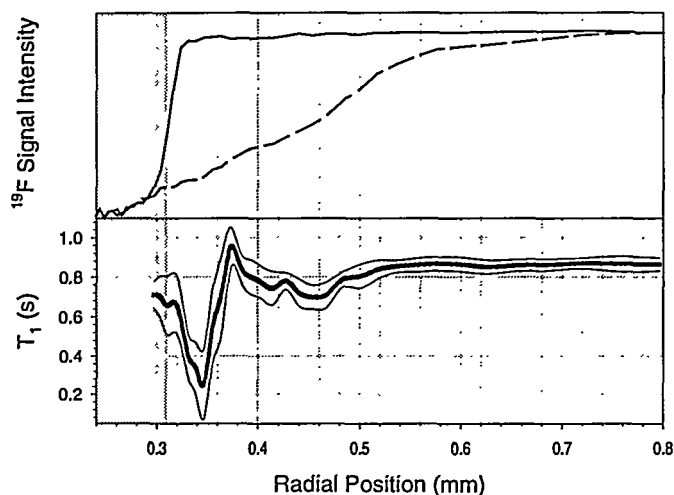
Fig. VII-4.

Concentration of $CF_3SO_3^-$ in Sample of Polyethylene Oxide/CF_3SO_3Li before (solid curve in upper plot) and after (dashed curve) Depositing Lithium. Lower plot shows the resultant T_1 spin relaxation time (thick solid curve) in the polarized cell, including confidence interval (thin curves).

[16] M. A. Ratner and D. F. Shriver, *Chem. Rev.* **88**, 109 (1988).

[17] P. G. Bruce and C. A. Vincent, *J. Chem. Soc. Faraday Trans.* **89**, 3187 (1993).

measure the NMR spin relaxation times, T_1 and T_2, as a function of distance from the electrode for the ionic species, as well as the polymer backbone across the region of the electrolyte concentration gradient.

The T_1 measurement requires inversion of the Boltzmann spin population. Yet, there is no common nutation angle for the nuclei within a toroid cavity following a simple transmitter pulse because of the large B_1 field dependence in the toroid cavity imager. Accordingly, we have developed specialized composite $90°$ and $180°$ pulse sequences for toroid cavities.[18] The resulting composite pulses are capable of simultaneously orienting the nuclear magnetization for all values of r across the entire sample in a phase-correlated manner with better than 98% efficiency. The composite $180°$ pulse allows the radial distribution of the T_1 spin relaxation time for the entire sample to be simultaneously measured by a simple adaptation of the standard inversion-recovery method for T_1 measurement.

This method was applied at ambient temperature to measuring T_1 for the ^{19}F resonance in the $CF_3SO_3^-$ anion across the electrolyte depletion zone indicated by the upper plot of Fig. VII-4, and the result is depicted in the lower plot of Fig. VII-4. The resultant T_1 within the electrolyte depletion zone exhibits significant variation from that which is characteristic of the bulk electrolyte. The latter quantity is constant for distances greater than 0.3 mm from the working electrode. Detailed interpretation of this trend must await a more complete investigation of the temperature dependence.

In future work, the ^1H and ^{13}C spin relaxation times of the polymer will be measured as a function of distance from the electrode to probe for differences in the segmental motion of the polymer across the salt concentration gradients. Differences are expected because the cations are believed to momentarily cross-link the polymer chains.[16,17] In addition, a spin-echo imaging pulse sequence can be used for determining the radial dependence of the T_2 spin relaxation time.[19] Observations of this nature are anticipated to provide insight into the effect of the electrolyte concentration gradients on the ion mobilities, phase composition of the polymer, and the segmental motion of the polymer subunits. Improved understanding of these key ion transport parameters will help in the design of the next generation of polymer-electrolyte battery materials.

B.   Research on Materials and Interfaces

The research on materials and interfaces addresses a broad range of fundamental issues in energy and environmental science that relate to passivation/corrosion of metals, decontamination of scrap and waste from nuclear facilities, the kinetics and mechanisms of interfacial/electrochemical processes, and molecular sieve catalysis. This research is characterized by the development and application of advanced electrochemical measurement techniques, synchrotron radiation analytical methods, and first-principle computational methods for determining molecular structures, molecular energies, and chemical reaction dynamics.

---

[18] K. Woelk and J. W. Rathke, *J. Magn. Reson. A* **115**, 106 (1995).

[19] R. M. Dixon and P. Styles, *J. Magn. Reson. Med.* **29**, 110 (1993).

1. *Corrosion and Decontamination of Metals*

The purpose of this activity is to elucidate the relationship between the structure and composition of surface films on metals and their properties which are relevant to a number of important technological applications, e.g., corrosion protection, environmental remediation, energy storage, and energy conversion. Synchrotron X-ray absorption spectroscopy, as well as infrared and laser Raman spectroscopy, is employed for *in situ* determinations of structure and composition. Electrochemical techniques such as cyclic voltammetry, dc polarization, and ac impedance are used to determine the energetics and mechanisms of the interfacial processes involved.

Synchrotron far infrared spectroscopy (SFIRS) continues to be applied to the *in situ* identification of corrosion films on metals in aqueous solutions. The nature of the surface film on copper in 0.1 $\underline{M}$ NaOH solution has now been completely elucidated. As had been reported before, the film in the pre-passive region at -0.05 V vs. standard calomel electrode (SCE) was found to consist of Cu_2O.[20] Recently, spectra have allowed us to determine unequivocally that the surface film in the passive region (at 0.3 V vs. SCE) consists of both CuO and $Cu(OH)_2$. The anodic corrosion film on silver in 0.01 $\underline{M}$ NaOCN + 0.1 $\underline{M}$ $NaClO_4$ solution has also been studied with SFIRS. Vibrational bands at wavelengths of 90 and 360 cm^{-1} have been observed *in situ* at +0.35 V vs. SCE for the first time. They have been assigned to the bending mode of surface NCO and to the Ag-N stretching mode of terminally bonded cyanate, respectively. This work is being carried out in collaboration with the University of Auckland, New Zealand, and the University of Poitiers, France. Future plans involve the development and use of a polarization division interferometer for the detection of monolayer and sub-monolayer amounts of materials adsorbed on a surface. Infrared spectroscopic studies of microelectrodes and pitting phenomena will be undertaken.

Synchrotron X-ray absorption spectroscopy (XAS) studies are being undertaken to determine the local structure of heavy metal ions incorporated into the corrosion-passivation films on Ni, Fe, and Cr. The subject is of interest in the development of effective procedures for the decontamination of radionuclide-contaminated storage tanks and piping systems in DOE nuclear facilities, as well as other applications, e.g., corrosion protection, batteries, and electrochromic devices. Electrodeposited oxide films are used to simulate the corrosion layers on metals. The incorporation of Ce and Sr into $Ni(OH)_2$ and NiOOH films has been investigated by XAS. The oxides (hydroxides) of these heavy metals have been found to co-deposit without forming solid solutions with the corresponding nickel oxide phases. It has also been possible to electrodeposit pure oxides of Ce and Sr. The structure of the $Ce(OH)_4$ and CeO_2 formed is highly disordered and may be important in its role as a corrosion inhibitor for aluminum. Initial results on the electrodeposition of iron oxide (hydroxide) films on a graphite substrate showed the extended X-ray absorption fine structure (EXAFS) spectrum of the materials (Fig. VII-5) to be remarkably similar to the spectrum of the corrosion-passivation layer on metallic iron, as had

---

[20] J. J. Laidler et al., *Chemical Technology Division Annual Technical Report, 1995*, Argonne National Laboratory Report ANL-96/10, p. 128 (1996).

been reported earlier by other workers.[21] The structure of the film is similar (but not identical) to γ-FeOOH. The EXAFS spectrum cannot be fitted by using parameters corresponding to the known oxides of iron. Future work will involve studies on the incorporation of Rb, Cr, and U into nickel oxide (hydroxide) films, as well as the electrochemical reduction and dissolution of the films.
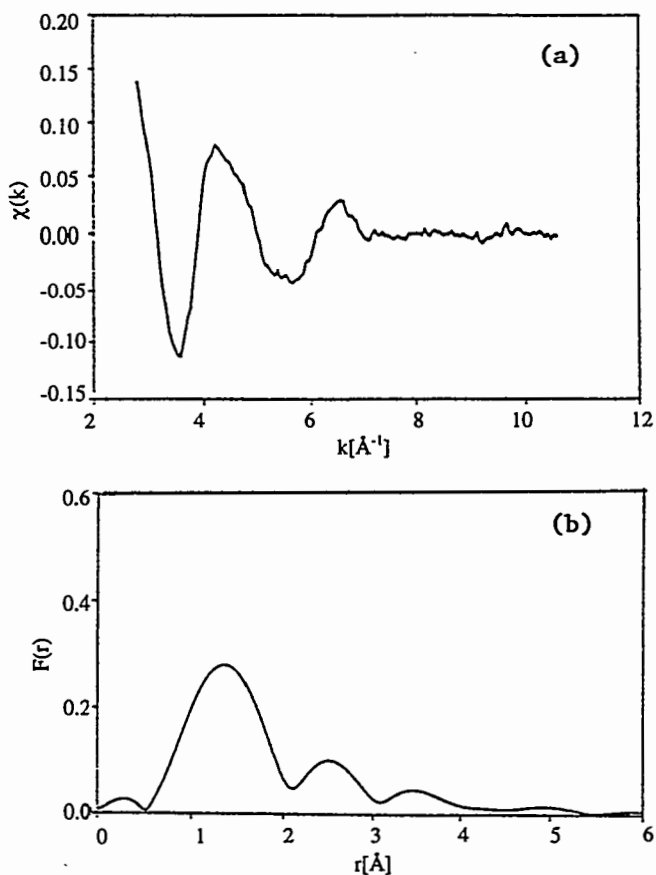
Fig. VII-5.

Iron K-edge from Extended X-ray Absorption Fine Structure Spectroscopy for Iron Oxide (hydroxide) Film Anodically Deposited on Graphite Substrate at 0.6 V vs. SCE. The k-weighted Fourier transform of (a) is shown in (b).

2.   Interfacial Electrochemistry and Ultracapacitor Studies

This research concentrates on understanding (1) the kinetic aspects and atomistic mechanisms of heterogeneous charge-transfer reactions in aqueous solutions over a wide range of temperatures (25 to 300°C) and (2) the atomic level structure of electrified interfaces that strongly influence the dynamics of these reactions. The electrode kinetic measurements of this study are carried out with relaxation techniques such as galvanostatic, coulostatic, or potentiostatic pulse transients; ac-impedance measurements; and the rotating-disk-electrode technique. The resulting data are analyzed with computerized data-evaluation methods. The interfacial structural studies use synchrotron X-ray scattering techniques. Heterogeneous charge transfer is an essential chemical step in the reactions occurring during many energy-related

---

[21] M. Kerkar, J. Robinson, and A. J. Forty, *Faraday Discuss. Chem. Soc.* **89**, 31 (1990).

processes, such as those involved in high power- and energy-density batteries and ultracapacitors for electrical vehicles and large-scale fuel cells for primary electrical power generation. Another electrochemical process that is relevant to practically all energy technologies is corrosion. Clearly, a fundamental understanding of the dynamics of these reactions could result in improvements to many energy technologies.

This year, we completed our kinetic studies of the Cu^{2+}/Cu electrode reaction, which is an important but poorly understood cathodic reaction occurring during stress corrosion cracking in light water nuclear reactors. We have extended our high-temperature/high-pressure kinetic measurements of the Cu^{2+}/Cu^+ reaction—the rate-determining step in the overall copper deposition/dissolution process—from a maximum temperature of 100°C to 200°C. The activation energy of the reaction was found to be 32 ± 5 kJ/mol, and the transfer coefficient was found to be independent of temperature. This work is carried out in close coordination with the theoretical modeling effort described in Sec. VII.B.3.a, and the results are in good agreement with theoretical predictions.

We also continued the structural investigation of buried electrified interfaces by using synchrotron X-ray techniques, in a collaborative effort with the Synchrotron Studies Group in the ANL Materials Science Division. As part of this effort, we are studying the crystallographic structure of underpotentially deposited (UPD) metals and the effect of anion coadsorption on the structure. The UPD metal layers on noble metals (e.g., Rh, Pd) are important electrocatalysts for fuel cells using hydrocarbon fuels, such as methanol, without the need for reforming to hydrogen. Preliminary measurements using rhodium single-crystal surfaces were carried out at the National Synchrotron Light Source (NSLS) of Brookhaven National Laboratory. However, the lower electron density of the anions makes their observation difficult with the relatively small X-ray flux at NSLS; therefore, our initial results were inconclusive. These measurements will be repeated at ANL's Advanced Photon Source (APS) in the near future. This project is carried out with the collaboration of the Chemistry Department of the University of Illinois, Urbana.

We have initiated a new project for the investigation of surface phenomena occurring in ultracapacitor energy storage devices. Ultracapacitors are electrochemical energy storage devices with characteristics between those of classical "dielectric" capacitors and those of batteries. The capacity of ultracapacitors arises predominantly from the following three phenomena: (1) the capacitance of the electrical double layer, (2) the adsorption/desorption pseudocapacitance, and (3) the capacitance caused by oxidation/reduction processes of the electrode material occurring at or near the interface. All three of these phenomena can be studied with synchrotron X-ray techniques. Initially, we are studying the solid-side phenomena occurring at RuO_2 surfaces because this oxide is one of the most promising electrode materials (often in combination with other oxides) for ultracapacitor applications. We have carried out some preliminary measurements at NSLS while the APS beamlines are under construction. A cyclic voltammogram of the $RuO_2(100)$ surface in 0.1 $\underline{M}$ H_2SO_4 solution is shown in the top panel of Fig. VII-6. The oxidation/reduction (Ru^4/Ru^3) peaks are closely followed by the scattered X-ray intensity shown in the bottom panel. Preliminary modeling of the corresponding structural changes suggests that the top surface layer expands upon reduction (probably due to the insertion of hydrogen ions). Future work will be carried out on different crystal faces of the RuO_2 in acidic and basic solutions.
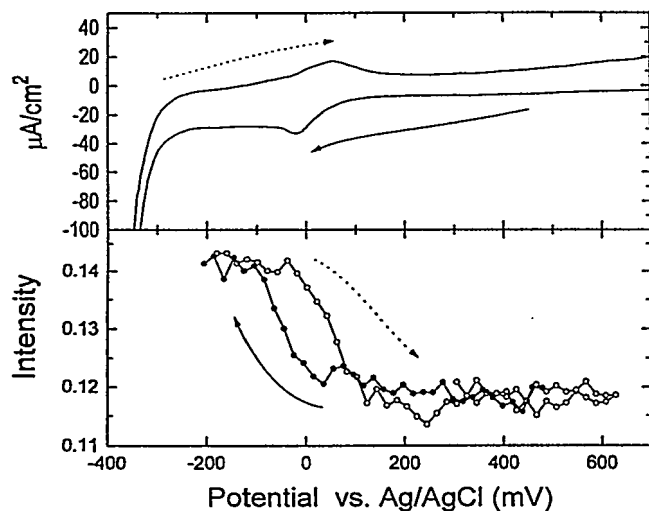
Fig. VII-6.

Cyclic Voltammetry and Reflected X-ray Intensity (in arbitrary units) of $RuO_2(100)$ Oxidation and Reduction. Arrows indicate direction of scan.

3. Theoretical Studies of Materials

The goal of this work is to develop new theoretical methods and apply them, along with previously established ones, to the study of the $Cu^{2+} \rightarrow Cu^{0}$ electrode reaction, molecular clusters, zeolites, thin diamond films, and lithium polymers.

a. Electrode Reactions

Electron transfer at electrode-electrolyte interfaces is a key step in a wide variety of chemical processes, including, for example, those occurring in stress corrosion cracking, in photoelectrochemical reactions of various types, and within fuel cells and batteries. The cuprous-cupric reaction is believed to play a role in limiting rates of stress corrosion cracking in some engineering environments.[22] A combined theoretical/experimental study of the cuprous-cupric electron transfer reaction at a copper electrode has been carried out. The experimental measurements (see Sec. VII.B.2) involve fast electrochemical relaxation measurements (in the microsecond to millisecond time frame) in a unique high-temperature/high-pressure electrochemical cell. The theoretical effort involves molecular dynamics simulations at the University of Minnesota and electronic structure calculations at Argonne National Laboratory. It has several different aspects: (1) simulation of the ion in water, (2) simulation of the electrolyte/electrode interface, and (3) a quantum mechanical model for the electron transfer process itself. The $Cu^{2+} \rightarrow Cu^{+}$ electron transfer reaction is, in most conditions, very quickly followed by the reaction $Cu^{+} \rightarrow Cu^{0}$, in which the copper atom is adsorbed on the electrode.

As reported above (Sec. VII.B.2), the measurements gave an activation barrier for the first electron transfer reaction of 32 kJ/mol. A value of 30 kJ/mol was obtained from the theoretical simulations, in good agreement with the experiment. The remarkable feature of our

---

[22] W. E. Ruther, W. K. Soppet, and T. F. Kassner, *Corrosion* **44**, 791 (1988).

theoretical results is that the barrier to electron transfer arises predominantly from the energy required for the ion to approach the surface. This is in contrast to the ferrous-ferric electron transfer, which we studied previously,[23] where the barrier was dominated by the rearrangement of the solvent molecules around the iron. This implies essentially different reaction coordinates for the two superficially similar reactions. In addition, the cuprous-cupric electron transfer differs from the ferrous-ferric reaction in that electronic coupling between the ion and the surface is very important in the former. The success of this study is an important step in the development of methodology for making reliable predictions of electron transfer reactions at electrode-electrolyte interfaces. In the future, we plan to extend these methods to the study of oxide surfaces.

b.   Gaussian-2 Theory

Gaussian-2 (G2) theory,[24] a method that we developed in collaboration with workers at Northwestern University and AT&T Bell Laboratories, has become widely used in computational quantum chemistry for thermochemical calculations. Originally, G2 theory was tested on 125 reaction energies, chosen because they have well-established experimental values.[24] All of the molecules contained only one or two non-hydrogen atoms with two exceptions (CO_2 and SO_2). In recent work, the test set has been expanded to include larger, more diverse molecules, with enthalpies of formation at 25°C (298 K) being used for comparison between experiment and theory.[25] During the past year, we have expanded the set of ionization energies and electron affinities in the original G2 test set from 63 to 148. From an assessment of G2 and density functional theories on this test set, we found that G2 theory is the most reliable method. It has an average absolute deviation of 0.06 eV for both ionization potentials and electron affinities. The two modified versions of G2 theory, G2(MP2)[26] and G2(MP2,SVP)[27] theory, perform nearly the same, with average absolute deviations of about 0.08 eV for both ionization potentials and electron affinities. Of the seven density functional methods tested for ionization potentials, the hybrid B3-LYP method[28,29] had the smallest average absolute deviation (0.18 eV). Of the same seven density functional methods tested for electron affinities, the BLYP method[28,29] had the smallest average absolute deviation (0.10 eV). In future work, we plan to use the enlarged test set to improve the reliability of G2 and density functional theories.

c.   Molecular Sieve Materials

We are carrying out a theoretical study of zeolites, which are used in the petrochemical industry for acid-catalyzed hydrocarbon cracking. We use a finite cluster model for the Brönsted acid site, and as a first step toward the inclusion of larger hydrocarbon

[23] L. A. Curtiss, J. W. Halley, J. Hautman, Z. Nagy, Y.-J. Rhee, and R. M. Yonco, *J. Electrochem. Soc.* **138**, 2032 (1994).

[24] L. A. Curtiss, K. Raghavachari, G. W. Trucks, and J. A. Pople, *J. Chem. Phys.* **94**, 7221 (1991).

[25] L. A. Curtiss, K. Raghavachari, G. W. Trucks, and J. A. Pople, *J. Chem. Phys.* **106**, 1063 (1997).

[26] L. A. Curtiss, K. Raghavachari, and J. A. Pople, *J. Chem. Phys.* **98**, 1293 (1993).

[27] L. A. Curtiss, P. C. Redfern, B. J. Smith, and L. Radom, *J. Chem. Phys.* **104**, 5148 (1996).

[28] A. D. Becke, *J. Chem. Phys.* **98**, 5648 (1993).

[29] C. Lee, W. Yang, and R. G. Parr, *Phys. Rev. B* **37**, 785 (1988).

molecules, we consider the interaction of ethane with the zeolite cluster. Our $H_3SiO(H)Al(OSiH_3)_4$ cluster model, which includes five tetrahedral atoms, allows an adsorbed molecule to interact with three oxygen atoms adjacent to the substitutional aluminum site. Our calculations, which consist of geometry optimizations, have identified several stationary points on the potential energy surface for the interaction of ethane with the zeolite acid site (ZH). These include the following: the neutral-adsorption complex for ethane (ZH...C_2H_6); the transition state complex for proton transfer from the zeolite to ethane (Z^-...H^+...C_2H_6); the equilibrium ion-pair complex between protonated ethane and the zeolite framework (Z^-...$C_2H_7^+$); and the adsorption complex between methane and the zeolite cluster in which the proton has been replaced by a methyl group (ZCH$_3$...CH_4). The location of these structures on the potential energy surface is shown schematically in Fig. VII-7. We are currently searching for the additional transition state for C-C cracking, so its energy is uncertain. Our results to date are noteworthy for two reasons. First, they provide evidence for the existence of a stable ion-pair structure (Z^-...$C_2H_7^+$), whose existence has been considered controversial and probably unlikely. Secondly, we have calculated a value for the proton transfer barrier from the zeolite to the adsorbed hydrocarbon that is in much closer agreement with typical experimental values than has been obtained by earlier studies.[30,31] We consider these results to be significant steps in our continuing efforts to provide a detailed atomic-level understanding of acid-catalyzed cracking in zeolites.
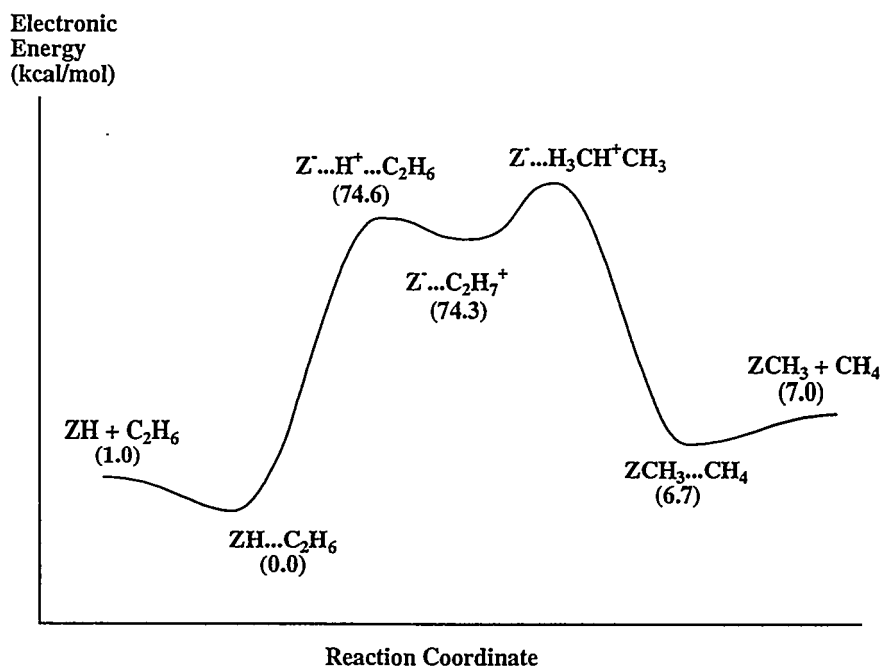
Fig. VII-7.   Computed Potential Energy Surface for Proton Transfer from an Acid Site on a Cluster Model of a Zeolite to an Ethane Molecule

[30] A. M. Rigby, G. J. Kramer, and R. A. van Santen, *J. Catalysis* **170**, 1 (1997).

[31] S. R. Blaskowski, M. A. C. Nascimento, and R. A. van Santen, *J. Phys. Chem.* **100**, 3463 (1996).

d.   Growth Mechanisms of Nanocrystalline Diamond Films

We have previously investigated growth on the diamond (110) surface with C_2 as the growth species, using density functional theory and hydrogen-terminated carbon clusters.[32] Insertion of C_2 into C-H bonds on the surface followed by growth of the (110) surface was found to have small barriers and exothermic reactions, indicating that growth is favorable. The possible mechanisms for growth on the diamond (100) surface with C_2 as the growth species differ from those on the (110) surface, and we have been investigating the implications of this observation for growth of nanocrystalline diamond films.[33] In contrast to the (110) surface, several reconstructions of the (100) surface are possible. Growth from carbon dimer, C_2, on the (100) monohydride surface can occur via insertion into the C-H bonds or into the C-C single bonds. Insertion into C-H bonds is likely to lead to growth of the (100) diamond surface similar to what we have found for the (110) surface.[32] Alternatively, growth on the nonhydride (100) surface, which has dimer rows with C=C double bonds, can occur by insertion of a carbon dimer into C=C double bonds. The insertion of C_2 into a C-C or C=C dimer bond on the surface will lead to a carbene-like product, and further addition of C_2 dimers to this carbene may lead to nucleation sites for growth of a new diamond crystal. In *ab initio* calculations on ethylene and a C_9H_{12} cluster, we have found that C_2 inserts into a carbon-carbon double bond without a barrier and with an energy lowering of about 80 kcal/mol. In future work, we will investigate the reaction involving C_2 insertion into a C-C single bond and the energetics of graphite vs. diamond growth on the (100) surface.

e.   Polymer Electrolytes

This project involves a fundamental study of lithium polymer electrolytes used in lithium battery systems. In this effort, we are investigating the effects of the polymer host on ion solvation and the attendant effects of ion pairing, which strongly affect the ionic transport in these systems. *Ab initio* molecular orbital theory is being used to investigate energetic, structural, and dynamical properties of ion-ion and ion-polymer interactions at the molecular level, in combination with molecular dynamics simulations being carried out at the University of Minnesota. During the past year, calculations using *ab initio* molecular orbital theory were performed to derive potentials for use in the molecular dynamics simulations[34] and to study the interaction of lithium cation with a polyethylene oxide chain. The polymer is being modeled for alkyl oxide chains. The interaction of a lithium cation with the oxygens from one and two chains was investigated to examine the stability of different coordinations of lithium and barriers to migration of the lithium cation from one coordination site to another. Structures corresponding to coordination of lithium cation with one to six oxygens of either one or two alkyl oxide chains were located (e.g., see Fig. VII-8). The binding energies of the complexes were found to increase with coordination of the cation by oxygen, although the binding energy per Li-O bond decreases. The barriers for lithium cation migration between coordination sites and transition states were

[32] D. M. Gruen, S. Lui, A. R. Krauss, and X. Pan, *J. Appl. Phys.* **75**, 1758 (1994).

[33] P. C. Redfern, D. A. Horner, L. A. Curtiss, and D. M. Gruen, *J. Phys. Chem.* **100**, 11654 (1996).

[34] P. T. Boinske, L. A. Curtiss, J. W. Halley, B. Lin, and A. Sutjianto, *J. Computer-Aided Mater. Design* **3**, 385 (1996).

located. While the barriers are found to be small for lithium cation migration from lower to higher coordination of lithium with oxygen, the barriers are large for higher to lower coordination. In future work we will investigate the effect of different anions on the potential energy surface and will develop additional pair potentials as is needed for the molecular dynamics studies.
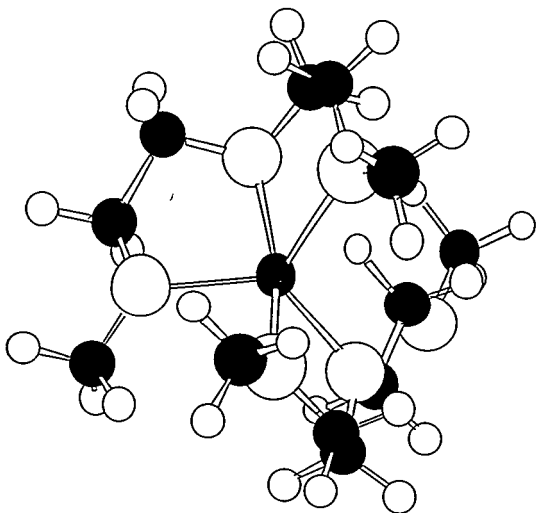
Fig. VII-8.

Illustration of Lithium Cation Coordinated to Five Oxygens from Two Alkyl Oxide Chains Used to Model Polyethylene Oxide (dark gray in center with five bonds, lithium; light-gray circles, oxygen; black circles, carbon; white circles, hydrogen)

VIII

Analytical Chemistry Laboratory

A. Introduction

The Analytical Chemistry Laboratory (ACL) operates in the Argonne system as a full-cost-recovery service center, but it has a mission that includes a complementary research and development component in analytical chemistry and its applications. Because of the diversity of research and development work at ANL, the ACL handles a wide range of analytical problems in its technical support role. Some routine or standard analyses are done, but the ACL usually works with commercial laboratories if high-volume, production analyses are required by our clients. It is common for the Argonne R&D programs to generate unique problems that require significant development of methods and adaption of techniques to obtain useful analytical data. Thus, much of the support work done by the ACL is very similar to applied research in analytical chemistry.

The ACL is administratively within CMT, its principal ANL client, but it provides technical support for many of the other technical divisions and programs at ANL. The ACL has four technical groups—Chemical Analysis, Instrumental Analysis, Organic Analysis, and Environmental Analysis—which together include about 30 technical staff members. Talents and interests of staff members cross group lines, as do many projects within the ACL. The ACL receives about 1600 jobs annually, many of which involve several samples.

The Chemical Analysis Group uses wet-chemical and instrumental methods for elemental, compositional, and isotopic determinations in solid, liquid, and gaseous samples and provides specialized analytical services. The Instrumental Analysis Group uses nuclear counting techniques to determine the radiochemical constituents in a wide range of sample types, from environmental samples with low radioactivity to samples with high radioactivity that require containment. The Organic Analysis Group uses a number of complementary techniques to separate organic compounds and measure them at trace levels and has performed development work in sensors, chemometrics, and detectors. The Environmental Analysis Group analyzes environmental, hazardous-waste, and coal samples for the inorganic constituents and provides quality assurance support to the DOE and other clients for various kinds of analytical data.

A major equipment improvement was completed this year with the installation of a replacement for our inductively coupled plasma/atomic emission spectrometer. The new instrument has detection limits that are about an order of magnitude lower than those of the older instrument. In addition, the ACL installed a new carbon/sulfur determinator this year for inorganic analyses, while a new gamma spectrometry system was installed for radiological measurements.

B. Technical Highlights

The ACL provides analytical chemistry support to CMT, other ANL divisions and programs, other DOE sites, DOE's Chicago Operations Office, and DOE Headquarters. In addition, ACL conducts research and development programs funded by DOE and other sponsors. Selected accomplishments for 1997 are summarized here. In addition, the ACL did analytical work on many other projects, which are described in more detail elsewhere.[1]

1. Support for Nuclear Technology Programs

The ACL analyzed samples from experiments conducted by the Nuclear Technology Department of CMT. Results from analysis of these samples supported efforts that included development of a zeolite waste form, treatment of spent oxide fuel and simulated fuel debris from the Three Mile Island reactor accident, treatment of spent metallic fuels, and treatment of fuels from the Molten Salt Reactor Experiment. The samples required a variety of dissolution techniques prior to measurement of the requested analytes. Analytical tools applied to individual measurements included inductively coupled plasma/atomic emission spectrometry (ICP/AES), inductively coupled plasma/mass spectrometry (ICP/MS), X-ray diffraction (XRD) spectrometry, and thermal ionization mass spectrometry (TIMS). These instruments were used for obtaining elemental, isotopic, and compound information. Many of the samples submitted contained radioactive materials, such as plutonium. These types of samples were analyzed with instruments, such as the ICP/AES that has been modified for use with the radioactive samples. Some results are given in Sections V and VI of this report.

2. Continuous Emission Monitoring of Plasma Hearth Furnace

A continuous emission monitor (CEM) based upon Fourier transform infrared (FTIR) technology that was developed at ANL has been used at the plasma hearth furnace, a unique waste-treatment facility at ANL-West, to monitor stack gases. The objective of the 1997 tests was to determine how operating conditions affect the combustion efficiency. Combustion parameters were changed for both the primary and the secondary combustion chambers, and the consequences were monitored by the CEM to determine the most efficient mode of operation for a variety of feeds.

---

[1] D. W. Green et al., *Analytical Chemistry Laboratory Progress Report for FY 1997*, Argonne National Laboratory Report ANL/ACL-97/5 (December 1997).

The stack gas at the plasma hearth furnace differs significantly from that at the Toxic Substances Control Act (TSCA) incinerator in Oak Ridge, TN, which we had studied previously with the CEM.[2] Several methods that we had used to monitor stack gases at the TSCA incinerator had to be modified to accommodate the different stack gas compositions. Using an older method to detect and quantify sulfur hexafluoride, carbon dioxide, water, tetrachloroethylene, and ethylene caused marginal matrix spike recoveries and false positive detection of tetrachloroethylene. A new method was developed for these constituents. This method is a significant improvement over the original one, which tended to misidentify tetrachloroethylene.

3.   Characterization of Products and Residues from Automobile Shredder Fluff Recycling

About 225 kg (25%) of every scrapped automobile that is processed by automobile shredders to recover ferrous-metal scrap is made up of a mixture of plastics, glass, fibers, and foam. This mixture is referred to as "fluff" and represents a substantial waste stream, which currently is sent to landfills. Argonne scientists are testing a potentially economical process to separate and recycle fluff recovered from scrapped automobiles.

The ACL has been supporting the recycling process development by analyzing various intermediates and products to determine their compositions and by measuring potential contaminants in recovered oils, foams, and residual materials classified as "fines." The ACL has analyzed samples for metals, chlorine, sulfur, water, polychlorinated biphenyls (PCBs), and residual cleaning solvents. Multiple analytical techniques were applied, including the Karl Fischer titration method, oxygen bomb combustion ion chromatography, cold vapor atomic absorption, microwave-assisted acid digestion, and ICP/AES. In 1997, we developed special procedures to estimate the oil content of selected samples as the nonvolatile residue from a hexane extraction and to measure PCBs by using a modification of the Environmental Protection Agency (EPA) procedures for waste analysis. We also applied purge-and-trap and gas chromatography/mass spectrometry techniques to measure organic constitutents. The data obtained from these analyses help to evaluate the quality of recovered products and to establish the hazard classification of the waste streams from the process so that they may be disposed of properly.

4.   Support for High-Temperature Superconductor Development

The ACL continued to provide extensive analytical support to ANL's high-temperature superconductivity programs. Much of this work involved analysis of starting materials, process samples, and products related to fabrication, as well as characterization studies on various ceramic compositions, including $YBa_2Cu_3O_{7-x}$ ("1,2,3-compound") and lead-doped bismuth/strontium/calcium/copper oxides ("BSCCO" ceramics). Our measurements included determining elemental composition by ICP/AES or classical wet chemical methods, anions by ion chromatography, carbon with a LECO™ analyzer, and phase composition by X-ray powder diffraction. We also used an

---

[2]   J. E. Battles et al., *Chemical Technology Division Annual Technical Report, 1993*, Argonne National Laboratory Report ANL-94/15, p. 145 (1994).

iodometric titration method to determine excess valence of the metals in a given ceramic (e.g., Cu^{3+}), which is related to the oxygen stoichiometry of the compound.

Measurements by ACL have included the characterization of impurities in different lots of silver tubing used in the fabrication process, as well as determination of the BSCCO-to-silver ratio. Through these and related activities, the teamwork among chemists, ceramists, and analysts is helping to move the technology of superconducting ceramics toward practical applications.

5. Performance Demonstration Programs for the WIPP Characterization Program

The Waste Isolation Pilot Plant (WIPP) is a DOE installation (near Carlsbad, NM) consisting of large interconnecting cavities hollowed out of deep geologic salt beds approximately 600 m underground. The facility is designed to demonstrate the safe handling, transportation, and disposal of transuranic (TRU) waste in the salt beds. The TRU waste destined for emplacement in the WIPP site stems from waste generated during the 1940s from the nation's nuclear weapons program at various DOE sites.

Wastes to be shipped to WIPP must first be characterized to identify any hazardous materials that might be present, in addition to the radioactive components. The ACL assisted in the implementation of a Performance Demonstration Program (PDP) that is designed to test laboratory performance in determining specified metals, semivolatile and volatile organic compounds, and PCBs in solidified wastes. Acceptable laboratory performance is demonstrated by the successful analysis of blind audit PDP samples. In 1997, the ACL prepared approximately 1 kg each of cemented and uncemented samples of simulated solidified waste and determined the levels of metal analytes in these materials. During 1997, materials were supplied for two cycles of the PDP.

In addition, the ACL is involved with the preparation and distribution of performance demonstration samples of gas samples that simulate the headspace in WIPP waste canisters. Every six months, the ACL prepares standard gas mixtures containing known concentrations of various volatile organic compounds, hydrogen, and methane. Labeled canisters are shipped to laboratories that the WIPP Carlsbad Area Office wants to qualify for headspace gas analysis. The ACL provides confirmation analysis on an aliquot of each of the gas mixtures for volatile organic compounds, methane, and hydrogen.

6. Screening of Semivolatile Organic Compounds in Solidified Waste

In 1997, the ACL initiated a project to evaluate the use of Fourier transform (FT) Raman spectroscopy for rapid screening of radioactive samples of solidified waste for the following WIPP semivolatile target analytes: o-cresol, m-cresol, p-cresol, 2,4-dinitrotoluene, hexachlorobenzene, nitrobenzene, pentachlorophenol, and pyridine. Our objective was to develop a method that required minimal sample preparation and identified samples containing high levels (parts per thousand, ppt) of WIPP-specified semivolatile organic compounds. These samples could then be segregated and

classified as containing high levels of semivolatile organic compounds without extensive characterization.

Samples of simulated sludge were prepared as the interfering matrix, and sand was used as a noninterfering matrix. An FT-Raman analysis was performed using an In/Ga/As detector with a CaF_2 beam splitter. Without any preconcentration of analytes, a detection limit of 1 ppt was established in the noninterfering sand matrix for most of the WIPP semivolatile organic compounds. In the simulated sludge, however, detection limits were much higher, approximately 200 ppt.

7.   Characterization of Used Filters for Disposal

Used high-efficiency particulate air (HEPA) filters removed from ANL laboratory exhaust systems represent a sizable waste stream from site operations. After composite samples are taken of HEPA waste destined for disposal at DOE's Hanford Reservation, the ACL characterizes them by chemical analysis to permit evaluation of the waste relative to Hanford's waste acceptance criteria.

In this characterization, each composite sample is homogenized by manual cutting and then analyzed for metals, semivolatile organics, PCBs, and radionuclides. Samples found to contain high concentrations of heavy metals are also tested according to the Toxicity Characteristic Leaching Procedure to determine whether the metals they contain exceed regulatory limits for mobility under landfill conditions. During 1997, the ACL characterized five composite HEPA filter samples. Each composite consisted of portions of approximately 48 filters. Thus, all filters replaced at ANL-East in 1997 (approximately 250 filters) were tested by this process. By shipping these wastes to Hanford on a regular basis, ANL avoids accumulating large volumes of HEPA waste in its storage facilities.

8.   Analysis of Process Liquors Used in Removing Zinc from Galvanized Steel

Because the U.S. automobile industry is using more and more galvanized (i.e., zinc-coated) steel, an unprecedented volume of galvanized steel scrap is being generated. These low-carbon steels are ideal scrap feed for iron and steel furnaces, but only if the zinc coating is removed. Argonne is working with Metal Recovery Technologies, Inc. (East Chicago, IN) to develop a technology that will remove the zinc coating from steel surfaces so that both the steel and zinc in galvanized scrap can be reused.

The ACL is contributing to this effort by performing chemical analyses on caustic process liquors and related materials. We have determined metal, chloride, and carbonate concentrations in strong sodium hydroxide solutions from the zinc-removal process, and also process parameters described as "total" and "free" alkali. The ACL analysts developed methods for determining the alkali parameters that are simpler than those recommended by the recycling industry, as well as a method for determining the carbonate content of the caustic liquors and process sludges. The ACL's measurements provided not only data for process characterization and control, but also information of environmental interest, including the chemical behavior of such toxic metal impurities as Pb, Cd, and Sb and the composition of waste streams associated with the zinc-removal technology.

Argonne is also developing a zinc electrowinning process for recovering the zinc after it is removed from galvanized scrap by dissolution. The ACL is participating in these studies by analyzing process samples to track such impurity elements as copper and by measuring physical and chemical properties of the metal product. The data from these measurements help the process engineers understand the effects of process variables and conditions on the electrowinning operations.

9. *Characterization of Phosphate-Ceramic-Stabilized Hazardous Wastes*

Argonne is developing a stabilization process that converts solid waste materials into chemically bonded phosphate ceramics. These ceramics have physical properties that make them good candidates for use as structural products. The process is broadly applicable to a variety of wastes, including combustion-process ashes, low-level mixed radioactive and chemical waste, and hazardous sludges. The ceramics formed are not only inexpensive to fabricate but also dense, leach resistant, and stronger than concrete. During 1997, ACL staff assisted this development by performing tests to determine the leach resistance of both simulated and actual wastes at several stages in the stabilization process. In this work, the Toxicity Characteristic Leaching Procedure, as described in U.S. EPA Method 1311, and other standard leaching tests were applied.

In accordance with the Toxicity Characteristic Leaching Procedure, waste samples were extracted with an acetic acid buffer to simulate leaching that might occur under landfill conditions. By leaching the wastes and analyzing the extracts by ICP/AES, ICP/MS, and cold vapor atomic absorption, we have obtained concentrations for Pb, Cd, Cr, Ni, As, Ba, Se, Ag, Mo, Fe, Cs, Ru, Sr, La, Nd, Y, Hg, Ce (a nonradioactive simulant for plutonium), and Re (a nonradioactive simulant for technetium). Concentrations of the radioactive isotopes ^{137}Cs, ^{238}U, ^{235}U, and ^{241}Am were determined in actual waste samples by gamma spectroscopy, and ^{99}Tc was measured by application of a solid-phase extraction technology (Empore^{TM} Disks) that ACL analysts helped develop for commercialization. Ion chromatography was used to determine the concentrations of phosphate, nitrate, sulfate, and chloride leached from the ceramic matrix.

10. *Support to Counternarcotics Efforts*

As part of collaborative work with the Houston Advanced Research Center, the ACL was asked to evaluate and to recommend technologies for the destruction of large quantities of seized illicit substances. The major criteria used in evaluation and selection of the recommended technologies were safety of Drug Enforcement Agency personnel, security of materials, cost of acquisition and operation of destruction technology, and compliance with EPA's air emissions regulations. The ACL's evaluation indicated that medical waste incinerators had advantages over rotary kiln incinerators in meeting most of the evaluation criteria. This work will continue in 1998 with the permitting of a facility to thermally destroy illicit substances.

As an extension of our prior work on transfer of cocaine from U.S. currency to people,[3] we examined British currency and determined that the fibers used in U.S. and British currencies are different; consequently, they retain cocaine differently. The two samples of British currency that we studied were not contaminated by cocaine. Future work will expand on our efforts to characterize money samples from large cities to see if currency from rural areas is as contaminated as that found in large metropolitan areas.

11. Development of a Rapid Water Sampling and Analysis System

Since 1994, ANL and the 3M Company have been collaborating to develop Empore™ Rad Disks, which are based on a new solid-phase extraction technology for radiochemical analysis. These disks are thin membranes that are loaded with element-selective particles embedded in stable, inert polytetrafluoroethylene fibrils. The Empore™ Rad Disks selectively collect radioisotopes from aqueous samples, even in the presence of very large concentrations of competing ions. To date, disks have been developed for Tc, Sr, and Ra.

In 1997, the ACL was part of a team that used the disks for technetium separation to evaluate the field performance of a rapid water sampling and analysis system developed by the team. The sampling system was designed to be easily portable and to work in remote locations. It was designed for large sample sizes (>4 L), for high flow rates (>200 mL/min), and for prefiltration, as required. The system was successfully tested on a variety of natural and process waters at several DOE sites. Results from the membrane-based system agreed favorably with the analytical results for technetium obtained from traditional methods.

The rapid water sampling and analysis system using these solid-phase extraction disks offers several advantages: (1) extremely large specimens (1-12 L) can easily be collected so that very low levels of detection can be obtained; (2) the sample preparation is done at the time of sampling by the field personnel so that overall sample preparation time can be reduced by a factor of 10; (3) bulk shipping and storage can be reduced by a factor ranging from 300 to 4000 by using the field sampler; and (4) the membranes lend themselves to field analysis. A portable beta spectrometer based upon solid scintillation was demonstrated in this project to allow counting of the radioactivity in these membranes in the field.

12. Analysis of Scale and Filter Residues in Cooling-Water Systems at the Advanced Photon Source

Operation of the synchrotron particle accelerators and storage ring at ANL's Advanced Photon Source (APS) requires substantial volumes of high-quality cooling water to regulate the heat load from power supplies, magnets, and other components. The ACL has provided support to the team of engineers responsible for maintaining the APS cooling water system by helping to identify

---

[3] J. J. Laidler et al., *Chemical Technology Division Annual Technical Report, 1996*, Argonne National Laboratory Report ANL-97/13, pp. 154-155 (1997).

deposits found on some system components and by making measurements to assess the nature and extent of corrosion taking place in the system.

This past year, we examined several fittings associated with hoses on inlet and outlet lines from selected components in the storage ring. Two types of deposit were present on these fittings. One was a bright yellow film that was identified by FTIR spectroscopy as an epoxy resin. The other was a dark deposit identified as cuprite (Cu_2O) by XRD analysis and scanning electron microscopy/energy dispersive spectroscopy. We also examined a number of filters from various locations in the cooling water system and determined the nature and quantity of particulate matter they had collected. Optical and scanning-electron microscopy showed that many of the filters contained tiny particles of copper metal (roughly 10-μm diameter). By burning off the polypropylene filter medium, dissolving the ash in mineral acids, and analyzing the solution by ICP/AES, we determined that some filters contained as much as 0.25 g of copper. We were unable to pinpoint the source of the copper particles through measurements of the copper concentration in several sets of water samples and in residues obtained by filtering small volumes (1 L) of water because the concentrations were extremely low in all cases. Apparently, the copper loading on the filters resulted from accumulation of a small number of particles per unit volume as thousands of gallons of water passed through each filter.

13.   Chemical Analysis for Electrometallurgical Treatment Program

The DOE expects that 128 metric tons of spent aluminum-matrix reactor fuel will be produced from U.S. and foreign research reactors over the next 40 years and has been evaluating alternative means of dealing with the fuel after processing in the canyons at the Savannah River Site is discontinued, as planned, in 2005. As a backup option to direct geologic disposal of the fuel, DOE advisors recommended an electrometallurgical process for treating the aluminum-based fuels, which is being investigated by researchers in CMT (Sec.V.A.4).

The ACL has provided a variety of chemical analyses in support of these studies. Measurements of the composition of electrolyte samples taken over a period of time helped to demonstrate that the electrolyte mixture is stable. Analysis of product deposits from electrotransport tests helped demonstrate that aluminum recovery from the spent fuel is viable. Finally, measurements of the component elements in simulated fuel materials and treatment residues helped confirm that the process can retain uranium in its desired location while the aluminum is removed and recovered.

The molten fluoride salt electrolyte in which the aluminum electrotransport process is carried out has provided interesting challenges to the analysts supporting this work. Some of the fluoride components in the product deposits are exceptionally difficult to dissolve and require decomposition by fusion techniques or other means.

14.   Preparation of Materials for Physics Experiments

The ACL was asked by ANL researchers to remove trace amounts of Na and Zn radioisotopes from a sample of ^{54}Mn intended for use in an experiment to measure the positron decay

branch in ^{54}Mn. The Na and Zn radionuclides emit particles that can interfere with the measurement of the ^{54}Mn positrons. This interference is particularly detrimental because the positron decay branch for ^{54}Mn is expected to be on the order of 1×10^{-9}; consequently, effective removal of the Na and Zn was mandatory.

The ACL devised a separation scheme in which the zinc was separated from manganese by anion exchange in 2 $\underline{M}$ HCl, and the sodium was removed by cation exchange in 0.5 $\underline{M}$ HCl. This scheme was used to purify 2 mCi of ^{54}Mn, and from it a 660 µCi source was prepared for placement in the APEX positron-electron spectrometer in the ATLAS linear accelerator facility. The spectrum of ^{54}Mn decay from the ACL-purified source was acquired over a period of two weeks. The physicists have reported that the experiment was successful.

In addition, the ACL prepared an osmium target for photon excitation studies by electroplating osmium metal onto a copper backing. The resulting metal planchet was then used as a target for photon excitation studies in which the high flux of photons from the APS would excite osmium nuclei by a process called NEET (Nuclear Excitation by Electronic Transition). A procedure for electroplating osmium is available in the literature, but direct application of the procedure did not work. By modifying the procedure so that the concentration of osmium in the plating solution was <0.006 $\underline{M}$, the ACL was able to produce a number of osmium targets, ranging in content from 3 to 20 mg/cm^2, on both copper and gold planchets. After an irradiation of approximately 12 h in the APS, an osmium target was counted by the physicists with a germanium detector to measure osmium X-rays. The use of these targets led to a successful experiment because evidence for an excited-state isomer with half-life of 5.7 h was found.

15.   The Integrated Performance Evaluation Program

In collaboration with the DOE's Radiological and Environmental Sciences Laboratory (RESL), the ACL is developing and piloting a comprehensive Integrated Performance Evaluation Program (IPEP) for DOE's Office of Environmental Management (EM) as part of its National Analytical Services Program. The IPEP is designed to provide information on the quality of radiological and nonradiological analysis data being produced by all analytical chemistry laboratories that provide DOE and its contractors with data on environmental restoration and waste management samples. The ACL has been assisting in developing program requirements and implementation strategies, especially in the nonradiological portions of the program. The CMT Computer Applications, Network, and Security Group is assisting the ACL in the development of strategies and systems for handling large data sets and for compiling and analyzing data from performance evaluation (PE) program studies.

The Interagency Agreement between ANL and EPA's Region V allows the IPEP to nominate laboratories performing analyses for EM into the Water Supply and Water Pollution PE Program Studies sponsored by the EPA's National Exposure Research Laboratory (Cincinnati, OH) and to access relevant information about laboratories from these programs. Historical and current data from these PE programs are now routinely transferred here electronically from the EPA's database at Research Triangle Park, NC. Historical and current data from the PE Program Studies of DOE, the Quality Assessment Program of the Environmental Measurements Laboratory, and the Mixed

Analyte Performance Evaluation Program of RESL are also routinely transferred into the IPEP database.

Pilot studies for the production and evaluation of IPEP reports have been conducted at DOE's Idaho Operations Office, the Sample Management Office at Idaho National Engineering and Environmental Laboratory, DOE's Albuquerque Operations Office, and the Sample Management Offices for several of the contractors that report through the Albuquerque Office. These pilot studies were designed to provide IPEP developers with an opportunity to test the feasibility of proposed operating mechanisms and to allow report users to have direct input on the report formats, technical content, and other needs during the development stage prior to implementation.

A World Wide Web server has been established that contains general information about DOE's IPEP, including contact names, PE program study distribution schedules, and hyperlinks to other servers of interest.

16. Corrections for ICP/MS Spectral Interference in the Determination of Arsenic, Selenium, and Vanadium

The ACL has procedures for the determination of heavy elements in a variety of solid and liquid media using ICP/MS. However, for elements with atomic numbers less than 36, spectral interferences can be severe. Under a Support Development Funds Project, the ACL has developed and tested the validity of a computer program that will simultaneously correct for many interferences in a single mass spectrum. Current research involved the correction procedures for As, Se, and V in a known interference matrix. These interference correction procedures will allow the accurate determination of interference-prone elements by ICP/MS, instead of by more mature analytical techniques that are either more labor-intensive (graphite furnace atomic absorption spectrophotometry) or have higher detection limits (ICP/AES). Measurement of these elements by ICP/MS will, therefore, result in lower detection limits and cost savings for ACL clients.

17. Determination of Minerals and Metals in Milk

In 1993, Argonne scientists successfully tested a magnetic separation process (MAG*SEP^{TM}) developed and patented by Bradtec Ltd., a British company, for removing radioactive ^{137}Cs from milk produced in the Ukraine. The milk is contaminated above safe drinking levels as a result of the 1986 accident at the Chernobyl nuclear power plant.

As a continuation of this work in 1997, Argonne researchers investigated the effects of the cesium removal process on levels of beneficial nutrient minerals (e.g., Ca, K, Fe, and P) as well as heavy-metal contaminants in the milk. In support of this investigation, the ACL established a methodology to measure the mineral elements and contaminant metals in samples of raw and processed (pasteurized and homogenized) milk before and after cesium removal treatment. For these measurements, we implemented a microwave-assisted acid digestion procedure for preparing the milk samples based on U.S. EPA Method 3051. This procedure involved treating 5 g of milk with 10 mL of concentrated nitric acid in a closed-vessel system. This procedure produced a digestate

suitable for ICP/AES measurement of Al, As, Ba, Be, Ca, Cd, Cr, Cu, Fe, K, Na, P, Mg, Mn, Pb, Sn, Sr, and Zn; ICP/MS measurement of As, Cd, Sn, Cs, and Pb; and cold vapor atomic absorption measurement of mercury.

The preparation and analysis methods were demonstrated to visiting Ukrainian scientists who came to observe the treatment studies. The data from these measurements will help determine whether removing the radioactive cesium might lower the nutritional value of the milk or introduce undesirable contaminants into it. Early results showed no adverse effects.

18. Chemical Analysis of Lithium Aluminate for Tritium Target Qualification Project

In its Tritium Target Qualification Project (TTQP), Battelle Pacific Northwest National Laboratory (PNNL) was charged by DOE with coordinating the manufacture of ^{6}Li-enriched lithium aluminate powders and pellets for use as tritium production targets. In support of this effort, Argonne prepared batches of the $LiAlO_2$ powder, which were subsequently sintered into ceramic pellets by a commercial vendor. The pellets were ultimately to be incorporated into a test assembly (the "Lead Test Assembly").

The ACL became involved in this project when we were asked to provide chemical analysis of developmental batches of the powder and pellet materials to determine whether the products met program specifications. The ACL was in a unique position to provide these measurements because we had established capabilities for analyzing these extremely refractory materials with high precision and accuracy when we supported early development of the $LiAlO_2$ target matrix (1983-1990). By far the most challenging aspect of these analyses is dissolving the materials to prepare them for Li and Al assay. A sealed-tube procedure using concentrated hydrochloric acid at 300°C is usually required, although we also had limited success with a microwave-assisted dissolution method at high pressure. For the powders and pellets, we determined the isotopic composition of lithium in each material by thermal ionization mass spectrometry, assayed lithium by isotope dilution and aluminum by 8-hydroxyquinolate gravimetry, measured carbonate impurity by carbon dioxide evolution, and measured leachable chloride by ion chromatography.

In addition to supporting the process-development activities for the TTQP, the ACL also participated in a qualification exercise conducted by the Idaho National Engineering and Environmental Laboratory as part of a project to identify commercial laboratories that could perform the needed measurements. This exercise required the rapid analysis, in duplicate, of seven prototype production pellets. Our results were pooled with similar data from other laboratories, including the National Institute of Standards and Technology, to evaluate method and laboratory performance in terms of precision and accuracy.

Based on ACL's historical experience with $LiAlO_2$ analysis, our performance in analyzing the developmental and prototype production materials, and our readiness to provide high-quality data with short turnaround time, the ACL was selected to provide chemical analysis data for certification of two production lots of pellets incorporated into the test assembly. To meet the schedule needs of the TTQP, we undertook an intensive campaign to complete all measurements on the two pellet lots

in less than four weeks. This successful effort made the data available in time for a planned review of the test assembly by the Nuclear Regulatory Commission. The test assembly was approved for use and shipped from PNNL on schedule during August 1997.

19.   Characterization of Materials from Fernald Silos

Fluor Daniel Fernald is evaluating options for the remediation of material stored in Silos 1 and 2 of Operable Unit 4 at the Fernald Environmental Management Project site in Ohio. The material in these silos consists predominantly of residues from pitchblende ore processed to extract uranium. To aid in selecting among available treatment options for remediating the silo contents, Fluor Daniel Fernald requested that the ACL analyze material from each of the two silos to identify the primary chemical compounds present.

In this effort, we determined the elemental composition of three subportions of each silo material and examined corresponding subsamples by XRD to provide information on specific compounds present. In the elemental analysis, each subsample was analyzed to determine 33 elements, including carbon, sulfur, phosphorus, and an assortment of metals. Of these, 31 elements were determined by ICP/AES after total dissolution of each sample by lithium tetraborate fusion. Carbon and sulfur were measured with commercial combustion analyzers. We also determined the distribution of carbon between organic and inorganic (carbonate) forms in selected samples. Ultimately, the information from the elemental determinations and XRD patterns was combined and interpreted to allow assignment of the major components in each material to specific compounds. This analysis resulted in our assigning approximately 86% of the Silo 1 material's mass to the compounds SiO_2 (65%), $PbCO_3$ (11.8%), $BaSO_4$ (7.7%), $PbSO_4$ (1.2%), and $CaCO_3$ (0.5%). In the Silo 2 material, an average of 81% of the material's mass was assigned to $(Ca,Mg)CO_3$ (38%), SiO_2 (31%), Fe_2O_3 (6.4%), $PbCO_3$ (3.5%), and $BaSO_4$ (2.6%). Fluor Daniel Fernald is evaluating these results with regard to potential implications for various processes to stabilize the silo materials for disposal.

20.   Demonstration of Field Portable X-ray Fluorescence Spectrometer

The Large-Scale Demonstration Project at ANL's Chicago Pile-5 (CP-5) reactor is testing innovative technologies that offer potential benefits to the decontamination and decommissioning of aging nuclear reactors and other facilities. In collaboration with researchers from the Technology Development, Environmental Research, and Energy Systems Divisions, ACL staff participated in a demonstration of two commercial field portable X-ray fluorescence (FPXRF) spectrometers for screening of heavy metal contaminants on surfaces and on used HEPA filters removed from service at the demonstration facility. The FPXRF systems utilize sealed radioactive sources to provide the exciting radiation needed to induce emission of fluorescent X-rays. The instrument includes a device to expose a sample to the excitation source, a detector and energy-dispersive analyzer to acquire and record the fluorescent X-ray energy spectrum, and a data processor to convert the spectral data to elemental concentrations.

In the demonstration, measurements were made with two units from TN Spectrace (Fort Collins, CO). These units were the TN Lead Analyzer (designed to analyze for lead in matrices such as soil, paint, surface dust, or air filters) and the TN Spectrace 9000 (designed to determine the elemental composition of a broad range of materials for environmental applications, industrial quality control, or other uses). The demonstration activities showed that, although the FPXRF technology cannot completely displace the baseline technology of collecting samples for analysis by regulator-approved laboratory methods, these field-portable analyzers offer considerable advantages in cost and time when used as a screening tool to identify areas of potential concern, to define dimensions of a contaminated area, to track progress of remediation activities, or to guide waste management strategies.

21. Fourier Transform Infrared Analysis of Oils

Oil samples from Fermi National Accelerator Laboratory were submitted to the ACL for analysis by FTIR-microscopy analysis. The FTIR spectra of the sample oils were collected, and they matched the library spectrum of mineral oil. Since Fermi Laboratory was interested in whether silicone oil was present in the samples, another spectrum of each sample was collected, this time using a thicker film of the sample to increase the signal of any low-level components. The spectrum of each sample was scaled to emphasize the absorption bands in the 1300-800 cm^{-1} range, because mineral oil absorption bands do not occur in this region but major silicone oil absorption bands do occur. The spectrum in this region for each sample was carefully examined against the library spectrum of silicone oil. The presence of silicone oil in one of the Fermi sample spectra was noted. To determine the concentration, an FTIR spectrum was collected for a mixture of known concentration of silicone oil in mineral oil. By comparing the relative heights of the silicone oil absorption bands to the mineral oil absorption bands, we were able to ascertain that the concentration of silicone oil in the Fermi sample is low (~1%).

22. Determination of Compounds Formed in Simulated Arcing of Cables

A set of 11 gas samples was submitted by an engineering company for determination of certain inorganic and organic compounds formed as a result of simulated arcing of electrical cables. Each of the gas samples was contained in a glass sample bulb. Analysis of each gas was performed in several stages. First, each gas was analyzed by gas mass spectrometry for determination of hydrogen, methane, ethane, oxygen, argon, carbon dioxide, and propane. Values were also obtained for nitrogen, but these values were subject to potential interference by carbon monoxide.

In the second step, low-molecular-weight organic compounds present in each gas sample were determined by a gas chromatography/mass spectrometry system fitted with a gas-handling injection valve to permit introduction of a measured amount of gas sample for analysis. We determined the response factors (area counts per nanogram) for carbon monoxide, ethene, ethyne, and ethane by using commercial gas standards that were available in our laboratories. Response factors determined from our previous work with headspace gas analysis were used for quantitation of benzene and toluene. As for the other compounds detected in the submitted samples, the response

factor for ethene was used for quantitation of all olefinic compounds, ethyne for all alkynes, and ethane for all alkanes. Therefore, quantification of organic compounds had to be considered semiquantitative, except for ethene, ethyne, ethane, and carbon monoxide.

The third step in analyzing each gas sample involved a gas chromatographic analysis to determine carbon monoxide. Carbon monoxide and nitrogen both have peaks in their mass spectra at m/e 28, but carbon monoxide has a peak at m/e 12 that is not present in the mass spectrum of nitrogen, and this peak could be shown to give reliable quantitation for CO.

In all, 56 organic compounds were identified in one or more of the individual gas samples. The predominant species were light, unsaturated hydrocarbons, especially ethene and ethyne. Besides air components, inorganic gases present consisted of hydrogen and carbon monoxide (both at fairly high concentration in some samples) and carbon dioxide. Hydrogen cyanide was detected in four of the 11 gas samples.

23. Development of the Sensor Algorithm Generation Environment

Current ACL work in chemometrics is focused on development of the Sensor Algorithm Generation Environment (SAGE), a graphical software "workbench" for designing automated monitoring algorithms for sensors of any type (optical, chemical, electrochemical, nuclear, etc.). By using SAGE, the developer of a sensor can selectively combine diverse procedures for digital filtering, pattern recognition, and multivariate calibration to produce an optimized algorithm for automated qualitative and/or quantitative analysis. This optimized SAGE algorithm can then be implemented on-board the sensor by using software or appropriate hardware to perform automated data analysis in real time.

Another goal in establishing the SAGE is to develop novel algorithms for creating smart chemical sensors. The term "smart" means that the sensor can (1) interpret multivariate data in real time; (2) perform data reduction and decision making; (3) communicate processed results to a user, multisensor data fusion system, or process control loop; and (4) alter its own operation based on the nature of these results. By developing automated numerical procedures that mimic the analytical reasoning and data analysis skills of a human expert, smart sensor algorithms can be produced.

The SAGE consists of three modules: digital filter, pattern recognition, and multivariate calibration. A submodule, which will contain code for analysis of hyperspectral images, has also been added. During 1997, the digital filter and pattern recognition modules were essentially completed. In addition to standard chemometric techniques, neural network analysis has been applied for multispectral and hyperspectral image analysis.

We are currently investigating the effect of spectral resolution on pattern recognition with SAGE. This study will establish the protocol for selecting the optimal resolution at which remote-sensing FTIR data need to be collected to obtain good pattern recognition without sacrificing the information content of the signal. With optimized resolution, disk space for storing high-resolution data that do not contribute to improved pattern recognition can be reduced. Collection of low-resolution data that give poor quality results can also be avoided.

The target analyte in this study is diisopropyl methyl phosphonate (DIMP). Dimethyl methyl phosphonate (DMMP) is used as an interferant to DIMP. The very strong absorption band of DMMP centered around 1055 cm^{-1} overlaps the weaker 995 cm^{-1} absorption band of DIMP, making a strong test case for accurate identification from FTIR spectra. Initial results indicate that it is possible to establish a protocol for optimal spectral resolution that performs well even in the presence of interfering species and gives pattern recognition results comparable to those obtained with very high resolution data.

In the experimental design, short segments of a single-beam spectrum were identified that had maximum analyte information and were optimal in correctly identifying DIMP by use of pattern recognition techniques. In the training procedure, the interferograms were converted to single-beam spectra through fast Fourier transformation, and short segments of single-beam spectra that had analyte information were isolated. These short segments were subjected to piecewise discriminant analysis pattern recognition methodology to calculate and optimize a set of discriminants sequentially in order to separate maximum DIMP data from DMMP data and backgrounds. These discriminants were tested in the prediction procedure by using a separate data set of interferograms not used in the training procedure. The results obtained in both training and prediction procedures were analyzed to establish the protocol for resolution to be used in data collection. Analysis of the results indicates that acceptable species identification will occur with remote-sensing FTIR interferograms (4 kilobyte file size) that result in a nominal spectral resolution of 8 cm^{-1}.

24. Analysis of Radioactive Environmental Samples

The ACL analyzes samples from ANL submitted for the determination of hazardous or radiological components, many as a part of various site remediation programs. Samples are also received from outside programs focused on site cleanup and facilities decontamination and decommissioning. This year, 340 analytical samples were received for the determination of specific radionuclides ($^{226/228}$Ra, ^{232}Th, $^{235/238}$U) as part of two major site remediation programs carried out by U.S. EPA Region V: the Ottawa landfill site in Ottawa, IL, and the Belding Warehouse site in Belding, MI. Matrices included soil and water from Ottawa and shredded debris (paper/cardboard, plastic, rubber, wood, etc.) from Belding. The Ottawa samples involved the use of standard gamma spectroscopy and alpha spectroscopy methods; data included analytical results, raw data (e.g., quality control data, instrument output), and associated documentation (e.g., notebook entries, chain-of-custody forms). The Belding Warehouse samples required (1) development of a gamma spectroscopy counting technique appropriate for the sample container geometry (a 1-gal paint can) and (2) generation of a five-point self-absorption curve unique to the sample matrix and geometry. Documentation in support of each technique was prepared and forwarded to the U.S. EPA.

.

IX

Publications and Presentations—1997

The Division's publications and oral presentations for 1997 were entered into a bibliographic data base. The pages that follow are a printout of this information sorted into six categories: (1) journal articles, books, and book chapters, (2) patents, (3) ANL progress and topical reports, as well as contributions to reports published by organizations other than ANL, (4) abstracts and papers published in proceedings of conferences, symposia, workshops, etc., (5) oral presentations at scientific meetings and seminars not referenced in the fourth category, and (6) papers accepted for publication but not yet published.

Chemical Technology Division
Publications and Presentations—1997

A. Journal Articles, Books, and Book Chapters

Formation of the $Fe_{23}Zr_6$ Phase in an Fe-Zr Alloy
    D. P. Abraham, J. W. Richardson, and S. M. McDeavitt
        Scr. Mater. **37**(2), 239–244 (1997)

Laves Intermetallics in Stainless Steel-Zirconium Alloys
    D. P. Abraham, J. W. Richardson, and S. M. McDeavitt
        Mater. Sci. Eng. **A239–240**, 658–664 (1997)

Isolation of Wastes in Electrometallurgical Treatment of Spent Nuclear Fuel
    J. P. Ackerman, L. S. H. Chow, S. M. McDeavitt, C. Pereira, and R. H. Woodman
        J. Miner. Met. Mater. **49**(7), 26–28 (1997)

Gasoline to Hydrogen: A New Route for Fuel Cells
    S. Ahmed, R. Doshi, R. Kumar, and M. Krumpelt
        Electric & Hybrid Vehicle Technology '97, pp. 77–80 (1997)

Stability of Low-Concentration Calibration Standards for Graphite Furnace Atomic Absorption Spectroscopy
    D. A. Bass and L. B. TenKate
        At. Spectrosc. **18**(1), 1–12 (1997)

Lithium Site Preference and Electronic Structure of $Li_4V_3O_8$
    R. Benedek, M. M. Thackeray, and L. H. Yang
        Phys. Rev. B **56**(17), 10,707–10,710 (1997)

Optimized Gaussian Basis Sets for Use with Relativistic Effective (Core) Potentials: K, Ca, Ga–Kr
    J.-P. Blaudeau and L. A. Curtiss
        Int. J. Quantum Chem. **61**(6), 943–952 (1997)

Extension of Gaussian-2 (G2) Theory to Molecules Containing Third-Row Atoms K and Ca
    J.-P. Blaudeau, M. P. McGrath, L. A. Curtiss, and L. Radom
        J. Chem. Phys. **107**(13), 5016–5021 (1997)

Synthesis of Nanoscale Transition Metal Particles Through the Use of Microwave Plasmas
    J. R. Brenner, G. Krumdick, J. Harkness, M. Knickelbein, R. E. Winans, and
    C. L. Marshall
        Nanostructured Mater. **8**(1), 1–17 (1997)

Structural Characterization of Rhodium-Containing Hydrodesulfurization (HDS) Catalysts
Derived from a Laser Vaporization Cluster Source
    J. R. Brenner, E. Parks, G. Nieman, S. Riley, C. L. Marshall, and R. E. Winans
        J. Catal. **166**(2), 294–305 (1997)

Dissolution Kinetics of U_3Si_2 Particles in Alkaline Hydrogen Peroxide
    B. A. Buchholz, J. C. Hutter, and G. F. Vandegrift
        Nucl. Technol. **118**(3), 225–232 (1997)

Optimizing the Coating Process of Organic Actinide Extractants on Magnetically Assisted
Chemical Separation Particles
    B. A. Buchholz, H. E. Tuazon, M. D. Kaminski, S. B. Aase, L. Nuñez, and
    G. F. Vandegrift
        Sep. Purif. Technol. **11**(3), 211–219 (1997)

Detecting Low Levels of Transuranics with Electron Energy Loss Spectroscopy
    E. C. Buck and J. Fortner
        Ultramicroscopy **67**, 69–75 (1997)

A New Uranyl Oxide Hydrate Phase Derived from Spent Fuel Alteration
    E. C. Buck, D. J. Wronkiewicz, P. A. Finn, and J. K. Bates
        J. Nucl. Mater. **249**, 70–76 (1997)

The Crystal Structure of Ianthinite, $[U_2^{4+}(UO_2)_4O_6(OH)_4(H_2O)_4](H_2O)_5$: A Possible
Phase for Pu^{4+} Incorporation during the Oxidation of Spent Nuclear Fuel
    P. C. Burns, R. J. Finch, F. C. Hawthorne, M. L. Miller, and R. C. Ewing
        J. Nucl. Mater. **249**, 199–206 (1997)

Characterization and Dissolution Behavior of a Becquerelite from Shinkolobwe, Zaire
    I. Casas, J. Bruno, E. Cera, R. J. Finch, and R. C. Ewing
        Geochim. Cosmochim. Acta **61**, 3879–3884 (1997)

TRUEX Processing of Plutonium Analytical Solutions at Argonne National Laboratory
    D. B. Chamberlain, C. Conner, J. C. Hutter, R. A. Leonard, D. G. Wygmans, and
    G. F. Vandegrift
        Sep. Sci. Technol. **32**(1–4), 303–326 (1997)

Fluorescence of the 1,4-Benzoquinone Radical Anion
    A. R. Cook, L. A. Curtiss, and J. R. Miller
        J. Am. Chem. Soc. **119**(24), 5729–5734 (1997)

Assessment of Gaussian-2 and Density Functional Theories for the Computation of
Enthalpies of Formation
    L. A. Curtiss, K. Raghavachari, P. C. Redfern, and J. A. Pople
        J. Chem. Phys. **106**(3), 1063–1079 (1997)

Investigation of the Use of B3LYP Zero-Point Energies and Geometries in the Calculation of Enthalpies of Formation
    L. A. Curtiss, K. Raghavachari, P. C. Redfern, and J. A. Pople
        Chem. Phys. Lett. **270**, 419–426 (1997)

Binding Energies of Germanium Clusters, Ge_n (n = 2–5)
    P. W. Deutsch, L. A. Curtiss, and J.-P. Blaudeau
        Chem. Phys. Lett. **270**, 413–418 (1997)

Alkaline Peroxide Processing of Low-Enriched Uranium Targets for [99]Mo Production—Decomposition of Hydrogen Peroxide
    D. Dong and G. F. Vandegrift
        Nucl. Sci. Eng. **126**, 213–223 (1997)

Clarkeite: New Chemical and Structural Data
    R. J. Finch and R. C. Ewing
        Am. Mineral. **82**, 607–619 (1997)

Distinguishing among Schoepite, $[(UO_2)_8O_2(OH)_{12}](H_2O)_{12}$, and Related Minerals by X-ray Powder Diffraction
    R. J. Finch, F. C. Hawthorne, M. L. Miller, and R. C. Ewing
        Powder Diffr. **12**(4), 230–238 (1997)

EELS Analysis of Redox in Glasses for Plutonium Immobilization
    J. Fortner, E. C. Buck, A. J. G. Ellison, and J. K. Bates
        Ultramicroscopy **67**, 77–81 (1997)

Electrorefining Reduces Rad Waste
    E. C. Gay
        Pollution Prevention Advisor **7**(2), 15 (1997)

Thermodynamics of Mixed-Oxide Compounds, $Li_2O \cdot Ln_2O_3$ (Ln = Nd or Ce)
    K. V. Gourishankar, G. K. Johnson, and I. Johnson
        Metall. Mater. Trans. B **28B**, 1103–1110 (1997)

ACL Racks Up Three P2 Scores—"Right Tool for the Job" Saves DOE $ in Cleanup
    D. W. Green
        Pollution Prevention Advisor **7**(1), 12 (1997)

Kill Performance Evaluations
    D. W. Green
        Managing the Modern Laboratory **2**(3), 24A–25A (1997)

Requirements for a Successful Performance Evaluation System
    D. W. Green
        Managing the Modern Laboratory **2**(3), 32A–36A (1997)

Uncommon Sense
    D. W. Green
        Managing the Modern Laboratory **2**(4), 44A–45A (1997)

EV-erybody Talks About It, Argonne Does Something for EVs
    G. L. Henriksen
        Pollution Prevention Advisor **7**(1), 10 (1997)

Reporting of Relative Sulfur Isotope-Ratio Data
    K. G. Heumann, T. B. Coplen, J. K. Bohlke, H. D. Dietze, M. Ebihara,
    J. W. Gramlich, H. R. Krousew, R. D. Loss, G. I. Ramendik, D. E. Richardson,
    K. J. R. Rosman, L. Schultz, P. D. P. Taylor, L. Turpin, R. D. Vocke, P. DeBievre,
    Y. Xiao, M. Shima, A. Pires de Matos, and N. N. Greenwood
        Pure Appl. Chem. **69**(2), 293–295 (1997)

The Effects of Variable Oxygen Partial Pressures during Bi-2223 Tape Processing
    T. G. Holesinger, J. F. Bingert, J. O. Willis, V. A. Maroni, A. K. Fischer, and
    K. T. Wu
        J. Mater. Res. **12**(11), 3046–3054 (1997)

Conversion of Chlorinated Volatile Organic Compounds to Carbon Dioxide and Methyl
Chloride for Isotopic Analysis of Carbon and Chlorine
    B. D. Holt, N. C. Sturchio, T. A. Abrajano, and L. J. Heraty
        Anal. Chem. **69**(14), 2727–2733 (1997)

Anisotropic Xe Chemical Shifts in Zeolites. The Role of Intra- and Intercrystallite Diffusion
    C. J. Jameson, A. K. Jameson, R. E. Gerald, and H. M. Lim
        J. Phys. Chem. B **101**, 8418–8437 (1997)

Advanced Understanding of the Tritium Recovery Process from the Ceramic Breeder
Blanket
    C. E. Johnson, J. P. Kopasz, and S.-W. Tam
        J. Nucl. Mater. **248**, 91–100 (1997)

Structural and Electrochemical Studies of Alpha Manganese Oxide (α-MnO_2)
    C. S. Johnson, D. W. Dees, M. F. Mansuetto, M. M. Thackeray, D. R. Vissers,
    D. Argyriou, C.-K. Loong, and L. Christensen
        J. Power Sources **68**(2), 570–577 (1997)

Stabilized α-MnO_2 Electrodes for Rechargeable 3-V Lithium Batteries
    C. S. Johnson, M. F. Mansuetto, M. M. Thackeray, Y. Shao-Horn, and S. A. Hackney
        J. Electrochem. Soc. **144**, 2279 (1997)

Light Element Thermodynamics Related to Actinide Separations
    I. Johnson and C. E. Johnson
        J. Nucl. Mater. **247**, 177–182 (1997)

Application of Surface-Enhanced Infrared Absorption Spectroscopy as a Sensor for Volatile Organic Compounds
> S. A. Johnson, N.-H. Pham, V. J. Novick, and V. A. Maroni
>> Appl. Spectrosc. **51**(9), 1423–1426 (1997)

Sorption Capacity of Ferromagnetic Microparticles Coated with CMPO
> M. D. Kaminski, S. Landsberger, L. Nuñez, and G. F. Vandegrift
>> Sep. Sci. Technol. **32**(1–4), 115–126 (1997)

Electrochemical Energy Conversion
> M. Krumpelt
>> In Section 27 of *Perry's Chemical Engineer's Handbook*, Ed., D. Green, 7th ed., McGraw-Hill, New York, pp. 27-55–27-60 (1997)

CMT Fuel Cell More Practical for Automobiles
> R. Kumar
>> Pollution Prevention Advisor **7**(1), 11 (1997)

Liquid Waste Goes into Spin Cycle
> R. A. Leonard
>> Pollution Prevention Advisor **7**(1), 13 (1997)

Centrifugal Contactors for Laboratory-Scale Solvent Extraction Tests
> R. A. Leonard, D. B. Chamberlain, and C. Conner
>> Sep. Sci. Technol. **32**(1–4), 193–210 (1997)

Meteoroid Streams as Sources for Meteorite Falls: A Status Report
> M. E. Lipschutz, S. F. Wolf, and R. T. Dodd
>> Plan. Space Sci. **45**(5), 517–523 (1997)

Ion Beam Induced Surface Modification of Chemical Vapor Deposition Diamond for X-ray Beam Position Monitor Applications
> C. Q. Liu, D. Shu, T. M. Kuzay, L. Wen, and C. A. Melendres
>> J. Vac. Sci. Technol. A **15**(3), Part 2, 1200–1205 (1997)

X-ray Absorption Spectra and the Local Structure of Nickel in Some Oxycompounds and Fluorides
> A. N. Mansour and C. A. Melendres
>> Journal de Physique IV **7**, C2–1171 (1997)

X-ray Absorption Spectra and the Structure of the Higher Oxide Forms of Nickel
> A. N. Mansour and C. A. Melendres
>> *New Materials for Fuel Cell and Modern Battery Systems III*, Eds., O. Savadogo and P. R. Roberge, Ecole Polytechnique de Montreal, Quebec, p. 166 (1997)

Examination of Phase Evolution in High-T_c Superconducting Ceramics by Raman Microspectroscopy and Imaging Raman Microscopy
> V. A. Maroni, A. K. Fischer, and K. T. Wu
>> Spectroscopy **12**(7), 38–45 (1997)

Review of Dimethyl Carbonate (DMC) Manufacture and Its Characteristics as a Fuel
Additive
    C. L. Marshall and M. A. Pacheco
        Energy & Fuels 11(1), 2–29 (1997)

Stainless Steel-Zirconium Waste Forms from Electrometallurgical Treatment of Spent
Nuclear Fuel
    S. M. McDeavitt, D. P. Abraham, J. Y. Park, and D. D. Keiser
        J. Miner. Met. Mater. 49(7), 29–32 (1997)

Measurement of Kinetic Rate Law Parameters on a Na-Ca-Al Borosilicate Glass for
Low-Activity Waste
    B. P. McGrail, W. L. Ebert, A. J. Bakel, and D. K. Peeler
        J. Nucl. Mater. **249**, 175–189 (1997)

Electrometallurgically Treating Metal, Oxide, and Al-Alloy Spent Nuclear Fuel Types
    C. C. McPheeters, E. C. Gay, E. J. Karell, and J. P. Ackerman
        J. Miner. Met. Mater. 49(7), 22–25 (1997)

Application of the Pyrochemical Process to Recycle of Actinides from LWR Spent Fuel
    C. C. McPheeters, R. D. Pierce, and T. P. Mulcahey
        Prog. Nucl. Energy **31**(1/2), 175–186 (1997)

Synchrotron Far Infrared Spectroscopy of Surface Films on a Copper Electrode in Aqueous
Solutions
    C. A. Melendres, G. A. Bowmaker, J. M. Leger, and B. Beden
        Nucl. Instrum. Methods Phys. Res. B **133**, 109–113 (1997)

X-ray Absorption Spectroelectrochemical Cell for *In-Situ* Studies of Thin Films
    C. A. Melendres and A. N. Mansour
        Electrochim. Acta **43**, 631 (1997)

Identification and Quantification of Phases Formed during the Processing of
$(Bi,Pb)_2Sr_2Ca_2Cu_3O_x$/Ag Composite Conductors
    N. N. Merchant, A. K. Fischer, V. A. Maroni, W. L. Carter, and R. D. Parrella
        IEEE Trans. on Applied Superconductivity 7(2), 1608–1611 (1997)

Leaching
    S. A. Miller
        In Section 18 of *Perry's Chemical Engineers' Handbook*, Ed., D. Green, 7th ed.,
        McGraw-Hill, New York, pp. 18-55–18-59 (1997)

Applicability of d.c. Relaxation Techniques to Multistep Reactions
    Z. Nagy, N. C. Hung, K. C. Liddell, M. Minkoff, and G. K. Leaf
        J. Electroanal. Chem. **421**, 33–44 (1997)

Isotopic Analysis of Ca from Extraterrestrial Micrometer-Sized SiC by Laser Desorption and Resonant Ionization Mass Spectroscopy
> G. K. Nicolussi, M. J. Pellin, W. F. Calaway, R. S. Lewis, A. M. Davis, S. Amari, and R. N. Clayton
>> Anal. Chem. **69**, 1140–1147 (1997)

Magnetic Particles Remove Metals and Radionuclides
> L. Nuñez and J. M. Andrew
>> Pollution Engineering, p. 10 (1997)

Magnets Grab Contaminants, Hazardous Wastes
> L. Nuñez and J. M. Andrew
>> Chemical Process Alert **3**(37), 4 (1997)

Application of Single-Ion Activity Coefficients to Determine the Solvent Extraction Mechanism for Components of High-Level Nuclear Waste
> L. Nuñez, M. D. Kaminski, and G. F. Vandegrift
>> Sep. Sci. Technol. **32**(1–4), 211–221 (1997)

Evidence for Dimeric and Tetrameric Water Clusters in HZSM-5
> D. H. Olson, S. A. Zygmunt, M. K. Erhardt, L. A. Curtiss, and L. E. Iton
>> Zeolites **18**, 347–349 (1997)

Electrochemical and *In Situ* Neutron Diffraction Investigations of La-Ni-Al-H Alloys
> W. Peng, L. Redey, A. N. Jansen, D. R. Vissers, K. M. Myles, J. M. Carpenter, J. W. Richardson, G. L. Burr, and J. R. Selman
>> J. Electrochem. Soc. **144**(11), 3836–3844 (1997)

Ceramic-Composite Waste Forms from Electrometallurgical Treatment of Spent Nuclear Fuel
> C. Pereira, M. C. Hash, M. A. Lewis, and M. K. Richmann
>> J. Miner. Met. Mater. **49**(7), 34–37 (1997)

Application of Quantum Beams to Analysis of Radioactive Materials
> M. C. Petri, L. Leibowitz, and C. E. Johnson
>> J. Nucl. Mater. **248**, 412–417 (1997)

Energy Resources, Conversion, and Utilization
> W. F. Podolski and S. A. Miller, Eds.
>> Section 27 of *Perry's Chemical Engineers' Handbook*, Ed., D. Green, 7h ed., McGraw-Hill, New York (1997)

Accurate Density Functional Thermochemistry for Larger Molecules
> K. Raghavachari, B. B. Stefanov, and L. A. Curtiss
>> Mol. Phys. **91**(3), 555–559 (1997)

Accurate Thermochemistry for Larger Molecules: Gaussian-2 Theory with Bond
Separation Energies
>   K. Raghavachari, B. B. Stefanov, and L. A. Curtiss
>   >   J. Chem. Phys. **106**(16), 6764–6767 (1997)

Review of *Environmental and Health & Safety Management: A Guide to Compliance*, by
N. P. Cheremisinoff and M. L. Graffia
>   J. B. Rajan
>   >   Environ. Prog. **16**(4), W9–W10 (1997)

Review of *Hazardous Air Pollutants: Assessment, Liabilities, and Regulatory Compliance*,
by J. W. Bradstreet
>   J. B. Rajan
>   >   Environ. Prog. **16**(4), W10–W11 (1997)

Toroids in NMR Spectroscopy
>   J. W. Rathke, R. J. Klingler, R. E. Gerald, K. W. Kramarz, and K. Woelk
>   >   Prog. Nucl. Magn. Reson. Spectrosc. **30**, 209–253 (1997)

Assessment of Modified Gaussian-2 (G2) and Density Functional Theories for Molecules
Containing Third-Row Atoms Ga–Kr
>   P. C. Redfern, J.-P. Blaudeau, and L. A. Curtiss
>   >   J. Phys. Chem. A **101**(46), 8701–8705 (1997)

Effect of Extremely Fine Y_2BaCuO_5 Precipitates on the Critical Current Density of
Melt-Processed $YBa_2Cu_3O_x$
>   S. Sengupta, D. Shi, J. S. Luo, A. Buzdin, V. Gorin, V. R. Todt, C. Varanasi, and
>   P. J. McGinn
>   >   J. Appl. Phys. **81**(11), 7396–7408 (1997)

Microstructural Stability of Electrochemically Active α-MnO_2
>   Y. Shao-Horn, S. A. Hackney, C. S. Johnson, and M. M. Thackeray
>   >   Prog. Batteries & Battery Mater. **16**, 141 (1997)

Off-Specular X-ray Scattering Studies of the Morphology of Thin Films
>   S. K. Sinha, Y. P. Feng, C. A. Melendres, D. D. Lee, T. P. Russel, S. K. Satija,
>   E. B. Sirota, and M. K. Sanyal
>   >   Physica A **231**, 99 (1996)

Optimization of Magnetite Carrier Precipitation Process for Plutonium Waste Reduction
>   S. A. Slater, D. B. Chamberlain, S. B. Aase, B. D. Babcock, C. Conner, J. Sedlet, and
>   G. F. Vandegrift
>   >   Sep. Sci. Technol. **32**(1–4), 127–147 (1997)

An Evaluation of Radium-Specific, Solid Phase Extraction Membranes
>   L. L. Smith, F. Markun, J. S. Alvarado, K. M. Hoffmann, D. C. Seely, and
>   R. T. Shannon
>   >   Radioact. Radiochem. **8**(1), 30–37 (1997)

Theoretical Study of the Potential Energy Surface of Diglyme
A. Sutjianto and L. A. Curtiss
Chem. Phys. Lett. **264**, 127–133 (1997)

Thermodynamic and Nonstoichiometric Behavior of the Lead-Doped and Lead-Free Bi-2212 Systems
M. Tetenbaum, M. C. Hash, B. S. Tani, J. S. Luo, and V. A. Maroni
Physica C **282–287**, 441–442 (1997)

A Comment on the Structure of Thin-Film $LiMn_2O_4$ Electrodes
M. M. Thackeray
J. Electrochem. Soc. **144**(5), L100–L102 (1997)

Manganese Oxides for Lithium Batteries
M. M. Thackeray
Prog. Solid State Chem. **25**(1-2), 1–71 (1997)

Structural Stability of $LiMn_2O_4$ Electrodes for Lithium Batteries
M. M. Thackeray, M. F. Mansuetto, and J. B. Bates
J. Power Sources **68**(1), 153 (1997)

Development of a Bench-Scale Metal Distillation Furnace
M. A. Vest, E. F. Lewandowski, R. D. Pierce, and J. L. Smith
Nucl. Technol. **120**(3), 232–242 (1997)

Sputtering Products of Sodium Sulfate: Implications for Io's Surface and for Sodium-Bearing Molecules in the Io Torus
R. C. Wiens, D. S. Burnett, W. F. Calaway, C. S. Hansen, K. R. Lykke, and M. J. Pellin
Icarus **128**, 386–397 (1997)

Physical and Chemical Characterization of Actinides in Soil from Johnston Atoll
S. F. Wolf, J. K. Bates, E. C. Buck, N. L. Dietz, J. Fortner, and N. R. Brown
Environ. Sci. Technol. **31**(2), 467–471 (1997)

Chemical Studies of H Chondrites—VIII. On Contemporary Meteoroid Streams
S. F. Wolf, M.-S. Wang, R. T. Dodd, and M. E. Lipschutz
J. Geophys. Res. Planets **102**(E4), 9273–9288 (1997)

Elevated-Temperature Creep Strength of $LiFeO_2$, $LiCoO_2$, and NiO—5 (at.%) Li_2O
J. Wolfenstine, C. D. Sperry, K. C. Goretta, J. L. Routbort, M. T. Lanagan, I. Bloom, T. D. Kaun, and M. Krumpelt
Mater. Lett. **31**, 251–254 (1997)

Application of Neutron Activation Analysis in a Fission Molybdenum Separation Study
D. Wu, S. Landsberger, and G. F. Vandegrift
J. Radioanal. Nucl. Chem. **216**(1), 101–105 (1997)

Raman Microscopy Examination of Phase Evolution in Bi(Pb)-Sr-Ca-Cu-O
Superconducting Ceramics
>K. T. Wu, A. K. Fischer, V. A. Maroni, and M. W. Rupich
>>J. Mater. Res. **12**(5), 1195–1204 (1997)

X-ray Scattering Study of Porous Silicon Growth during Anodic Dissolution
>H. You, Z. Nagy, and K. Huang
>>Phys. Rev. Lett. **78**(7), 1367–1370 (1997)

A New Quality Control Test for Biological and Recombinant Products
>B. Y. Zaslavsky and D. J. Chaiko
>>*Validation Practices for Biotechnology Products*, Ed., J. K. Shillenn, American
>>Society for Testing and Materials, ASTM STP 1260, Philadelphia, PA (1997)

B. Patents and Inventions

Aqueous Biphasic Plutonium Oxide Extraction Process with pH and Particle Control
    D. J. Chaiko and R. Mensah-Biney
        Patent No. 5,625,862, issued April 29, 1997

THTPV—A Transient Heat Transfer Program for Process Vessels
    A. A. Frigo, D. E. Preuss, and J. L. Bailey
        Invention No. ANL-SF-97-035 (1997)

Electrorefining Cell with Parallel Electrode/Concentric Cylinder Cathode
    E. C. Gay, W. E. Miller, and J. J. Laidler
        Patent No. 5,650,053, issued July 22, 1997

Method of Preparing Sodalite from Chloride Salt Occluded Zeolite
    M. A. Lewis and C. Pereira
        Patent No. 5,613,240, issued March 18, 1997

Thermal and Chemical Remediation of Mixed Wastes
    P. A. Nelson and W. M. Swift
        Patent No. 5,697,307, issued December 16, 1997

Method of Solubilizing Phthalocyanines and Metallophthalocyanines
    J. W. Rathke, M. J. Chen, and C. M. Fendrick
        Statutory Invention Registration No. H1695, issued November 4, 1997

Porous Silicon with Embedded Tritium as a Stand-Alone Prime Power Source for
Optoelectronic Applications
    S.-W. Tam
        Patent No. 5,605,171, issued February 25, 1997

Process of Preparing Tritiated Porous Silicon
    S.-W. Tam
        Patent No. 5,604,162, issued February 18, 1997

C. Reports

A Survey of Decontamination Processes Applicable to DOE Nuclear Facilities
       L. Chen, D. B. Chamberlain, C. Conner, and G. F. Vandegrift
              ANL-97/19 (May 1997)

Determination of Labile Copper, Cobalt, and Chromium in Textile Mill Wastewater
       J. S. Crain, A. M. Essling, J. T. Kiely, E. A. Huff, D. R. Huff, and D. G. Graczyk
              ANL/ACL-97/1 (January 1997)

Laboratory Testing of Glasses for Lockheed Idaho Technology Company: Final Report
       A. J. G. Ellison, E. C. Buck, N. L. Dietz, W. L. Ebert, J. S. Luo, S. F. Wolf, and
       J. K. Bates
              ANL-97/12 (June 1997)

Uranium Isotopic Composition and Uranium Concentration in Special Reference Material
SRM A (Uranium in KCl/LiCl Salt Matrix)
       D. G. Graczyk, A. M. Essling, C. S. Sabau, F. P. Smith, D. L. Bowers, and
       J. P. Ackerman
              ANL/ACL-97/3 (July 1997)

Analytical Chemistry Laboratory Progress Report for FY 1997
       D. W. Green, A. S. Boparai, D. L. Bowers, D. G. Graczyk, and P. C. Lindahl (with
       contributions from ACL staff)
              ANL/ACL-97/5 (December 1997)

Advanced Integrated Solvent Extraction Systems
       E. P. Horwitz, M. L. Dietz, and R. A. Leonard
              Pacific Northwest National Laboratory Report PNNL-SA-28461, pp. 4.13–4.15
              (1997)

Chemical Technology Division Annual Technical Report, 1996
       J. J. Laidler et al.
              ANL-97/13 (June 1997)

Solvent Extraction of Radionuclides from Aqueous Tank Waste
       B. A. Moyer, P. V. Bonnesen, R. A. Sachleben, R. A. Leonard, and G. J. Lumetta
              Pacific Northwest National Laboratory Report PNNL-SA-28461, pp. 4.5–4.11
              (1997)

Mobile Evaporator Corrosion Test Results
       A. E. V. Rozeveld and D. B. Chamberlain
              ANL-97/2 (May 1997)

Extraction of Semivolatile Organic Compounds from High-Efficiency Particulate Air
(HEPA) Filters by Supercritical Carbon Dioxide
       J. B. Schilling
              ANL/ACL-97/6 (September 1997)

Development of Test Acceptance Standards for Qualification of the Glass-Bonded Zeolite
Waste Form, Interim Annual Report, October 1995–September 1996
    L. J. Simpson, D. J. Wronkiewicz, and J. Fortner
        ANL-98/5 (September 1997)

Separation Science and Technology Semiannual Progress Report, October 1993–March 1994
    G. F. Vandegrift, S. B. Aase, B. A. Buchholz, D. B. Chamberlain, C. Conner,
    J. M. Copple, K. Foltz, B. Gebby, J. C. Hutter, R. A. Leonard, L. Nuñez,
    A. Philippides, M. C. Regalbuto, A. E. V. Rozeveld, J. Sedlet, S. A. Slater,
    B. Srinivasan, D. Strellis, and D. G. Wygmans
        ANL-97/21 (December 1997)

Volatile Trace Element Composition and Shock in Equilibrated H Chondrites
    S. F. Wolf and M. E. Lipschutz
        Lunar and Planetary Institute Technical Report 97–02, Eds., M. E. Zolensky,
        A. N. Krot, and E. R. D. Scott, Part 1, 67–68 (1997)

Radiation Effects in Moist-Air Systems and the Influence of Radiolytic Product Formation
on Nuclear Waste Glass Corrosion
    D. J. Wronkiewicz, J. K. Bates, E. C. Buck, J. C. Hoh, J. W. Emergy, and
    L. M. Wang
        ANL-97/15 (July 1997)

D. Abstracts and Proceedings Papers

Partial Oxidation Reformer Development for Fuel Cell Vehicles
>   S. Ahmed, R. Doshi, S. H. D. Lee, R. Kumar, and M. Krumpelt
>> Proc. of the 32nd Intersoc. Energy Conversion Eng. Conf., Honolulu, HI,
>> July 27–August 1, 1997, Vol. 2, pp. 843–846 (1997)

Pu and Gd Chemistry of Zirconolite Polytypes in a Titanate Ceramic
>   A. J. Bakel, E. C. Buck, and B. B. Ebbinghaus
>> Proc. of the Plutonium Futures—The Science Conf., Santa Fe, NM,
>> August 25–27, 1997, pp. 135–136 (1997)

Glass Dissolution at 20, 40, 70, and 90°C
>   A. J. Bakel, W. L. Ebert, D. M. Strachan, and N. R. Brown
>> Ceram. Trans. **72**, 271–278 (1997)

Structure and Electrochemical Potential Simulation for the Cathode Material $Li_{1+x}V_3O_8$
>   R. Benedek, M. M. Thackeray, and L. H. Yang
>> Abstracts, Materials Research Soc. Meeting, Boston, MA, December 1–5, 1997,
>> Abstract Y1.8, p. 507 (1997)

Chemical Reactivity of Delithiated Stoichiometric and Lithium Substituted $Li_{1+\delta}Mn_{2-\delta}O_4$ ($0 \leq \delta \leq 0.33$) Spinel Oxides
>   T. E. Bofinger, C. S. Johnson, S. A. Hackney, and M. M. Thackeray
>> Abstracts, Materials Research Soc. Meeting, Boston, MA, December 1–5, 1997,
>> Abstract Y8.27, p. 521 (1997)

Reduction of Delithiated Manganese Dioxide Structures
>   T. E. Bofinger, C. S. Johnson, S. A. Hackney, and M. M. Thackeray
>> Abstracts, 192nd Electrochem. Soc. Meeting, Paris, France, August 31–
>> September 5, 1997, Vol. 97–2, p. 176 (1997)

Microscopic Analysis of Pu-Contaminated Incinerator Ash: Implications for Immobilization
>   E. C. Buck
>> Proc. of the Plutonium Futures—The Science Conf., Santa Fe, NM,
>> August 25–27, 1997, pp. 139–141 (1997)

Study of Corrosion of a Titanate Ceramic for Plutonium Immobilization with EELS
>   E. C. Buck, A. J. Bakel, and J. K. Bates
>> Proc. of the Microscopy and Microanalysis '97 Conf., Cleveland, OH,
>> August 10–14, 1997, pp. 747–748 (1997)

Characterization of a Plutonium-Bearing Zirconolite-Rich Synroc
>   E. C. Buck, B. B. Ebbinghaus, A. J. Bakel, and J. K. Bates
>> Mater. Res. Soc. Symp. Proc. **465**, 1259–1266 (1997)

The Crystal Structure of Ianthinite, a Mixed-Valence Uranium Oxide Hydrate
  P. C. Burns, R. J. Finch, F. C. Hawthorne, M. L. Miller, and R. C. Ewing
      Mater. Res. Soc. Symp. Proc. **465**, 1193–1200 (1997)

Resonance Ionization of Sputtered Atoms: Quantitative Analysis in the Near-Surface
Region of Silicon Wafers
  W. F. Calaway, D. R. Spiegel, A. H. Marshall, S. W. Downey, and M. J. Pellin
      Proc. of the 14th Int. Conf. on the Application of Accelerators in Research
      and Industry, Denton, TX, November 6–9, 1996, Am. Institute of Physics Conf.
      Proc. 392, Eds., J. L. Duggan and I. L. Morgan, pp. 739–742 (1997)

Development and Testing of a Glass Waste Form for the Immobilization of Plutonium
  D. B. Chamberlain, J. M. Hanchar, J. W. Emery, J. C. Hoh, S. F. Wolf, R. J. Finch,
  J. K. Bates, A. J. G. Ellison, and D. B. Dingwell
      Mater. Res. Soc. Symp. Proc. **465**, 1229–1236 (1997)

Iron Phthalocyanine-Catalyzed Oxygen Atom Transfer Reactions
  M. J. Chen and J. W. Rathke
      Abstracts, Catalysis Club of Chicago, Spring Symp., Evanston, IL, April 2, 1997

Cathodes for Ceria-Based Fuel Cells
  R. Doshi, V. L. Richards, and M. Krumpelt
      Proc. of the Fifth Int. Symp. on Solid Oxide Fuel Cells, Electrochem. Soc.
      Meeting, Aachen, Germany, June 2–5, 1997, Vol. 97–40 (1997)

Short-Term Consistency Testing vs. Long-Term Behavior
  W. L. Ebert, A. J. Bakel, S. F. Wolf, and D. M. Strachan
      Proc. of the 18th USDOE Low-Level Radioactive Waste Management
      Conf., Salt Lake City, UT, May 20–22, 1997, Track 1.07, USDOE Report
      CONF-970537 (1997)

Dissolution Rates of DWPF Glasses from Long-Term PCT
  W. L. Ebert and S.-W. Tam
      Mater. Res. Soc. Symp. Proc. **465**, 149–156 (1997)

$LiMn_{2-x}Cu_xO_4$ Spinels—5 V Cathode Materials
  Y. Ein-Eli, W. F. Howard, S. H. Lu, S. Mukerjee, J. McBreen, J. T. Vaughey, and
  M. M. Thackeray
      Abstracts, Materials Research Soc. Meeting, Boston, MA, December 1–5, 1997,
      Abstract Y7.3, p. 516 (1997)

The Role of H_2O in Minerals Containing the Uranyl Ion
  R. J. Finch
      Trans. of the Am. Geophys. Union Spring Meeting, EOS, Vol. 78, p. S328
      (1997)

Thermodynamic Stabilities of U(VI) Minerals: Estimated and Observed Relationships
  R. J. Finch
      Mater. Res. Soc. Symp. Proc. **465**, 1185–1192 (1997)

Spent Fuel Reaction—The Behavior of the ε-Phase over 3.1 Years
>   P. A. Finn, J. C. Hoh, S. F. Wolf, M. T. Surchik, E. C. Buck, and J. K. Bates
>   Mater. Res. Soc. Symp. Proc. **465**, 527–534 (1997)

Plutonium Alteration Phases from Vapor Hydration of Lanthanide Borosilicate Glass for Weapons Material Disposition: A TEM Study
>   J. Fortner, C. J. Mertz, D. B. Chamberlain, and J. K. Bates
>   Proc. of the Microscopy and Microanalysis '97 Conf., Cleveland, OH,
>   August 10–14, 1997, pp. 663–664 (1997)

Solution-Borne Colloids from Drip Tests Using Actinide-Doped and Fully-Radioactive Waste Glasses
>   J. Fortner, S. F. Wolf, E. C. Buck, C. J. Mertz, and J. K. Bates
>   Mater. Res. Soc. Symp. Proc. **465**, 165 (1997)

Ring Opening Metathesis Polymerizations in Supercritical Fluids
>   D. E. Fremgen, M. J. Chen, and J. W. Rathke
>   Abstracts, Catalysis Club of Chicago, Spring Symp., Evanston, IL, April 2, 1997
>   (1997)

In Situ Imaging of Charge Carriers in an Electrochemical Cell

>   R. E. Gerald, R. J. Klingler, J. W. Rathke, G. Sandí, and K. Woelk
>   Abstracts, Fourth Int. Conf. on Magnetic Resonance Microscopy, Albuquerque,
>   NM, September 21–25, 1997, p. 48 (1997)

In Situ Measurements of Ion Mobility in an Electrochemical Cell
>   R. E. Gerald, R. J. Klingler, J. W. Rathke, and K. Woelk
>   Program Binder for the 38th Experimental Nuclear Magnetic Resonance Conf.,
>   Orlando, FL, March 23–27, 1997, p. 10 (1997)

Analytical Chemistry of Aluminum Salt Cake
>   D. G. Graczyk, A. M. Essling, E. A. Huff, F. P. Smith, and C. T. Snyder
>   *Light Metals, 1997*, Ed., R. Huglen, Proc. of the Technical Sessions Presented
>   by the TMS Aluminum Committee at the 126th Annual Meeting of the
>   Minerals, Metals, and Materials Soc., Orlando, FL, February 9–13, 1997,
>   pp. 1135–1140 (1997)

^{129}Xe MRM of Gaseous Probes in Silica Aerogels
>   D. M. Gregory, R. E. Gerald, and R. E. Botto
>   Abstracts, Fourth Int. Conf. on Magnetic Resonance Microscopy, Albuquerque,
>   NM, September 21–25, 1997, p. 49 (1997)

MRM Characterization of Microporous Materials Using Gaseous Probes
>   D. M. Gregory, R. E. Gerald, and R. E. Botto
>   Program Binder for the 38th Experimental Nuclear Magnetic Resonance Conf.,
>   Orlando, FL, March 23–27, 1997, p. 215 (1997)

Rare Earth Elements and the Ce Anomaly in Terrestrial Zircons
  J. M. Hanchar, P. W. O. Hoskin, S. G. Jackson, E. B. Watson, R. W. Hinton,
  Y. Thibault, R. J. Finch, S. F. Wolf, S. Hemming, B. Hanson, and D. J. Lindstrom
        Trans. of the Am. Geophys. Union Fall Meeting, EOS, Vol. 78, No. 46, p. F783
        (1997)

Three-Color Resonance Ionization Spectroscopy of Zr in Si
  C. S. Hansen, W. F. Calaway, M. J. Pellin, R. C. Wiens, and D. S. Burnett
        Resonance Ionization Spectroscopy 1996, Proc. of the Eighth Int. Symp.
        on Resonance Ionization Spectroscopy and Its Applications (RIS '96),
        State College, PA, June 30–July 5, 1996, Am. Institute of Physics Conf. Proc.
        338, Eds., N. Winograd and J. E. Park, pp. 215–219 (1997)

Irradiation Performance of Lithium Ceramic Breeder Materials
  C. E. Johnson
        Proc. of the Fifth Int. Workshop on Ceramic Breeder Blanket Interactions,
        Rome, Italy, September 23–25, 1996, pp. 77–85 (1997)

Electrometallurgical Treatment of TMI-2 Fuel Debris
  E. J. Karell, K. V. Gourishankar, and G. K. Johnson
        Trans. of the Am. Nucl. Soc. Annual Meeting, Orlando, FL, June 1–5, 1997,
        Vol. 76, pp. 73–74 (1997)

Application of the Electrometallurgical Treatment Technique to Long-Term Disposition of
DOE Spent Fuel
  E. J. Karell, K. V. Gourishankar, and C. C. McPheeters
        Trans. of the Am. Nucl. Soc. Winter Meeting and Embedded Topical Meetings,
        Albuquerque, NM, November 16–20, 1997, Vol. 77, pp. 81–82 (1997)

Ion Transport Properties Determined by *In-Situ* NMR Imaging
  R. J. Klingler, R. E. Gerald, and J. W. Rathke
        Abstracts, Advanced Non-Aqueous Battery Technology Research and
        Development Workshop, Hunt Valley, MD, October 15–17, 1997, pp. 82–84
        (1997)

High-Pressure NMR Studies of Oxo-Type Catalysts
  R. J. Klingler, K. W. Kramarz, and J. W. Rathke
        Book of Abstracts, Part 1, 214th Am. Chem. Soc. National Meeting,
        Las Vegas, NV, September 7–11, 1997, Abstract No. 168 (1997)

High Pressure *In Situ* NMR Spectroscopy of Cobalt Oxo Catalysts
  K. W. Kramarz, R. J. Klingler, and J. W. Rathke
        Abstracts, 15th North American Catalysis Soc. Meeting, Chicago, IL,
        May 18–23, 1997, p. 149 (1997)

Glovebox Atmosphere Pressure and Flow Controls
  R. F. Malecha and M. A. Slawecki
        Proc. of the Tenth Annual Conf. and Equipment Exhibit of the Am. Glovebox
        Soc., Lakewood, CO, July 21–24, 1997, p. 101 (1997)

Ag/Bi-2223 Composite Conductors: What's Going on during Thermomechanical
Processing?
> V. A. Maroni
>> Program and Extended Abstracts, Int. Workshop on Superconductivity,
>> Co-Sponsored by the Int. Superconductivity Technology Center and the
>> Materials Research Society, Kona, HI, June 15–18, 1997, pp. 167–170 (1997)

Applications and Limitations of Surface Enhanced Infrared Spectroscopy
> V. A. Maroni, S. A. Johnson, V. J. Novick, and Y. Tsai
>> Abstracts, 48th Pittsburgh Conf. and Exposition on Analytical Chemistry and
>> Applied Spectroscopy, Atlanta, GA, March 16–21, 1997, Abstract No. 1279
>> (1997)

Raman Microspectroscopy and Imaging Raman Microscopy of High-T_c Ceramic
Superconductors
> V. A. Maroni, K. T. Wu, and A. K. Fischer
>> Abstracts, 48th Pittsburgh Conf. and Exposition on Analytical Chemistry
>> and Applied Spectroscopy, Atlanta, GA, March 16–21, 1997, Abstract No. 605
>> (1997)

Effect of Lead Content on Phase Evolution and Microstructural Development in Ag-Clad
Bi-2223 Composite Conductors
> N. N. Merchant, V. A. Maroni, A. K. Fischer, S. E. Dorris, W. Zhong, and N. Ashcom
>> Proc. of the 126th Annual Meeting of the Minerals, Metals, and Materials Soc.,
>> Symp. on High-Temperature Superconductors: Synthesis, Processing, and
>> Applications II, Orlando, FL, February 9–13, 1997, pp. 25–34 (1997)

Testing and Evaluation of Batteries for a Fuel Cell Powered Hybrid Bus
> J. F. Miller, C. E. Webster, A. F. Tummillo, and W. H. DeLuca
>> Proc. of the 32nd Intersoc. Energy Conversion Eng. Conf., Honolulu, HI,
>> July 27–August 1, 1997, pp. 894–898 (1997)

Transuranium Element Incorporation into the β-U_3O_8 Uranyl Sheet
> M. L. Miller, R. J. Finch, P. C. Burns, and R. C. Ewing
>> Mater. Res. Soc. Symp. Proc. 465, 581–588 (1997)

Copper Deposition/Dissolution at High Temperatures and Pressures
> Z. Nagy, R. O. Rigney, N. C. Hung, and R. M. Yonco
>> Abstracts, 191st Electrochem. Soc. Meeting, Montreal, Quebec, Canada,
>> May 4–9, 1997, Vol. 97–1, pp. 863–864 (1997)

Comparison of the Corrosion Behavior of Tank 51 Sludge-Based Glass and a Nonradioactive
Homologue Glass
> L. Nuñez, W. L. Ebert, S. F. Wolf, and J. K. Bates
>> Mater. Res. Soc. Symp. Proc. 465, 237–244 (1997)

Transient Heat Transfer Program for Glovebox Process Vessels
> D. E. Preuss, A. A. Frigo, and J. L. Bailey
>> Proc. of the Tenth Annual Conf. and Equipment Exhibit of the Am. Glovebox
>> Soc., Lakewood, CO, July 21–24, 1997, pp. 8–32 (1997)

Copper Deposition/Dissolution at High Temperatures and Pressures
>R. O. Rigney, N. C. Hung, R. M. Yonco, and Z. Nagy
>>Proc. of the Symp. on Electrode Materials and Processes for Energy Conversion and Storage IV, Eds., J. McBreen, S. Mukerjee, and S. Srinivasan, The Electrochem. Soc., Pennington, NJ, Vol. 97–13, pp. 354–366 (1977)

Novel Carbonaceous Materials for Lithium Secondary Batteries
>G. Sandi, R. E. Winans, K. A. Carrado, and C. S. Johnson
>>Proc. of the Second Int. Symp. on New Materials for Fuel Cell and Modern Battery Systems, Montreal, Canada, July 6–10, 1997, pp. 415–425 (1997)

TEM and XRD Studies of Layered $LiMnO_2$ and Delithiated Products
>Y. Shao-Horn, S. A. Hackney, A. R. Armstrong, P. G. Bruce, C. S. Johnson, and M. M. Thackeray
>>Abstracts, 192nd Electrochem. Soc. Meeting, Paris, France, August 31–September 5, 1997, Vol. 97–2, p. 98 (1997)

Structural and Electrochemical Features of Low-Temperature $LiCoO_2$ and Delithiated Products
>Y. Shao-Horn, S. A. Hackney, C. S. Johnson, A. J. Kahaian, and M. M. Thackeray
>>Abstracts, Materials Research Soc. Meeting, Boston, MA, December 1–5, 1997, Abstract Y3.5, p. 510 (1997)

Structural and Electrochemical Features of Low-Temperature $LiCoO_2$ and Delithiated Products
>Y. Shao-Horn, S. A. Hackney, C. S. Johnson, A. J. Kahaian, and M. M. Thackeray
>>Abstracts, 192nd Electrochem. Soc. Meeting, Paris, France, August 31–September 5, 1997, Vol. 97–2, pp. 150–151 (1997)

Evaluation of Standard Durability Tests towards the Qualification Process for the Glass-Zeolite Ceramic Waste Form
>L. J. Simpson and D. J. Wronkiewicz
>>Mater. Res. Soc. Symp. Proc. **465**, 441–448 (1997)

Methods and Criteria Development for Qualification of the Glass-Zeolite Ceramic
>L. J. Simpson, D. J. Wronkiewicz, and S. F. Wolf
>>Abstracts, 99th Am. Ceram. Soc. Meeting, Cincinnati, OH, May 4–7, 1997, p. 152 (1997)

Electrochemical Separation of Aluminum from Uranium for Research Reactor Spent Nuclear Fuel Applications
>S. A. Slater, J. L. Willit, and E. C. Gay
>>Proc. of the Topical Conf. on Separation Science and Technology, AIChE Annual Meeting, Los Angeles, CA, November 16–21, 1997, pp. 650–653 (1997)

Materials Research for Lithium Batteries
>M. M. Thackeray
>>Abstract, Advanced Non-Aqueous Battery Technology Workshop, Hunt Valley, MD, October 15–17, 1997

Electrical Installation Considerations of Brushless DC Motors
R. L. Tollner and J. J. Heiberger
Proc. of the Tenth Annual Conf. and Equipment Exhibit of the Am. Glovebox
Soc., Lakewood, CO, July 21–24, 1997, p. 144 (1997)

Converting ^{99}Mo Production from High- to Low-Enriched Uranium
G. F. Vandegrift, C. Conner, J. Sedlet, and D. G. Wygmans
Trans. of the Am. Nucl. Soc. Winter Meeting and Embedded Topical Meetings,
Albuquerque, NM, November 16–20, 1997, Vol. 77, pp. 98–100 (1997)

Testing of HEPA Filters in Gloveboxes
S. G. Wiedmeyer
Proc. of the Tenth Annual Conf. and Equipment Exhibit of the Am. Glovebox
Soc., Lakewood, CO, July 21–24, 1997, p. 145 (1997)

Imaging Diffusion in Gels, Polymers, and Solids
K. Woelk, B. L. J. Zwank, J. Bargon, R. J. Klingler, R. E. Gerald, and J. W. Rathke
Abstracts, Fourth Int. Conf. on Magnetic Resonance Microscopy, Albuquerque,
NM, September 21–25, 1997, p. 61 (1997)

Grain Boundary Corrosion and Alteration Phase Formation during the Oxidative
Dissolution of UO_2 Pellets
D. J. Wronkiewicz, E. C. Buck, and J. K. Bates
Mater. Res. Soc. Symp. Proc. **465**, 519 (1997)

X-ray Scattering and Photoluminescence Studies of Porous Silicon
H. You, J. A. Tanzer, Z. Nagy, Z. Gaburro, and D. Babic
Proc. of the Symp. on Pits and Pores: Formation, Properties, and Significance
for Advanced Luminescent Materials, Eds., P. Schmuki, D. J. Lockwood,
H. S. Isaacs, and A. Bsiesy, The Electrochem. Soc., Pennington, NJ, Vol. 97–7,
pp. 215–223 (1997)

X-ray Scattering and Photoluminescence Studies of Porous Silicon
H. You, J. A. Tanzer, Z. Nagy, Z. Gaburro, and D. Babic
Abstracts, 191st Electrochem. Soc. Meeting, Montreal, Quebec, Canada,
May 4–9, 1997, Vol. 97–1, p. 199 (1997)

Sodium Zirconium Phosphate-Structured HLW Forms and Synroc for High-Level Nuclear
Waste Immobilization
V. N. Zyryanov and E. R. Vance
Mater. Res. Soc. Symp. Proc. **465**, 409–415 (1997)

E. Papers Presented at Scientific Meetings

Laves Intermetallics in Stainless Steel-Zirconium Alloys
>D. P. Abraham, S. M. McDeavitt, and J. W. Richardson
>>Presented at the Fourth Int. Conf. on High-Temperature Intermetallics, San Diego, CA, April 27–May 1, 1997

Fuel Processor Development
>S. Ahmed
>>Presented at the DOE Fuel Cells for Transportation Program—National Laboratory R&D Meeting, Washington, DC, July 22–23, 1997

Catalytic Partial Oxidation Reactor for Gasoline and Alternative Transportation Fuels
>S. Ahmed, R. Kumar, and M. Krumpelt
>>Presented at the Windsor Workshop on Transportation Fuels, Windsor, Ontario, Canada, June 9–11, 1997

A System for Rapid Water Sampling and Analysis Based on Empore^{TM} Membranes and Solid Scintillation Spectrometry
>J. H. Aldstadt, K. A. Orlandini, L. L. Smith, K. M. Hoffman, D. C. Seely, and I. R. Shaw-Epperson
>>Presented at the 43rd Annual Conf. on Bioassay, Analytical, and Environmental Radiochemistry, Charleston, SC, November 9–13, 1997

Thermodynamics of the Li_4SiO_4/H_2O System
>C. Alvani, S. Casadio, and C. E. Johnson
>>Presented at the Sixth Int. Workshop on Ceramic Breeder Blanket Interactions, Mito, Japan, October 22–24, 1997

Mobile Laboratory Screening of VOC's in Soil Using Static Headspace
>D. V. Applegate, J. F. Schneider, L. L. Chromizky, and A. S. Boparai
>>Presented at the 28th Analytical Chemistry Laboratory Technical Meeting, Argonne National Laboratory, IL, November 6, 1997

Corrosion Testing of MD Ceramic Materials
>A. J. Bakel, E. C. Buck, and D. B. Chamberlain
>>Presented at the Fissile Materials Disposition Program—Technical Evaluation Panel Meeting, Lawrence Livermore National Laboratory, Livermore, CA, July 30, 1997

Corrosion of a Pu-Doped Ceramic
>A. J. Bakel, E. C. Buck, S. F. Wolf, J. K. Bates, and D. B. Chamberlain
>>Presented at the 99th Am. Ceram. Soc. Meeting, Cincinnati, OH, May 4–7, 1997

Effects of Aerobic and Anaerobic Chelate Biodegradation on Actinide Speciation
>J. E. Banaszak, B. E. Rittmann, and D. T. Reed
>>Presented at the Fifth Int. Conf. on the Chemistry and Migration Behavior of Actinides and Fission Products in the Geosphere, MIGRATION '97, Sendai, Japan, October 26–31, 1997

Mathematical Modeling of the Effects of Aerobic and Anaerobic Chelate Biodegradation on Actinide Speciation
>J. E. Banaszak, J. VanBriesen, B. E. Rittmann, and D. T. Reed
>>Presented at the Fifth Int. Conf. on the Chemistry and Migration Behavior of Actinides and Fission Products in the Geosphere, MIGRATION '97, Sendai, Japan, October 26–31, 1997

Evaluation of Waste Glass Corrosion Mechanisms through Laboratory Testing and Analysis
>J. K. Bates, W. L. Ebert, and D. M. Strachan
>>Presented at the Am. Chem. Soc. Meeting, Las Vegas, NV, September 7–11, 1997

A Comparison of Corrosion Protection Methods in the Wet Seal of Molten Carbonate Fuel Cells
>I. Bloom, J. E. Indacochea, T. G. Benjamin, and M. Krumpelt
>>Presented at the 32nd Intersoc. Energy Conversion Eng. Conf., Honolulu, HI, July 27–August 1, 1997

Determination of Volatile and Semivolatile Organic Compounds in WIPP Sludges
>A. S. Boparai
>>Presented at the 27th Annual Analytical Chemistry Laboratory Technical Talks, Argonne, IL, April 22, 1997

Determination of Semivolatile Organic Compounds in Highly Alkaline Cemented and Uncemented Waste Water Sludges
>A. S. Boparai, K. J. Parish, Y. Tsai, P. D. Postlethwait, and M. J. Schipma
>>Presented at the 48th Pittsburgh Conf. and Exposition on Analytical Chemistry and Applied Spectroscopy, Atlanta, GA, March 16–21, 1997

Switchable Radioactive Neutron Source—Proof-of-Principle
>D. L. Bowers, E. A. Rhodes and C. E. Dickerman
>>Presented at the Fourth Int. Conf. on Methods and Applications of Radioanalytical Chemistry, MARC-IV, Kailua-Kona, HI, April 6–11, 1997

Structural Effects of the Addition of Late Transition Metals to Molybdenum Disulfide
>J. R. Brenner, C. L. Marshall, J. Heising, and M. Kanatzidis
>>Presented at the 15th North American Catalysis Soc. Meeting, Chicago, IL, May 18–23, 1997

Retention of Neptunium in Uranyl Alteration Phases Formed during Spent Fuel Corrosion
>E. C. Buck, R. J. Finch, P. A. Finn, and J. K. Bates
>>Presented at the European Meeting of the Materials Research Soc., Davos, Switzerland, September 28–October 3, 1997

Qualitative Analysis of Passive FTIR Sensor Data Using Partial Least Squares Discriminant
>S. E. Carpenter and Y. X. Noyes
>>Presented at the 48th Pittsburgh Conf. and Exposition on Analytical Chemistry and Applied Spectroscopy, Atlanta, GA, March 16–21, 1997

Extraction and Encapsulation of Metals from Aqueous Waste Streams
> D. J. Chaiko
>> Presented at the Am. Chem. Soc. Special Symp., Pittsburgh, PA,
>> September 15–17, 1997

DOE/EE Transporation Perspective
> S. G. Chalk and J. F. Miller
>> Presented at the Fuel Cells '97 Review Meeting, Morgantown, WV,
>> August 26–28, 1997

The U.S. Department of Energy—Investing in Clean Transportation
> S. G. Chalk, J. Milliken, and J. F. Miller
>> Presented at the Fifth Grove Fuel Cell Symp., London, United Kingdom,
>> September 22–25, 1997

Dissolution of Glass and Ceramic Materials
> D. B. Chamberlain
>> Presented at the Fissile Materials Disposition Program—Technical Evaluation
>> Panel Meeting, Lawrence Livermore National Laboratory, Livermore, CA,
>> July 30, 1997

Status: Corrosion Testing of MD Immobilization Forms
> D. B. Chamberlain, A. J. Bakel, C. J. Mertz, J. Fortner, E. C. Buck, S. F. Wolf, and
> D. M. Strachan
>> Presented at the Savannah River Technical Center, Aiken, SC, February 1997

Corrosion Testing of the MD LaBS Glass
> D. B. Chamberlain, E. C. Buck, and C. J. Mertz
>> Presented at the Fissile Materials Disposition Program—Technical Evaluation
>> Panel Meeting, Lawrence Livermore National Laboratory, Livermore, CA,
>> July 30, 1997

Dissolution of Low-Enriched UO_2/Al Dispersion Plates in Alkaline Peroxide Solution
> C. Conner, S. B. Aase, D. G. Wygmans, G. F. Vandegrift, D. Wu, and S. Landsberger
>> Presented at the IAEA Int. Meeting on Reduced Enrichment for Research and
>> Test Reactors (RERTR), Jackson Hole, WY, October 5–10, 1997

Decontamination of Tritiated Water by a Fuel-Cell Cascade
> C. Conner, R. Kumar, and G. F. Vandegrift
>> Presented at the Tritium Focus Group Meeting, Toronto, Canada, May 27–30,
>> 1997

Determination of Labile Copper, Cobalt, and Chromium in Textile Mill Wastewater
> J. S. Crain, A. M. Essling, J. T. Kiely, E. A. Huff, D. R. Huff, and D. G. Graczyk
>> Presented at the 30th Great Lakes Regional Am. Chem. Soc. Meeting,
>> Chicago, IL, May 28–30, 1997

Determination of Labile Transition Metal Species in Treated Wastewater
> J. S. Crain, A. M. Essling, J. T. Kiely, E. A. Huff, D. R. Huff, and D. G. Graczyk
>> Presented at the 30th Great Lakes Regional Am. Chem. Soc. Meeting, Chicago, IL, May 28–30, 1997

Radioanalytical ICP-MS: Principles and Applications
> J. S. Crain, L. L. Smith, F. P. Smith, J. T. Kiely, J. S. Yaeger, D. G. Graczyk, and J. A. Alvarado
>> Presented at the USDOE Environmental Measurements Laboratory, New York, NY, May 15, 1997

Development of Acceptance Specifications for Lower Activity Waste from the Hanford Tanks
> J. C. Cunnane, P. H. Kier, and N. R. Brown
>> Presented at the 18th USDOE Low-Level Radioactive Waste Management Conf., Salt Lake City, UT, May 20–22, 1997

Computational Studies of Molecular Adsorption in Zeolites
> L. A. Curtiss, L. E. Iton, and S. A. Zygmunt
>> Presented at the Thermodynamics and Statistical Mechanics Conf., Williams Bay, WI, May 15–16, 1997

Theoretical Studies of Long-Range Electronic Coupling
> L. A. Curtiss and J. R. Miller
>> Presented at the 21st DOE Solar Photochemistry Research Conf., Copper Mountain, CO, June 7–11, 1997

Ab Initio Molecular Orbital Studies of Ion-Polymer and Ion-Ion Interactions in Lithium Polymer Electrolytes
> L. A. Curtiss, A. Sutjianto, and A. G. Baboul
>> Presented at the Advanced Non-Aqueous Battery Technology and Development Workshop, Hunt Valley, MD, October 15–17, 1997

Development of a Portable FTIR Vapor and Liquid Sensor
> J. C. Demirgian
>> Presented at the Second Tri-Service Environmental Technology Workshop, St. Louis, MO, June 10–12, 1997

Comparison of Partial and Classical Least Squares Algorithms for the Analysis of Stack Emissions Using FTIR Spectroscopy
> J. C. Demirgian, K. Carney, Z. Mao, and J. M. Ewing
>> Presented at the 48th Pittsburgh Conf. and Exposition on Analytical Chemistry and Applied Spectroscopy, Atlanta, GA, March 16–21, 1997

A Novel Fermentation Pathway in a Mutant *Escherichia coli* Producing Succinic Acid, Acetic Acid, and Ethanol
> M. I. Donnelly, C. S. Millard, D. R. Clark, M. J. Chen, and J. W. Rathke
>> Presented at the 19th Symp. on Biotechnology for Fuels and Chemicals, Colorado Springs, CO, May 4–8, 1997

Ceramic Direct Methanol Fuel Cells
>   R. Doshi and M. Krumpelt
>> Presented at the DOE Fuel Cells for Transportation Program—National Laboratory R&D Meeting, Washington, DC, July 22–23, 1997

Micro-Engineered Cathode Interface Studies
>   R. Doshi, T. W. Kueper, Z. Nagy, and M. Krumpelt
>> Presented at the Fuel Cells '97 Review Meeting, Morgantown, WV, August 26–28, 1997

Effect of Alteration Phase Formation on the Glass Dissolution Rate
>   W. L. Ebert
>> Presented at the Conf. on Glass: Scientific Research toward High Performance Confinement, CEA-Valrho Summer Workshop, Mejannes-le-Clap, France, August 31–September 7, 1997

Laboratory Measurement of the Forward Dissolution Rate
>   W. L. Ebert
>> Presented at the 99th Am. Ceram. Soc. Meeting, Cincinnati, OH, May 4–7, 1997

The Incorporation of Technetium into a Representative Low-Activity Waste Glass
>   W. L. Ebert, A. J. Bakel, D. L. Bowers, E. C. Buck, and J. W. Emery
>> Presented at the 99th Am. Ceram. Soc. Meeting, Cincinnati, OH, May 4–7, 1997

Corrosion Mechanisms of Spent Fuel under Oxidizing Conditions
>   P. A. Finn, R. J. Finch, E. C. Buck, and J. K. Bates
>> Presented at the European Meeting of the Materials Research Soc., Davos, Switzerland, September 28–October 3, 1997

Plutonium Alteration Phases from Lanthanide Borosilicate Glass
>   J. Fortner, C. J. Mertz, D. B. Chamberlain, and J. K. Bates
>> Presented at the Plutonium Futures—The Science Conf., Santa Fe, NM, August 25–27, 1997

In Situ X-ray Scattering and Luminescence Studies of Porous Silicon
>   Z. Gaburro, H. You, J. A. Everhart, Z. Nagy, and D. Babic
>> Presented at the Am. Phys. Soc. Meeting, Kansas City, MO, March 17–21, 1997

In Situ Diffusion Measurements in an Electrochemical Cell
>   R. E. Gerald, R. J. Klingler, J. W. Rathke, and K. Woelk
>> Program Binder for the 38th Experimental Nuclear Magnetic Resonance Conf., Orlando, FL, March 23–27, 1997

In Situ Measurements of Ion Mobility in an Electrochemical Cell
>   R. E. Gerald, R. J. Klingler, J. W. Rathke, and K. Woelk
>> Presented at the 30th Great Lakes Regional Am. Chem. Soc. Meeting, Chicago, IL, May 28–30, 1997

Reduction of UO_2 by the Lithium Process
> K. V. Gourishankar
>> Presented at the 21st Annual Actinide Separations Conf., Charleston, SC,
>> June 23–26, 1997

Analytical Chemistry of Aluminum Salt Cake
> D. G. Graczyk
>> Presented at the 27th Annual Analytical Chemistry Laboratory Technical
>> Talks, Argonne, IL, April 22, 1997

Thermal Ionization Mass Spectrometry as Applied to Trace Element Isotopic Analysis
> J. W. Gramlich
>> Presented at the 30th Great Lakes Regional Am. Chem. Soc. Meeting,
>> Chicago, IL, May 28–30, 1997

Scientists as Managers
> D. W. Green
>> Presented at the 48th Pittsburgh Conf. and Exposition on Analytical
>> Chemistry and Applied Spectroscopy, Symp. on "Managing the Modern
>> Analytical Laboratory," Atlanta, GA, March 16–21, 1997

Recent Advances in Magnetic Resonance Microscopy to the Physical Structure
Characterization of Carbonaceous and Inorganic Material
> D. M. Gregory, R. E. Gerald, G. D. Cody, and R. E. Botto
>> Presented at the 213th Am. Chem. Soc. National Meeting, San Francisco, CA,
>> April 13–17, 1997

Preparation Techniques for Ceramic Waste Form Powder
> M. C. Hash, C. Pereira, V. N. Zyryanov, M. A. Lewis, G. L. Burns, J. J. Smith,
> J. P. Thalacker, and J. P. Ackerman
>> Presented at the 99th Am. Ceram. Soc. Meeting, Cincinnati, OH, May 4–7,
>> 1997

Advanced Development in Radioanalytical Sample Preparation Using Empore^{TM}
Strontium, Technetium, and Radium Rad Disks
> K. M. Hoffmann, D. C. Seely, M. D. Erickson, K. A. Orlandini, L. L. Smith,
> R. T. Shannon, R. Bruening, and S. Izatt
>> Presented at the Fourth Int. Conf. on Methods and Applications of
>> Radioanalytical Chemistry, Kailua-Kona, HI, April 6–11, 1997

A Combined CSEX-SREX Extraction/Recovery Process
> E. P. Horwitz, M. L. Dietz, and R. A. Leonard
>> Presented at the 21st Annual Actinide Separations Conf., Charleston, SC,
>> June 23–26, 1997

Ceramic Breeder Materials: Status and Needs
> C. E. Johnson, K. Noda, and N. Roux
>> Presented at the Eighth Int. Conf. on Fusion Reactor Materials, Sendai, Japan,
>> October 26–31, 1997·

Manganese Oxide Materials for Lithium Batteries
>C. S. Johnson and M. M. Thackeray
>>Presented at the Chicago-Midwest Battery Workshop, Illinois Institute of Technology, Chicago, IL, April 15, 1997

Spectroscopic Study of the Proton Dynamics in Manganese Dioxide Electrode Materials
>C. S. Johnson, M. M. Thackeray, J. C. Nipko, and C.-K. Loong
>>Presented at the Int. Conf. on Neutron Scattering, Toronto, Canada, August 17–21, 1997

Analysis of Lead Cable Experiment Samples Using X-ray Diffraction, Scanning Electron Microscope/Energy Dispersive Spectrometry, Inductively Coupled Plasma/Atomic Emission Spectrometry, Gas Mass Spectrometry, and Gas Chromatography/Mass Spectrometry
>P. L. Johnson
>>Presented at the 27th Annual Analytical Chemistry Laboratory Technical Talks, Argonne, IL, April 22, 1997

Recovery of Surplus Weapons—Usable Plutonium for Mixed Oxide Reactor Fuels
>T. R. Johnson, R. D. Pierce, and C. C. McPheeters
>>Presented at the Plutonium Futures—The Science Conf., Santa Fe, NM, August 25–27, 1997

Evaluation of Ferromagnetic Microparticles for Recovery of Hazardous Metals from Waste Solutions
>M. D. Kaminski, L. Nuñez, and C. Tsouris
>>Presented at the Tenth Symp. on Separation Scince and Technology for Energy Applications, Gatlinburg, TN, October 20–24, 1997

Extraction of Radionuclides and Hazardous Metals from Solution Using Extractant Coated Magnetic Microparticles
>M. D. Kaminski, L. Nuñez, and C. Tsouris
>>Presented at the Tenth Symp. on Separation Science and Technology for Energy Applications, Gatlinburg, TN, October 20–24, 1997

Evaluation of Extractant-Coated Magnetic Microparticles for the Recovery of Hazardous Metals from Waste Solution
>M. D. Kaminski, L. Nuñez, and A. E. Visser
>>Presented at the Tenth Symp. on Separation Science and Technology for Energy Applications, Gatlinburg, TN, October 20–24, 1997

Engineering-Scale Testing of the Lithium Reduction Process for DOE Oxide Spent Fuels
>E. J. Karell
>>Presented at the 21st Annual Actinide Separations Conf., Charleston, SC, June 23–26, 1997

Non-Segregating Electrolytes for Molten Carbonate Fuel Cells
>T. D. Kaun, I. Bloom, S. P. Nied, and M. Krumpelt
>>Presented at the Fuel Cells '97 Review Meeting, Morgantown, WV, August 26–28, 1997

Non-Segregating Li/Na Carbonate Electrolytes for Molten Carbonate Fuel Cells
> T. D. Kaun, S. Nied, S. Zelle, M. T. Lanagan, and M. Krumpelt
>> Presented at the Fifth Int. Symp. on Molten Salt Chemistry and Technology,
>> Dresden, Germany, August 24–29, 1997

High-Pressure NMR Studies of Oxo-Type Catalysts
> R. J. Klingler, K. W. Kramarz, and J. W. Rathke
>> Presented at the Am. Chem. Soc. Meeting, Las Vegas, NV, September 7–11,
>> 1997

Fuel Cells for Transportation R&D at Argonne National Laboratory
> R. Kumar, S. Ahmed, I. Bloom, J. D. Carter, R. Doshi, K. W. Kramarz, S. H. D. Lee,
> M. Krumpelt, and K. M. Myles
>> Presented at the Annual Automotive Technology Development Customers'
>> Coordination Meeting, Dearborn, MI, October 27–30, 1997

Catalytic Partial Oxidation Reforming of Hydrocarbon Fuels
> S. H. D. Lee, S. Ahmed, R. Kumar, and M. Krumpelt
>> Presented at the IAPG Chemical Working Group Meeting, Naval Surface
>> Warfare Center, West Bethesda, MD, September 16–18, 1997

CO Removal from Reformate
> S. H. D. Lee, K. W. Kramarz, D. J. Carter, R. Kumar, and M. Krumpelt
>> Presented at the DOE Fuel Cells for Transportation Program—National
>> Laboratory R&D Meeting, Washington, DC, July 22–23, 1997

Development and Testing of the SRTALK Process
> R. A. Leonard, C. Conner, M. W. Liberatore, P. V. Bonnesen, B. A. Moyer,
> D. J. Presley, and G. J. Lumetta
>> Presented at the Tenth Symp. on Separation Science and Technology for Energy
>> Applications, Gatlinburg, TN, October 20–24, 1997

The Activity of Cobalt and Silicon in the Co-Si System with Special Focus on the α-Co
Solid Solution
> D. Lexa, R. J. Kematick, and C. E. Myers
>> Presented at the Ninth Int. Conf. on High-Temperature Materials Chemistry,
>> State College, PA, May 19–23, 1997

DOE's Integrated Performance Evaluation Program: A Tool in a Total Quality System
> P. C. Lindahl, J. R. Dahlgran, W. E. Streets, and W. R. Newberry
>> Presented at the 43rd Annual Conf. on Bioassay, Analytical and Environmental
>> Radiochemistry, Charleston, SC, November 9–13, 1997

The Department of Energy's Integrated Performance Evaluation Program (IPEP): Pilot
Studies for Implementation
> P. C. Lindahl, W. E. Streets, J. J. Marr, K. J. Parish, W. R. Newberry,
> J. R. Dahlgran, C. Watkins, J. Connolly, J. Fisk, and L. A. Souza
>> Presented at the 39th Rocky Mountain Conf. on Analytical Chemistry, Denver,
>> CO, August 3–7, 1997

Results of Pilot Implementation Studies of DOE's Integrated Performance Evaluation Program (IPEP)
>   P. C. Lindahl, W. E. Streets, J. J. Marr, K. J. Parish, A. E. Scandora, G. A. Anast, W. R. Newberry, J. R. Dahlgran, C. Watkins, J. Connolly, and J. Fisk
>>   Presented at the 37th ORNL-DOE Conf. on Analytical Chemistry in Energy Technology, Gatlinburg, TN, October 7–9, 1997

An AEM Study of Glass-Palagonite Interfaces Formed in Hawaiian Basalt Glasses
>   J. S. Luo, W. L. Ebert, N. L. Dietz, and J. K. Bates
>>   Presented at the 99th Am. Ceram. Soc. Meeting, Cincinnati, OH, May 4–7, 1997

Characterization of Contaminated Soils and Solid Waste Streams with Electron Microscopy and Synchrotron X-rays
>   J. S. Luo, J. Wang, and E. C. Buck
>>   Presented at the U.S. EPA Region 5 Waste Minimization/Pollution Prevention Conf. for Hazardous Waste Generators, Chicago, IL, February 25–27, 1997

In-Situ X-ray Absorption Spectroscopy Study of the $LiNiO_2$ Electrode
>   A. N. Mansour, J. McBreen, and C. A. Melendres
>>   Presented at the Am. Phys. Soc. Meeting, Kansas City, KS, March 1997

The Advanced Photon Source and CMT: Getting Ready to Work at the MRCAT
>   V. A. Maroni
>>   Presented as a Chemical Technology Division Seminar, March 11, 1997

The Ag/Bi-2223 Composite Superconductor: Using Process Knowledge to Improve Performance
>   V. A. Maroni
>>   Presented as a Materials Science Division Seminar, Argonne, IL, October 8, 1997

Understanding the Aging of Fluidized Cracking Catalysts Through the Use of Density Gradient Separation Techniques
>   C. L. Marshall, G. R. Dyrkacz, L. Ruščić, I. Vasalos, and W. J. Reagan
>>   Presented at the 15th North American Catalysis Soc. Meeting, Chicago, IL, May 18–23, 1997

Ab Initio Investigation of HDS Catalysts
>   C. L. Marshall, J. L. Tilson, M. R. Palmer, and J. R. Brenner
>>   Presented at the 213th Am. Chem. Soc. National Meeting on Applications of Quantum Chemical and Molecular Simulation to Heterogeneous Catalysis, Division of Petroleum Chemistry, San Francisco, CA, April 13–17, 1997

Development of Processing Methods for Stainless Steel-Zirconium Nuclear Waste Forms Alloys
>   S. M. McDeavitt and D. P. Abraham
>>   Presented at the 126th Annual Meeting of the Minerals, Metals, and Materials Soc., Symp. on Materials Processing Fundamentals, Orlando, FL, February 9–13, 1997

Recent Developments in Electrometallurgical Treatment Technology at Argonne
    C. C. McPheeters, E. C. Gay, E. J. Karell, and J. P. Ackerman
        Presented at the 21st Annual Actinide Separations Conf., Charleston, SC,
        June 23–26, 1997

Synchrotron Infrared Spectroscopy for the *In-Situ* Study of Electrode Surfaces and
Interfaces
    C. A. Melendres
        Presented at the Am. Chem. Soc. Regional Meeting, Midland, MI, May 27–30,
        1997

Synchrotron Techniques for the *In-Situ* Study of Corrosion-Passivation Phenomena in
Metals
    C. A. Melendres
        Presented at the 191st Electrochem. Soc. Meeting, Montreal, Quebec, Canada,
        May 4–9, 1997

In-Situ Synchrotron Studies of the Passivation and Localized Corrosion of Copper in
Aqueous Solutions
    C. A. Melendres
        Presented at the Joint Int. Meeting of the Electrochemical Soc. of the USA and
        the Int. Soc. of Electrochemistry, Paris, France, August 31–September 5, 1997

In-Situ Infrared Spectroscopy of Electrode Surfaces with a Synchrotron Source
    C. A. Melendres, G. A. Bowmaker, J. M. Leger, B. Beden, and A. Tadjeddine
        Presented at the Joint Int. Meeting of the Electrochemical Soc. of the USA and
        the Int. Soc. of Electrochemistry, Paris, France, August 31–September 5, 1997

High J_c Ag/Bi-2223 Composite Conductors: The Importance of Reaction Induced Texture
    N. N. Merchant, V. A. Maroni, S. E. Dorris, and A. K. Fischer
        Presented at the Spring Meeting of the Materials Research Soc., San Francisco,
        CA, March 31–April 4, 1997

Phase and Microstructure Evolution in Ag/Bi-2223 Multifilaments: Optimizing Process
Chemistry to Improve Performance
    N. N. Merchant, V. A. Maroni, G. N. Riley, W. L. Carter, E. Podtburg, and
    M. W. Rupich
        Presented at the Fall Meeting of the Materials Research Soc., Boston, MA,
        December 1–5, 1997

Comparison of the Corrosion Behavior of Plutonium Glasses
    C. J. Mertz, A. J. Bakel, J. K. Bates, D. B. Chamberlain, J. Fortner, J. M. Hanchar,
    and S. F. Wolf
        Presented at the 99th Am. Ceram. Soc. Meeting, Cincinnati, OH, May 4–7,
        1997

Trace Anion Catalysis of Elementary Heterogeneous Charge-Transfer Reactions
    Z. Nagy
        Presented at the DOE/BES Corrosion Contractors' Meeting, University of
        Minnesota, Minneapolis, MN, September 19–20, 1997

Kinetic Measurements of Copper Deposition/Dissolution at High Temperature and Pressures
>   Z. Nagy, R. O. Rigney, N. C. Hung, and R. M. Yonco
>   Presented at the Gordon Research Conf. on Electrochemistry, Ventura, CA, January 12–17, 1997

Application of Adaptive Neural Network Processing to Passive FTIR Sensor Data
>   Y. X. Noyes and S. E. Carpenter
>   Presented at the 48th Pittsburgh Conf. and Exposition on Analytical Chemistry and Applied Spectroscopy, Atlanta, GA, March 16–21, 1997

Superconducting Open-Gradient Magnetic Separation for the Pretreatment of Radioactive or Mixed Waste Vitrification Feeds
>   L. Nuñez, R. D. Doctor, M. D. Kaminski, and A. E. Visser
>   Presented at the Tenth Symp. on Separation Science and Technology for Energy Applications, Gatlinburg, TN, October 20–24, 1997

Metals Separation Using Solvent Extractants on Magnetic Microparticles
>   L. Nuñez and M. Pourfarzaneh
>   Presented at the 213th Am. Chem. Soc. National Meeting, San Francisco, CA, April 13–17, 1997

Determination of Polychlorinated Biphenyls in Water Containing Citrikleen^{TM}
>   K. J. Parish, D. V. Applegate, A. S. Boparai, and M. J. Schipma
>   Presented at the 48th Pittsburgh Conf. and Exposition on Analytical Chemistry and Applied Spectroscopy, Atlanta, GA, March 16–21, 1997

Fuel Cell R&D at Argonne National Laboratory
>   W. F. Podolski
>   Presented to the Chinese Fuel Cell Bus Delegation, Argonne National Laboratory, May 23, 1997

The Reduction of Np(VI) and Pu(VI) by Organic Chelating Agents
>   D. T. Reed, S. B. Aase, and J. E. Banaszak
>   Presented at the Fifth Int. Conf. on the Chemistry and Migration Behavior of Actinides and Fission Products in the Geosphere, MIGRATION '97, Sendai, Japan, October 26–31, 1997

Kinetic Measurements of Copper Deposition/Dissolution at High Temperatures and Pressures
>   R. O. Rigney, N. C. Hung, and Z. Nagy
>   Presented at the 29th Central Regional Meeting of the Am. Chem. Soc., Midland, MI, May 27–30, 1997

High Gradient Magnetic Separation for the Pretreatment of Radioactive and Mixed Waste
>   J. A. Rith, A. D. Ebner, J. Shen, and L. Nuñez
>   Presented at the Tenth Symp. on Separation Science and Technology for Energy Applications, Gatlinburg, TN, October 20–24, 1997

Ceramic Breeder Material Development
> N. Roux, S. Tanaka, C. E. Johnson, and R. A. Verrall
>> Presented at the Fourth Int. Symp. on Fusion Nuclear Technology, Tokyo, Japan, April 6–11, 1997

Computational, Electrochemical and ^{7}Li NMR Studies of Lithiated Disordered Carbon Electrodes in Lithium Ion Cells
> G. Sandí, R. E. Gerald, L. G. Scanlon, K. A. Carrado, and R. E. Winans
>> Presented at the Fall Meeting of the Materials Research Soc. on Materials for Electrochemical Energy Storage and Conversion II—Batteries, Capacitors, and Fuel Cells, Boston, MA, December 1–5, 1997

Separation of Uranium from Actinides Using a High Throughput Electrorefiner
> S. A. Slater and E. C. Gay
>> Presented at the 21st Annual Actinide Separations Conf., Charleston, SC, June 23–26, 1997

Electrochemical Separation of Aluminum from Uranium for Spent Fuel Applications
> S. A. Slater, J. L. Willit, and E. C. Gay
>> Presented at the Tenth Symp. on Separation Science and Technology for Energy Applications, Gatlinburg, TN, October 20–24, 1997

Electroplating Fission-Recoil Barriers onto LEU-Metal Foils for ^{99}Mo-Production Targets
> J. A. Smaga, J. Sedlet, C. Conner, M. W. Liberatore, D. E. Walker, D. G. Wygmans, and G. F. Vandegrift
>> Presented at the Int. Meeting on Reduced Enrichment for Research and Test Reactors (RERTR), Jackson Hole, WY, October 5–10, 1997

An Evaluation of Empore^{TM} Radium Rad Disks
> L. L. Smith, F. Markun, J. S. Alvarado, D. C. Seely, and J. A. Osterheim
>> Presented at the 3M Empore^{TM} Rad Disk Technical Workshop at the 43rd Annual Conf. on Bioassay, Analytical, and Environmental Radiochemistry, Charleston, SC, November 9–13, 1997

The Characterization and Testing of Candidate Immobilization Forms for the Disposal of Plutonium
> D. M. Strachan, A. J. Bakel, E. C. Buck, D. B. Chamberlain, J. Fortner, C. J. Mertz, S. F. Wolf, W. L. Bourcier, B. B. Ebbinghaus, H. F. Shaw, R. A. Van Konynenburg, B. P. McGrail, J. D. Vienna, J. C. Marra, and D. K. Peeler
>> Presented at the 21st Annual Actinide Separation Conf., Charleston, SC, June 23–26, 1997

Development of Evaluation Protocols for DOE's Integrated Performance Evaluation Program (IPEP)
> W. E. Streets, P. C. Lindahl, J. J. Marr, K. J. Parish, A. E. Scandora, G. A. Anast, and W. R. Newberry
>> Presented at the 37th ORNL-DOE Conf. on Analytical Chemistry in Energy Technology, Gatlinburg, TN, October 7–9, 1997

Status of Implementation of DOE's Integrated Performance Evaluation Program (IPEP)
W. E. Streets, P. C. Lindahl, J. J. Marr, K. J. Parish, A. E. Scandora, J. M. Copple, G. A. Anast, and J. R. Dahlgran
Presented at the 43rd Annual Conf. on Bioassay, Analytical, and Environmental Radiochemistry, Charleston, SC, November 9–13, 1997

Thermodynamic and Nonstoichiometric Behavior of the Lead-Doped and Lead-Free Bi-2212 Systems
M. Tetenbaum, M. C. Hash, B. S. Tani, J. S. Luo, and V. A. Maroni
Presented at the Fifth Int. Conf., Materials and Mechanisms of Superconductivity, High Temperature Superconductors, Beijing, China, February 28–March 4, 1997

Battery Research at Argonne National Laboratory
M. M. Thackeray
Presented at the Exploratory Technology Research Session at the DOE-sponsored Automotive Technology Development Customers' Coordination Meeting, Dearborn, MI, October 27–30, 1997

Manganese Oxides for Lithium Batteries
M. M. Thackeray
Presented at the Electrochem. Soc. Meeting, Minneapolis, MN, November 12, 1997

Metal Oxides for Lithium Batteries
M. M. Thackeray
Presented at the Royal Netherlands Academy of Science, Amsterdam, The Netherlands, April 7–11, 1997

The Structural Stability of Manganese Oxide Electrodes for Lithium Batteries
M. M. Thackeray, C. S. Johnson, Y. Shao-Horn, and S. A. Hackney
Presented at the Am. Phys. Soc. Meeting, Kansas City, MO, March 17–21, 1997

The Use of High Performance Computers to Solve Problems in Catalytic Chemistry
J. L. Tilson and C. L. Marshall
Presented at the 213th Am. Chem. Soc. National Meeting on Industrial Applications of Computational Chemistry, Division of Computers in Chemistry, San Francisco, CA, April 13–17, 1997

Treatment of Molten Salt Reactor Experiment Fuel and Flush Salts
Z. Tomczuk, W. E. Miller, and J. J. Laidler
Presented at the Am. Nucl. Soc. Annual Meeting, Orlando, FL, June 1–5, 1997

ANL Nuclear Cleanup Activities
G. F. Vandegrift
Presented at Argonne National Laboratory for CHM Corporation, Argonne, IL, August 19, 1997

Discussion Notes: Production of ^{99}Mo from Low-Enriched Uranium
    G. F. Vandegrift
        Presented at PUSPIPTEK, Serpong, Indonesia, April 28–May 7, 1997 and
        October 24–November 1, 1997

Challenges in Actinide and Fission-Product Separations in Production of ^{99}Mo from
Irradiated Low-Enriched Uranium
    G. F. Vandegrift, S. B. Aase, C. Conner, R. A. Leonard, J. Sedlet, J. L. Snelgrove,
    D. G. Wygmans, and S. Landsberger
        Presented at the 21st Annual Actinide Separations Conf., Charleston, SC,
        June 23–26, 1997

Progress in Chemical Processing of LEU Targets for ^{99}Mo Production—1997
    G. F. Vandegrift, C. Conner, J. Sedlet, D. G. Wygmans, D. Wu, F. Iskander, and
    S. Landsberger
        Presented at the IAEA Int. Meeting on Reduced Enrichment for Research and
        Test Reactors (RERTR), Jackson Hole, WY, October 5–10, 1997

Development and Processing of LEU Targets for ^{99}Mo Production
    G. F. Vandegrift, J. L. Snelgrove, and G. L. Hofman
        Presented at the University of Texas Nuclear Engineering Teaching Laboratory,
        Austin, TX, April 24, 1997

Development and Processing of LEU Targets for ^{99}Mo Production
    G. F. Vandegrift, J. L. Snelgrove, and G. L. Hofman
        Presented at the IAEA Meeting, Production Technologies for Molybdenum-99
        and Technetium-99m, Faure, South Africa, April 10–12, 1997

Application of Instrumental Radioanalytical Techniques to Nuclear Waste Testing and
Characterization
    S. F. Wolf
        Presented at the Fourth Int. Conf. on Methods and Applications of
        Radioanalytical Chemistry, MARC-IV, Kailua-Kona, HI, April 6–11, 1997

Volatile Trace Element Composition and Shock in Equilibrated H Chondrites
    S. F. Wolf and M. E. Lipschutz
        Presented at the Workshop on Parent Body and Nebular Modification of
        Chondritic Materials, Sponsored by the University of Hawaii Lunar and
        Planetary Institute, and NASA Origins of Solar Systems Program, Maui,
        Hawaii, July 17–19, 1997

Volatile Trace Element Content and Petrographic Type in Equilibrated H Chondrites
    S. F. Wolf and M. E. Lipschutz
        Presented at the 60th Meteoritical Soc. Meeting, Maui, HI, July 21–25, 1997

Ion Exchange in a Zeolite-Molten Chloride System
    R. H. Woodman and C. Pereira
        Presented at the 99th Am. Ceram. Soc. Meeting, Cincinnati, OH, May 4–7,
        1997

Study of Electrochemical Interfaces at the Advanced Photon Source
> H. You and Z. Nagy
>> Presented at the Advanced Non-Aqueous Battery Technology Research and Development Workshop, Hunt Valley, MD, October 15–17, 1997

In Situ Study of Porous Silicon: Growth and Luminescence
> H. You, Z. Nagy, J. A. Tanzer, Z. Gaburro, and D. Babic
>> Presented at the Fifth Int. Conf. on Surface X-ray and Neutron Scattering, Oxford, England, July 13–17, 1997

Direct Methanol Fuel Cells as Portable Power Sources
> D. J. Zurawski
>> Presented at the University of Puerto Rico, San Juan, Puerto Rico, February 3, 1997

Fuel Cell Technology: Ushering in a New Age in Transportation Technology
> D. J. Zurawski
>> Presented at Tristate University, Angola, IN, January 22, 1997

DMFC Program at ANL
> D. J. Zurawski, M. Krumpelt, R. Kumar, and A. J. Aldykiewicz
>> Presented at the Army Research Office Review of the Minority Institution Fuel Cell/Battery/Manufacturing Research Hub, Illinois Institute of Technology, Chicago, IL, May 2, 1997

A Computational Study of Proton Transfer between a Zeolithic Brønsted Acid Site and an Adsorbed H_2O Dimer
> S. A. Zygmunt, L. A. Curtiss, and L. E. Iton
>> Presented at the 15th North American Catalysis Soc. Meeting, Chicago, IL, May 18–23, 1997

F. Papers Accepted for Publication

Modeling of a Zeolite Column for the Removal of Fission Products from Molten Salt
      R. K. Ahluwalia, H. K. Geyer, C. Pereira, and J. P. Ackerman
            To be published in Ind. Eng. Chem. Res.

Corrosion of a Pu-Doped Zirconolite-Rich Ceramic
      A. J. Bakel, E. C. Buck, S. F. Wolf, B. B. Ebbinghaus, and D. B. Chamberlain
            To be published in *Environmental Issues and Waste Management Technologies
            in the Ceramic and Nuclear Industries III*, Proc. of the Am. Ceram. Soc. Conf.

X-ray Absorption Specroscopy Study of the Local Structure of Heavy Metal Ions
Incorporated into Electrodeposited Nickel Oxide Films
      M. Balasubramanian, C. A. Melendres, and A. N. Mansour
            To be published in J. Electrochem. Soc.

Structure and Electrochemical Potential Simulation for the Cathode Material $Li_{1+x}V_3O_8$
      R. Benedek, M. M. Thackeray, and L. H. Yang
            To be published in Mater. Res. Soc. Symp. Proc.

Investigation of the Vibrational Properties of OCN^- on a Silver Electrode by *In-Situ*
Synchrotron Far Infrared Spectroscopy and Visible-Infrared Sum Frequency Generation
Spectroscopy
      G. A. Bowmaker, J. M. Leger, A. LeRille, C. A. Melendres, and A. Tadjeddine
            To be published in J. Chem. Soc., Faraday Transactions

Microstructural Characterization of a Highly HDS-Active Co_6S_8-Pillared Molybdenum
Sulfide
      J. R. Brenner, C. L. Marshall, R. E. Winans, J. Heising, R. Bissessur, and
      M. Kanatzidis
            To be published in Chem. Mater.

Materials Derived from Synthetic Organo-Clay Complexes as Novel Hydrodesulfurization
Catalyst Supports
      K. A. Carrado, C. L. Marshall, J. R. Brenner, K. Song
            To be published in Microporous Mater.

Use of Sol-Gel Systems for Solid/Liquid Separation
      D. J. Chaiko, J. P. Kopasz, and A. J. G. Ellison
            To be published in Ind. Eng. Chem. Res.

Oxygen Atom Transfer from μ-Oxo-bis[1,4,8,11,15,18,22,25-octakis(trifluoromethyl)phthalocyaninato]
diiron(III): Evidence for an Fe(IV) = O Intermediate
      M. J. Chen and J. W. Rathke
            To be published in J. Porphyrins and Phthalocyanines

Dissolution of Low-Enriched UO_2/Al Dispersion Plates in Alkaline Peroxide Solution
>   C. Conner, S. Aase, D. G. Wygmans, G. F. Vandegrift, D. Wu, and S. Landsberger
>>   To be published in the Proc. of the 1997 Int. Meeting on Reduced Enrichment
>>   for Research and Test Reactors

Computational Methods for Calculating Accurate Enthalpies of Formation, Ionization
Potentials, and Electron Affinities
>   L. A. Curtiss and K. Raghavachari
>>   To be published in *Computational Thermochemistry*

Gaussian-2 Theory
>   L. A. Curtiss and K. Raghavachari
>>   To be published in *Encyclopedia of Computational Chemistry*

Assessment of Complete Basis Set Methods for Calculation of Enthalpies of Formation
>   L. A. Curtiss, K. Raghavachari, P. C. Redfern, and B. B. Stefanov
>>   To be published in J. Chem. Phys.

The Incorporation of Technetium into a Representative Low-Activity Waste Glass
>   W. L. Ebert, A. J. Bakel, D. L. Bowers, E. C. Buck, and J. W. Emery
>>   To be published in *Environmental Issues and Waste Management Technologies
>>   in the Ceramic and Nuclear Industries III*, Proc. of the Am. Ceram. Soc. Conf.

$LiMn_{2-x}Cu_xO_4$ Spinels—5 V Cathode Materials
>   Y. Ein-Eli, W. F. Howard, S. H. Lu, S. Mukerjee, J. McBreen, J. T. Vaughey, and
>   M. M. Thackeray
>>   To be published in Mater. Res. Soc. Symp. Proc.

In Situ Imaging of Charge Carriers in an Electrochemical Cell

>   R. E. Gerald, R. J. Klingler, J. W. Rathke, G. Sandí, and K. Woelk
>>   To be published in Chapter X of *Spatially Resolved Magnetic Resonance*, Proc.
>>   of the Fourth Int. Conf. on Magnetic Resonance Microscopy

Chemistry and Management Education
>   D. W. Green
>>   To be published in Managing the Modern Laboratory

Forum on Hiring the Right Person the First Time
>   D. W. Green
>>   To be published in Managing the Modern Laboratory

Missed Communication
>   D. W. Green
>>   To be published in Managing the Modern Laboratory

[129]Xe MRM Characterization of Pore Structures in Silica Aerogels
>   D. M. Gregory, R. E. Gerald, D. J. Clifford, and R. E. Botto
>>   To be published in Chapter X of *Spatially Resolved Magnetic Resonance*, Proc.
>>   of the Fourth Int. Conf. on Magnetic Resonance Microscopy

Energy and Yield Distributions of Calcium Atoms and Clusters Undergoing 4 keV Ar+ Ion Bombardment
> C. S. Hansen, W. F. Calaway, B. V. King, and M. J. Pellin
>> To be published in Surf. Sci.

Ceramic Waste Form Powder Preparation Techniques
> M. C. Hash, C. Pereira, V. N. Zyryanov, M. A. Lewis, G. L. Burns, J. J. Smith, J. P. Thalacker, and J. P. Ackerman
>> To be published in *Environmental Issues and Waste Management Technologies in the Ceramic and Nuclear Industries III*, Proc. of the Am. Ceram. Soc. Conf.

Spectroscopic Study of the Proton Dynamics in Manganese Dioxide Electrode Materials
> C. S. Johnson, M. M. Thackeray, J. C. Nipko, and C.-K. Loong
>> To be published in Physica B

Evaluation of Extractant-Coated Magnetic Microparticles for the Recovery of Hazardous Metals from Waste Solution
> M. D. Kaminski, L. Nuñez, and A. E. Visser
>> To be published in Sep. Sci. Technol.

Methods for the Determination of Metals and Inorganic Chemicals in Environmental Samples
> P. C. Lindahl
>> Book Review to be published for *Environmental Progress*, Noyes Publications, Westwood, NJ

Analysis of X-ray Absorption Spectra of Some Nickel Oxycompounds Using Theoretical Standards
> A. N. Mansour and C. A. Melendres
>> To be published in J. Phys. Chem.

In-Situ X-ray Absorption Spectroscopic Study of Electrodeposited Nickel Oxide Films during Redox Reactions
> A. N. Mansour, C. A. Melendres, and J. Wong
>> To be published in J. Electrochem. Soc.

Ab Initio Molecular Orbital Study of the Acidity of Hydrated Sodium Hydroxide
> C. L. Marshall, J. Nicholas, K. A. Carrado, H. V. Brand, and R. E. Winans
>> To be published in J. Phys. Chem.

Evaluation of Stainless Steel-Zirconium Alloys as High-Level Nuclear Waste Forms
> S. M. McDeavitt, D. P. Abraham, and J. Y. Park
>> To be published in J. Nucl. Mater.

In-Situ Synchrotron Studies of the Passivation and Localized Corrosion of Copper in Aqueous Solutions
> C. A. Melendres
>> To be published in Passivity and Breakdown

In-Situ Synchrotron Far Infrared Spectroscopy of Surface Films on a Copper Electrode in Aqueous Solutions
>   C. A. Melendres, G. A. Bowmaker, J. M. Leger, and B. Beden
>   >   To be published in J. Electroanal. Chem.

Comparison of the Corrosion Behavior of Plutonium Glasses
>   C. J. Mertz, A. J. Bakel, J. K. Bates, D. B. Chamberlain, J. Fortner, J. M. Hanachar, and S. F. Wolf
>   >   To be published in *Environmental Issues and Waste Management Technologies in the Ceramic and Nuclear Industries III*, Proc. of the Am. Ceram. Soc. Conf.

Review of *Hazardous Waste Planning*
>   J. B. Rajan
>   >   To be published in Environ. Prog.

Structural Features of Low-Temperature $LiCoO_2$ and Acid-Delithiated Products
>   Y. Shao-Horn, S. A. Hackney, C. S. Johnson, A. J. Kahaian, and M. M. Thackeray
>   >   To be published in J. Solid State Chem.

Microstructural Features of α-MnO_2 Electrodes for Lithium Batteries
>   Y. Shao-Horn, S. A. Hackney, C. S. Johnson, and M. M. Thackeray
>   >   To be published in J. Electrochem. Soc.

Electrochemically Generated $CaCO_3$ Deposits on Iron Studied with FTIR and Raman Spectroscopy
>   L. J. Simpson
>   >   To be published in Electrochim. Acta

Methods and Criteria Development for Qualification of the Glass-Zeolite Ceramic Waste Form
>   L. J. Simpson, D. J. Wronkiewicz, and S. F. Wolf
>   >   To be published in *Environmental Issues and Waste Management Technologies in the Ceramic and Nuclear Industries III*, Proc. of the Am. Ceram. Soc. Conf.

Electroplating Fission-Recoil Barriers onto LEU-Metal Foils for [99]Mo-Production Targets
>   J. A. Smaga, J. Sedlet, C. Conner, M. W. Liberatore, D. E. Walker, D. G. Wygmans, and G. F. Vandegrift
>   >   To be published in the Proc. of the 1997 Int. Meeting on Reduced Enrichment for Research and Test Reactors

Radiostrontium Analysis Using Sorbent Disks
>   L. L. Smith, F. Markun, J. S. Alvarado, K. A. Orlandini, K. M. Hoffmann, D. C. Seely, and R. T. Shannon
>   >   To be published in *Current Protocols in Field Analytical Chemistry*

The Characterization and Testing of Candidate Immobilization Forms for the Disposal of Plutonium
> D. M. Strachan, A. J. Bakel, E. C. Buck, D. B. Chamberlain, J. Fortner, C. J. Mertz,
> S. F. Wolf, W. L. Bourcier, B. B. Ebbinghaus, H. F. Shaw, R. A. Van Konynenburg,
> B. P. McGrail, J. D. Vienna, J. C. Marra, and D. K. Peeler
>> To be published in Waste Management '98

Electrical Design
> R. L. Tollner
>> To be published in *Guideline for Gloveboxes*, Release 2, Am. Glovebox Soc.

Progress in Chemical Processing of LEU Targets for ^{99}Mo Production—1997
> G. F. Vandegrift, C. Conner, J. Sedlet, D. G. Wygmans, D. Wu, F. Iskander, and
> S. Landsberger
>> To be published in the Proc. of the 1997 Int. Meeting on Reduced Enrichment for Research and Test Reactors

Converting Targets and Processes for Fission-Product ^{99}Mo from High- to Low-Enriched Uranium
> G. F. Vandegrift, J. L. Snelgrove, S. B. Aase, M. M. Bretscher, B. A. Buchholz,
> L. Chen, C. Conner, D. Dong, G. L. Hofman, G. C. Knighton, R. A. Leonard,
> J. Sedlet, D. E. Walker, T. C. Wiencek, E. L. Wood, D. G. Wygmans, A. Travelli,
> S. Landsberger, D. Wu, A. Suripto, A. Mutalib, H. Nasution, Adang H. G.,
> Hotman, L., S. Amini, Dedi S., Martalena R., A. Gogo, B. Purwadi, D. L. Amin,
> Zahiruddin, A. Sukmana, Kadarisman, Sriyono, D. Hafid, and M. Sayad
>> To be published as a Book Chapter in Int. Atomic Energy Agency *TECHDOC*

On the Mechanism of Hematite Deposition on a Metal Surface under Nucleate Boiling Conditions
> L. Wen and C. A. Melendres
>> To be published in Colloids Surf.

Imaging Diffusion with Non-Constant B_1 Gradients
> K. Woelk, B. L. J. Zwank, J. Bargon, R. J. Klingler, R. E. Gerald, and J. W. Rathke
>> To be published in Chapter X of *Spatially Resolved Magnetic Resonance*, Proc. of the Fourth Int. Conf. on Magnetic Resonance Microscopy

Structure and Morphology of Electrodeposited $CaCO_3$: X-ray Diffraction and Microscopy Studies
> S. Xu, C. A. Melendres, J. H. Park, and M. A. Kamrath
>> To be published in J. Electrochem. Soc.

An Assessment of Density Functional Methods for Studying Molecular Adsorption in Cluster Models of Zeolites
> S. A. Zygmunt, R. M. Mueller, L. A. Curtiss, and L. E. Iton
>> To be published in J. Mol. Struct. (Theochem.)

Distribution for ANL-98/13

Internal:

D. P. Abraham	F. Y. Fradin	D. J. Myers
J. P. Ackerman	E. C. Gay	K. M. Myles
S. Ahmed	M. M. Goldberg	L. Nuñez
K. Amine	K. V. Gourishankar	C. Pereira
J. M. Andrew	D. G. Graczyk	W. H. Perry
J. G. Asbury	D. W. Green	W. F. Podolski
A. J. Bakel	D. M. Gruen	R. B. Poeppel
J. K. Bates	J. E. Harmon (3)	J. W. Rathke
J. E. Battles	J. E. Helt	D. T. Reed
P. R. Betten (5)	G. L. Henriksen	M. K. Richmann
S. K. Bhattacharyya	D. J. Hill	W. W. Schertz
I. D. Bloom	L. R. Johnson	D. K. Schmalzer
A. S. Boparai	E. J. Karell	S. A. Slater
D. L. Bowers	T. D. Kaun	D. L. Smith
L. M. Boxberger	J. P. Kopasz	J. L. Smith
E. C. Buck	T. R. Krause	M. J. Steindler
J. D. Carter	M. Krumpelt	W. M. Swift
D. J. Chaiko	R. Kumar	S.-W. Tam
D. B. Chamberlain	J. J. Laidler (75)	M. Thackeray
Y. I. Chang	L. Leibowitz	M. C. Thurnauer
L. S. H. Chow	R. A. Leonard	Z. Tomczuk
J. C. Cunnane	M. A. Lewis	G. F. Vandegrift
D. W. Dees	P. C. Lindahl	D. C. Wade
L. W. Deitrich	M. J. Lineberry	L. C. Walters
W. H. DeLuca	J. S. Luo	R. W. Weeks
H. Drucker	V. A. Maroni	C. L. Wilkinson
B. D. Dunlap	S. M. McDeavitt	J. L. Willit
W. L. Ebert	W. D. McFall	S. F. Wolf
R. E. Einziger	C. C. McPheeters	A. M. Wolsky
P. A. Finn	J. F. Miller	R. D. Wolson
J. Fortner	W. E. Miller	TIS Files
S. C. Foster	T. P. Mulcahey	

External:

DOE-OSTI (2)
ANL-E Library
ANL-W Library
Manager, Chicago Operations Office, DOE
A. Bindokas, DOE-CH
P. M. Ferrigan, DOE-CH

J. C. Haugen, DOE-CH
S. Ludwig, DOE-CH
A. L. Taboas, DOE-CH
J. R. LaFevers, DOE-UC
Chemical Technology Division Review Committee Members:
 H. U. Anderson, University of Missouri-Rolla, Rolla, MO
 E. R. Beaver, Monsanto Company, St. Louis, MO
 A. L. Bement, Purdue University, West Lafayette, IN
 M. V. Koch, University of Washington, Seattle, WA
 R. A. Osteryoung, North Carolina State University, Raleigh, NC
 V. P. Roan, University of Florida, Palm Beach Gardens, FL
 G. R. St. Pierre, Ohio State University, Columbus, OH
R. C. Alkire, University of Illinois, Champaign, IL
R. A. Bajura, USDOE, Federal Energy Technology Center, Morgantown, WV
S. Barker, Lockheed Martin Hanford Company, Richland, WA
S. E. Berk, USDOE, Office of Fusion Energy, Germantown, MD
A. L. Boldt, Lockheed Martin Hanford Company, Richland, WA
S. S. Borys, Gas Research Institute, Chicago, IL
D. F. Bowersox, Los Alamos National Laboratory, Los Alamos, NM
G. G. Boyd, USDOE, Office of Science and Technology, Washington, DC
E. Brueckner, US CAR, Dearborn, MI
D. B. Bullen, Nuclear Waste Technical Review Board, Arlington, VA
S. A. Butter, USDOE, Office of Basic Energy Sciences, Washington, DC
L. Camara, MC Power Corporation, Burr Ridge, IL
M. H. Campbell, MACTECH, Richland, WA
K. A. Chacey, USDOE, Office of Environmental Management, Germantown, MD
S. G. Chalk, USDOE, Office of Transportation Technologies, Washington, DC
S. W. Chun, USDOE, Federal Energy Technology Center, Pittsburgh, PA
H. Cost, Chrysler Corporation, Auburn Hills, MI
P. Davis, USDOE, Office of Transportation Technologies, Washington, DC
C. Donnelly, 3M Center, St. Paul, MN
J. Dunning, GM EV, Troy, MI
T. Dvong, USDOE, Office of Transportation Technologies, Washington, DC
J. J. Eberhardt, USDOE, Office of Transportation Technologies, Washington, DC
R. E. Erickson, USDOE, Office of Environmental Management, Germantown, MD
G. Escobar, LATO Office Rocky Flats Plant, Golden, CO
R. C. Ewing, University of Michigan, Ann Arbor, MI
R. J. Fiskum, USDOE, Office of Building Energy Research, Washington, DC
M. W. Frei, USDOE, Office of Waste Management, Germantown, MD
T. Fryberger, Pacific Northwest National Laboratory, Richland, WA
D. R. Funk, USDOE, Office of Nuclear Energy, Germantown, MD
D. Geiser, USDOE, Office of Technology Development, Germantown, MD
M. R. Ghate, USDOE, Federal Energy Technology Center, Morgantown, WV
R. Gilchrist, Pacific Northwest National Laboratory, Richland, WA
T. J. Gross, USDOE, Office of Transportation Technologies, Washington, DC
C. Hanson, USDOE, Richland Operations Office, Richland, WA

H. Haskins, Ford Motor Company, Dearborn, MI
K. L. Heitner, USDOE, Office of Transportation Technologies, Washington, DC
T. M. Hohl, Lockheed Martin Hanford Company, Richland, WA
N. Iyer, Westinghouse Savannah River Company, Aiken, SC
G. Jansen, Lockheed Martin Hanford Company, Richland, WA
L. J. Jardine, Lawrence Livermore National Laboratory, Livermore, CA
E. F. Johnson, Princeton University, Princeton, NJ
E. Jones, Pacific Northwest National Laboratory, Richland, WA
F. Kane, University of Idaho, Moscow, ID
R. D. Kelley, USDOE, Office of Basic Energy Sciences, Germantown, MD
C. Kincaid, USDOE, Office of Nonproliferation and National Security, Washington, DC
R. Kinney, 3M Industrial and Electronic Sector Research Laboratory, St. Paul, MN
R. S. Kirk, USDOE, Office of Transportation Technologies, Washington, DC
B. Knutson, Lockheed Martin Hanford Company, Richland, WA
L. J. Krause, 3M Industrial and Electronic Sector Research Laboratory, St. Paul, MN
K. Krist, Gas Research Institute, Chicago, IL
P. Lascoe, USDOE, Richland Operations Office, Richland, WA
S. C. T. Lien, USDOE, Office of Technology Development, Germantown, MD
G. J. Lumetta, Pacific Northwest National Laboratory, Richland, WA
W. D. Magwood, USDOE, Office of Nuclear Energy, Washington, DC
P. Marpin, USDOE, Office of Energy Research, Germantown, MD
B. P. McGrail, Pacific Northwest National Laboratory, Richland, WA
J. Milliken, USDOE, Office of Transportation Technologies, Washington, DC
A. C. Muscatello, Rocky Flats Plant, Golden, CO
R. J. Nowak, DARPA/DSO Defense Sciences Office, Arlington, VA
J. B. O'Sullivan, Electric Power Research Institute, Palo Alto, CA
A. L. Olson, Lockheed Idaho Technology Company, Idaho Falls, ID
J. Owendoff, USDOE, Office of Environmental Management, Washington, DC
P. G. Patil, USDOE, Office of Transportation Technologies, Washington, DC
R. Paur, Army Research Office, Research Triangle Park, NC
D. Pepson, USDOE, Office of Waste Management, Germantown, MD
R. Person, USDOE, Materials Disposition, Washington, DC
L. Petrakis, Brookhaven National Laboratory, Upton, NY
S. T. Picraux, Sandia National Laboratories, Albuquerque, NM
G. Reddick, Lockheed Martin Hanford Company, Richland, WA
S. Rogers, USDOE, Office of Transportation Technologies, Washington, DC
P. S. Schaus, Lockheed Martin Hanford Company, Richland, WA
L. H. Schwartz, National Institute of Standards and Technology, Gaithersburg, MD
A. W. Searcy, Lawrence Berkeley Laboratory, Berkeley, CA
R. W. Shivers, USDOE, Office of Conservation, Washington, DC
W. A. Siegel, USDOE, Office of Transportation Technologies, Washington, DC
A. Simmons, USDOE, Las Vegas, NV
M. I. Singer, USDOE, Advanced Research/Special Technologies, Washington, DC
S. Singhal, Westinghouse Electric Corporation, Pittsburgh, PA
E. Slaathug, Lockheed Martin Hanford Company, Richland, WA
C. Sloane, GM Research and Development Center, Warren, MI

D. Stahl, Framatome Cogema Fuels, Las Vegas, NV
R. B. Stout, Lawrence Livermore National Laboratory, Livermore, CA
J. P. Strakey, USDOE, Federal Energy Technology Center, Pittsburgh, PA
R. A. Sutula, USDOE, Office of Transportation Technologies, Washington, DC
R. Swaroop, Electric Power Research Institute, Palo Alto, CA
T. A. Thornton, Framatome Cogema Fuels, Las Vegas, NV
J. A. Turi, USDOE, Office of Environmental Management, Germantown, MD
University of California, Government Documents Department, Berkeley, CA
M. Williams, USDOE, Federal Energy Technology Center, Morgantown, WV
R. E. York, General Motors Corporation, Warren, MI
C. Zeh, USDOE, Federal Energy Technology Center, Morgantown, WV
S. Zimmer, Chrysler Corporation, Auburn Hills, MI
R. J. Harrison, Atomic Energy of Canada, Ltd., Chalk River, Ontario, CANADA
M. Ozawa, PNC Tokai-Works, Ibaraki-ken, JAPAN